Aus dem Institute for Cardiovascular Prevention (IPEK) der Ludwig-Maximilians-Universität München (LMU)

Dissertation

zum Erwerb des Doctor of Philosophy (Ph.D.) an der

Medizinischen Fakultät der

Ludwig-Maximilians-Universität zu München

The role of the atypical chemokine receptor ACKR3 in Bone Marrow homeostasis

vorgelegt von:

Maria Aslani

aus: Panorama, Thessaloniki, Griechenland

2022

Mit Genehmigung der Medizinischen Fakultät der

Ludwig-Maximilians-Universität zu München

First evaluator (1. TAC member):	Prof. Dr. med. Christian Weber
Second evaluator (2. TAC member):	Prof. Dr. rer. nat. Jürgen Bernhagen
Third evaluator:	Prof. Dr. Christian Schulz
Fourth evaluator:	Prof. Dr. Peter J. Nelson

Dean: **Prof. Dr. med. Thomas Gudermann**

Date of the defense:
13th May 2022

Table of Contents

A. Abstract

Daily hematopoietic cells are produced in the bone marrow (BM) in a process termed as hematopoiesis. At the apex of hematopoiesis, the hematopoietic stem cells (HSC) reside, the cells which produce all other hematopoietic cells (Haas et al., 2018). The chemokine CXCL12 and its receptor CXCR4 regulate hematopoiesis, retaining the HSC within the BM (Nagasawa et al., 1996, Ma et al., 1998). Additionally, CXCL12 binds to the atypical chemokine receptor ACKR3 (Burns et al., 2006). However, the expression and the role of ACKR3 within the BM remains undetermined, whereas the mechanism by which CXCL12 and CXCR4 maintain HSCs in the BM remains elusive.

In this regard, the expression of ACKR3 was assessed using an ACKR3 reporter mouse line. In addition, the expression of the receptor was conditionally deleted *in vivo* and the effect in steady state and during emergency hematopoiesis, with the administration of the cytotoxic agent 5-Fluorouracil (5FU), was assessed. Furthermore, ACKR3 was pharmacologically inhibited and the role of the receptor in regulating CXCL12 was investigated. Finally, the role of the axis in HSC BM retention was evaluated in *Ackr3*$^{-/-}$, *Cxcl12*$^{-/-}$ and *Cxcr4*$^{-/-}$ mice.

The present study demonstrates that ACKR3 is not expressed in HSC and progenitor cells, but rather in the endosteal cells and in BM plasma cells. In addition, the conditional deletion of ACKR3 in all tissues, did not affect blood cell production, but induced HSCs to exit quiescence and acquire a proliferating phenotype. Similarly, conditional deletion of CXCL12 forced HSCs to exit dormancy, demonstrating that ACKR3 maintains HSC quiescence via CXCL12.

The role of ACKR3 in HSC maintenance is even more pronounced during emergency hematopoiesis. In the absence of the receptor, mice exhibit enhanced mortality at day 10 after the administration of the cytotoxic agent. Under these conditions, ACKR3 also regulates *Cxcl12* gene expression in aortic cells and hence, the concentration of CXCL12 in circulation.

Nevertheless, ACKR3 deletion and the pharmacological inhibition of the receptor does not affect HSC mobilization. Deletion of CXCL12 and the artificial increase of circulating CXCL12 concentration further suggest that CXCL12 is not sufficient to regulate HSC retention and mobilization. On the contrary, the expression of CXCR4 on hematopoietic, but not on stromal cells, is essential for the maintenance of the cells in the BM.

In conclusion, the present study unravels the differences in the expression pattern of CXCR4 and ACKR3 within the BM and reveals an unprecedented role for ACKR3 in the maintenance of HSC quiescence and the regulation of CXCL12 concentration under certain conditions. Finally, this study suggests that HSCs anchor in the BM via CXCR4, demonstrating that CXCR4 is the critical element for BM cell retention.

List of Figures

List of Tables

List of abbreviations

ACKR3	Atypical Chemokine Receptor 3
AEC	Arterial Endothelial cells
ApoE	Apolipoprotein E
ATP	Adenosine Triphosphate
BMT	Bone Marrow Transplantation
CAR cells	CXCL12 Abundant Reticular cells
CM	Classical Monocytes
CMP	Common Myeloid Progenitor
DHR	Dihydrorhodamine
GAG	Glycosaminoglycan
G-CSF	Granulocyte Colony-Stimulating Factor
GDP	Guanosine Diphosphate
GMP	Granulocyte-Monocyte Progenitor
GTP	Guanosine Triphosphate
Hct	Hematocrit
Hgb	Hemoglobin
HIF1a	Hypoxia Inducible Factor 1 Subunit Alpha
HSC	Hematopoietic Stem Cells
HSPC	Hematopoietic Stem and Progenitor cells
HUVEC	Human Umbilical Vein Endothelial Cells
i.v.	intravenously
i.p.	Intraperitonially
LSK	$Lineage^{-}$ $Sca1^{+}$ $c\text{-}kit^{+}$ cells
MCV	Mean Corpuscular Volume
MEP	Megakaryocyte-Erythroid Progenitor
MPP	Multiple Progenitor Population
MSC	Mesenchymal Stem cells
NCM	Non-classical Monocytes
Osx	Osterix
PBS	Phosphate-Buffered Saline
PFA	Paraformaldehyde
RBC	Red Blood Cells
ROS	Reactive Oxygen Species
SCF	Stem Cell Factor
SEC	Sinusoidal endothelial cells
Ubc	Ubiquitin
WHIM	Warts, Hypogammaglobulinemia, Infections, and Myelokathexis

1. Introduction

1.1. Hematopoietic stem cells: the cornerstone of the hematopoietic system

Hematopoiesis is the process of blood cell production in the adult bone marrow. Blood cells are vital for life as they are responsible for the constant oxygen transport in all tissues (Hook et al., 1988). At the same time, the hematopoietic system is detrimental for the development and the suppression of diseases. Immunodeficiencies, leukemias and anemias develop due to mutations in hematopoietic cells (Fischer et al., 2015, Passegué et al., 2003, Hoggatt et al., 2016, Cascio and DeLoughery, 2017, Kato et al., 2018). In addition, endogenous and exogenous pathogens trigger hematopoietic cells to initiate the process of inflammation. During inflammation, hematopoietic cells sense the pathogenic factors, and mediate immune responses in order to exterminate them, and restore the affected tissue. Of note, although the immune responses are necessary for the elimination of the pathogens and the suppression of the disease, the malfunction of the immune responses can induce "para-inflammation", a condition of low-grade inflammation. This condition stresses the tissue and if not restored can become chronic (Medzhitov, 2008). Chronic inflammation characterizes aging, a state described as inflamm-aging (Pietras, 2017) and is also associated with the development of cardiovascular diseases, dementia, type 2 diabetes, and cancer (Ferrucci and Fabri, 2018). Thus, it is evident that the understanding of hematopoiesis and the immune responses is detrimental in order to prevent and treat human diseases.

The blood cells produced during hematopoiesis are discerned into 2 lineages: the myeloid, and the lymphoid lineage (Nombela- Arrieta and Manz, 2017). Erythroid cells, granulocytes (neutrophils, mast cells, eosinophils, basophils), monocytes, plasmacytoid dendritic cells, and megakaryocytes constitute the myeloid lineage. On the contrary, lymphoid lineage contains T and B cells (Orfao et al., 2019). The hematopoietic stem cells (HSCs) produce all hematopoietic cells and are, thus, the core of hematopoiesis. Consequently, their role during disease development is detrimental, while they have also been therapeutically explored.

Aging and inflammation affect the metabolic properties of HSCs and deteriorate their capacity to generate blood cells of both lineages (de Haan and Lazare, 2018, Evans et al., 2020, Nagai et al., 2006, Rodriguez et al., 2009, Esplin et al., 2011, Regan-Komito et al., 2020, Mitroulis et al., 2018). Similarly, the accumulation of mutations, and epigenetic changes in HSCs, as well as the enhanced metabolic activity (Kurosawa and Iwama, 2020, Carroll and St. Clair, 2018) can eventually lead to the development of hematopoietic malignancies (Valent et al., 2019). Nevertheless, in addition to mediating disease development, HSCs have been therapeutically exploited.

The ablation of cancer cells by chemotherapy (Amjad et al., 2021) is a standard therapeutic approach in cases of hematological malignancies (Israels et al., 1969, Klener et al., 2019). However, to restore hematopoiesis and immune responses after the cell ablation, the transplantation of hematopoietic stem cells has been widely used in clinic (Thomas et al., 1957, Simpson and Dazzi, 2019). In the case of Multiple Myeloma or Hodgkin's lymphoma, HSCs are collected from the patients prior to chemotherapy (autologous transplantation). In other cases, like Acute Lymphocytic Leukemia, Acute Myeloid Leukemia, Chronic Myeloid Leukemia/Chronic Lymphocytic Leukemia, and some severe cases of Myelodysplastic Syndrome a distinct compatible HSC donor is required as the source of the HSC transplant (allogeneic transplantation) (Dessie et al., 2020, Khaddour et al., 2021). In addition to hematologic malignancies, novel studies pinpoint the potency of allogeneic transplantation as treatment for non-malignant diseases, like anemia (Khaddour et al., 2021), and autoimmune diseases, such as type 1 diabetes and lupus (Kondo et al., 2003). Hence, HSC mobilization is a process with many perspectives in clinical practice.

1.2. HSC biology

HSCs are characterized by two critical properties: self-renewal and multipotency (Haas et al., 2018, Laurenti and Göttgens, 2018, Seita and Weissman, 2010). Self-renewal is the ability of HSCs to proliferate, producing two stem cells that maintain these two properties. In this manner, the HSC pool expands (Kiel et al., 2007, Ito et al., 2016, Nakamura-Ishizu et al., 2014). At the same time, HSCs exhibit multipotency, as they can differentiate into hematopoietic cells of both the myeloid and the lymphoid lineage. Transcriptome analysis of human HSCs revealed that the differentiation of HSCs to specialized hematopoietic cells is a continuous process (Velten et al., 2017), during which lineage-biased progenitor cells are produced as intermediate cells (Velten et al., 2017, Notta et al., 2016) (Figure 1). Lineage bias and eventually lineage commitment of HSCs and progenitor cells is tightly regulated by transcription factors. More than 80 transcription factors orchestrate HSC differentiation (Göttgens, 2015), with the most important being the C/EBPa for the induction of the myeloid lineage (Zhang et al., 1997) and the PU.1, necessary to produce both myeloid and B cells (Yeamans et al., 2007). Therefore, both proliferation and differentiation of HSCs are orchestrating hematopoiesis.

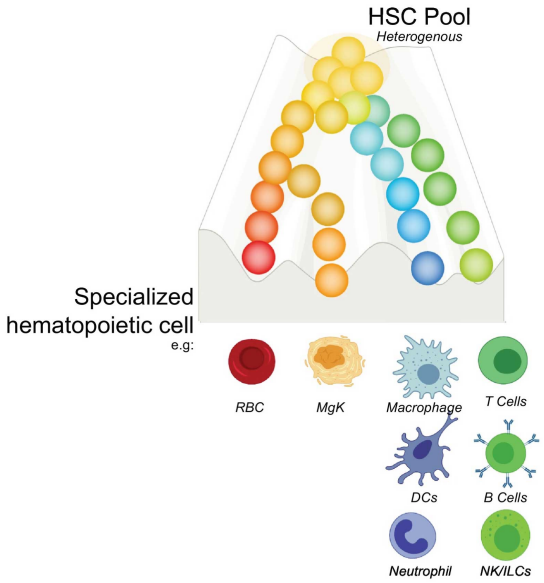

Figure 1 The hematopoiesis cloud.

A continuum model of bone marrow hematopoiesis. HSCs via multipotent and later committed progenitors, produce the differentiated hematopoietic cells.

DCs: Dendritic cells, RBC: red blood cells, MgK: megakaryocytes, NK: Natural killer cells, ILCs: innate-lymphocyte cells. Adapted from Rodrigues et al., 2021.

In order to preserve these properties and remain functional, HSCs acquire a dormant phenotype in steady state conditions. More specifically, tracking *in vivo* HSCs revealed a slow differentiation turnover to progenitor and differentiated cells of approximately 8 weeks (Säwen et al., 2018, Busch et al., 2015), and a low proliferative rate (Wilson et al., 2008, Fukushima et al., 2019). Wilson et al. reported that less than 2% of HSCs undergo proliferation at steady state, while this percentage increases in the progenitor populations, in which 20% of the cells are proliferating during unperturbed hematopoiesis (Wilson et al., 2008). On the contrary, a highly proliferative profile of HSCs has been correlated with defective response in case of emergency and enhanced cell apoptosis (Baba et al., 2016, Uckelmann et al., 2016). Interestingly, Bernitz et al., proposed that 4% of the murine HSCs remain dormant for a period of at least 2 years, as demonstrated using a doxycycline induced GFP system, which labels and, subsequently allows tracking of HSCs (Bernitz et al., 2016). This finding suggests that the HSC pool exhibits heterogeneity in the cell metabolic profile. In addition, according to the same study the number of dormant HSCs remained stable for a period of approximately a year, which implies the existence of a memory system that distinguishes the proliferative HSCs from the dormant cells (Bernitz et al., 2016).

One such factor defining the dormant and the proliferative HSCs is the mitochondrial activity. Mitochondria are cellular organelles surrounded by membrane where the cellular energy source, Adenosine Triphosphate (ATP), is produced. The presence of intracellular oxygen is necessary in this process, which is termed as oxidative phosphorylation (Deshpande and Mohiuddin, 2021). In

the absence of oxygen, ATP is produced in a less efficient way with the degradation of glucose (Semenza, 2007). HSCs exhibit attenuated metabolic activity compared to other hematopoietic cells in steady state conditions. They produce low levels of ATP (Simsek et al., 2010), but more importantly, HSCs exploit the anaerobic production of energy in contrast to differentiated hematopoietic cells (Simsek et al., 2010). Thus, they exhibit low mitochondrial activity in steady state (Almeida et al., 2017). Of note, a transcription factor induced in the absence of oxygen, the Hypoxia Inducible Factor 1 Subunit Alpha (HIF1a), is highly expressed in HSCs (Takubo et al., 2010), further supporting the existence of an anaerobic intracellular environment in these cells. On the contrary, when the cells exit dormancy and HSCs enter the metabolically active G1 or S/G2/M phases of their proliferating cycle, the production of energy on the mitochondrial membrane increases (Liang et al., 2020). However, even in the active HSCs, cellular mitochondrial respiration is tightly controlled. In this regard, mitophagy, the process of mitochondria degradation by autophagy, is enhanced in proliferating HSCs (Ito et al., 2016). Blockade of the mitophagy circle blocks HSC differentiation (Jin et al., 2019), revealing the significance of the mitochondrial activity for the HSC maintenance, and blood cell production.

One reason for the critical role of the mitochondrial activity in HSC maintenance is that the byproducts of this cycle negatively affect HSCs. Reactive Oxygen Species (ROS) are produced during the aerobic metabolism and accumulate intracellularly (Maryanovich et al., 2015). Their intracellular presence oxidizes proteins, and subsequently alters their function, while causing breaks to the DNA strands (Ray et al., 2012). As a result, ROS enhance the expression of the γH2AX histone, which is responsible for DNA repair, in active HSCs (Yahata et al., 2011). Furthermore, ROS affect functionally the HSCs, as ROS accumulation deteriorates the cells' engraftment potency (Yahata et al., 2011, Ito et al., 2006). In this regard, it has been proposed that ROS accumulation force HSCs to enhance their proliferation rate. As a result, HSCs lose their self-renewing capacity, which leads to cell exhaustion (Ito et al., 2006), and poor hematopoietic cell production. Similarly, in humans, accumulation of ROS in HSCs is correlated with low repopulating efficacy of HSCs (Bai et al., 2018), and *in vitro* production of less and smaller colonies (Rönn et al., 2017). Of note, the intracellular ROS content increases during the maturation of HSPC cells to differentiated blood cells (Cao et al., 2016), thus, suggesting that ROS may exhibit some functional role during differentiation. Hence, the metabolic profile of the HSCs mirrors the differentiation and proliferation potency of the stem cells, and it changes dynamically according to the conditions.

1.3.1. HSC modulation in the HSC niche

The factors that determine the HSC proliferation and differentiation compose the specialized HSC microenvironment, the HSC niche. A niche (Scofield, 1978, Scadden, 2012), is defined by specific factors that regulate the physical and biochemical features of the microenvironment. Any cell in a niche can dynamically change in numbers or metabolically (Scadden, 2006). Subsequently, in the HSC niche, HSCs sense paracrine factors and respond to them, at steady state and during

pathogenic conditions (Chavakis et al., 2019, Emmons et al., 2017). Thus, the characterization of the factors composing the HSC niche and the identification of their role in HSC maintenance are detrimental for the understanding of inflammatory disease progression and the development of novel therapeutic agents.

A great amount of work has been done to identify the factors regulating HSC biology within the BM niche. The significance of these cells and proteins is better understood when considering the recent computational data, which reveal an interdependency of the HSC metabolism and the niche cells. Depletion of the niche cells drives HSCs to exit quiescence, whereas loss of HSCs depletes the niche cells (Becker et al., 2019). A simplified model of the cells and factors composing the HSC niche is illustrated in Figure 2.

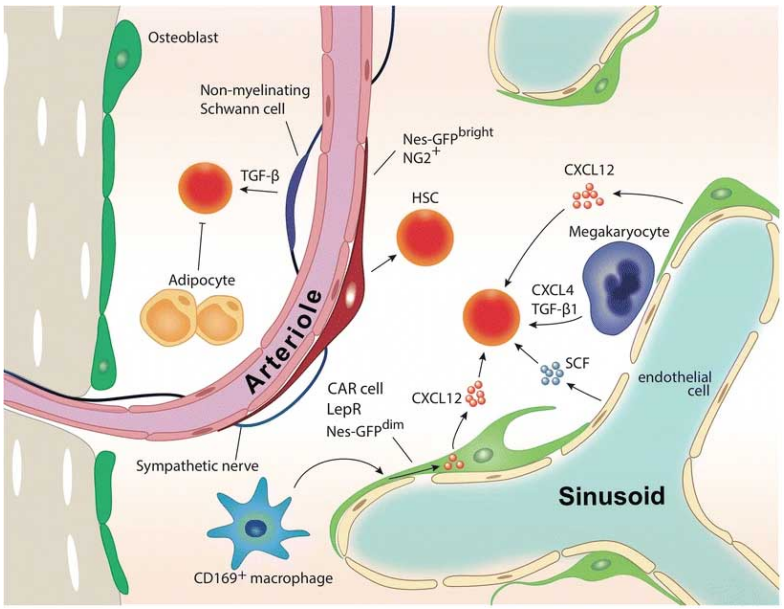

Figure 2 The BM niche.
Osteolineage and vascular cells compose the BM niche. *Nestin*$^{+}$, LEPR^{+} CAR cells express CXCL12 and SCF. Megakaryocytes regulate HSCs via CXCL4 and TGF-β1. Adipocytes and Non-myelinating Schwann cells further regulate HSCs via TGF-β.
CAR cells: CXCL12 abundant reticular cells; TGF-β: transforming growth factor β; SCF: stem cell factor.
Taken from Asada et al., 2017

As shown in Figure 2, two stromal cell types define the HSC niche in the long bones: the endosteal and the vascular cells. The major subsets that comprise the endosteal niche are the osteoblasts and the osteoclasts that line the inner surface of the bone (endosteum) (Frost, 1969, Rucci, 2008). Trapped between the endosteum and the outer surface (periosteum) are the osteocytes, mature cells deriving from osteoblasts (Holmbeck et al., 2005, Bonewald, 2011). Depletion of the osteocytes (Asada et al., 2013), or of the osteopontin, a protein that lines the inner bone surface (Nilsson et al., 2005), induces HSC and progenitor cell proliferation. Hence, endosteal cells are a

critical component of the BM niche for the regulation of Hematopoietic Stem and Progenitor Cell (HSPC) metabolism.

In contrast to the endosteal cells, a complex network of vessels, arterioles, and sinusoids (very small vessels) make up the vascular HSC niche (Coutu et al., 2017). Depletion of a small subset of $NG2^+$ cells that surrounds arterioles decreases BM cellularity (Kunisaki et al., 2013). In addition, Chen et al described *Apelin*$^+$ endothelial cells in proximity to HSCs. Depletion of the $Apelin^+$ ECs also reduces the number of HSCs in the BM (Chen et al., 2019). Accordingly, depletion of the extracellular protein Jagged-1, which is expressed in arterial and sinusoidal cells of the BM, reduces the number of HSCs and prevents HSC engraftment after transplantation (Poulos et al., 2013). Hence, it is evident that the BM vasculature is also detrimental for HSC maintenance.

In addition to cells of the endosteal and vascular lineage, several different cell types and their secretome have been described to be part of the HSC niche. Macrophages are essential for HSC retention in the BM (Winkler et al., 2010, Chow et al., 2011) and the regulation of cell mobilization (Christopher et al., 2011). Megakaryocytes are an important cell type of the HSC microenvironment, found in proximity to HSCs in murine BM (Bruns et al., 2014). Ablation of megakaryocytes results in loss of HSC quiescence (Bruns et al., 2014, Zhao et al., 2014). Dormancy is restored by injection of either CXCL4 (Bruns et al., 2014) or Transforming growth factor β1 (TGF-β1) (Zhao et al., 2014, Di Giandomenico et al., 2020), two factors produced by megakaryocytes. These findings suggest the major role of CXCL4 and TGFb in the regulation of HSC biology. Adipocytes are also essential for HSC regulation, as deletion of the adipose tissue decreased the number of BM HSC and promoted instead extramedullary hematopoiesis in spleen (Wilson et al., 2018). Finally, the BM niche is also subjected to nerve control. Denervation of the BM results in loss of BM cells and induces aberrant HSC proliferation (Yamazaki et al., 2011). In addition, adrenergic neurons of the sympathetic nervous system are essential for HSC mobilization (Katayama et al., 2006, Méndez-Ferrer et al., 2008), whereas recently sensory, nociceptive neurons were also identified in proximity to HSCs (Gao et al., 2021).

However, the most interesting cell population comprising the HSC niche is the CXCL12 Abundant Reticular (CAR) cells. CAR cells are found around endothelial cells of the vasculature and are, thus, described as pericytes. They exhibit multipotency, as they differentiate into both adipocytes, as well as endosteal cells, and have similar antigenic profile to Mesenchymal Stem Cells (MSC) (Zhou et al., 2014). In addition to producing CXCL12 they are also characterized by the expression of PDGFRβ (Gomariz et al., 2018, Adapala et al., 2019), CD73 (Breitbach et al., 2018) and LEPR. Of note, LEPR expression marks pericytes on BM sinusoids, but not in arterioles (Zhou et al., 2014, Ramalingam et al., 2017), suggesting that CAR cells are perisinusoidal cells. Finally, another proposed marker for CAR cells is Nestin. $Nestin^+$ cells are perivascular, multipotent and when depleted HSC maintenance is disrupted (Mendez-Ferrer et al., 2010). Recently, a multipotent cell population expressing LEPR (Aoki et al., 2021), as well as CD271 and the Stage-Specific Embryonic Antigen (Matsuoka et al., 2015) has been identified in humans, revealing the presence of a similar CAR cell population, and, hence, common regulatory networks in the BM of the two systems.

For these reasons, the proteome of CAR cells has been extensively studied. CAR cells express the glycoprotein Developmental endothelial locus (Del) 1, which is essential for HSC differentiation towards the myeloid lineage (Mitroullis et al., 2017). Additionally, *Lepr*$^{+}$ CAR cells express the stem cells factor (SCF), (Zhou et al., 2014), the ligand of the c-kit receptor that is broadly expressed to all HSPC (Ogawa et al., 1991, Ikuta and Weissman, 1992). SCF is an essential HSC cytokine, as deletion of the SCF, is lethal in mice at embryonic stage. SCF$^{-/-}$ embryos displayed reduced primitive hematopoietic cells in the fetal liver (Ding et al., 2012), whereas in adults, deletion of the SCF under the *LepR* promoter disrupted HSC maintenance (Comazzetto et al., 2019) and induced HSC mobilization (Ding et al., 2012), revealing a role of the cytokine in HSC production, as well as cell retention within the BM. Nevertheless, as the name suggests, the major component of the CAR cells' secretome is the chemokine CXCL12.

1.3.2. The role of the CXCL12/CXCR4 axis in hematopoiesis

Chemokines are chemical molecules that induce the movement. The human chemokine system consists of 48 chemokines binding to 23 receptors (Zlotnik and Yoshie, 2012). Figure 3 illustrates an overview of the human chemokine system. It can be appreciated that the chemokine/chemokine receptor interaction is characterized by ligand, and receptor bias. In other words, despite many chemokine receptors interact with multiple chemokines, each chemokine favors a specific activation pathway to the receptor, acting either as agonist or antagonist. At the same time, the chemokine binding to different receptors results in the activation of alternative pathways (Steen et al., 2014), enhancing the complexity of the chemokine system.

All chemokines share structural features, as they are organized into a N terminal loop and a subsequent β-sheet (the core of the chemokine) that leads to an α-helix at the C terminus (Miller and Mayo, 2017). Accordingly, the structure of the human CXCL12 is illustrated in Figure 4. The N residues of CXCL12 are detrimental for in the initial binding to the N terminal of the receptor (Janssens et al., 2018). Subsequent interaction with the core of the receptor, eventually, triggers the signaling cascade (Crump et al., 1997). Due to the significant functional role of the N terminus, the region is characterized by 4 highly conserved cysteine residues. The positioning of the first 2 cysteines (C) categorizes the chemokines into 4 groups: the CC, when the two cysteines are sequential, the CXC, when an amino acid intervenes between the two cysteines, the CX3C, when three amino acids are found between the cysteines, and the XC chemokines, with only one conserved cysteine (Zlotnik and Yoshie, 2012).

In addition to their structure, the biological relevance of the chemokines classifies them as homeostatic, inflammatory or both (Zlotnik and Yoshie, 2012, Hughes and Nibbs, 2018). The major difference between the homeostatic and the inflammatory chemokines, is that homeostatic chemokines are constitutively expressed in tissues, whereas the inflammatory chemokines are expressed only after cell stimulation (Zlotnik et al., 2006). Of note, homeostatic chemokines are vital during organogenesis by regulating cell trafficking. Table 1 lists the

homeostatic chemokines, which together with the respective receptors regulate tissue organization. As shown in Table 1, CXCL12 is directing the homing of alveolar stromal cells, but more importantly it is necessary for the leukocyte homing in brain and the bone marrow (Chen et al., 2018).

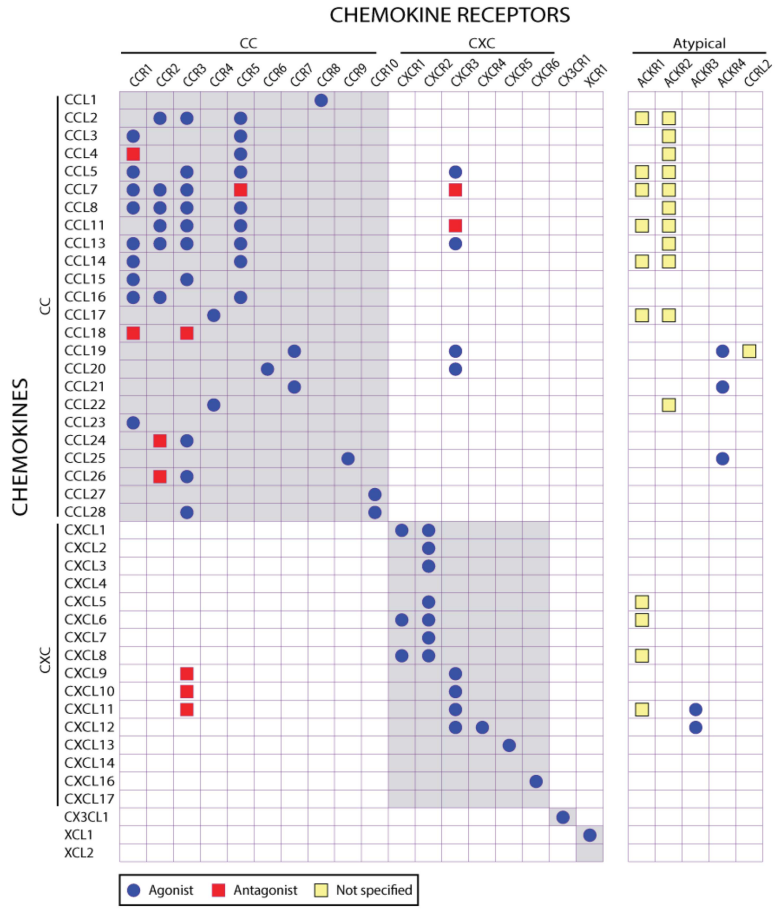

Figure 3 The human chemokine system.
Chemokines are classified based on the response they mediate in the receptors, as Agonists, Antagonists, or not specified.
Adapted from Stone et al., 2017.

In fact, the discovery of CXCL12 was groundbreaking for the HSC research and the chemokine field. In 1996, CXCL12 was described as the ligand for the chemokine receptor that is now known as CXCR4 and is found on leukocytes (Oberlin et al., 1996). Later the same year, a knockout (ko) mouse model was developed for the ligand. Strikingly, the deletion of CXCL12 was lethal in mice, as *Cxcl12*$^{-/-}$ mice died perinatally at day 15.5. Thus, CXCL12 was the first chemokine found to be

vital for development (Nagasawa et al., 1996). As a result, 3 independent groups generated mice, in which the gene for the described receptor, the *Cxcr4* gene, was deleted to further investigate the axis. Similarly to *Cxcl12*$^{-/-}$, only 30% of the *Cxcr4*$^{-/-}$ mice were viable (Zou et al., 1998, Ma et al., 1998, Tachibana et al., 1998), revealing the CXCL12/CXCR4 axis and demonstrating its critical role in organogenesis.

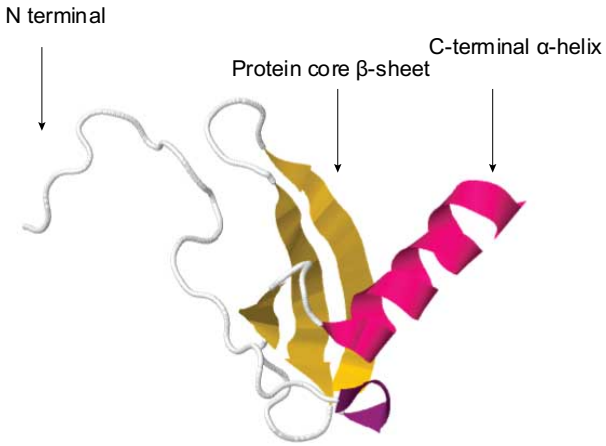

Figure 4 Secondary structure of the human CXCL12.
CXCL12 is composed by a C-terminal α-helix (pink), a three stranded β-sheet (yellow) that compose the core of the protein structure, a hinge (purple), and a flexible N terminal.
Accessed in PDB, code 2KEE, Veldkamp et al., 2009, doi: 10.2210/pdb2KEE/pdb

Table 1 Homeostatic chemokines and their receptors are involved in tissue organization.
Adapted by Chen et al., 2018.

Location	***Chemokines***	***Receptors***	***Function***
Skin	CCL27	CCR10	Skin homing of T cells
Brain	CXCL12	CXCR4	Brain homing of leukocytes
Lung	CXCL12	CXCR4	Stromal cell homing
Spleen	CCL19, CCL21, CXCL13	CCR7, CXCR5	T cell, B cell and DC homing
Small intestine	CCL25	CCR9	Lymphocyte homing
Secondary lymphoid tissues	CCL21, CCL19, CCL13	CCR7, CXCR5	T cell, B cell and DC homing
Bone marrow	CXCL12	CXCR4	Neutrophil retention in BM

DC: dendritic cell.

One major tissue defect in both *Cxcl12*$^{-/-}$ (Nagasawa et al., 1996), and *Cxcr4*$^{-/-}$ mice (Zou et al., 1998), was the abnormal formation of the heart ventricles. Nevertheless, in addition to the major role of CXCR4/CXCL12 in heart development, these two factors are also essential for BM development. More specifically, both *Cxcl12*$^{-/-}$ (Nagasawa et al., 1996) and *Cxcr4*$^{-/-}$ mice were characterized by inefficient BM colonization (Zou et al., 1998, Ma et al., 1998). Moreover, in *Cxcr4*$^{-/-}$ mice, aberrant B cell and neutrophil progenitors were present in the periphery (Ma et al., 1999), suggesting that CXCR4 is detrimental for the retention of the progenitors within the BM. However, to further elucidate the mechanisms involved it was necessary to overcome the model lethality and, consequently, inducible *Cxcr4*$^{-/-}$ and *Cxcl12*$^{-/-}$ mouse models were developed, in which the researchers inactivate the targeted genes in a spatial and temporal controlled manner.

In accordance with the data in total ko mice, induction of CXCR4 depletion in adult mice significantly reduces the number of BM cells. Simultaneously, the remaining BM HSCs exhibit a highly proliferative profile (Sugiyama et al., 2006). In contrast to CXCR4 deletion, aberrant CXCR4 signaling is also deleterious for hematopoiesis. More specifically, the familial Warts, Hypogammaglobulinemia, Infections, and Myelokathexis (WHIM) syndrome is caused by mutations in the *Cxcr4* locus that result in the production of a truncated in the C terminus protein (Tassone et al., 2009). The mutation abrogates CXCR4 internalization and, thus, the desensitization after the stimulation. As a result, the CXCR4 receptor is constantly active (Tassone et al., 2009, McDermott et al., 2011, McDermott et al., 2015). WHIM mice, that contains such mutation in CXCR4, exhibit reduced number of circulating cells and increased BM cell counts (Freitas et al., 2017). Interestingly, blockade of CXCR4 reverses the WHIM associated leukopenia in mice (Balabanian et al., 2012), further demonstrating the key role of CXCR4 in the regulation of BM cell retention and circulation egress.

However, contradicting results have been reported in inducible CXCL12$^{-/-}$ mouse models regarding the role of the ligand in BM cell retention. Tzeng et al., reported that deletion of CXCL12 in all cells of adult mice mobilizes HSPC cells to the circulation, while enhancing the proliferative status of BM HSC. Of note, no reduction in the total BM cellularity was observed (Tzeng et al., 2011), as it would be expected due to the leukocyte blood egress. On the contrary, inducible CXCL12$^{-/-}$ mice that were developed by Ding and Morrison did not exhibit HSPC mobilization in the periphery. In fact, the number of circulating cells was decreased approximately by half (Ding and Morrison, 2013), which would rather suggest a role in HSC differentiation and blood cell production. The contradicting results in these two mouse models, in which CXCL12 was ubiquitously deleted in all cells, reveal the significance of identifying and specifically targeting the CXCL12 producing cells in the BM.

1.3.3. The source of CXCL12 within the HSC niche

Cxcl12 gene produces 6 different protein isoforms in humans and 3 in mice, denoted with the Greek letters: α, β, γ, δ, ε, and ϕ for humans, and respectively α, β, and γ for mice (Janssens et al., 2018). Interestingly, in murine BM only the isoforms CXCL12α and CXCL12β have been detected at mRNA level (Torres and Ramirez, 2009). In addition to the CAR cells (Zhou et al., 2014), other BM stromal cells have also been attributed with CXCL12 expression. In this regard, the expression of CXCL12 in osteoblasts has been confirmed in mRNA and protein level (Ponomaryov et al., 2000, Katayama, et al., 2006), as well as in reporter mice (Ding and Morrison, 2013). Of note, apart from the osteoblasts, also *Osterix*$^{+}$ (*Osx*) osteoblast progenitor cells express CXCL12 (Greenbaum et al., 2013). It can be, thus, concluded that multiple cell types express CXCL12 within the BM.

The different sources of BM CXCL12 led to the development of multiple hypotheses for the exact location of the HSCs within the BM and a debate between the supporters of the endosteal versus the vascular niche. Despite the early evidence on the role of the endosteal cells in HSPC maintenance (Asada et al., 2013, Nilsson et al., 2005, Driessen et al., 2003), it is now widely accepted that HSCs reside mainly in a perivascular niche. This hypothesis is supported by immunofluorescence data on BM sections (Kunisaki et al., 2013), as well as *in vivo* tracking of fluorescently labeled HSCs (Acar et al., 2015), and live cell imaging data (Christodoulou et al., 2020). However, to identify the sole cell type responsible for HSC retention, several mouse models targeting CXCL12 and SCF have been developed. An elaborate list of these mouse models, and the phenotype observed is presented in Figure 5. In accordance with the phenotype described by Tzeng et al., (Tzeng et al., 2011), CXCL12 deletion in *Lepr*$^{+}$ pericytes and *Ng2*$^{+}$ endothelial cells result in HSC mobilization (Szade et al., 2017). In addition to the models of Figure 5, deletion of CXCL12 in Osterix^{+} cells (Greenbaum et al., 2013), but not in mature osteoblasts (Ding and Morrison, 2013, Greenbaum et al., 2013) mobilizes HSPC to the circulation. These data suggest that CXCL12 secretion by multiple cell types regulates HSC retention in the BM, although an overlap in the cells expressing *Lepr* and *Osterix* should not be excluded, due to the expression of *Osterix* in multipotent stromal cells in the vascular region of the BM (Greenbaum et al., 2013).

However, a great amount of data challenges the idea of the static HSC niche altogether. First, sinusoids are evenly distributed within the BM (Kunisaki et al., 2013). In this regard, perivascular HSC are at the same time located within 50μm from the endosteum in the human BM (Bourke et al., 2009), disclosing a complex microenvironment and overlap between the niches. In addition, recent evidence suggest that CAR cells align to the extracellular collagen in the BM matrix (Gomariz et al., 2018) and are, thus, distributed within the BM. Finally, in addition to the cells expressing CXCL12, the extracellular matrix also regulates the protein properties.

	Bone marrow location			Observed phenotype			
				Cxcl12 deletion		Scf deletion	
	Sinusoid	Arteriole	Endosteum	Bone marrow HSC	Peripheral blood HSC	Bone marrow HSC	Peripheral blood HSC
Lepr-Cre	✓	✓	X	↔	↑	↓	↔
NG2-Cre	✓	✓	X	↓	↑	↓	↔
NG2-Cre^{ERTM} 2-week induction	X	✓	X	↓	↔	↔	↔
NG2-Cre^{ERTM} 6-week induction	X	✓	X	↔	↔	↔	↔
Myh11-Cre^{ERT2}	X	✓	X	↓	↔	N/A	N/A
Vav1-Cre	N/A	N/A	X	↔	↔	↔	↔
Col2.3-Cre	N/A	N/A	✓	↔	↔	↔	↔
Nes-Cre	N/A	N/A	N/A	↔	↔	↔	↔
Nes-CreER	N/A	N/A	N/A	↔	↔	↔	↔
Tie2-CreER	✓	✓	X	↓	N/A	↓	N/A
Sp7-Cre	N/A	N/A	✓	↔	↔	N/A	N/A
Prx1-Cre	N/A	N/A	N/A	↓	N/A	N/A	N/A
Oc-1-Cre	N/A	N/A	✓	↔	↔	N/A	N/A

Figure 5 Mouse models developed for targeting CXCL12 and SCF in the HSC niche.
Transgenic mouse models target the expression of CXCL12 and SCF in BM sinusoids, arterioles, or endosteum. The observed effect in HSPC retention and mobilization is noted when assessed.
Adapted from Szade et al., 2017

The binding of chemokines on sugar molecules, the glycosaminoglycans (GAGs) is a significant step in chemokine-induced cell migration (Rot, 2010, Hughes and Nibbs, 2018). Chemokines constantly associate and disassociate with GAGs at the site of their production. This association and disassociation of the chemokines on the extracellular matrix creates a local chemokine gradient. Non-immobilized chemokines interact with the chemokine receptors on proximal leukocytes (Graham et al., 2019) in a 1:1 stoichiometry (Kufavera et al., 2014) and subsequently direct cell migration (Rot, 2010, Hughes and Nibbs, 2018). CXCL12 interaction with GAGs, stabilizes the chemokine, and, thus, determines the half-life of the chemokine (O'Boyle et al., 2009), as well as its chemotactic properties (Connell et al., 2016). Imaging data of the CXCL12 protein distribution within the BM suggest that CXCL12 concentration is rather equally dispersed within the BM, with some hot spots close to the endosteum (Kunz and Schroeder, 2019). Thus, CXCL12 expression and its interactions within the BM are complex, and detrimental for HSC maintenance.

1.3.4. The role of the CXCL12/CXCR4 axis on Hematopoietic Stem and Progenitor Cell retention

Despite the advances in the characterization of the CXCL12 expressing cells in the BM, the mechanism that retains HSCs has not been fully elucidated (Panch et al., 2017). Two main theories have been proposed to explain HSC retention in the BM. In the first one, the relative difference in CXCL12 concentration between the BM and the circulation determines hematopoietic cell egress. According to the second hypothesis, Hematopoietic Stem and Progenitor Cells (HSPCs) anchor on extracellular CXCL12 via CXCR4 (Hopman and DiPersio, 2014).

The data originating from the total *Cxcl12*$^{-/-}$ (Nagasawa et al., 1996) and *Cxcr4*$^{-/-}$ mice (Ma et al., 1999) suggest that the direct binding of CXCL12 on CXCR4 is necessary for HSPC retention. Accordingly, the CXCR4 antagonist AMD3100 is a clinically used agent for HSPC mobilization. AMD3100 is a bicyclam originally identified for abrogating HIV entry in T cells by antagonizing for CXCR4 binding (Donzella et al., 1998, De Clercq, 2003). However, during the clinical studies as a potent HIV inhibitor, the recipients exhibited a drastic increase of circulating white blood cells 6 hours after AMD3100 administration (Hendrix et al., 2000). The impact of this finding was huge, since AMD3100 was rejected as an HIV drug, but was approved in clinical practice as a mobilizing agent. Currently, it is used in clinic together with another mobilizing agent, the cytokine G-CSF, for poor responders to G-CSF alone. In addition, AMD3100 has been tested in clinical trials in the WHIM syndrome patients, where it is expected to reverse the leukopenia observed, by abrogating the CXCR4 signaling. AMD3100 was also tested in clinical trials to treat thalassemia, a disorder characterized by defective tissue oxygenation by the erythrocytes (Miao et al., 2020). In mice, mobilization through AMD3100 leads to a profound increase of circulating HSPC within 1 hour (Winkler et al., 2012), whereas a synergistic effect with G-CSF administration was also observed (Broxmeyer et al., 2005), similarly to the effect observed in humans.

Furthermore, adhesion molecules have been postulated to act synergistically with CXCR4 for the anchoring of HSPC within the BM. On the cell membrane there are specialized lipid formations so-called lipid rafts. CXCR4 has been postulated to be part of the lipid rafts, together with other transmembrane proteins. As a result, these rigid lipid formations enable the interaction of the proximal proteins (Hermetet et al., 2019, Ratajczak and Adamiak, 2015, Capitano et al., 2015). In this manner, the interaction of CXCR4 with a family of transmembrane retention molecules, the integrins, is facilitated. It has been, thus, hypothesized that CXCR4 activation induces the subsequent activation of the integrins, and, finally, retains the leukocytes (Donzella et al., 1998). In this regard, inhibition of the VLA4 (α4β1) integrin complex together with the CXCR4 blockade, by AMD3100, enhances HSPC mobilization (Ramirez et al., 2009). In addition to integrins, the transactivation of the c-kit receptor after CXCR4 stimulation also suggests an interplay between the two receptors (Cheng et al., 2010). These observations demonstrate that HSPC retention may involve multiple molecules, rather than solely one receptor and its ligand.

Intriguingly, the administration of AMD3100 also affects the concentration of CXCL12 as the levels of the chemokine in the BM decreases and the concentration of CXCL12 in circulation increases

(Redpath et al., 2017, Jørgensen et al., 2021, Dar et al., 2011). Thus, the existence of a CXCl12 gradient between the BM and the circulation has been proposed to regulate HSC retention and mobilization. The observation that BM stromal cells translocate CXCL12 from circulation to the BM, in a CXCR4-dependent way (Dar et al., 2005), resulted in the formation of the hypothesis that the release of CXCL12 from the BM to the circulation is necessary for the AMD3100-mediated HSPC mobilization (Dar et al., 2011). In accordance with this, injection of recombinant CXCL12 induced the release of HSPC after 1 hour (Dar et al., 2011), whereas, on the contrary, inactivation of CXCL12 with a specific antibody abrogated the mobilization (Redpath et al., 2017). The hypothesis was further strengthened by the fact that the mobilizing agent G-CSF also affects BM CXCL12 levels. However, in contrast to AMD3100, G-CSF has been shown to decrease *Cxcl12* expression in bone marrow cells (Day et al., 2015) and osteoblasts (Christopher et al., 2009). In addition, the concentration of circulating CXCL12 increases in human G-CSF recipients 5 days after its administration (Gębura et al., 2019), further strengthening the hypothesis regarding the involvement of the CXCL12 gradient in hematopoietic cell mobilization. Nevertheless, the identification of an alternate CXCR4 antagonist that mobilize HSPC without affecting the concentration of CXCL12 (Redpath et al., 2017) and the evidence that AMD3100 acts as a partial agonist to CXCR4, rather than an inhibitor (Jørgensen et al., 2021), demonstrate that the exact mechanism of HSPC retention in BM remains elusive.

1.4.1. Balancing the axis- the ACKR3 receptor

To fully elucidate the mechanisms involved in the regulation of systemic CXCL12 it is necessary to assess all chemokine interactions and the signaling pathways involved. Chemokine receptors, like CXCR4, span in 7 transmembrane regions, while being coupled to a G protein. In this manner, the binding of CXCL12 in the extracellular region of CXCR4 induces conformational changes in the helixes III, V, VI and VII that activate an intracellular G protein (Wescott et al., 2016, Kufareva et al., 2017). The G proteins are trimeric proteins, with each subunit labeled with a greek letter α, β, and γ. The activation of the receptor mediates the exchange of the Guanosine-5'-diphosphate (GDP) molecule to a high energy-molecule of Guanosine-5'-triphosphate (GTP). The GTP provides the required energy for the release of one subunit (Gα) from the G protein, which consequently, activates downstream pathways (Hilger et al., 2018). In addition to the Gα-mediated signaling, G protein coupled chemokine receptors activate downstream pathways also via the Gβγ subunits (Thelen, 2001).

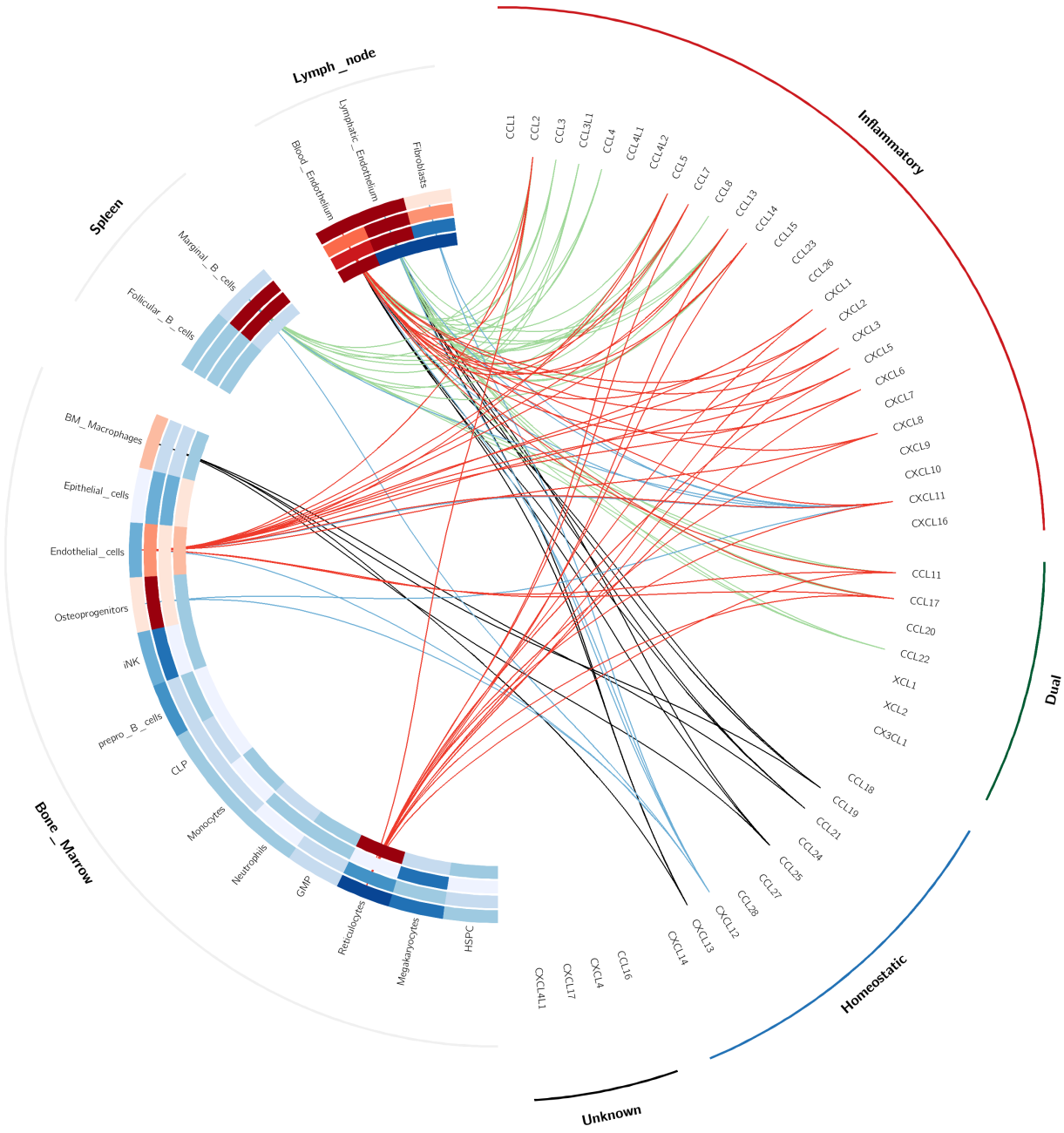

Figure 6 The murine atypical chemokine receptors.
The murine chemokines are classified based on their biological relevance (inflammatory, homeostatic, dual, unknown). The expression of the 4 atypical chemokine receptors (starting from inside: ACKR1, ACKR2, ACKR3, ACKR4) in lymph node, spleen and bone marrow is plotted in a heatmap. The binding of each receptor to chemokines is illustrated with the colored ribbons (ACKR1: RED, ACKR2: GREEN, ACKR3: BLUE, ACKR4: BLACK).

However, in contrast to CXCR4 and the G-protein coupled chemokine receptors described above, four chemokine receptors carry a mutation in the 2nd intracellular loop that prevents the activation of a G-protein after stimulation. Due to this attribute, these receptors are termed as

atypical chemokine receptors (ACKRs) (Zlotnik and Yoshie,2012, Bachelerie et al., 2014). Figure 6 illustrates the expression of the 4 murine ACKRs (ACKR1, ACKR2, ACKR3, ACKR4) in BM, spleen, and lymph nodes, based on RNAseq data (gexc.rinken.jp). The ribbons on the figure demonstrate the receptors interactome, according to the literature (Bonecchi et al., 2004, Zarbock et al., 2007, Szabo et al., 1995, Kashiwazaki et al., 2003, Jamieson et al., 2005, Hansell et al., 2011, Gosling et al., 2000, Gardner et al., 2004, Fukuma et al., 2003). It can be, hence, noted the strong expression of all ACKRs in stromal cell populations in BM and lymph nodes. All receptors are expressed on endothelial cells, whereas, based on the data set, *Ackr3* is additionally present on BM osteoprogenitor cells and fibroblasts. Another characteristic is that, except for ACKR3 the other 3 receptors exhibit a broad spectrum of chemokine binding. Of note, ACKR1 and ACKR2 interact only with inflammatory chemokines, which suggests a role for both receptors during inflammatory responses.

The expression of ACKRs on stromal cells, the multiple binding partners that characterize these receptors, together with the alternative downstream pathways, compared to the G-protein coupled receptors, characterize ACKRs and define their importance in the hematopoietic system. ACKRs possess the ability to bind and internalize chemokines (Stone et al., 2017, Graham et al., 2012). Chemokine internalization subsequently leads to the subcellular chemokine transfer in the case of ACKR1, or the chemokine degradation in the case of ACKR2, 3, and 4. Despite the differences in the mechanisms involved, ACKRs regulate the local chemokine concentration, consequently, determining the availability of chemokines for the hematopoietic cells (Vacchini et al., 2016). Finally, ACKR3 signal through β-arrestin dependent pathways (Stone et al., 2017, Graham et al., 2012). There are two β-arrestins, the β-arrestin 1 and 2, and in contrast to the trimeric G proteins, they are monomeric structures, characterized by two β-sheet domains (Hilger et al., 2018). β-Arrestins mediate receptor internalization after stimulation (Galliera et al., 2004), via the formation of intracellular vesicles (Laporte et al., 2002, Goodman et al., 1996). The intracellular transfer of the receptor terminates the signaling cascade that was initiated after the chemokine binding. However, the interaction of a receptor with a β-arrestin is not silent, as β-arrestins initiate kinase cascades that, finally, result in changes in gene expression (DeWire et al., 2007). In summary, by regulating the availability of chemokines in the microenvironment, and by stimulating β-arresting signaling cascades, ACKRs alter the microenvironment and regulate indirectly hematopoietic cells.

The atypical chemokine receptor that interferes with CXCR4/CXCL12 axis is the atypical chemokine receptor 3 (ACKR3). The receptor, initially cloned in dog thyroid cells, was named Receptor Dog cDNA1 (RDC1) and was initially characterized as a G protein, based on its sequence and the similarities observed with known GPCRs (Libert et al., 1990). Interestingly, the first ligand described for RDC1 was the vasoactive intestinal peptide (VIP) (Sreedharan et al., 1991), a hypothesis that was corrected 2 years later, after the identification of the human VIP receptor (HVR) (Sreedharan et al., 1993). The observation that murine $CXCR4^{-/-}$ liver cells could still bind to CXCL12 led Burns et al., to search for an additional CXCL12 receptor and to finally identify ACKR3. In addition to CXCL12, ACKR3 binds with lower affinity to the inflammatory chemokine CXCL11 (Burns et al., 2006). Moreover, similarly to $CXCR4^{-/-}$ and $CXCL12^{-/-}$ mice, $ACKR3^{-/-}$ mice exhibit

enhanced mortality, due to cardiac malformation (Yu et al., 2011, Gerrits et al., 2008, Sierro et al., 2007). Interestingly, CXCR4 and ACKR3 share additionally another ligand. The cytokine macrophage Migration Inhibitory Factor (MIF) binds to the heterodimer of CXCR4 and the transmembrane protein CD74 inducing murine B cell migration (Schwartz et al., 2009; Klasen et al., 2014). In addition, MIF interacts also with ACKR3, as the cytokine blocks CXCL11 binding to ACKR3 expressing cells (Alampour-Rajabi et al., 2015). The shared binding pattern between MIF and CXCL12 stage MIF as a factor in the CXCR4/ACKR3/CXCL12 axis. However, in contrast to $CXCR4^{-/-}$, $CXCL12^{-/-}$ and $ACKR3^{-/-}$ mice, $MIF^{-/-}$ mice are viable (Harper et al., 2010), and, hence, the cytokine could be considered as a supplementary element of the CXCR4/CXCL12/ACKR3 axis.

The structural differences between CXCR4 and ACKR3 orchestrate alternative downstream pathways after the receptor activation. The activation of the G protein downstream of CXCR4 leads to the disassociation of the Gα subunit and the activation of the c-Jun, and NF-kB transcription factors, or the mTORC2 pathway (Kawaguchi et al., 2019). On the contrary, as discussed above, ACKR3 does not signal through a G-protein (Zlotnik and Yoshie, 2012, Burns et al., 2006, Canals et al., 2012, Levoye et al., 2009), but rather via β-arrestin 2 (Zabel et al., 2009, Rajagopal et al., 2010, Min et al., 2020), which subsequently activates the Extracellular signal Regulated Kinases (ERK) pathway (Rajagopal et al., 2010). In addition to the differential downstream pathways, both receptors are subject to regulatory mechanisms. In this regard, a family of kinases, the G protein-coupled receptor kinases (GRK), differentially phosphorylates the serine/threonine residues in both CXCR4 and ACKR3, consequently regulating the receptor activity. CXCR4 can be phosphorylated by the GRK2, 3, and 6, whereas ACKR3 is only phosphorylated by GRK2. These phoshorylations regulate the activation of the receptors and their deregulation is correlated with disease pathogenesis (Fumagalli et al., 2019). In addition, binding dynamics are different between the receptors, as the ACKR3/CXCL12 interaction is characterized by a slow dissociative rate (Gustavsson et al., 2019), while, finally, ACKR3 has been shown to internalize and scavenge the bound chemokine (Zabel et al., 2009, Canals et al., 2012), regulating in this way the chemokine availability.

Based on these features, different hypotheses have been proposed for the role of ACKR3 in the CXCR4/CXCL12 axis (Figure 7). The first hypothesis (Figure 7A) claims the direct activation of ACKR3 upon CXCL12 binding via the β-arrestin 2 (Zabel et al., 2009, Rajagopal et al., 2010, Min et al., 2020). Accordingly, early studies on ACKR3 underlined a key role for the receptor in cell survival (Burns et al., 2006) and migration (Balabanian et al., 2005, Zabel et al., 2009). Another proposed mechanism is the regulation of the CXCR4/CXCL12 signaling through the formation of CXCR4/ACKR3 heterodimers (Figure 7B). Cells expressing both receptors form both homo- and heterodimers (Lipfert et al., 2013, Décaillot et al., 2011, Gao et al., 2020). The formation of ACKR3/CXCR4 heterodimers abrogated the CXCR4-mediated response after CXCL12 stimulation (Décaillot et al., 2011, Levoye et al., 2009). Finally, the last hypothesis supports that ACKR3 controls CXCL12 availability for the alternative binding partner, the receptor CXCR4 (Figure 7C). Pharmacological inhibition of ACKR3 in healthy human volunteers using the antagonist ACT-1004-1239 induced a transient increase in circulating CXCL12 concentration (Huynh et al., 2021). Similarly, despite the perinatal lethality described before (Berahovich et al., 2010), Berahovich et

al claim that the surviving *Ackr3*$^{-/-}$ mice exhibit 5 times higher concentration of circulating CXCL12 (Berahovich et al., 2014). In addition, the deletion of ACKR3 resulted in enhanced CXCR4 activation in murine brain cells (Abe et al., 2014). Finally, it is possible that ACKR3 scavenging properties mediate local effects in CXCL12 concentration, enabling the formation of a local chemokine gradient. The best characterized *in vivo* model for the CXCL12 gradient is the chemotaxis of the primordial germ cells in zebrafish. The zebrafish primordial germ cells migrate where gametes will eventually form. This migration depends on the CXCL12-mediated CXCR4 stimulation (Lau et al., 2020). ACKR3 deletion on somatic cells of the zebrafish abrogated the primordial cell migration, whereas ectopic injection of the ACKR3 transcript altered the migration pattern (Boldajipour et al., 2008). *In vitro*, Torisawa et al., developed a system to assess gradient formation with HEK293 cells overexpressing either CXCL12 or the chemokine receptors CXCR4 and ACKR3. The system revealed that CXCR4 cells migrate towards CXCL12 only when in proximity to ACKR3 expressing cells (Torisawa et al., 2010), revealing the importance of ACKR3 in the formation of the gradient. To my knowledge, these hypotheses on the mechanisms by which ACKR3 regulates the CXCR4/CXCL12 axis have not been so far assessed within the BM niche.

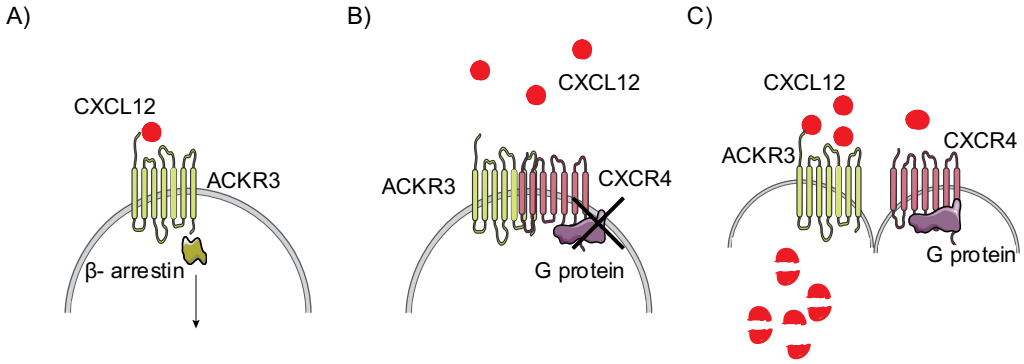

Figure 7 Models of ACKR3/CXCR4/CXCL12 axis.
A) ACKR3 signals through the β-arrestin pathway after binding of CXCL12. B) In cells that co-express ACKR3 and CXCR4, the formation of a heterodimer abrogates the G-protein mediated signaling of CXCR4. C) ACKR3 degrades CXCL12, decreasing the availability of CXCL12 in the local microenvironment.

1.4.2. ACKR3 in hematopoiesis

ACKR3 is broadly expressed in human and murine tissues. In humans, ACKR3 has been detected in liver, placenta, and spleen, at both mRNA, and protein level. In addition, using a CXCL12 binding assay it was demonstrated that human umbilical vein endothelial cell (HUVEC) line express ACKR3 (Berahovich et al., 2014). In mice, *Ackr3* is expressed in the murine brain (Schönemeier et al., 2008, Banisadr et al., 2016), while both the mRNA and the protein are also present in kidney, heart, and spleen (Heesen et al., 1998, Berahovich et al., 2014). In addition, two reporter mouse models have been developed to assess ACKR3 expression (Gerrits et al., 2008, Banisadr et al., 2016). The insertion of the lacZ gene under the *Ackr3* reporter revealed the expression of ACKR3

in the endosteal region of long bones (Gerrits et al., 2008). Similarly, the generation of a GFP knock in model demonstrated that the receptor is also present in the cranial vasculature (Cruz-Orengo et al., 2011), thus, confirming the expression of ACKR3 on stromal cells.

Nevertheless, the expression of ACKR3 on hematopoietic cells remains controversial (Infantino et al., 2006, Humpert et al., 2012, Humpert et al., 2014, Torossian et al., 2014, Tarnowski et al., 2010). *Ackr3* mRNA is not detected in human hematopoietic cells (Berahovich et al., 2010). Berahovich et al., reported the expression of ACKR3 only in murine primitive erythroid cells (Berahovich et al., 2010). Interestingly, the role of the receptor on BM hematopoiesis and HSC biology remains unknown. On the contrary, flow cytometric analysis of *Ackr3*^{GFP} reporter mice revealed a small population of splenic B cells expressing ACKR3, which was not present in lymph nodes (Cruz-Orengo et al., 2011). Radice et al., identified these ACKR3^{+} cells as splenic marginal zone B cells. ACKR3 has a functional role in spleen organization and the establishment of immune responses, as the deletion of the receptor abrogated the formation of a marginal zone in spleen in mice (Radice et al., 2020). Hence, despite being expressed in a small B cell subset, ACKR3 possesses a regulatory role in the splenic microenvironment. However, the expression of the receptor in HSPC and the role of ACKR3 in HSPC maintenance and retention remain undetermined.

2. Aims of the study

Chemokines are key regulators of hematopoiesis under steady state and inflammatory conditions. The homeostatic chemokine CXCL12 and its receptors, CXCR4 and ACKR3 are crucial during development, as deletion of either component is lethal in mice at embryonic stage (Nagasawa et al., 1996, Zou et al., 1998, Ma et al., 1998, Sierro et al., 2007). CXCR4 is expressed on hematopoietic cells, as well as in stromal cells (Oberlin et al., 1996, Dar et al., 2005). CAR cells are the main cells producing CXCL12 within the BM (Sugiyama et al., 2006). ACKR3 has been shown to be present in the endosteal part of the BM, whereas the expression on hematopoietic cells remains controversial (Gerrits et al., 2008; Humpert et al., 2014; Torossian et al., 2014).
CXCR4/CXCL12 axis plays a major role in BM cell retention (Ma et al., 1999; Tzeng et al., 2011). However, different hypotheses have been proposed on the mechanism by which BM cell mobilization occurs. The two main models could be summarized as the "constant retention", in which CXCR4 is constantly binding to CXCL12, subsequently activating surface integrins and, thus, maintaining the cells within the BM. On the other hand, according to the "gradient" hypothesis, the relative difference on the CXCL12 concentration between the BM and the circulation regulates hematopoietic cells' localization. On the contrary, the role of ACKR3 in hematopoiesis remains elusive. Thus, my project aimed to elucidate:

A. The role of ACKR3 on HSPC maintenance

1. **Description of the ACKR3 expressing cells in the BM**
   employing *Ackr3*^{GFP} reporter mouse model
2. **Investigation of the role of ACKR3 in BM cell maintenance**
   Ubc-Cre^{ERT2} *Ackr3*$^{flox/flox}$ mice were employed in steady state conditions.
3. **Identification of the ACKR3-dependent mechanisms in the BM**
   employing knockout mouse models for the two main ligands, CXCL12 and MIF
4. **Evaluation of the role of ACKR3 in BM cell reconstitution**
   by immunohistochemistry and flow cytometry in BM cell-depleted mice after administration of the cytotoxic compound 5 Fluorouracil.

B. Scrutinizing the mechanism of the HSPC retention

1. **Investigation of the role of ACKR3 on BM cell retention**
   inhibiting ACKR3 in an inducible *Ubc-Cre*^{ERT2} *Ackr3*$^{flox/flox}$ mouse model and via a pharmacological inhibitor
2. **Evaluation of the "Gradient" hypothesis for BM cell retention**
   depleting CXCL12 in an inducible *Ubc-Cre*^{ERT2} *Cxcl12*$^{flox/flox}$ mouse model and by increasing the circulating CXCL12 after *in vivo* injection of AMD3100 or injection of recombinant CXCL12.
3. **Evaluation of the "Constant retention" hypothesis for BM cell retention**
   Employing an inducible *Ubc-Cre*^{ERT2} *Cxcr4*$^{flox/flox}$ mouse model, as well as the HSC specific *Fgd5*^{CreERT2} *Cxcr4*$^{flox/flox}$ mouse model
4. **Evaluation of the role of the stromal cells in BM cell maintenance**

by bone marrow transplantation of $CXCR4^{+/+}$ hematopoietic cells in $CXCR4^{-/-}$ murine recipients and by bone marrow transplantation of $CXCR4^{-/-}$ hematopoietic cells in $CXCR4^{+/+}$ murine recipients

3. Materials and Methods

3.1 Laboratory Equipment

Table 2 Laboratory equipment used in the study

Equipment	*Provider*
Laboratory Balance, TE124S	Sartorius
Laboratory Balance, M-Power	Sartorius
Centrifuge, 5810 R	Eppendorf
Centrifuge, Universal 32 R	Hettich
Microcentrifuge, Biofuge Pico	Heraeus
Vortex mixer, VV3	VWR
ThermoMixer, C	Eppendorf
Thermomixer, comfort	Eppendorf
Multichannel Pipets, PIPETMAN Neo	Gilson
Hotplate stirrer, Ruhromag MH12	Retsch
Pipettes	Gilson
Waterbath	Memmert
Incubator, CB210	Binder
Microcentrifuge tubes	Eppendorf
EDTA tubes	Sarstdedt
Pipette tips (10µl-1ml)	Starlab
Falcon tubes (15 and 50ml)	Corning
Falcon 5ml round bottom tubes	BD Falcon

3.2 Animal handling

All mouse lines were bred and maintained in the LMU Klinikum animal facility. All mice were housed in individually ventilated cage (IVC).

Ackr3^{GFP} reporter mice (Cruz-Orengo et al., 2011) were purchased from Jackson Laboratory (stock #008591). The mice carry an insertion of the *Gfp* gene instead of the second exon of the *Ackr3* locus. Thus, the mice carrying the GFP protein have only one *Ackr3* expressing allele. Due to the significant perinatal lethality observed in *Ackr3*$^{-/-}$ mice (Yu et al., 2011), the *Ackr3*^{GFP} line was maintained in heterozygous background. As control, mice without the *Gfp* insertion, *Ackr3*$^{+/+}$, were used. C57BL/6J (stock #000664) and C57BL/6N (stock #005304) mice were purchased from Jackson Laboratory. *Apoe*$^{-/-}$ mice (Piedrahita et al., 1992) were obtained from in house breeding or purchased from Jackson Laboratory (stock #002052). Tissues from MIF$^{-/-}$ mice were kindly provided by Prof. Jürgen Bernhagen (Klinikum der Universität München, Munich, Germany).

Mice carrying *Cxcr4*$^{flox/flox}$ allele (Nie et al., 2004) were kindly provided by Prof. Y. Zou (Columbia University, New York, US). These mice contain two loxP sites in intron 3 and exon 2 of the *Cxcr4* gene. *Ackr3*$^{flox/flox}$ mice (Berahovich et al., 2010) were kindly provided by ChemoCentryx, Inc

(Mountain View,CA). *Cxcl12*$^{flox/flox}$ mice were generated in our institute (Döring et al., 2019). All *flox*-containing mouse lines were maintained in *Apoe*$^{-/-}$ background.

In order to introduce cell specific gene deletions *in vivo*, the Cre recombinase technology was employed. The Cre recombinase was initially found on bacteriophages. Due to its ability to recognize loxP genetic regions and excise the DNA sequence found among these flag regions (Shaikh and Sadow, 1997), it has been widely used for *in vivo* DNA recombination. In this regard, *Ubiquitin (Ubc)-Cre*^{ERT2} mice (Ruzankina et al., 2007) were bought from Jackson Laboratory (stock #007001). In this line, a gene encoding the Cre recombinase fused with a mutated human estrogen receptor has been inserted under the promoter of the constitutively expressed human ubiquitin C. As a result, the transgenic protein is expressed in all cells (Ruzankina et al., 2007). However, due to the presence of the modified human estrogen receptor, the produced Cre recombinase is inactive. In order to activate the recombinase, the administration of the ligand, tamoxifen, is required (Feil et al., 1997). Thus, when crossing these mice with the *flox*-containing lines stated above, the gene of interest is excised in all tissues, after the administration of tamoxifen. All *Ubc-Cre*^{ERT2} lines were maintained in *Apoe*$^{-/-}$ background.

Tamoxifen (Sigma; cat.no. T 5648) was diluted in MIGLYOL® 812 (Caelo; cat.no. 52622-27-2) at 37°C. Subsequently, the solution was aliquoted in syringes containing 50µl. The tamoxifen was administered intraperitonially (i.p.) for 5 consecutive days in a dosage of 50µg per 20g of mouse weight. To assess the effect of gene deletion, mice were compared to *flox*-containing mice, which did not express the Cre recombinase.

Finally, *Fgd5*$^{ZsGr.CreERT2}$ mice (Gazit et al., 2014) were purchased from Jackson Laboratory (stock #027789). The mice are knock-in, as the *Fgd5* allele has been replaced with two genes coding the fluorescent protein Zoantus Green (ZsGreen), and the *Cre*^{ERT2} recombinase described above. Thus, *Fgd5* expressing cells are fluorescent due to the presence of the protein ZsGreen, and the administration of tamoxifen induces the intracellular production of the Cre recombinase. As a result, when crossed with a *flox*-containing line the desired gene is excised in the Fgd5^{+} cells. *Fgd5*$^{Cre/Cre}$ mice are lethal (Gazit et al., 2014), and, hence, mice were maintained in heterozygous background. *Fgd5*$^{+/+}$ mice, which were not expressing the Cre protein, were used as control. The *Fgd5*$^{ZsGr.CreERT2}$ line was maintained in *Apoe*$^{-/-}$ background.

Proliferating cells were depleted *in vivo* using the cytotoxic agent, 5-Fluorouracil (5FU) (Sigma; cat.no. F6627). The agent was diluted in 1x Phosphate Buffered Saline (PBS) (Gibco; cat.no. 10010-015) and was subsequently injected i.p. in a dosage of 250mg/kg of mouse. The effect of the cell depletion was determined with the comparison of the 5FU-treated mice to PBS-injected mice. Mice were sacrificed 4, 10, and 21 days (d) later.

In order to inhibit CXCR4 *in vivo*, the CXCR4 antagonist AMD3100 (Selleckhem; cat.no S8030) was used. The lyophilized inhibitor was dissolved in 1x PBS. 10mg/kg of AMD3100 were administered i.p., as previously described (Liu et al., 2015). 1x PBS was injected in the respective control group. Mice were sacrificed 1 hour (h) later.

Finally, in order to administer CXCL12 *in vivo*, recombinant murine CXCL12 (Biolegend; cat.no. 578706) was diluted in 1x PBS containing 0.1% Albumin (Roth; cat.no. 3737.3). The recombinant chemokine was injected intravenously (i.v.), whereas mice injected with the vehicle, 0.1% Albumin in PBS, were used as control group. Mice were sacrificed 30min later.

3.2.1 Bone marrow transplantation

Table 3 Antibiotic mix for BM transplantation

Antibiotic	*Grams/50ml of dH_2O*	*Provider; catalogue number*
Neomycin	5g	Gibco; cat.no. 538242
Polymyxin	0.5g	Sigma; cat.no. 544628

Whole BM cells obtained from *Apoe*$^{-/-}$ donor mice were transplanted to *Ubc-Cre*^{ERT2} *CXCR4*$^{flox/flox}$ and *CXCR4*$^{flox/flox}$ recipient mice. Accordingly, BM cells originating from *Ubc-Cre*^{ERT2} *CXCR4*$^{flox/flox}$ and *CXCR4*$^{flox/flox}$ donor mice were transplanted to *Apoe*$^{-/-}$ recipient mice. Age matched and sex matched donors were chosen for all bone marrow transplantation (BMT) experiments.

Prior to the BMT, the recipient mice were treated for 48h with the antibiotics described in Table 3. The recipient mice were irradiated twice, 24h and 4h before the transplantation, with 6 Gray (Gy), for 8.5 minutes (min), using a CP-160 Cabinet X-Radiator (Faxitron X-Ray Corp.).

To obtain the donor cells, donor mice were sacrificed, and the femurs were dissected. Femoral BM cells were flushed in 1x PBS under sterile conditions and $2.5x10^6$ cells were aliquoted in syringes to a final volume of 100µl. Recipient mice were shortly maintained under UV light, in order to induce vasodilation. Donor cells were injected i.v. to the recipients. Mice remained under antibiotics for 4 weeks. After this recovery phase, mice were treated with tamoxifen, as described above, to excise the *Cxcr4* gene.

3.2.2 *In vivo* Pharmacological inhibition of ACKR3

To pharmacologically inhibit ACKR3 *in vivo*, an antagonist that will be referred to the rest of the thesis as compound X was used, as previously described (Richard-Bildstein et al., 2020, Zabel et al., 2009). Male and female C57BL/6N and C57BL/6J mice were employed. Animals were sacrificed 1h, 6h or 3d later. Animals were allocated to groups in a randomized manner.

3.2.3 Animal anesthetization, blood and organ collection

Age matched, and sex matched mice were sacrificed for experimental purposes. At the experiment endpoint mice were deeply anesthetized with 6-8mg/kg Xylazin and 120mg/kg Ketamin solution. After loss of reflections, whole blood was collected from the retro orbital plexus in an EDTA-containing tube. Mice were then surgically dissected and were subsequently perfused

with 1x PBS. Finally, organs were collected. All animal experiments were planned and held according to the local legislation (District Government of Upper Bavaria, Germany; License Numbers: Gz ROB-55.2-2532.Vet_02-16-186 and Gz ROB-55.2.-2532.Vet_02-18-96) and the institutional and national guidelines for laboratory animals.

3.3 Molecular Methods

3.3.1 DNA isolation

Weaned mice were marked with ear punches, and a tail biopsy was stored for the determination of the genotype.

Tail DNA was isolated from the biopsy using the ReliaPrep™ gDNA Tissue Miniprep System (Promega; cat.no. A2051), according to manufacturer's instructions. More specifically, the tail tissue was homogenized in 100µl tail lysis buffer supplemented with 20µl Proteinase K solution at 56°C overnight. 300µl of cell lysis buffer supplemented with 20µl of RNAase A solution were subsequently added, and samples were incubated at 56°C for 10min. Samples were centrifuged for 1min at maximum speed and the supernatant was collected to a new centrifuge tube. 250µl of binding buffer was added and samples were transferred to ReliaPrep Binding Columns. The columns were centrifuged for 1min at maximum speed and the flow-through was discarded. The columns were washed three times with 500µl Column Wash Solution, followed by centrifugation for 2min at maximum speed, and the discard of the flow-through. After the last wash, the columns were placed in a sterile microcentrifuge tube. Finally, for the elution of the DNA, dH_2O was added to the columns and the tubes were centrifuged for 1min at maximum speed. The columns were discarded and the eluted DNA in the tube was stored at -20°C until further usage.

3.3.2 End Point PCR

To determine the mouse genotype, as well as to verify the deletion of the *Ackr3* gene after the injection of tamoxifen, end point Polymerase Chain Reaction (PCR) was performed. The PCR master mix is shown in Table 4. Each PCR reaction contained 5µl of DNA, whereas the polymerase used was the GoTaq DNA Polymerase (Promega; cat.no. M3001). The sequence of the primers used, and the expected size of the DNA products in base pair (bp), is listed in Appendix A. The reaction was performed in Mastercycler Nexus (Eppendorf) with the program shown in Table 5.

Table 4 PCR master mix

Component	***Volume***
GoTaq® DNA polymerase	7.5 µl
dH_2O	3 µl
Forward Primer (10µM)	0.75 µl
Reverse Primer (10µM)	0.75 µl
DNA	5 µl

Amplified DNA products were visualized by gel electrophoresis. 2% Agarose (Sigma, cat.no. A9539) gel was prepared in 1x TAE buffer (Applichem; cat.no. APA1691) containing 0.5µg/ml Ethidium Bromide (Sigma; cat.no. 1239-45-8). Samples were loaded on the gel and subjected to electrophoretic separation in a DNA electrophoresis Cell (Bio-Rad). 1kB TAE ladder (Invitrogen, cat.no. 10787-018) was also loaded on the gel to determine the size of the DNA products. Picture acquisition was done under UV light (Intas UV System). Genotype was determined according to the size of the DNA products.

Table 5 PCR Program for end point PCR

Step	*Temperature*	*Time*	*Cycles*
Initial Denaturation	95°C	2min	1x
Denaturation	95°C	30sec	35x
Annealing	55-63°C	30sec	
Extension	68-72°C	2min 30sec	
Final extension	72°C	5min	1x

3.3.3 RNA isolation

Harvested murine tissues were snap frozen in liquid nitrogen and stored in -20°C. Tissue samples were thawed, and the tissue weight was determined. An equal amount of tissue was used for the RNA isolation.

Total RNA was isolated using the RNeasy Mini kit (Qiagen; cat.no. 74104), according to the manufacturer's protocol. 700µl of Qiazol Lysis Reagent was added and the samples were homogenized for 2min in a TissueLyser LT (Qiagen) in the presence of a stainless-steel bead (Qiagen; cat.no. 69989). The homogenate was incubated at RT for 5min. 140µl of chloroform was added and samples were vortexed for 15 seconds (s). Samples were incubated for 2min at RT and were subsequently centrifuged for 15min at 12,000g. The aqueous phase was collected in a new microcentrifuge tube and 1.5 times the sample volume of 100% ethanol (Merck; cat.no. 64-17-5) were added. The sample was mixed vigorously and was immediately loaded into an RNAeasy Mini column. Samples were centrifuged at 12,000g for 1min and the flow-through was discarded. Columns were washed with 700µl of RWT, centrifuged for 1min at 12,000g and the flow-through was discarded. Columns were washed again with 500µl of RPE, centrifuged at 12,000g for 1min and the flow-through was also discarded. Finally, to dry the membrane, the samples were centrifuged at 12,000g for 2min. Columns were subsequently placed in a sterile microcentrifuge tube and the RNA was eluted with the addition of 30-50µl of dH_2O. The samples were centrifuged at 12,000g for 1min and the flow-through was stored at -20°C.

3.3.4 RNA quantification and cDNA synthesis

Prior to further use, the concentration of the isolated RNA was quantified, and the purity of the nucleic acid was assessed using a NanoPhotometer (Implen). 1µl of RNA sample was used to

determine the optical density (OD) at 260nm, 280nm and 230nm. A value of OD_{260}/OD_{280} above 1.5 was generally accepted, while samples with a value of OD_{260}/OD_{230} lower than 0.7 were disqualified. Using the sample with the lowest RNA concentration, the total amount of RNA used for the cDNA synthesis was determined, and all samples were normalized accordingly with the addition of dH_2O.

The cDNA synthesis was performed using the High Capacity cDNA Reverse Transcription kit (ThermoFisher; cat.no. 4368814) using a maximum of 2µg of RNA, according to the manufacturer's instructions. Briefly, a master mix was prepared, as shown in Table 6. 10µl of normalized RNA sample were mixed in a microcentrifuge tube with 10µl of Master mix. cDNA synthesis was then performed according to the program in Table 7. cDNA samples were stored at -20°C.

Table 6 Master mix for cDNA synthesis

Component	***Volume***
10x RT Buffer	2 µl
25x dNTP Mix (100mM)	0.8 µl
10x RT Random Primers	2 µl
MultiScribe Reverse Transcriptase	1 µl
Nuclease-free dH_2O	4.2 µl

Table 7 Program for cDNA synthesis

	Step 1	***Step 2***	***Step 3***
Temperature	25°C	37°C	85°C
Time	10min	120min	5min

3.3.4 Real time PCR

Quantitative PCR (qPCR) was performed with the GoTaq qPCR Master mix (Promega; cat.no. A6002). The components of each qPCR reaction are shown in Table 8. 25-50ng of reverse transcribed RNA were used per reaction. The sequence of the primers used is listed in Table 9. The amplification program is described in Table 10. qPCR reaction was performed in a 7900HT Fast Real-Time PCR (ThermoFisher) and gene expression was analyzed according to the $2^{-\Delta\Delta CT}$ method, with *Gapdh* used as reference gene.

Table 8 Master mix for qPCR

Component	*Volume*
GoTaq® qPCR Master Mix	10 µl
CXR Reference Dye	0.1 µl
Forward Primer (10µM)	0.6 µl
Reverse Primer (10µM)	0.6 µl
cDNA + ddH_2O	8.7 µl

Table 9 Primer Sequence for qPCR

Gene		*Sequence (5´> 3´)*
Cxcl12	Forward	CTT CAT CCC CAT TCT CCT CA
	Reverse	GAC TCT GCT CTG GTG GAA GG
Ackr3	Forward	AAC CTC TTT GGG AGC ATC TTC TT
	Reverse	GGT GCC GGT GAA GTA GGT GAT
Gapdh	Forward	GTG AAG GTC GGT GTG AAC G
	Reverse	GGT CGT TGA TGG CAA CAA TCT C

Table 10 Program for qPCR

Step	*Temperature*	*Time*	*Cycles*
Initial Denaturation	95°C	15min	1x
Denaturation	95°C	15sec	40x
Annealing	58°C	30sec	
Extension	72°C	30sec	

3.4 Tissue Processing

3.4.1 Blood analysis

To analyze hematological parameters one drop of blood was assessed using a hematology analyzer (Scil Vet abc). Blood was aspirated, and the number of erythrocytes (RBC) and platelets were assessed. In addition, the concentration of hemoglobin (Hgb), hematocrit (Hct) and the erythrocyte mean corpuscular volume (MCV) were measured.

3.4.2 Plasma and BM supernatant collection

Collected blood was aliquoted in EDTA tubes and one vial was maintained at 4°C for plasma isolation. For plasma collection, blood was centrifuged at 2,000g for 10min at 4°C. Plasma was isolated and, subsequently, stored at -20°C until further use.

After femoral dissection, the knee was removed, and the femurs were placed in a pipette tip. The tips were placed in a microcentrifuge tube which was then centrifuged at 10,000g for 1min. The BM cell pellet was resuspended in 250-500µl of sterile 1x PBS. The resuspended BM cells were further centrifuged at 2,000g for 10min at 4°C. BM supernatant was collected and stored at -20°C. BM cell pellets were then resuspended in 1ml 1x PBS and the cells were subsequently used for the assessment of protein expression by flow cytometry.

3.4.3 Flow Cytometry

3.4.3.1 Preparation of cell suspensions

Extracellular and intracellular protein expression was assessed by flow cytometry. Spleen and kidney tissues were minced by applying mechanical pressure on 30µm cell strainers placed upon falcon tubes. Filters were rinsed with 1x PBS and collected cells were transferred to 5ml falcon tubes with round bottom for flow cytometry. Lung, liver and aorta, were cut in pieces and were subsequently digested in the presence of 100µg/ml Liberase™ TM Research Grade (Roche; cat.no. 5401127001). Samples were incubated for 40min at 37°C at 500rpm orbital shaking. After digestion, cells were transferred in flow cytometry tubes equipped with cell strainer cap (Falcon; cat.no. 352235) in order to discard undigested pieces of tissue. BM and blood cells were directly transferred to flow cytometry tubes.

In order to quantify cell events 10µl of Precision Counting Beads (Biolegend; cat.no 424902) were added to all cell suspensions prior to any further processing. Red blood cells in spleen and blood samples were then lysed after incubation with 1x RBC lysis buffer (Biolegend; cat.no. 420301) for 10min at RT. Cell suspensions of all tissues were centrifuged at 350g for 5min and the supernatant was discarded. Cell pellets were subsequently used for extracellular and intracellular antibody staining.

3.4.3.2 Extracellular and intracellular staining

The extracellular CXCR4 expression was assessed in an *ex vivo* binding assay. The assay employed the fluorescently labeled ligand, CXCL12, whereas the specificity of the binding was determined using the CXCR4 inhibitor, AMD3100, according to the scheme on Figure 8. More specifically, BM cells from every mouse were transferred in two flow cytometry tubes. One sample was incubated with 1x PBS alone, whereas the other was incubated with 1x PBS supplemented with 2µM of AMD3100. Cells were incubated at 37°C for 5min. Then, 1x PBS supplemented with CXCL12 labeled with the fluorescent molecule Alexa Fluor 647 (Almac; cat.no. CAF-50) was added to all samples to a final concentration of 40nM. Cells were incubated for additional 15min at 37°C. Finally, samples were washed with 1x PBS, centrifuged at 350g for 5min and cell pellets were stained with antibodies targeting extracellular epitopes.

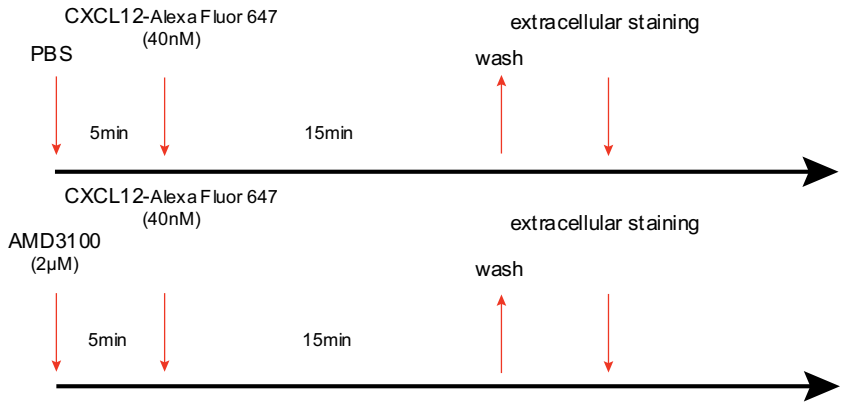

Figure 8 Scheme of ex vivo binding assay.
BM cells were treated with PBS or AMD3100. After 5min incubation CXCL12-Alexa Fluor 647 was supplemented for 15min incubation at 37 °C. Cells were washed and subsequently stained with the antibody mix for extracellular proteins.

In order to assess the intracellular ROS and the mitochondrial content, BM cells pellets were resuspended in IMDM culture medium (ThermoFisher; cat.no. 12440053), supplemented with 2% Fetal Bovine Serum (Sigma Aldrich; cat.no. F7524) and 2.5µg/ml Dihydrorhodamine (DHR) 123 (Sigma; cat.no. D 1054) or respectively 20nM MitoTracker Deep Red FM (ThermoFisher; cat.no. M22426). DHR 123 can passively diffuse across the mitochondrial membrane. There, in the presence of oxygen, the dye becomes fluorescent. Similarly, MitoTraker can passively diffuse membranes and stains active mitochondrial. Cells were incubated at 37°C for 20min. Afterwards, cells were washed with 1x PBS and centrifuged at 350g for 5min. The cell pellets were subsequently stained for extracellular epitopes.

To assess the extracellular epitopes, an antibody mix was prepared in 1x PBS containing 0.5% Albumin. Cell pellets were resuspended in 100µl of antibody mix and were incubated at 4°C. Appendix B contains all antibodies employed for flow cytometry and the dilution in which they were used. Unstained CD16/32 antibody was included in all antibody mixes that did not otherwise contain fluorescently labeled CD16/32, in order to block Fcγ receptors. After 45-60min incubation, samples were washed with 1x PBS and centrifuged at 350g for 5min. The supernatant was discarded, and cell pellets were resuspended in 200-500µl for sample acquisition.

Cell apoptosis was evaluated by assessing caspase 3 and caspase 7 activity. Cell suspensions were firstly stained extracellularly. Cells were washed by centrifugation and cell pellets were resuspended in 1x PBS supplemented with 1µM Caspase-3/7Green Reagent (ThermoFisher; cat.no. C10740). Samples were incubated at 37°C for 30min. In apoptotic cells, the active caspase 3 and caspase 7 cleave the four amino acid peptide (DEVD) of the reagent. The cleavage releases a DNA binding dye, which then fluorescently labels the apoptotic cells, and allows their detection. In order to determine the percentage of caspase$^+$ cells, an unstained control was used.

In order to assess intracellular epitopes, as well as the cell cycle, the Foxp3 / Transcription Factor Staining Buffer Set (ThermoFisher; cat.no. 00-5523-00) was used. Briefly, cells already stained for surface antigens, were washed and centrifuged. The pellets were initially fixed with 200μl Fixation/Permeabilization buffer for 20min at RT and were later washed with 100μl 1x Permeabilization buffer. An antibody mix was prepared using 1x Permeabilization buffer as diluent. Cell pellets were resuspended in the antibody mix and incubated for additional 20min at RT. Cells were finally washed with 1x PBS and resuspended at 200-400μl of 1x PBS for acquisition.

3.4.3.3 Sample acquisition and analysis

Cell events were recorded using the BD FACS Canto II (BD Biosciences) and the LSRFortessa (BD Biosciences). The FlowJo analysis program (BD Biosciences) was used for the analysis. Cell events were gated according to the gating strategies shown in Figures 9-18.

The absolute cell counts were calculated based on the number of counting beads recorded and the beads concentration in the samples, according to the formula:

$$\frac{Recorded\ cells\ x\ Counting\ beads\ Concentration\ (beads/\mu l)}{Recorded\ beads\ x\ Volume\ of\ sample}$$

The expression of ACKR3 in *Ackr3*^{GFP} mice, and of Fgd5 in Fgd5^{ZsGreen} mice was assessed by calculating the Δ mean Fluorescent Intensity (MFI) of the fluorescent molecules, according to the formula:

$$\Delta MFI = Sample\ \text{MFI} - \text{Average MFI of control samples}$$

of each independent experiment. When stated, the $\log_2$ of the ΔMFI values was calculated, after normalizing for the minimum value.

For the analysis of the intracellular ROS and the mitochondrial content staining data, samples were normalized as the fold change to the control samples of each independent experiment according to the formula:

$$Fold\ change = \frac{Sample\ MFI}{Average\ MFI\ of\ ctrl\ samples}$$

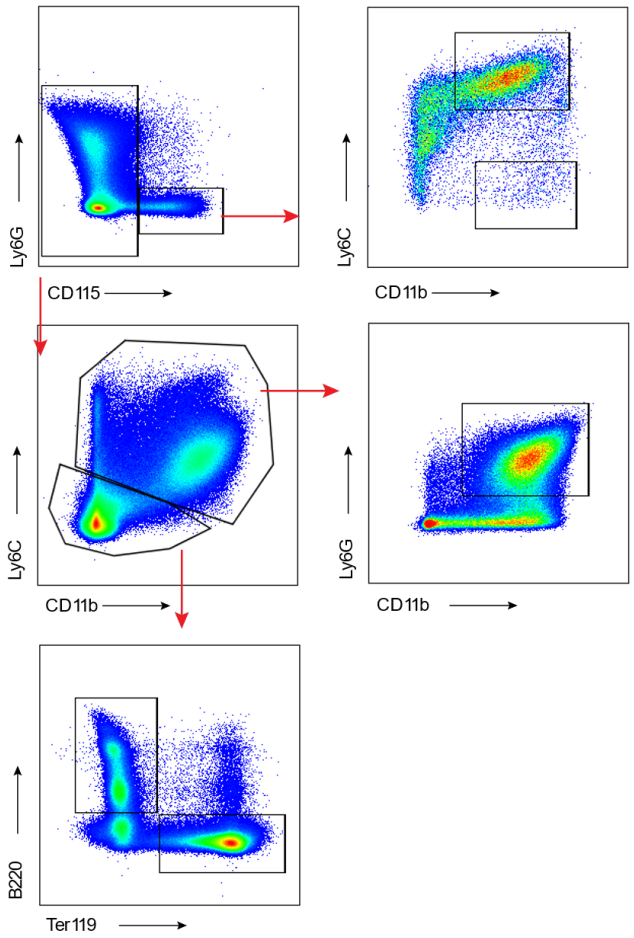

Figure 9 Gating strategy for BM mature leukocytes.
BM classical monocytes (CM) were identified as $CD115^{+}CD11b^{+}Ly6C^{high}$, whereas non-classical monocytes (NCM) were gated as $CD115^{+}$ $CD11b^{+}Ly6C^{low}$. Neutrophils were identified as $CD115^{-}CD11b^{+}Ly6G^{+}$. B cells were gated as $CD11b^{-}Ly6C^{-}B220^{+}$ and erythroid cells as $CD11b^{-}Ly6C^{-}B220^{-}Ter119^{+}$.

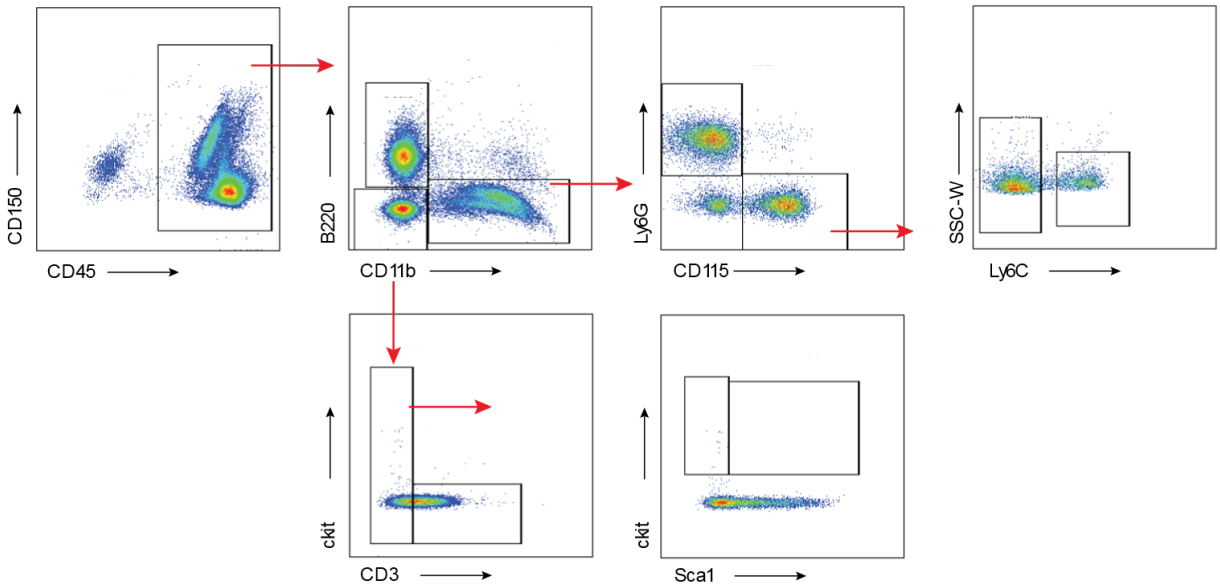

Figure 10 Gating strategy for leukocytes in blood and spleen.
Circulating and splenic CM were identified as $CD45^{+}CD11b^{+}CD115^{+}Ly6C^{high}$, whereas NCM were gated as $CD45^{+}CD11b^{+}CD115^{+}Ly6C^{low}$. Neutrophils were identified as $CD45^{+}CD11b^{+}Ly6G^{+}$.Circulating B cells were gated as $CD45^{+}CD11b^{-}B220^{+}$ and T cells as $CD45^{+}CD11b^{-}CD3^{+}$. $Lineage^{-}$ $Sca1^{+}$ $ckit^{+}$ (LSK) cells in blood and spleen were gated as $CD45^{+}CD11b^{-}B220^{-}CD3^{-}ckit^{high}Sca1^{+}$, whereas MPC as $CD45^{+}CD11b^{-}B220^{-}CD3^{-}ckit^{high}Sca1^{-}$.

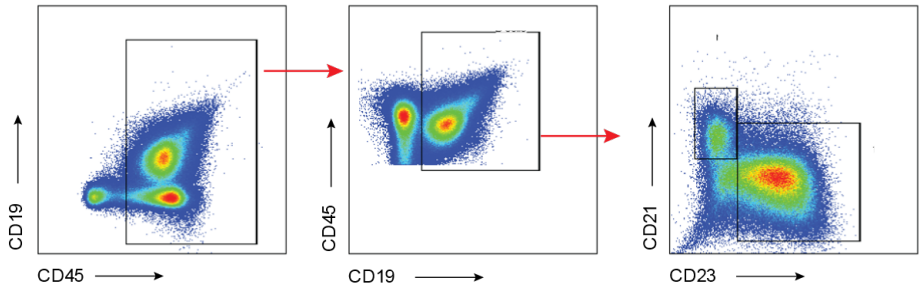

Figure 11 Gating strategy for splenic marginal cells.
Splenic marginal leukocytes were gated as $CD45^{+}CD19^{+}CD21^{+}$, whereas follicular cells were gated as $CD45^{+}CD19^{+}CD23^{+}$.

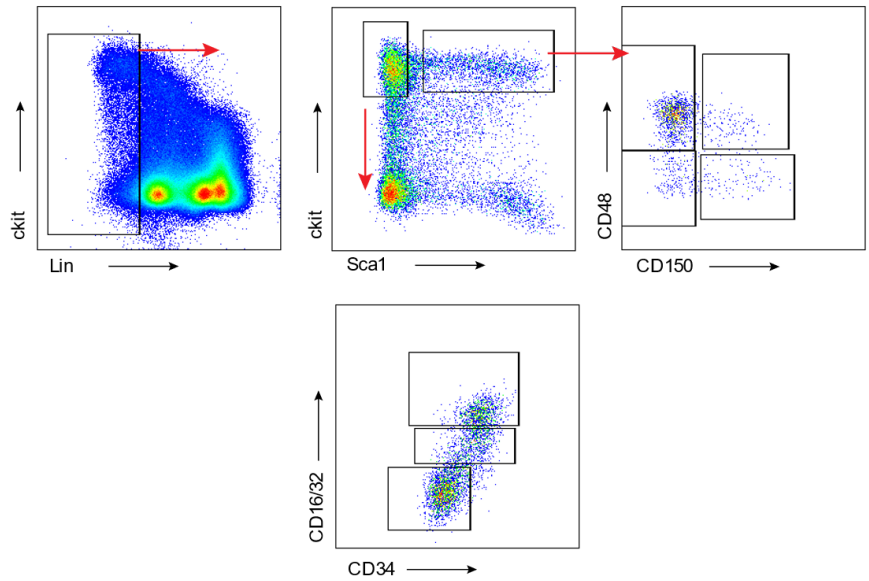

Figure 12 Gating strategy for BM HSPC.
LSK cells were gated as Lineage$^-$ Sca1$^+$ ckit$^+$, whereas MPC as Lin$^-$ckit^{high}Sca1$^-$. HSCs gated as Lin$^-$ckit$^+$Sca1$^+$CD150$^+$CD48$^-$, MPP1 as Lin$^-$ckit$^+$Sca1$^+$CD150$^-$CD48$^-$, MPP2 as Lin$^-$ckit$^+$Sca1$^+$CD150$^+$CD48$^+$, MPP3 as Lin$^-$ckit$^+$Sca1$^+$CD150$^-$CD48$^+$. Granulocyte-Monocyte Progenitor (GMP) cells were gates as Lin$^-$ckit$^+$Sca1$^-$CD16/32$^+$CD34$^+$, Common Myeloid Progenitor (CMP) as Lin$^-$ckit$^+$Sca1$^-$CD16/32^{low}CD34^{low}, and Megakaryocyte-Erythroid Progenitor (MEP) as Lin$^-$ckit$^+$Sca1$^-$CD16/32$^-$CD34$^-$.
Lin: CD3, Gr1, B220, Ter119, CD11b.

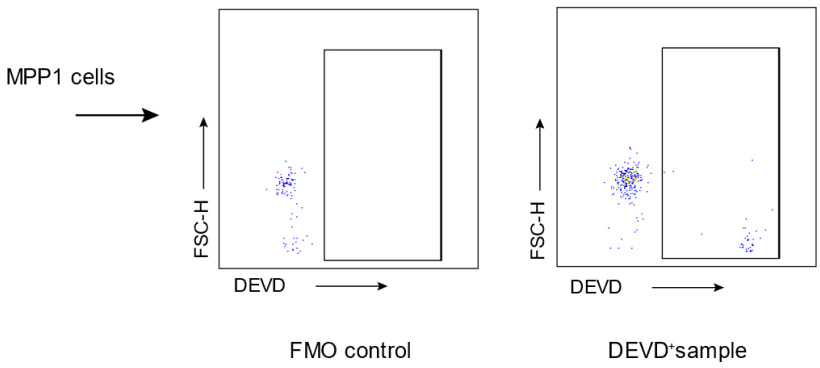

Figure 13 Representative figure of the gating strategy for assessment of apoptosis.
Representative figure of MPP1 cells gated as Caspase$^+$, based on the fluorescence of the DEVD substrate, and the background fluorescence of the Fluorescence Minus One (FMO) control.

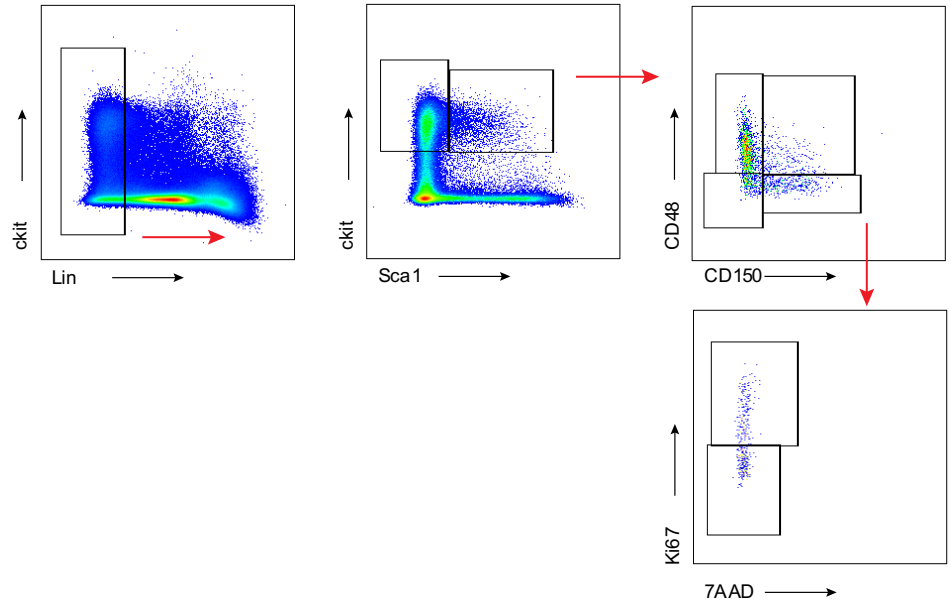

Figure 14 Representative figure of the gating strategy for assessment of the cell cycle.
Representative figure of HSCs gated as $Lin^{-}ckit^{+}Sca1^{+}CD150^{+}CD48^{-}$ assessed for the presence of the Ki67 nuclear protein. $Ki67^{+}$ cells were considered as proliferative cells, whereas $Ki67^{-}$ were considered as quiescent.

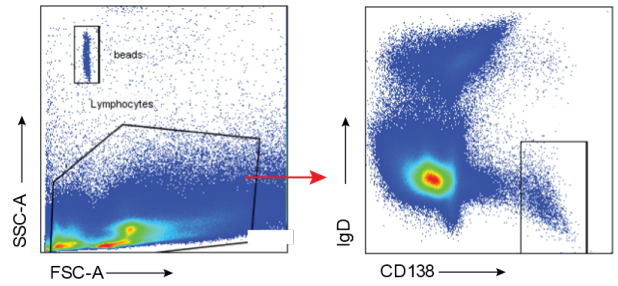

Figure 15 Gating strategy for the BM plasma cells.
Plasma cells were gated in the BM as $CD138^{+}IgD^{-}$ leukocytes.

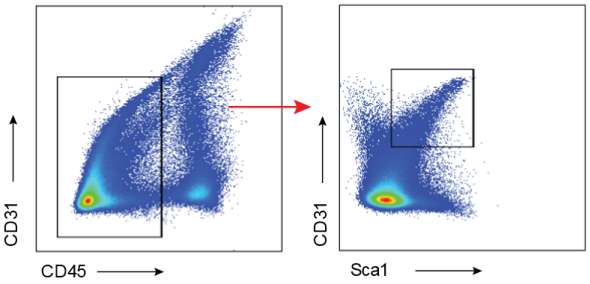

Figure 16 Gating strategy for the endothelial cells in lung, aorta, and liver.
The endothelial cells in the lung, aorta, and the liver were gated as $CD45^{-}CD31^{+}$ cells.

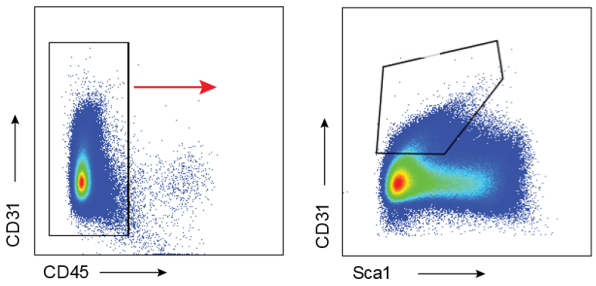

Figure 17 Gating strategy for the endothelial cells in kidney.
The endothelial cells in the kidney were gated as $CD45^{-}CD31^{+}Sca1^{-}$ cells.

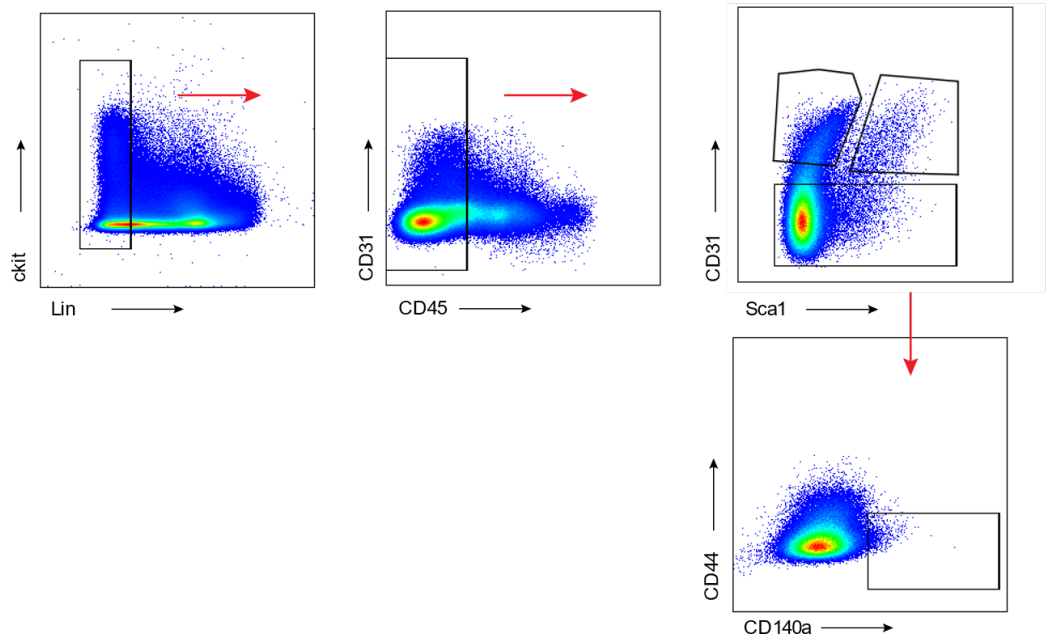

Figure 18 Gating strategy for the endothelial cells in BM.
Aortic endothelial cells (AECs) were gated as $Lin^{-}CD45^{-}CD31^{+}Sca1^{+}$ cells. Sinusoid endothelial cells (SEC) were gated as $Lin^{-}CD45^{-}CD31^{+}Sca1^{+}$, whereas fibroblasts as $Lin^{-}CD45^{-}CD31^{-}CD140a^{+}$ cells.
Lin: Ter119, CD11b, Gr1.

3.4.4 Enrichment of LSK cells

Hematopoietic $Lineage^{-}$ $Sca1^{+}$ $ckit^{+}$ (LSK) cells were isolated with the EasySep Mouse Hematopoietic Progenitor Cell Isolation Kit (STEMCELL Technologies; cat.no. 19856), according to the manufacturer's instructions. Briefly, BM cells were centrifuged at 350g for 5min and the supernatant was discarded. In 1ml of BM cell pellet 50µl of rat serum was added in order to block unspecific antibody binding. Cells were transferred into a flow cytometry tube, and 50µl of Isolation cocktail, containing antibodies against Lin^{+} cells, was added. Cells were stained for 15min

at 4°C. Then, RapidSpheres were vortexed for 30s and 75µl were added in the samples. After 10min incubation at 4°C, 2ml of 1x PBS containing 1% BSA were supplemented and the samples were placed into an Easysep Magnet for 3min. After that, the magnet was inverted and the unbound, LSK enriched cells were poured into a 15ml Falcon tube.

Quantification of the isolated cells was performed by flow cytometry, as described above, with the addition of counting beads, and the subsequent acquisition of the samples in a flow cytometer. Cell counts were normalized, and cells were used in the colony formation assay.

3.4.5 Colony Formation Assay from blood and BM cells

To assess the colony formation potential of cells in the periphery, 100µl of blood cells were lysed as previously described, and washed. Cell pellet was resuspended in 100µl IMDM containing 2% FBS and were mixed with 1ml mouse Methylcellulose Complete Media (R&D Systems; cat.no. HSC007). Cells were vortexed and plated in 10mm dishes (Starlab). Cells were cultured in a humidified incubator at 37°C in presence of 5% CO_2. At day 10, pictures of the colonies were taken using a Fusion Solo S Western blot and chemiluminescence imaging system (Vilber) and the number of colonies was counted.

Similarly, 1,000 of enriched BM LSK cells were centrifuged at 350g for 5min. Cell pellets were resuspended in 100µl IMDM containing 2% FBS. Cells were subsequently mixed with methylcellulose complete media, plated in dishes and cultured. The number of colonies originating from BM LSK cells was assessed at day 7. In addition, cells were harvested in 1x PBS and cell suspensions were used for flow cytometry analysis. The number of produced cells was assessed with the addition of counting beads, as previously described.

3.5 Immunosorbent assays

3.5.1 ELISA

BM SCF and CXCL12 concentration in plasma and BM supernatant were assessed by Enzyme-Linked Immunosorbent Assay (ELISA). SCF was quantified using the Murine SCF Standard ABTS ELISA Development kit (PeproTech; cat.no. 900-K78). ELISA 96-well plates (ThermoFisher Scientific) were coated with 1µg/ml of capture antibody against SCF. The antibody was diluted in 1x PBS and the plate was incubated overnight. The wells were aspirated and subsequently washed 3 times with 0.05% Tween in 1x PBS. After each washing step, the plate was inverted and blotted against paper towels in order to completely remove the buffer. After the last wash, 300µl of blocking buffer (1x PBS supplemented with 1% BSA) was added for 1 hour at RT. Standard samples were made by serial dilutions of 20ng/ml of SCF in diluent buffer (0.1% BSA and 0.05% Tween-20 in 1x PBS). After blocking, the plate was washed 3 times. The samples or the SCF standards were added to the plate. After 2h the samples were aspirated, and the wells were washed 3 more times. 100µl of detection antibody for SCF was added in a concentration of 0.25µg/ml and

incubated for 2 more hours. The plate was washed, and the Avidin-HRP Conjugate was added diluted 1/2000 in diluent. The plate was incubated for 30min at RT. Finally, the plate was washed 3 times and 100μl of ABTS Liquid Substrate were added. The plate was incubated in the dark for approximately 30min. For the detection, the absorbance was assessed in an Infinite F200 Pro Plate reader (Tecan) spectrophotometer at 405nm.

The quantification of BM and circulating CXCL12 was performed using the Mouse CXCL12 alpha Quantikine ELISA kit (R&D Systems; cat.no. MCX120) and the Legend Max Mouse CXCL12 beta ELISA kit (Biolegend; cat.no. 444207). These kits include pre-coated wells, and, hence, samples or standards were directly added to the plates without prior coating nor blocking of the ELISA plate.

In order to detect CXCL12β, standard samples were prepared with the serial dilution of 10ng/ml of recombinant protein. The samples and standards were then added to the plate and were incubated for 2h at RT. The plate was then washed 3 times, and the detection antibody for CXCL12β was added. After 1h incubation, the plate was washed again and 100μl of Avidin-HRP were added. The plate was incubated for 30min at RT. The plate was thoroughly washed 3 times. Finally, 100μl of Substrate solution, provided by the manufacturer, were added. The plate was incubated 20min at RT in the dark. The reaction was stopped with the addition of 100μl of Stop solution, and the plate was detected at the spectrophotometer at 450nm.

To assess the concentration of CXCL12α, standard samples were prepared with the serial dilution of 10ng/ml. The diluted samples and the standards were then added to the plate. After a 2h incubation at RT, the plate was washed 3 times. 100μl of the detection antibody against CXCL12α was added and the plate was incubated for additional 2h. The plate was washed 3 times and 200μl of Substrate solution, provided by the manufacturer, were added. The plate was incubated for 30min at RT, protected from light, until, finally, 50μl of Stop solution were added. The absorbance was then detected in the spectrophotometer at 450nm.

The absolute protein concentration of all ligands was determined with the generation of a standard curve. More specifically, the absorbance and the concentration of the standard samples were plotted in two axes in order to generate a sigmoidal curve. This curve was used to interpolate the protein concentration in the samples, based on the optical density values.

3.5.2 Legendplex Flow assay

For the screening of protein concentration in the BM supernatant, the 13-plex assay LEGENDplex™ Mouse HSC Panel (Biolegend; cat.no. 740677) was used. Briefly, the analyte standards were reconstituted and serially diluted. 25μl of undiluted samples or standards were added in duplicates in a 96-well plate. 25μl of fluorescently labeled beads were added into each well. The plate was incubated for 2h at RT under shaking. Then, the plate was centrifuged at 250g for 5min and washed twice with wash buffer, provided by the manufacturer. 25μl of detection antibodies against the 13 cytokines was added, and the plate was incubated for 1h under shaking. The fluorescent dye PE was finally supplemented, and the plate was incubated 30min in the dark. The plate was washed twice. After the final wash the samples were resuspended in wash buffer

and the samples were transferred into flow cytometry tubes. The samples were acquired in the LSRFortessa (BD Biosciences).

For the analysis of the results the .fcs files obtained from the cytometer were loaded to the LEGENDplex 8.0 Data analysis software. A standard curve was done for each analyte according to the fluorescence intensity of the serially diluted standards. The standard curves were used for the determination of the samples' concentration.

3.6 Immunohistochemistry techniques

3.6.1 Bone decalcification and preparation of sections

Femurs, tibias and spines harvested for imaging were incubated in Paraformaldehyde (PFA) (Sigma-Aldrich; cat.no. P 6148) for 2 days at 4°C. Bones were subsequently decalcified in EDTA 10% (Gerbu; cat.no. 1034) for 10 days. Finally, bones were incubated overnight in PBS with 30% sucrose (Sigma-Aldrich; cat.no. 84100) and the tissues were finally embedded in Tissue-Tek OCT compound (Sakura). 20μm thick BM sections were made in a cryostat Leica CM3050S, which were eventually used for immunohistochemistry.

Slides were rinsed with 1x PBS and blocked in 1x PBS containing 2% Albumin and goat serum for approximately 2h. Slides were subsequently incubated for 90min in permeabilization buffer containing 0.4% Triton X100 (Merck; cat.no. 9036-19-5) in 1x PBS supplemented with 1% Albumin. Slides were incubated with appropriate antibodies (Table 11), diluted in the permeabilization buffer. Slides were stained at RT for 2 days.

Table 11 List of antibodies used for immunohistochemistry

Epitope	*Fluorochrome*	*Clone*	*Company*	*Catalogue Number*
CD45	Pacific Blue	30-F11	Biolegend	103125
GFP	635P		Chromotek	gbas635p-100

3.6.2 Immunohistochemistry and image analysis

Prior to imaging, slides were thoroughly washed with 1x PBS and were mounted in Immu-Mount mounting medium (ThermoFisher; cat.no. 9990402). For the detection of the cellular nuclei, the Antifade Mounting Medium Vectashield was used supplemented with DAPI (Biozol; cat.no. H-1200). Finally, the samples were sealed with 1.5 thick coverslips (Menzel; cat.no. 631-0853). Pictures were acquired using the Leica TCS SP8 confocal laser scanning microscopy (CLSM), equipped with a 63/1.30 glycerol immersion objective and a 20/0.75 Multi-Immersion microscope objective.

The immunohistochemistry figures assessing the GFP expression, without any further computational analysis were deconvolved using the Huygens Professional software (Scientific Volume Imaging B.V.).

For the analysis of the GFP signal in the BM sections of *Ackr3*$^{GFP/+}$ mice the LASX 3D software was used. In more details, tilescan images of transverse BM sections were acquired. At the first step of the analysis, the Gaussian blur filter was applied. Then, the median fluorescent intensity (MFI) and the number of GFP$^+$ cells was determined for all sections. The number of GFP$^+$ cells was calculated to the area of the picture (in mm^2). In each imaging session, the average value for these two measurements was computed for every mouse. The two average values were subsequently normalized to the average value of the control, *Ackr3*$^{+/+}$ mice of that imaging session. In total 3-6 sections were acquired per mouse in multiple imaging sessions, until a normalized value for the MFI signal and the number of GFP$^+$ cells was calculated for each mouse. Finally, the average values and the standard deviation (SD) of all mice were pooled together and plotted.

3.8 Statistical analysis

Summary data is presented as mean ± standard error mean (SEM), whereas individual data is presented as mean. All statistical analyses were done using GraphPad Prism version 9.0 for Windows (GraphPad Software).

Data Gaussian distribution was assessed before the selection of statistical test using the Shapiro-Wilk test or the Kolmogorov-Smirnov test. Differences in data following a lognormal distribution were assessed using a Mann-Whitney *U* test. Prior to any statistical comparison, the data variance was compared among the groups were compared. For the comparison of two groups an unpaired 2-tail *t* test was used, with Welch's correction when appropriate. For multiple comparisons a False Discovery Rate (FDR) of 5% was used. For the comparison of multiple groups, 1 or 2-way ANOVA was used. For data with significant different variances Welch's ANOVA was used. Corrections for multiple comparisons were done using an appropriate *post hoc* test. A confidence interval of 95% was selected as threshold. The survival curves were compared using a Log-rank Mantel Cox test, with the confidence interval of 95% set as threshold.

4. Results

4.A Role of ACKR3 on HSPC maintenance

4.A.1 Description of the ACKR3 expressing cells in the BM

I used *Ackr3*^{GFP} reporter mouse line to map the expression of ACKR3 in the BM. In these mice, one allele encoding for *Ackr3* gene has been replaced by a *Gfp* sequence. As a consequence, GFP is produced when ACKR3 is expressed. To identify the ACKR3 expressing cells of the BM, bones were harvested, fixed, decalcified, and subsequently sectioned. Figure 19A shows a transverse section of the epiphysis of the BM. The GFP signal, and thus, the ACKR3 expression was limited only to the endosteal part. Islets of leukocytes are discerned on Figure 19A stained with the nuclei marker DAPI being GFP^{-}. The expression of ACKR3 in endosteal cells can be better visualized in the diaphysis of longitudinal sections in Figures 19B-C. The co-staining with the DAPI reveals that ACKR3-expressing cells were DAPI^{+} and were, thus, nucleated cells (Figure 19C). To verify that the observed GFP signal is not due to autofluorescence, I stained longitudinal sections with a GFP booster, an anti-GFP antibody emitting in a separate red channel. As shown in Figure 20A there was a certain background staining when using the GFP booster, even in the *Ackr3*$^{+/+}$ mice, which do not express GFP. Nevertheless, the anti-GFP antibody binds on the GFP^{+} endosteal cells, revealing the specificity of the GFP signal in these cells. Thus, these data suggest that ACKR3 is uniquely expressed in the endosteal part of the BM.

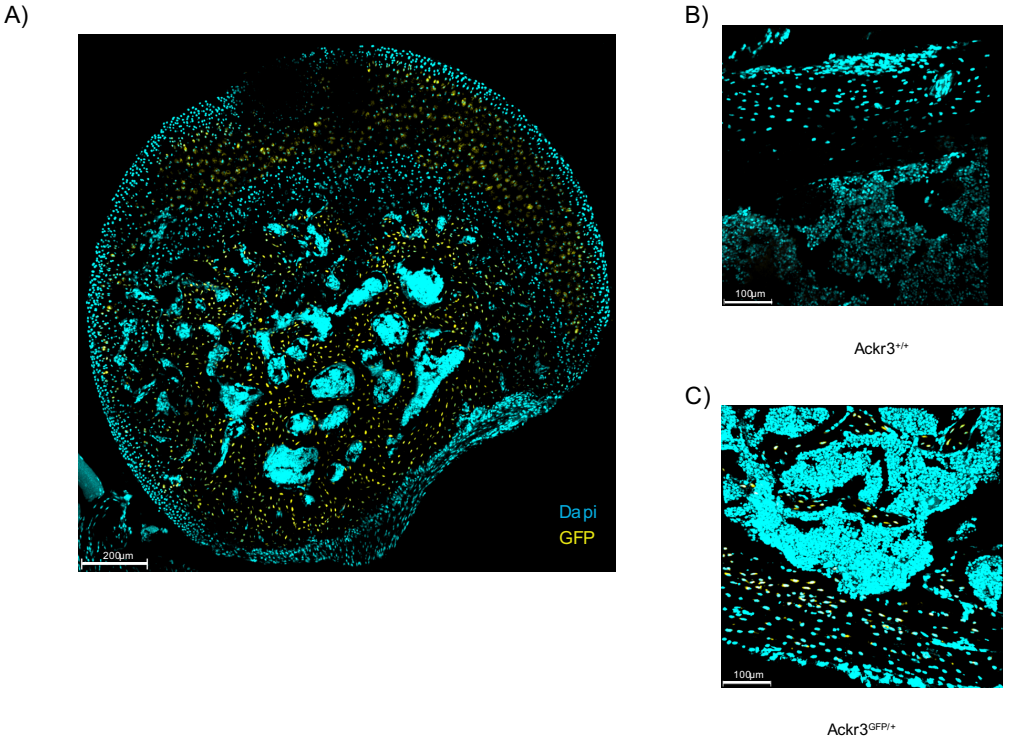

Figure 19 ACKR3 is expressed in the endosteum of murine femurs.

A) Representative immunofluorescence micrograph of transverse section of femur from *Ackr3*$^{GFP/+}$ mouse. B) Immunofluorescence of longitudinal sections of femurs from *Ackr3*$^{+/+}$ and C) *Ackr3*$^{GFP/+}$ mouse. GFP^{+} (yellow) cells and DAPI^{+} (blue) cells can be discerned.

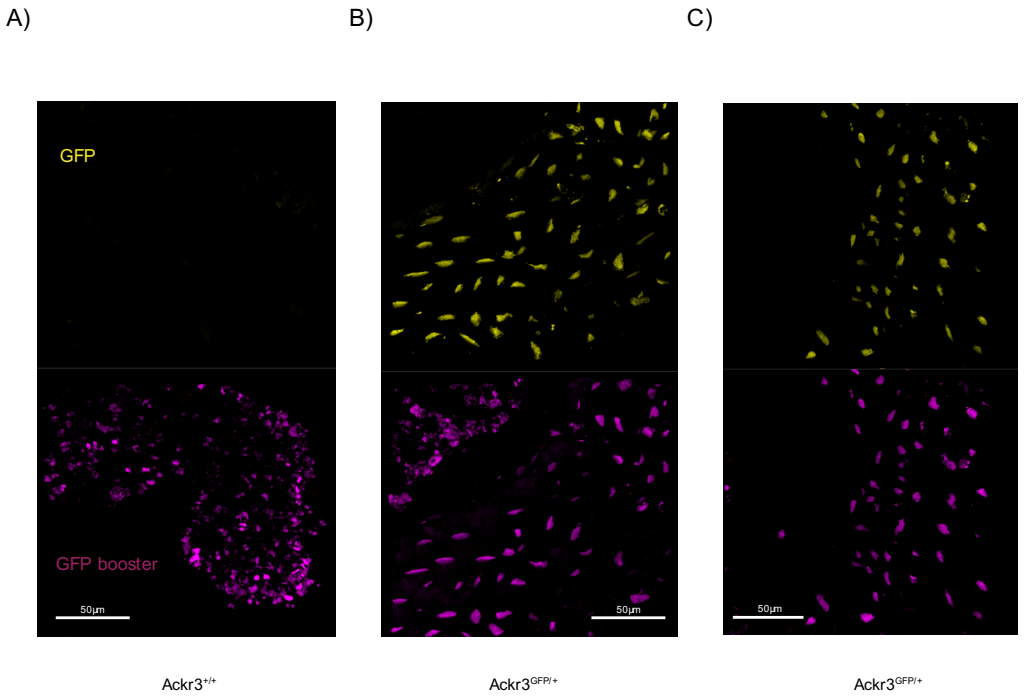

Figure 20 The GFP signal on endosteal cells is specific.
Representative immunofluorescence figure of longitudinal sections of femurs from A) *Ackr3*$^{+/+}$, and B-C) *Ackr3*$^{GFP/+}$ mouse assessed for the presence of GFP (yellow) (upper panel), and the GFP booster (magenta) (lower panel).

The primary data obtained by immunofluorescence did not indicate expression of ACKR3 on murine leukocytes. However, to scrutinize this hypothesis, I assessed the expression of the atypical chemokine receptor in BM leukocytes and stromal cells by flow cytometry. As shown in Figure 21A, BM HSC and progenitor cells did not significantly express ACKR3. Interestingly, BM plasma cells, identified by the expression of CD138, expressed high levels of ACKR3. BM stromal cells, aortic endothelial cells (AEC) and sinusoid endothelial cells (SEC), as well as fibroblasts were negative for ACKR3 expression. Similarly, in circulation, myeloid and lymphoid mature cells were ACKR3^{-} (Figure 21B). In spleen only marginal B cells were ACKR3^{+} (Figure 21C), in accordance with previously described findings (Radice et al., 2020), whereas splenic myeloid cells did not express the receptor. In summary, our results revealed that ACKR3 expression within the BM is restricted to the endosteal cells and plasma cells, while HSPC do not express the receptor.

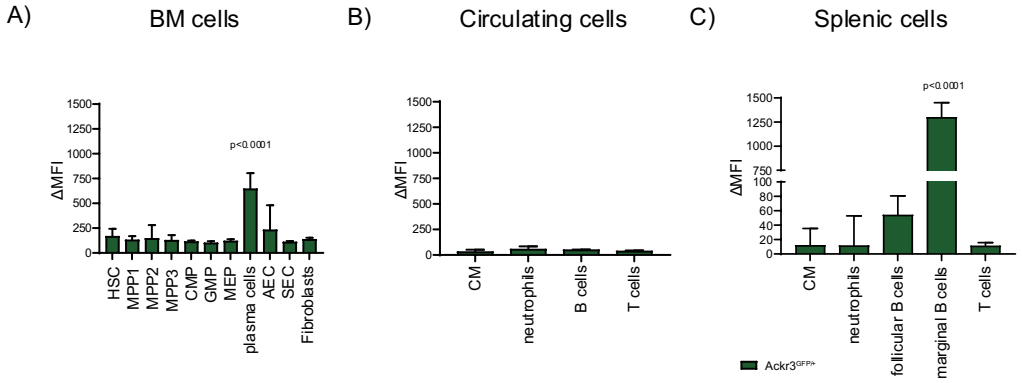

Figure 21 Expression pattern of ACKR3 on hematopoietic cells and BM stromal cells.
Expression of ACKR3 on A) BM leukocytes and stromal cells, B) circulating blood cells, C) splenic cells in *Ackr3*$^{GFP/+}$ (green) mice, assessed by flow cytometry. Data are shown as mean ± SEM. A-C) The expression of the *Ackr3*$^{GFP/+}$ mice was normalized to that of the control *Ackr3*$^{+/+}$ (n=3-5, in 2 independent experiments). Factorial ANOVA, with Šidák *post hoc* test.

Next, I asked whether a chronic inflammatory condition such atherosclerosis could induce ACKR3 expression. Mice which are deficient for the Apolipoprotein (Apo) E spontaneously display hypercholesterolemia, changes in hematopoiesis and as a consequence develop atherosclerotic plaques in the arterial wall (Zhang et al., 1992). I, thus, assessed the expression of ACKR3 in different tissues of the ApoE-deficient mice. In accordance with my previous observations in steady state, I found that ACKR3 was also expressed in the endosteal cells of *Apoe*$^{-/-}$ *Ackr3*$^{GFP/+}$ mice (Figure 22A). Interestingly, the expression of ACKR3 on endosteal cells was not restricted in femurs, as ACKR3 expression marked the endosteum of tibias (Figure 22B) and the endosteal cells of spines (Figure 22C). To assess the expression of ACKR3 on hematopoietic cells under these conditions, leukocytes from BM, blood, and spleen were assessed by flow cytometry for the GFP expression. No GFP signal was detected in any tested BM hematopoietic cells of these mice (Figure 23A). Circulating myeloid and lymphoid cells did not express ACKR3 either (Figure 23B). On the contrary, marginal B cells remained ACKR3^{+} under low grade inflammatory conditions (Figure 23C). To summarize, these data suggest that ACKR3 is a gene characterizing the endosteal cells in murine tissues, whereas murine HSPC do not express ACKR3 under steady state and low-grade inflammatory conditions.

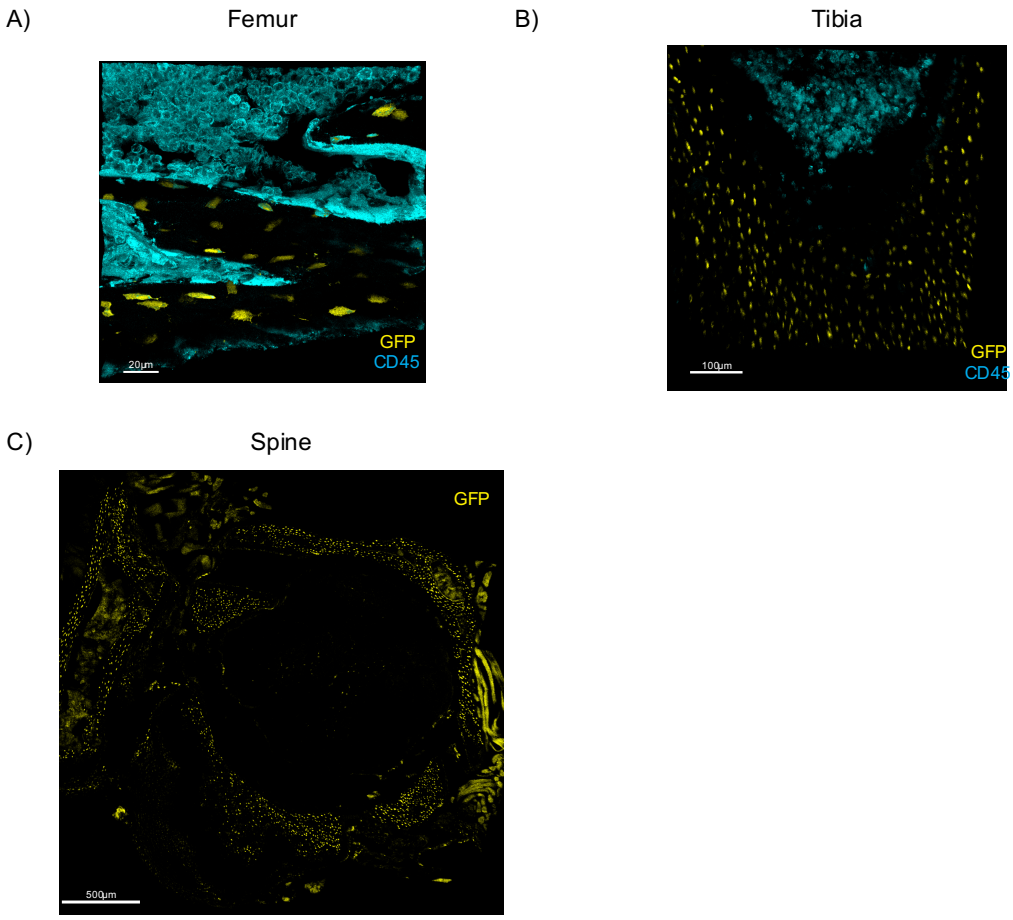

Figure 22 ACKR3 is expressed in the endosteum of bone tissues in Apoe$^{-/-}$ mice.
Representative immunofluorescence micrograph of GFP^{+} (yellow) cells and DAPI^{+} (blue) cells in longitudinal sections of A) femur and B) tibia from *Apoe*$^{-/-}$- *Ackr3*$^{GFP/+}$ mouse. C) Immunofluorescence micrograph of transverse section of spine from *Apoe*$^{-/-}$- *Ackr3*$^{GFP/+}$ mouse.

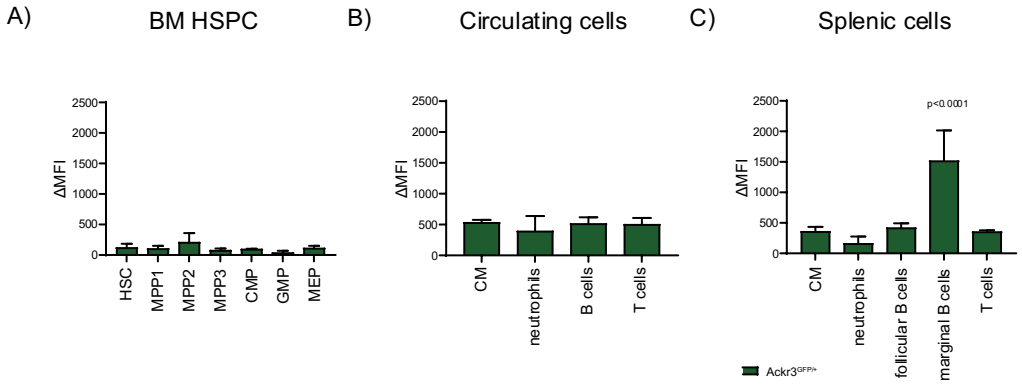

Figure 23 Expression pattern of ACKR3 on hematopoietic cells in Apoe$^{-/-}$ mice.

Expression of ACKR3 on A) BM hematopoietic cells, B) circulating blood cells, C) splenic cells in *Apoe*$^{-/-}$-*Ackr3*$^{GFP/+}$ (green) mice, assessed by flow cytometry. Data are shown as mean ± SEM. A-C) The expression of the *Ackr3*$^{GFP/+}$ mice was normalized to that of the control *Ackr3*$^{+/+}$ (n=2-5, in 2 independent experiments). Factorial ANOVA, with Šidák *post hoc* test.

4.A.2 Investigation of the role of ACKR3 in BM cell maintenance in steady state and in low grade inflammatory conditions

The expression of ACKR3 on BM stromal cells prompted me to investigate the role of ACKR3 on hematopoiesis. Since *Ackr3*$^{-/-}$ mice are 70% lethal (Sierro et al 2007), I backcrossed *Ackr3*$^{flox/flox}$ mice with the tamoxifen inducible *Ubc-Cre*^{ERT2} mouse model, to generate *Ubc-Cre*^{ERT2} *Ackr3*$^{flox/flox}$ mice that I named *Ubc-Ackr3*$^{-/-}$ mice here and in the rest of the thesis. Consequently, administration of tamoxifen results in the excision of the *Ackr3* gene in all cells. Mice were sacrificed 3 weeks after the initial tamoxifen injections, genomic DNA was isolated from murine tails and an end point PCR was performed to assess *Ackr3* deletion. As shown in Figure 24A, in the *Ubc-Ackr3*$^{-/-}$ mice the *Ackr3* gene has been excised and the PCR product is of lower molecular weight (approximately 300bp) compared to the control *Ackr3*$^{flox/flox}$ mice (1500bp). In addition, since marginal B cells exhibited distinct ACKR3 expression, I evaluated the presence of ACKR3 by flow cytometry, using a specific anti-ACKR3 antibody (clone 11G8). As shown in Figure 24B the expression of ACKR3 on marginal B cells was reduced approximately by >50% in the *Ubc-Ackr3*$^{-/-}$ mice, validating the efficiency of the deletion in the mouse model.

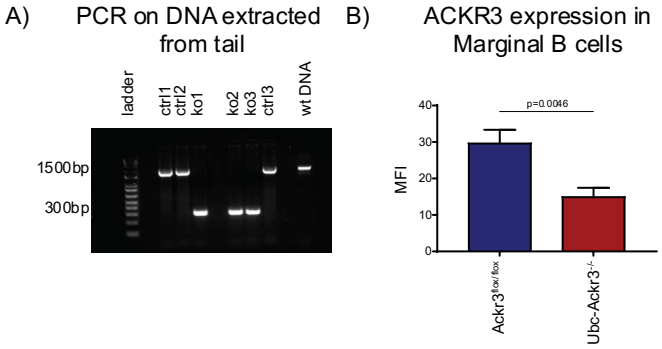

Figure 24 Validation of the ACKR3 deletion in *Ubc-Ackr3*$^{-/-}$ mice.
A) Representative gel with the PCR products on the *Ackr3* gene in 3 *Ackr3*$^{flox/flox}$ (ctrl) and 3 *Ubc-Ackr3*$^{-/-}$ (ko) mice. DNA from *Apoe*$^{-/-}$ mouse (wt DNA) was also included as additional control. B) Expression of ACKR3 on marginal B cells, as assessed by flow cytometry using the anti-ACKR3 antibody 11G8 in *Ackr3*$^{flox/flox}$ (blue) and *Ubc-Ackr3*$^{-/-}$ (red) mice (n=3). Data are shown as mean ± SEM. Unpaired *t* test.

Next, I asked whether ACKR3 affects the maintenance of HSCs, the cornerstone of hematopoiesis. To this end, I first assessed HSC metabolism, by measuring the intracellular accumulation of ROS using the fluorescent dye DHR 123. HSCs in *Ubc-Ackr3*$^{-/-}$ mice exhibited a 50% increase of ROS

content compared to the respective *ACKR3*$^{flox/flox}$ mice (Figure 25A). This effect was not observed in any other of the HSPC subsets. I, thus, wondered, whether this increase in the levels of ROS was associated with an accumulation of mitochondria in this population. To determine the mitochondrial content of HSPCs after ACKR3 deletion, BM cells were stained with the mitochondrial fluorescent label MitoTracker. Nevertheless, as shown in Figure 25B, HSC and progenitor cells from *Ubc-Ackr3*$^{-/-}$ mice did not contain more mitochondria compared to control group. Because the metabolic state and the ROS concentration in HSCs (Ito et al., 2006, Rodrigues-Moreira et al., 2017, Pilo and Angelucci, 2018) has been associated with cell quiescence, I then assessed the apoptosis and the proliferation rate of HSPC in *Ubc-Ackr3*$^{-/-}$ mice. To assess cell apoptosis, I treated BM HSPC with a fluorescently labeled substrate for caspase 3 and 7. However, the accumulation of ROS in HSCs did not result in increased apoptosis, as the percentage of Caspase^{+} cells was comparable between the two groups (Figure 25C). In order to assess cell proliferation, HSPC cells were stained intracellularly for the nuclear protein Ki67. Interestingly, there was a significant decrease on the quiescent Ki67^{-} cells in HSC, MPP1 and MPP3 populations in *Ubc-Ackr3*$^{-/-}$ mice. Accordingly, the percentage of proliferative Ki67^{+} HSC and MPP1 cells was approximately double in mice lacking ACKR3 (Figure 25D-F). The proliferation of the subpopulation MPP2 was not assessed, due to the low number of cells.

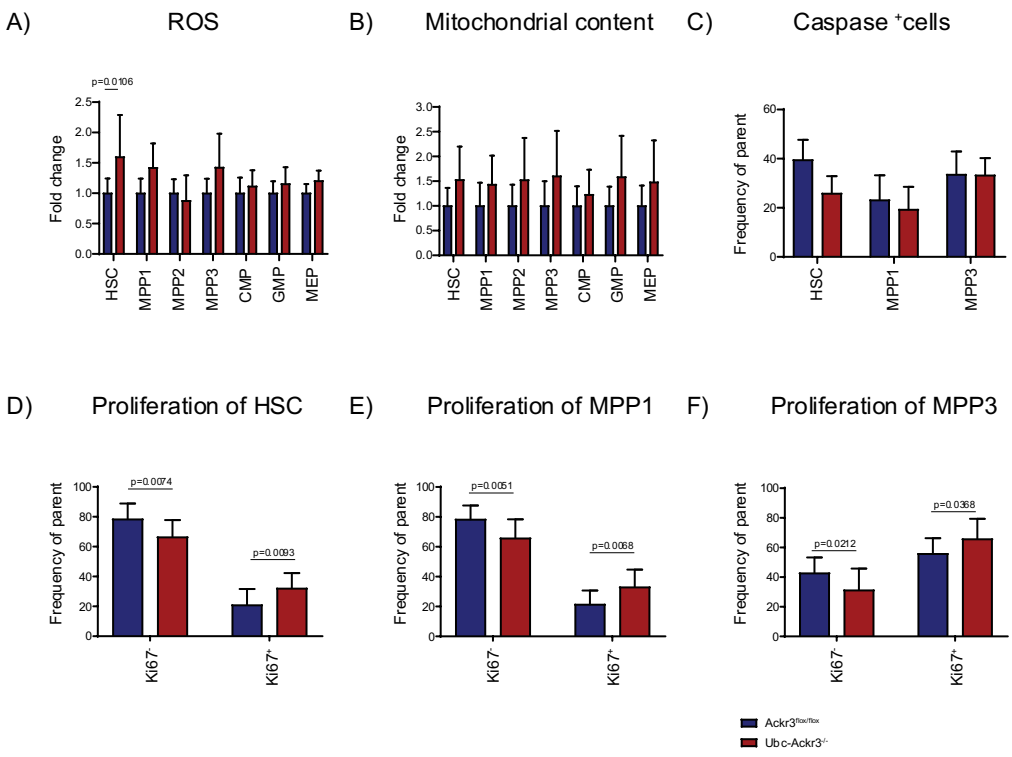

Figure 25 ACKR3 regulates ROS accumulation and HSC quiescence.
A) Intracellular ROS levels on HSPC in *Ackr3*$^{flox/flox}$ (blue) and *Ubc-Ackr3*$^{-/-}$ (red) mice (n=7, in 2 independent experiments). B) Mitochondrial content of HSPC (n=7, in 2 independent experiments). C) Percentage of Caspase^{+} HSPCs (n=6-7, in 2 independent experiments). D) Frequency of Ki67^{-} and Ki67^{+} cells for the

assessment of cellular proliferation in HSC, E) MPP1, F) MPP3 cells (n=12-16, in 4 independent experiments). Data are shown as mean ± SEM. A-B) MFI values of *Ubc-Ackr3*$^{-/-}$ cells were normalized to control *Ackr3*$^{flox/flox}$ cells of each independent experiment. A-C) 2way ANOVA, with Šidák *post hoc* test. D-F) Multiple unpaired *t* tests, with 5% FDR correction according to Benjamini, Hochberg step up approach.

The aberrant proliferation observed after the deletion of ACKR3 prompted me to hypothesize a deficient HSC differentiation towards mature cells. To this end, enriched LSK cells were plated in methylcellulose matrix and the number of colonies formed was quantified at day 7. The number of colonies produced did not significantly decrease in the *Ubc-Ackr3*$^{-/-}$ mice, as LSK cells produced an average of 33 colonies, in comparison to the 54 colonies deriving from the control mice (Figure 26A). Moreover, when assessing the number of cells produced in the colonies by flow cytometry, there was no difference between the two groups (Figure 26B).

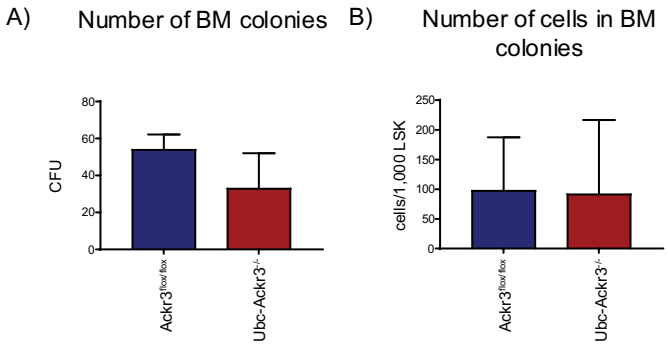

Figure 26 ACKR3 does not affect LSK differentiation.
A) Quantification of colonies formed by LSK cells from control *Ackr3*$^{flox/flox}$ (blue) and *Ubc-Ackr3*$^{-/-}$ (red) mice (n=3). B) Number of cells produced in the colonies, assessed by flow cytometry (n=5-6, in 2 independent experiments). Data are shown as mean ± SEM. A-B) Unpaired *t* test.

In accordance with the *ex vivo* data on LSK differentiation, ACKR3 deletion did not drastically affect hematopoietic cell production. In particular, the total BM cellularity in control and *Ubc-Ackr3*$^{-/-}$ mice was comparable, as assessed by flow cytometry (Figure 27A). Additionally, the number of BM HSPC remained unaltered (Figure 27B). Accordingly, no changes were observed in the counts of mature myeloid, erythroid as well as B cells in the BM (Figure 27C). Thus, our data suggest a role for ACKR3 in the maintenance of HSPC under low oxidative conditions and quiescent. Nevertheless, the receptor does not affect the HSC potency to differentiate into mature cells in steady state conditions.

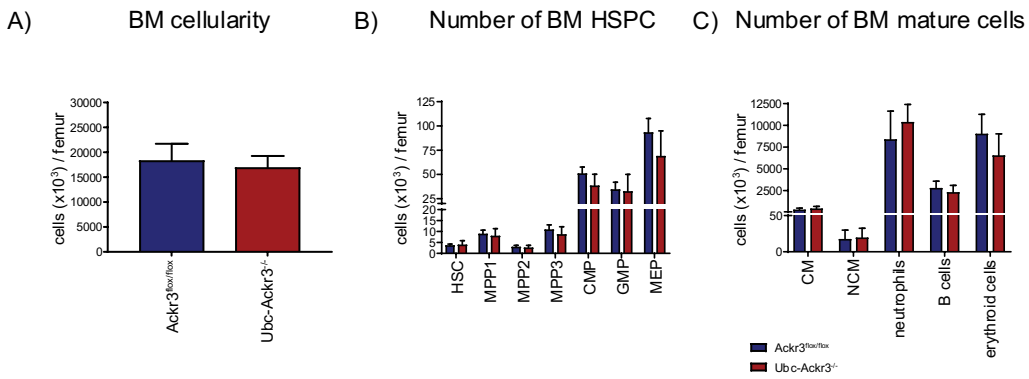

Figure 27 ACKR3 deletion does not affect BM cell production.
A) Quantification of total BM cells in *Ackr3$^{flox/flox}$* (blue) and *Ubc-Ackr3$^{-/-}$* (red) mice (n=8-11, in 2 independent experiments). B) Quantification of BM HSPC cells (n=10-11, in 3 independent experiments) and C) BM mature myeloid and lymphoid cells (n=6-10, in 2 independent experiments), assessed by flow cytometry. Data are shown as mean ± SEM. A) Unpaired Student´s *t* test. B-C) 2-way ANOVA, with Šidák *post hoc* test.

4.A.3 Identification of the ACKR3-related mechanisms in the BM

To elucidate the mechanism by which ACKR3 affects BM HSPC metabolism, I screened the presence of cytokines that are known to regulate HSC biology, in the BM supernatant of *Ubc-Ackr3$^{-/-}$* mice. Out of the 13 cytokines of the LEGENDplex assay, 10 were detectable in the samples. Nevertheless, no differences were observed between the two groups (Figure 28). Interestingly, the concentration of the well described ligand of ACKR3, the chemokine CXCL12, remained unaltered in the BM supernatant after ACKR3 depletion.

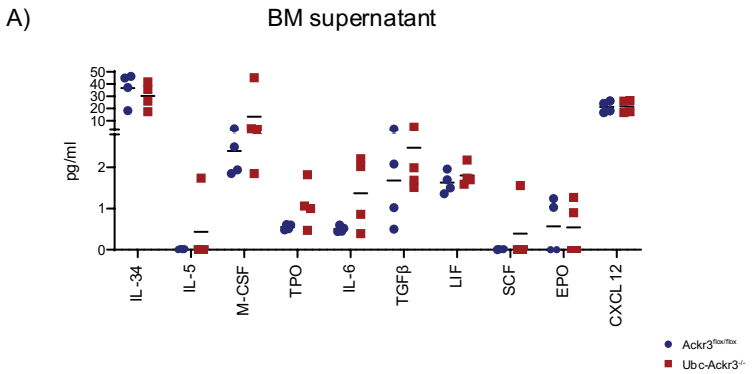

Figure 28 ACKR3 deletion does not alter the proteome of the BM supernatant.
A) LEGENDplex assay for the quantification of 10 cytokines in the BM supernatant in *Ackr3$^{flox/flox}$* (blue) and *Ubc-Ackr3$^{-/-}$* (red) mice (n=3). Data are shown as individual values with mean. Multiple *t* test, with 5% FDR correction according to Benjamini, Hochberg step up approach.

To determine whether ACKR3 maintains HSC quiescence via CXCL12, I evaluated the oxidative status of HSCs and cell proliferation in CXCL12 knock-out (CXCL12$^{-/-}$) mice. Due to the lethality of the global KO (Nagasawa et al., 1996), I utilized an inducible *Ubc-Cxcl12*$^{-/-}$ mouse model, by crossing *Cxcl12*$^{flox/flox}$ mice with the *Ubc-Cre*^{ERT2} mice. As control, *Cxcl12*$^{flox/flox}$ mice were used. Mice were harvested 2 months after the initial tamoxifen injection and the CXCL12 concentration was assessed in both BM and circulation. As shown in Figure 29A-B, the two main isoforms of CXCL12 in BM, the CXCL12α and CXCL12β were 6 times and 4 times respectively decreased in the BM supernatant of *Ubc-Cxcl12*$^{-/-}$ mice compared to control mice. In addition, circulating CXCL12α exhibited also an approximate 10-fold reduction in the plasma of the *Ubc-Cxcl12*$^{-/-}$ mice (Figure 29C), and, thus, I safely concluded that CXCL12 was massively reduced in this mouse model and thus could be used for further experiment.

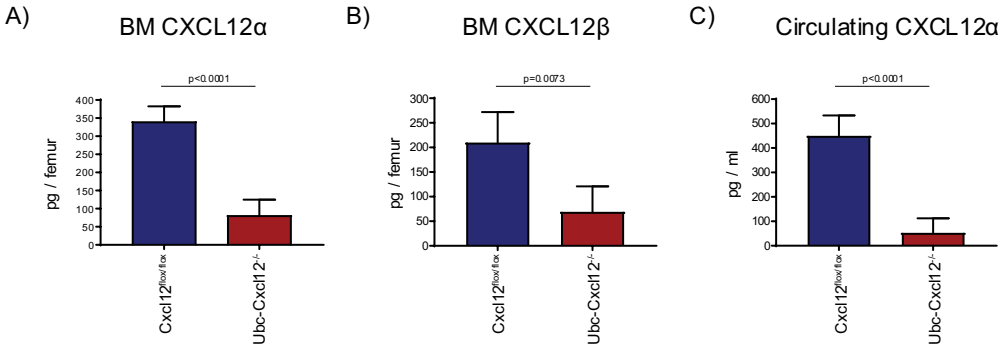

Figure 29 CXCL12 is adequately depleted in *Ubc-Cxcl12*$^{-/-}$ mice.
ELISA for A) CXCL12α (n=7, in 3 independent experiments) and B) CXCL12β (n=4-5, in 2 independent experiments) in BM supernatant of *Cxcl12*$^{flox/flox}$ (blue) and *Ubc-Cxcl12*$^{-/-}$ (red) mice. C) ELISA for CXCL12a in plasma (n=7, in 3 independent experiments). Data are shown as mean ± SEM. A-C) Unpaired *t* test.

Interestingly, the depletion of CXCL12 increased the ROS content in HSCs by approximately 40% (Figure 30A) and induced the intracellular accumulation of mitochondria. *Ubc-Cxcl12*$^{-/-}$ mice exhibited a 0.8-fold increase in the mitochondrial content of HSCs (Figure 30B). As expected, this increase in both ROS content and mitochondrial mass was followed by enhanced proliferation in HSCs (Figure 31A), MPP1 (Figure 31B) and MPP3 cells (Figure 31C). In summary, these data revealed that CXCL12 mediates the regulation of the oxidative status of HSC, and consequently HSPC quiescence.

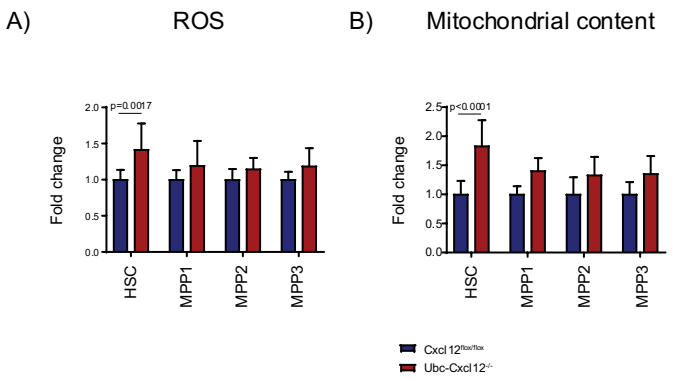

Figure 30 CXCL12 regulates ROS levels and the mitochondrial content on HSCs.
A) Intracellular ROS levels on HSPC in *Cxcl12*$^{flox/flox}$ (blue) and *Ubc-Cxcl12*$^{-/-}$ (red) mice (n=9, in 3 independent experiments). B) Mitochondrial content of HSPC (n=6, in 2 independent experiments). Data are shown as mean ± SEM. A-B) 2-way ANOVA, with Šidák *post hoc* test.

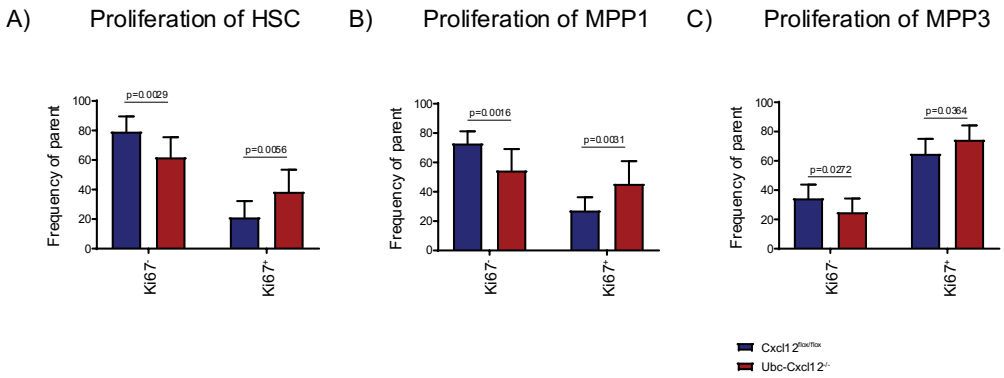

Figure 31 CXCL12 maintains HSPC quiescent.
A) Frequency of Ki67^{-} and Ki67^{+} cells for the assessment of cellular proliferation in HSC, B) MPP1, C) MPP3 cells in *Cxcl12*$^{flox/flox}$ (blue) and *Ubc-Cxcl12*$^{-/-}$ (red) mice (n=11, in 4 independent experiments). A-C) Data are shown as mean ± SEM. Multiple unpaired *t* tests, with 5% FDR correction according to Benjamini, Hochberg step up approach.

MIF has been described as an alternative ligand of ACKR3 (Alampour-Rajabi et al., 2015), thus *Mif*$^{-/-}$ mice were also employed to evaluate whether MIF affects HSC metabolism similarly to ACKR3 ko and CXCL12 ko mice. However, absence of MIF did not significantly alter the number of HSPC cells in the BM (Figure 32A). In addition, the concentration of ROS (Figure 32B), and the mitochondrial content (Figure 32C) of HSC and MPP cells did not significantly change in *Mif*$^{-/-}$ mice. In addition, the cell proliferative rate remained also at levels comparable to the steady state mice in both HSCs (Figure 32D), MPP1 (Figure 32E) and MPP3 cells (Figure 32F). Together these results indicate that despite the described role of ACKR3 as scavenging receptor, depletion of the

receptor does not significantly alter the CXCL12 concentration in the BM. Nevertheless, depletion of CXCL12 induces an oxidative profile on HSCs, and enhances cell proliferation, phenocopying the effects observed in *Ubc-Ackr3*$^{-/-}$ mice. On the contrary, deletion of MIF does not affect HSC proliferation, hence, suggesting that ACKR3 maintains HSC quiescence mainly via CXCL12.

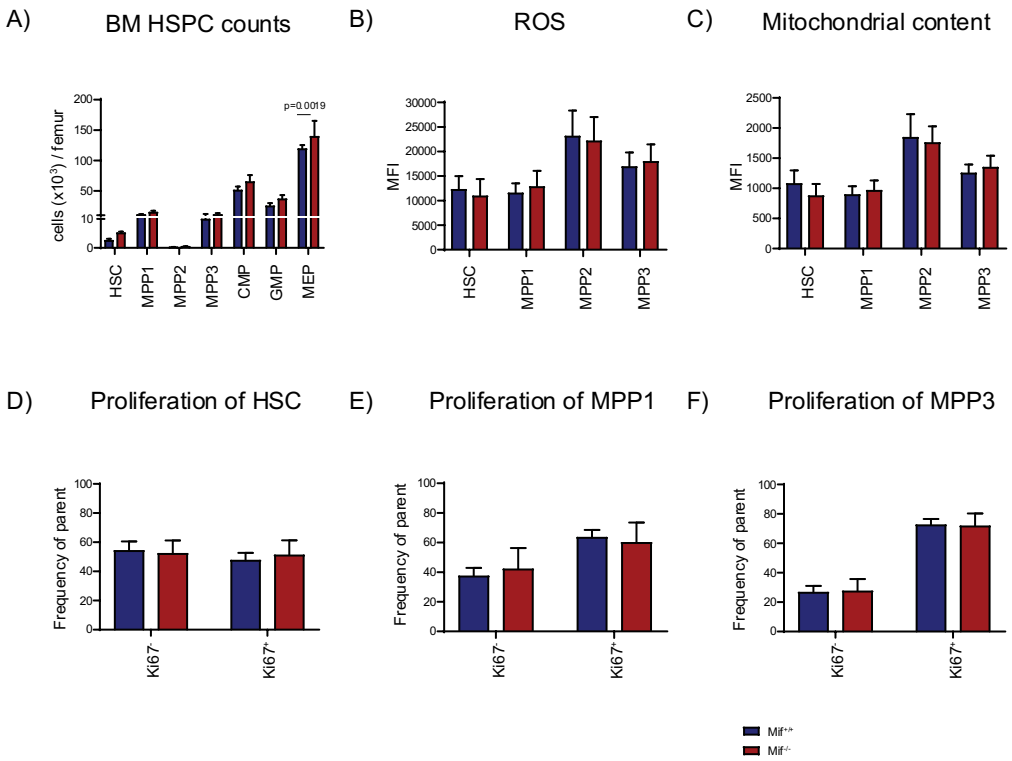

Figure 32 MIF does not regulate HSC quiescence.
A) Number of HSPC cells in the BM of *Mif*$^{+/+}$ (blue) and *Mif*$^{-/-}$ (red) mice (n=5), as assessed by flow cytometry. B) Assessment of intracellular ROS levels on HSPC (n=4-5). C) Mitochondrial content of HSPC (n=4-5). D) Frequency of Ki67$^-$ and Ki67$^+$ cells for the assessment of cellular proliferation in HSC, E) MPP1, and F) MPP3 cells (n=5). Data are shown as mean ± SEM. A-C) 2-way ANOVA, with Šidák *post hoc* test. D-F) Multiple unpaired *t* tests, with 5% FDR correction according to Benjamini, Hochberg step up approach.

4.A.4 Evaluation of the role of ACKR3 in BM cell reconstitution

The phenotypic changes in HSC metabolism after depletion of the ACKR3 prompted me to investigate the biological relevance of these changes in a model of emergency hematopoiesis. To this end, I employed 5 Fluorouracil (5FU), a cytotoxic drug used in clinic as a chemotherapeutic agent that depletes proliferative cells (Heidelberger et al., 1957, Casale and Crane, 2020). To assess whether myeloablation induces the expression of ACKR3 on hematopoietic cells, 5FU was, firstly, administered in *Ackr3*$^{+/+}$ and *Ackr3*$^{GFP/+}$ mice and ACKR3 expression was assessed 4, 10 and 21 days later.

The progression of cell depletion after 5FU administration was similar in control and *Ackr3*$^{GFP/+}$ mice and no significant differences were observed between the two groups. At day 4 BM monocytes were greatly reduced in both groups, as classical monocytes (CM) reached an average of approximately 29 cells in the femur of 5FU-treated *Ackr3*$^{+/+}$ mice and 65 cells in the 5FU-treated *Ackr3*$^{GFP/+}$ mice, respectively (Figure 33A). Similarly, non-classical monocytes (NCM) decreased approximately 30 times after 5FU treatment in the control mice, and 23 times in the 5FU-*Ackr3*$^{GFP/+}$ mice. The effect of the agent on neutrophils was less pronounced. Finally, erythroid cells and BM B cells were not significantly depleted (Figure 33A). In accordance with the BM cell depletion, an average of 247 circulating CM was measured in 1ml of peripheral blood in 5FU-treated *Ackr3*$^{+/+}$ mice (Figure 33B). The depletion was even more pronounced in the 5FU-treated *Ackr3*$^{GFP/+}$ mice as an average of 89 circulating CM was measured in 1ml of blood, which corresponds to a 10-fold drop compared to the steady state *Ackr3*$^{GFP/+}$ mice (Figure 33B). Circulating neutrophils, B, and T cells were not significantly depleted after 5FU treatment (Figure 33B). The ablation pattern was similar in spleen, where the number of CM and NCM was extremely low. Thus, the total number of CD11b^{+}CD115^{+} cells was gated as the monocyte population. The number of splenic monocytes had a 13 and 30-fold decrease in the control and the *Ackr3*$^{GFP/+}$ mice respectively after the 5FU administration. Interestingly, B cells were also decreased in the *Ackr3*$^{GFP/+}$ mice after the 5FU treatment (Figure 33C). Of note, 5FU affected also the LSK and MPC cells in both groups. The cell counts of both cell types reached an average of approximately 1,000 cells/spleen, when at steady state conditions range to approximately 30,000-40,000 cells (Figure 33C). In accordance with the observations made in spleen, BM HSPC cells were also depleted at day 4 after the 5FU treatment. Figure 34A illustrates a representative figure of the BM Lin^{-} gated cells, in which it is evident that the populations of LSK and MPC cells were absent in the 5FU treated BM. Figure 34B shows the quantification of the BM LSK cell depletion, further revealing the drastic effect 5FU had on BM HSPC. Thus, day 4 after the 5FU treatment reveals the effect of the agent on hematopoietic cells. Monocytes are the cells mainly affected, although it should be noted that HSPC cells are also depleted. However, no differences were observed on the effect of 5FU between the *Ackr3*$^{+/+}$ and *Ackr3*$^{GFP/+}$ mice. Thus, our model could be used for the assessment of the ACKR3 expression under these conditions.

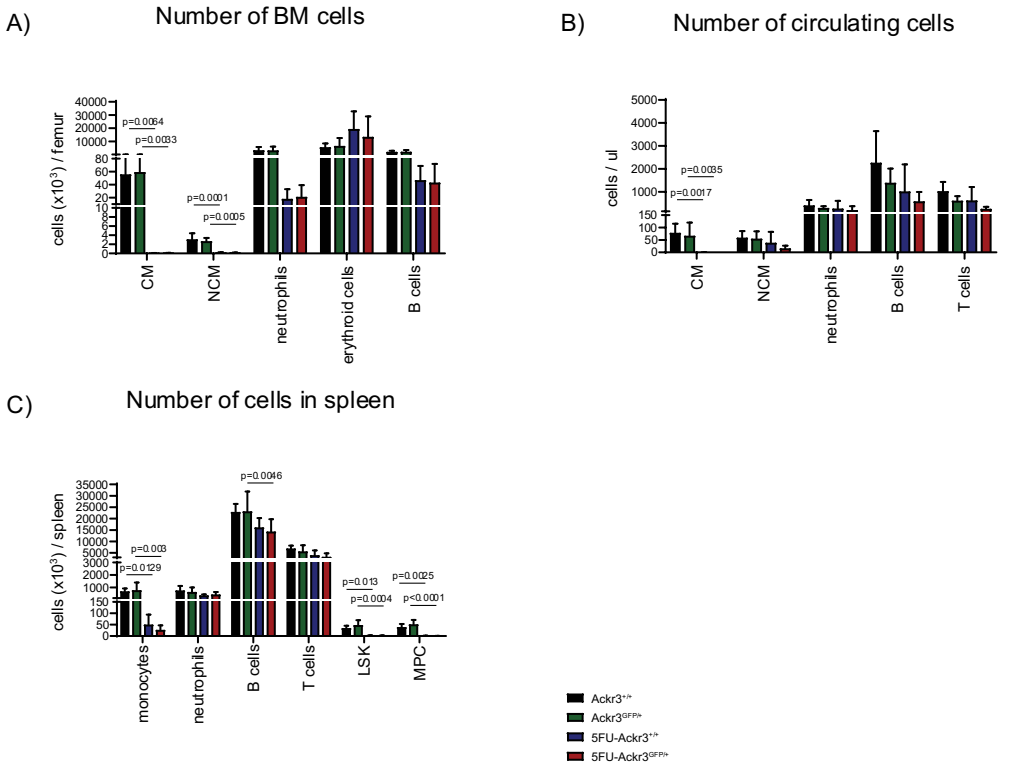

Figure 33 Administration of 5FU depletes monocytes in all tissues in control and *Ackr3*$^{GFP/+}$ mice.
A) Number of mature cells in the BM of 5FU-treated *Ackr3*$^{+/+}$ (blue) and *Ackr3*$^{GFP/+}$ (red) mice, in comparison to the steady state *Ackr3*$^{+/+}$ (black) and *Ackr3*$^{GFP/+}$ (green) mice (n=4-6, in 3 independent experiments), assessed by flow cytometry. B) Number of circulating cells (n=3-7, in 3 independent experiments). C) Number of hematopoietic cells in spleen (n=4-9, in 3 independent experiments). Data are shown as mean ± SEM. A-C) 2-way ANOVA, with Tukey *post hoc* test.

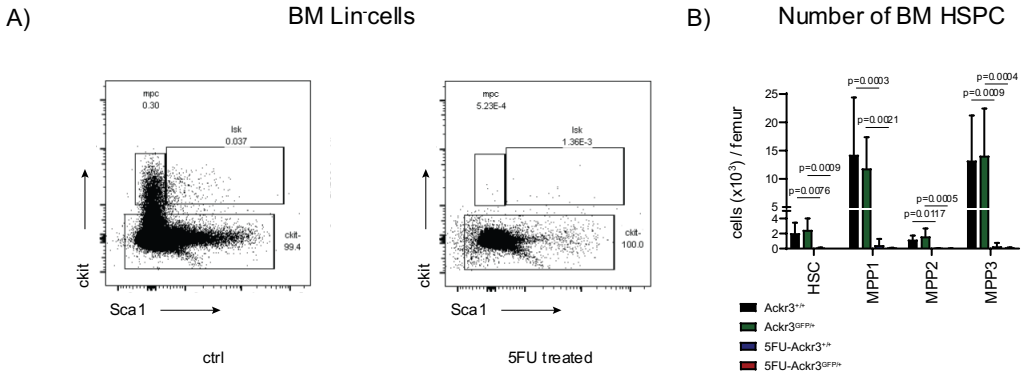

Figure 34 Administration of 5FU depletes BM HSPC in control and *Ackr3*^{GFP} mice.
A) Representative figure of flow cytometry for HSPC cells in control and 5FU treated BM. Cells have been previously gated as Lin$^-$. B) Quantification of the number of HSPC cells in the BM of 5FU treated-*Ackr3*$^{+/+}$ (blue) and 5FU treated- *Ackr3*$^{GFP/+}$ (red) mice, in comparison to the steady state *Ackr3*$^{+/+}$ (black) and

Ackr3$^{GFP/+}$ (green) mice (n=6-9, in 3 independent experiments). Data are shown as mean ± SEM. 2-way ANOVA, with Tukey *post hoc* test.

Nevertheless, despite the robust depletion of hematopoietic cells, BM leukocytes (Figure 35A) and BM stromal endothelial cells (Figure 35B) remained negative for ACKR3 expression. The expression of ACKR3 on HSCs could not be assessed, as, due to the depletion, no HSCs were acquired in the 5FU-treated *Ackr3*$^{GFP/+}$ mice (Figure 35A), as shown also in Figure 34B. To assess changes in the expression of ACKR3 on osteocytes, BM immunofluorescent pictures were acquired and the GFP signal was quantified. Figure 35C shows the average MFI value for each mouse normalized to the steady state *Ackr3*$^{GFP/+}$ mice of each individual experiment. Nevertheless, no difference was observed in the fluorescence intensity of the endosteal cells (Figure 35C). In addition, the number of ACKR3 expressing cells was evaluated, by quantifying the GFP$^+$ cells in the endosteum, and normalized to the number of cells in steady state *Ackr3*$^{GFP/+}$ mice. Similarly, the number of GFP$^+$ cells remained unaltered after the 5FU treatment (Figure 35D). Hence, 5FU treatment does not affect the expression levels of *Ackr3* endosteal cells of the BM.

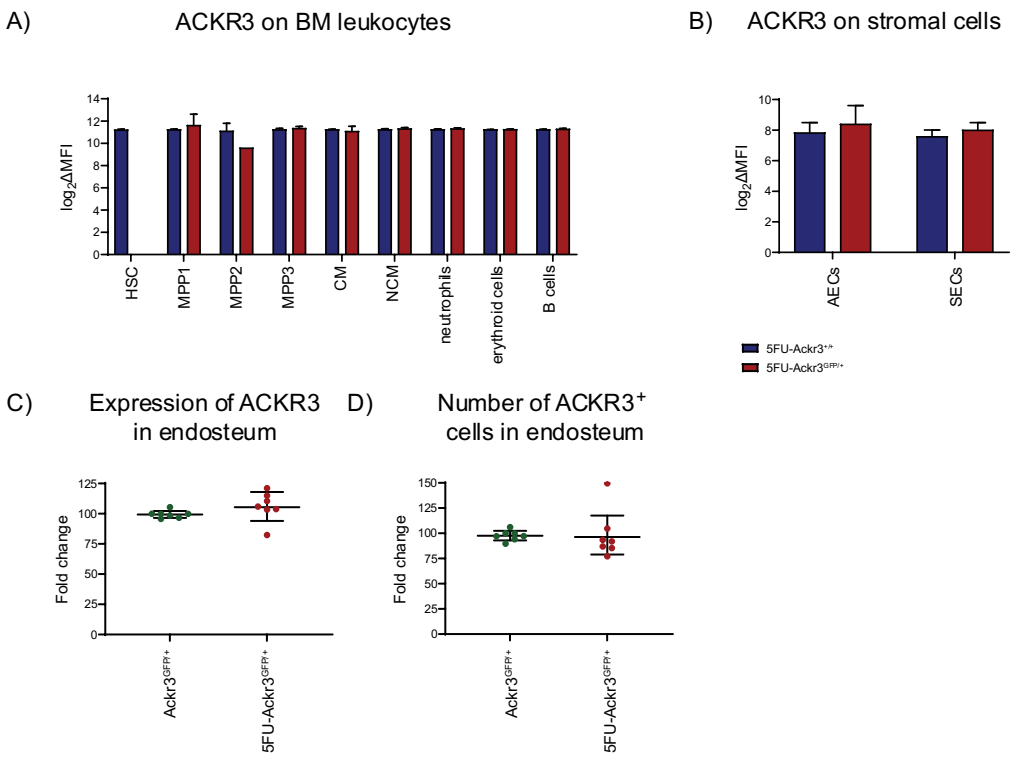

Figure 35 Myeloablation does not affect ACKR3 expression in BM leukocytes and stromal cells.
A) Expression of ACKR3 on BM leukocytes (n=1-7, in 3 independent experiments) and B) BM endothelial cells in 5FU- *Ackr3*$^{GFP/+}$ (red) mice compared to 5FU- *Ackr3*$^{+/+}$ (blue) mice (n=5, in 2 independent experiments), as assessed by flow cytometry. C) Quantification of the MFI of ACKR3 expression in BM endosteal cells (n=7, in 3 independent experiments) and D) of the number of ACKR3$^+$ endosteal cells in

5FU-*Ackr3*$^{GFP/+}$ mice compared to steady state *Ackr3*$^{GFP/+}$ (green) mice, as assessed by immunofluorescence (n=7, in 3 independent experiments). A-B) Data are shown as mean ± SEM. Mann-Whitney *U* test, with 5% FDR correction according to Benjamini, Hochberg step up approach. C-D) Data are shown as individual values with mean. Unpaired *t* test with Welch´s correction.

At day 10 after the 5FU injection, all mature cells remained drastically reduced in the BM (Figure 36A). In both groups of 5FU treated mice there was a 7-fold reduction in CM. NCM were also decreased in both 5FU treated groups. BM neutrophils were also 7 times decreased in 5FU treated *Ackr3*$^{GFP/+}$ mice (Figure 36A). In comparison to what observed at day 4, even BM B cells were significantly reduced at this time point in both groups, whereas the number of erythroid cells significantly decreased only in the *Ackr3*$^{GFP/+}$ mice (Figure 36A). Circulating CM, NCM and neutrophils remained significantly reduced in the 5FU-treated *Ackr3*$^{GFP/+}$ mice (Figure 36B). In spleen, only neutrophils exhibited a 5-fold decrease at day 10, as all other populations had reconstituted the tissue (Figure 36C). In accordance with the data on the mature cells, at day 10 after the 5FU administration, HSCs had reconstituted the BM. In fact, in both groups, there was a tendency for increased HSPC in the BM of the 5FU treated mice compared to the steady state mice, which reached statistical significance in the case of MPP2 cells (Figure 37A). In addition, the proliferation rate of HSPC cells was assessed at this time point. Nevertheless, there were not significant differences between the myeloablated and the steady state mice (Figure 19B-D), which mirrored the fact that hematopoiesis was already re-established, and the cell counts of HSC were comparable to the baseline.

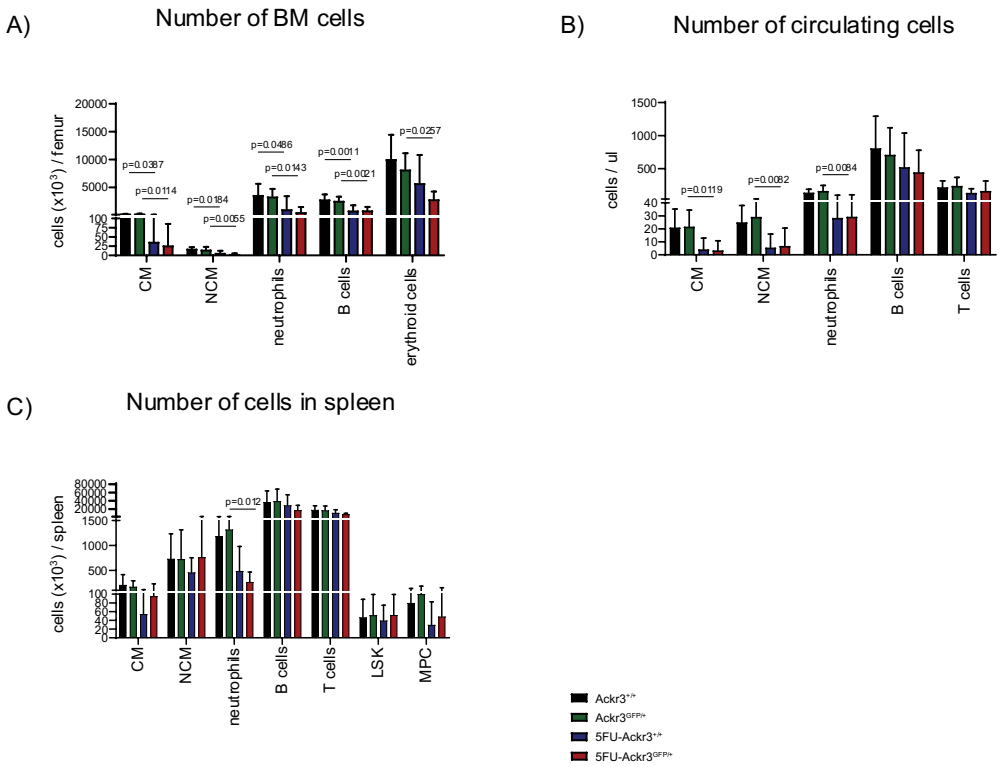

Figure 36 Mature cells have reconstituted peripheral tissues at day 10 after the 5FU administration.
A) Number of mature cells in the BM of steady state *Ackr3*$^{+/+}$ (black), *Ackr3*$^{GFP/+}$ (green) mice, 5FU-A*ckr3*$^{+/+}$ (blue) and 5FU-*Ackr3*$^{GFP/+}$ (red) mice (n=7-9, in 3 independent experiments), assessed by flow cytometry. B) Number of circulating cells (n=5-10, in 3 independent experiments). C) Number of cells in spleen (n=7-9, in 3 independent experiments). Data are shown as mean ± SEM. A-C) 2-way ANOVA, with Tukey *post hoc* test.

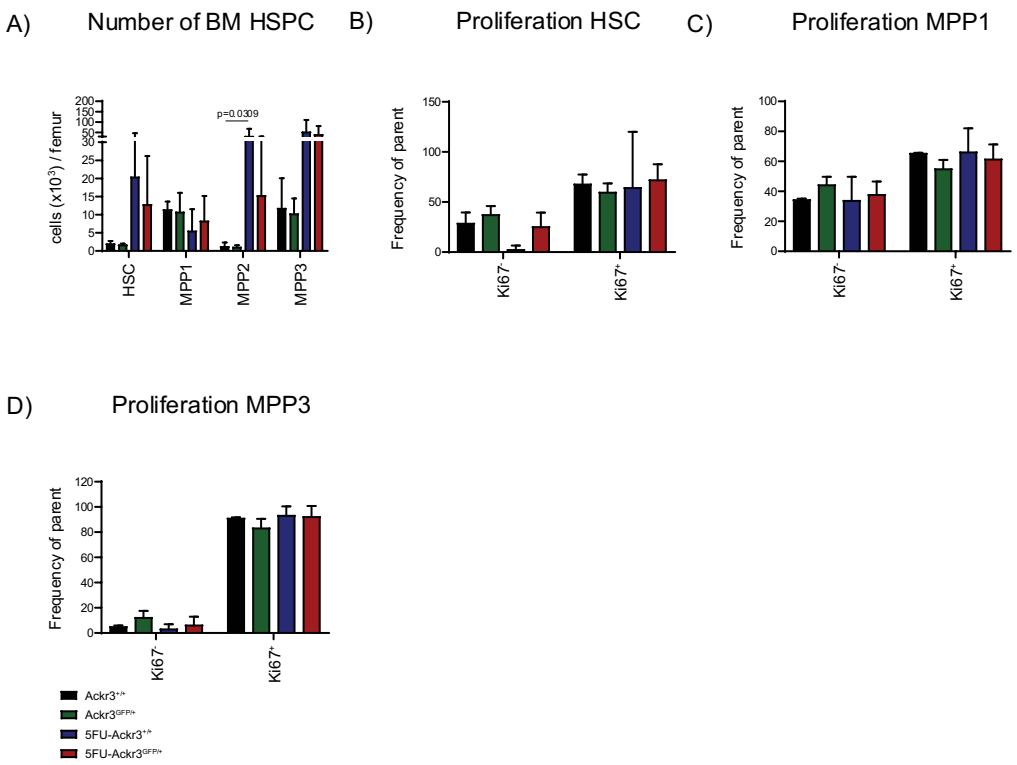

Figure 37 HSPC have reconstituted the BM at day 10 after the 5FU administration.
A) Number of HSPC in the BM of steady state *Ackr3*$^{+/+}$ (black), *Ackr3*$^{GFP/+}$ (green) mice, 5FU-*Ackr3*$^{+/+}$ (blue) and 5FU-*Ackr3*$^{GFP/+}$ (red) mice (n=7-9, in 3 independent experiments), assessed by flow cytometry. B) Frequency of quiescent Ki67^{-} and proliferating Ki67^{+} cells in HSC, C) MPP1 and D) MPP3 cells (n=2-3). Data are shown as mean ± SEM. A-D) 2-way ANOVA, with Tukey *post hoc* test.

However, similar to the previous time point examined, the reconstitution of the BM after the myeloablation did not induce the expression of ACKR3 on BM hematopoietic cells, as assessed by flow cytometry (Figure 38A). BM endothelial cells remained also ACKR3^{-} (Figure 38B). Finally, osteocytes 10d after the myeloablation were expressing ACKR3 in levels comparable to that of steady state mice, as shown by the MFI (Figure 38C) and the quantification of ACKR3^{+} cells (Figure 38D) in the endosteal part of the BM, thus suggesting that ACKR3 expression is not affected also during the reconstitution of hematopoiesis.

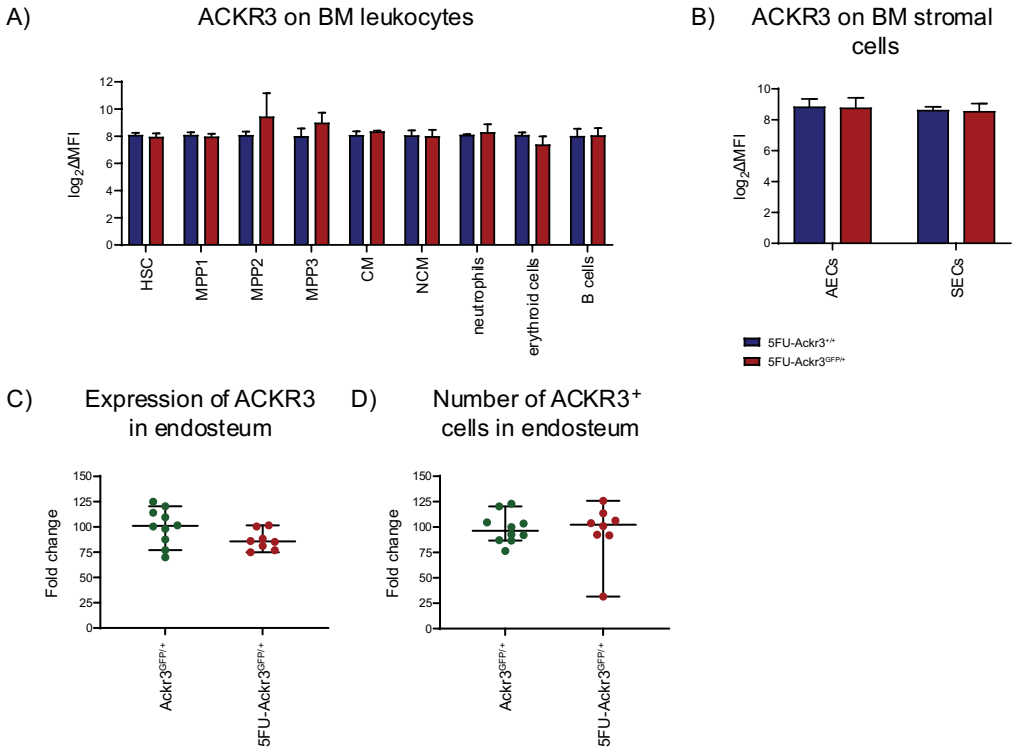

Figure 38 The expression pattern of ACKR3 remains unaltered during the reconstitution of hematopoiesis at day 10 after myeloablation.

A) Expression of ACKR3 on BM leukocytes (n=3-5, in 2 independent experiments) and B) BM endothelial cells in 5FU- *Ackr3*$^{GFP/+}$ (red) mice compared to 5FU- *Ackr3*$^{+/+}$ (blue) mice (n=5-6, in 2 independent experiments), as assessed by flow cytometry. C) Quantification of the MFI of ACKR3 expression in BM endosteal cells and D) of the number of ACKR3^{+} endosteal cells in 5FU- *Ackr3*$^{GFP/+}$ mice compared to steady state *Ackr3*$^{GFP/+}$ (green) mice, as assessed by immunofluorescence (n=8-10, in 3 independent experiments) (n=8-10, in 3 independent experiments). A-B) Data are shown as mean ± SEM. Mann-Whitney *U* test, with 5% FDR correction according to Benjamini, Hochberg step up approach. C-D) Data are shown as individual values with mean. Unpaired *t* test with Welch´s correction.

The last time point assessed after the myeloablation was the 21 days. At this time point leukocytes had fully reconstituted all tissues examined. Myeloid cells in BM (Figure 39A), blood (Figure 39B) and spleen (Figure 39C) reached the numbers observed in steady state mice. Similarly, no differences were observed in the number of HSPC between steady state and 5FU-treated mice (Figure 40A). The successful reconstitution of the BM imposed a more quiescent prolife to the HSC of the 5FU treated *Ackr3*$^{GFP/+}$ mice, compared to the steady state mice, as the population of Ki67^{-} cells increased, in contrast to the proliferative Ki67^{+} cells (Figure 40B). Although, this effect was not observed in MPP1 cells (Figure 40C), a similar effect was observed in the MPP3 population of the 5FU-treated *Ackr3*$^{+/+}$ mice. More specifically, the number of Ki67^{+} cells was approximately half compared to the steady state *Ackr3*$^{+/+}$ mice (Figure 40D).

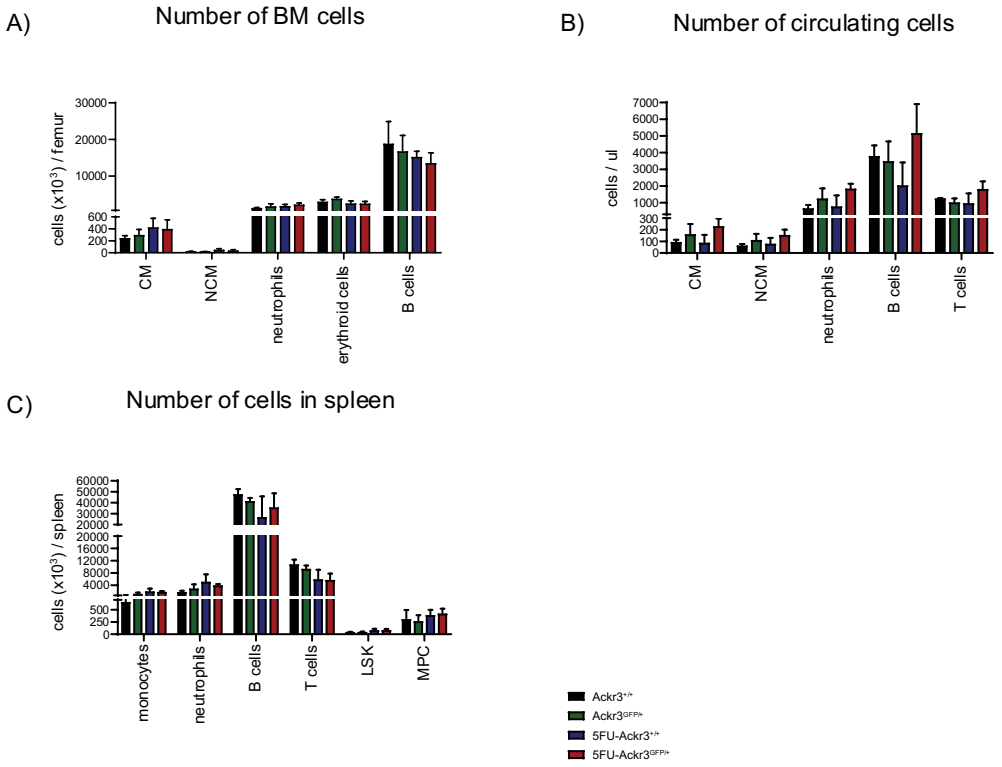

Figure 39 Full reconstitution of mature cells at day 21 after myeloablation.
A) Number of mature cells in the BM of steady state *Ackr3*$^{+/+}$ (black), *Ackr3*$^{GFP/+}$ (green) mice, 5FU-*Ackr3*$^{+/+}$ (blue) and 5FU-*Ackr3*$^{GFP/+}$ (red) mice, assessed by flow cytometry. B) Number of circulating cells. C) Number of cells in spleen. Data are shown as mean ± SEM. A-C) 2-way ANOVA, with Tukey *post hoc* test (n=3-4).

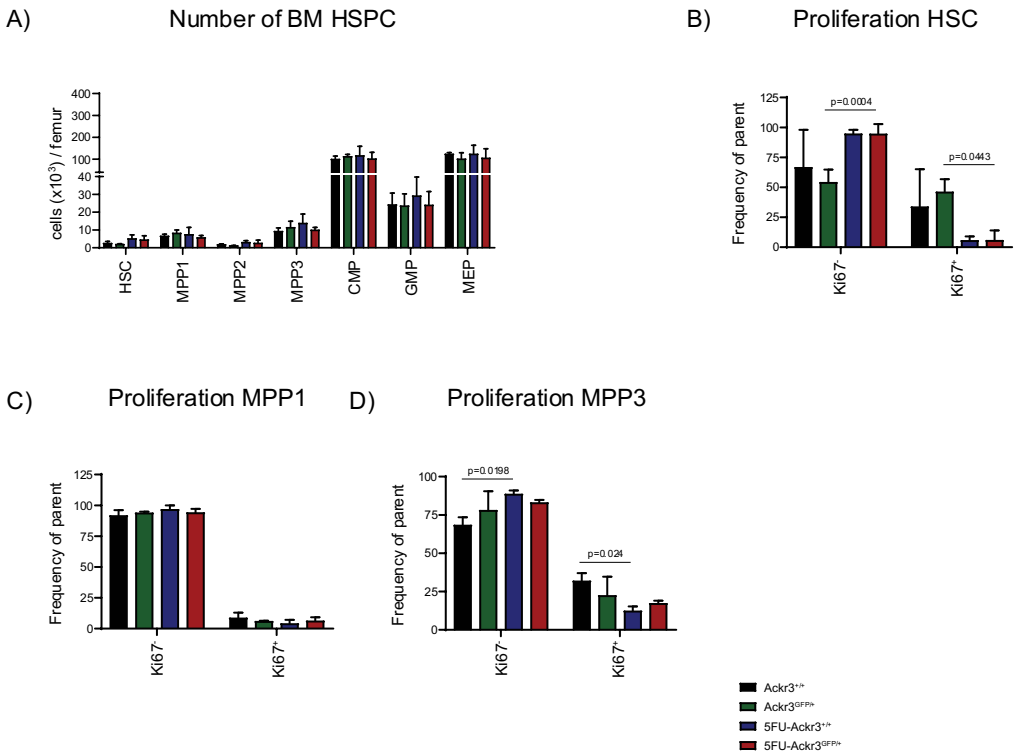

Figure 40 HSPC return to quiescence 21 days after the myeloablation.
A) Number of HSPC in the BM of steady state *Ackr3*$^{+/+}$ (black), *Ackr3*$^{GFP/+}$ (green) mice, 5FU-*Ackr3*$^{+/+}$ (blue) and 5FU-*Ackr3*$^{GFP/+}$ (red) mice (n=2-4), assessed by flow cytometry. B) Frequency of quiescent Ki67^{-} and proliferating Ki67^{+} cells in HSC, C) MPP1 and D) MPP3 cells (n=3-4). Data are shown as mean ± SEM. A-D) 2-way ANOVA, with Tukey *post hoc* test.

The expression of ACKR3 was also assessed after the complete reconstitution of hematopoiesis at day 21, as previously described. Nevertheless, BM leukocytes remained negative for ACKR3 expression at this stage, as well (Figure 41A). Likewise, no expression was noted in BM endothelial cells (Figure 41B). Similarly, the GFP signal on BM endosteal cells was equal to that of steady state mice (Figure 41C) and the number of GFP^{+} cells was also comparable (Figure 41D). Thus, it can be safely concluded that myeloablation by 5FU does not induce ACKR3 expression on BM HSPC at any stage of the hematopoietic reconstitution and that the expression on endosteal cells remains unaffected.

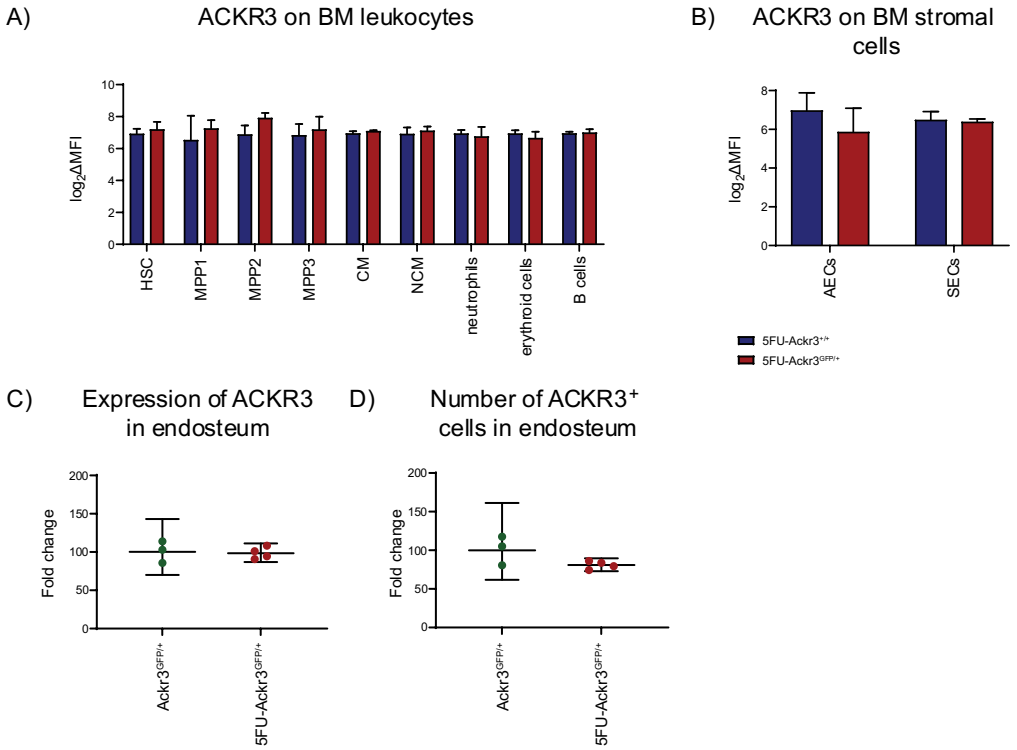

Figure 41 ACKR3 expression remains unmodified at day 21 after myeloablation.
A) Expression of ACKR3 on BM leukocytes and B) BM endothelial cells in 5FU-*Ackr3*$^{GFP/+}$ (red) mice compared to 5FU-*Ackr3*$^{+/+}$ (blue) mice (n=2-4), as assessed by flow cytometry. C) Quantification of the MFI of ACKR3 expression in BM endosteal cells and D) of the number of ACKR3^{+} endosteal cells in 5FU-*Ackr3*$^{GFP/+}$ mice compared to steady state *Ackr3*$^{GFP/+}$ (green) mice, as assessed by immunofluorescence (n=3-4). A-B) Data are shown as mean ± SEM. Mann-Whitney *U* test, with 5% FDR correction according to Benjamini, Hochberg step up approach. C-D) Data are shown as individual values with mean. Unpaired *t* test.

The expression of ACKR3 is strong in the endosteum of steady state mice and remains as such still after myeloablation. This observation prompted me to investigate the role of ACKR3 on the hematopoietic reconstitution process. To this end, I administered 5FU to the *Ubc-Ackr3*$^{-/-}$ mice. Given the data discussed above regarding the reconstitution phase at the different time points assessed, control *Ackr3*$^{flox/flox}$ and *Ubc-Ackr3*$^{-/-}$ mice were examined at days 10 and 21 after myeloablation. As shown in Figure 42, in the control group 94% of the mice survived at the later time point assessed, the 21d. On the contrary, 50% of the *Ubc-Ackr3*$^{-/-}$ mice survived to day 21. Critical day was day 10, as at that point the survival probability reduced by 23% (Figure 42). At the same time, no major differences were observed in the ablation of the monocytes between the two 5FU treated groups. Interestingly, there was a profound effect on B cells in *Ubc-Ackr3*$^{-/-}$ mice compared to the ACKR3 expressing mice, as circulating B cells (Figure 43A), and splenic B cells (Figure 43B) exhibited a 5-fold and 2-fold reduction in the *Ubc-Ackr3*$^{-/-}$ mice compared to the

5FU-treated *Ackr3*$^{flox/flox}$ mice. In the BM, there was an approximate 10-fold reduction in the number of neutrophils in the *Ubc-Ackr3*$^{-/-}$ mice, compared to the *Ackr3*$^{flox/flox}$ mice (Figure 43C). However, no significant changes were observed in the number of HSPC cells in the BM between the two groups (Figure 44A), nor in the proliferative status of these cells (Figure 44B-D). Approximately all (99.68%) HSCs in *Ubc-Ackr3*$^{-/-}$ mice were highly proliferative, as they were positive for the antigen Ki67, whereas in *Ackr3*$^{flox/flox}$ mice approximately 20% of the cells were Ki67^{-} suggesting that they had already acquired a quiescent phenotype (Figure 44B).

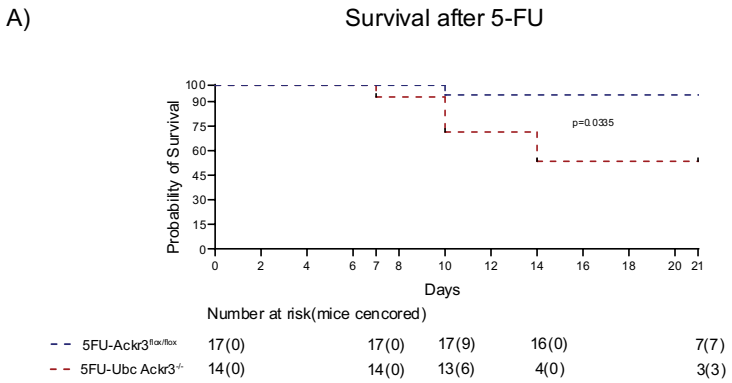

Figure 42 ACKR3 is vital for mouse survival after myeloablation.
A) Kaplan Meier Survival curve for 5FU-*Ubc-Ackr3*$^{-/-}$ mice (red) mice compared to 5FU-*Ackr3*$^{flox/flox}$ (blue) mice n=14-17, in 5 independent experiments). Data are shown as percentage of surviving mice per time point. Mantel-Cox test.

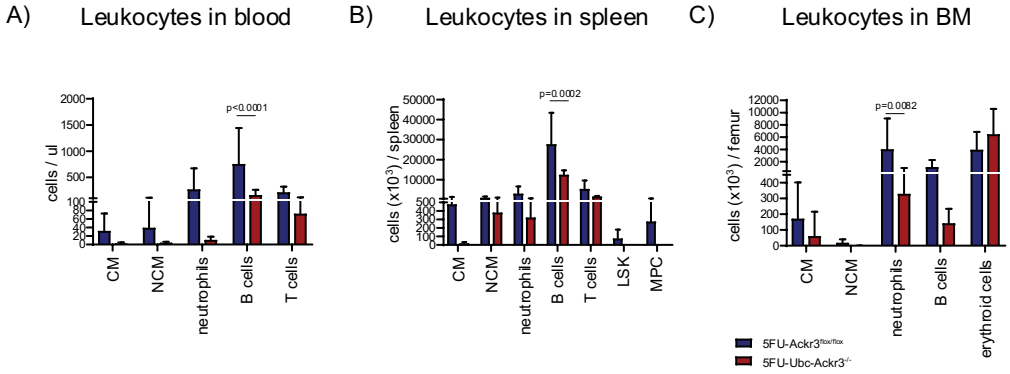

Figure 43 Reconstitution of mature leukocytes in *Ubc-Ackr3*$^{-/-}$ mice at day 10 after myeloablation.
A) Number of mature cells in the circulation of 5FU-*Ackr3*$^{flox/flox}$ (blue) and 5FU-*Ubc-Ackr3*$^{-/-}$(red) mice (n=9, in 4 independent experiments), assessed by flow cytometry. B) Number of splenic cells (n=4-6, in 2 independent experiments). C) Number of cells in BM (n=8-9, in 4 independent experiments). Data are shown as mean ± SEM. A-C) 2-way ANOVA, with Šidák *post hoc* test.

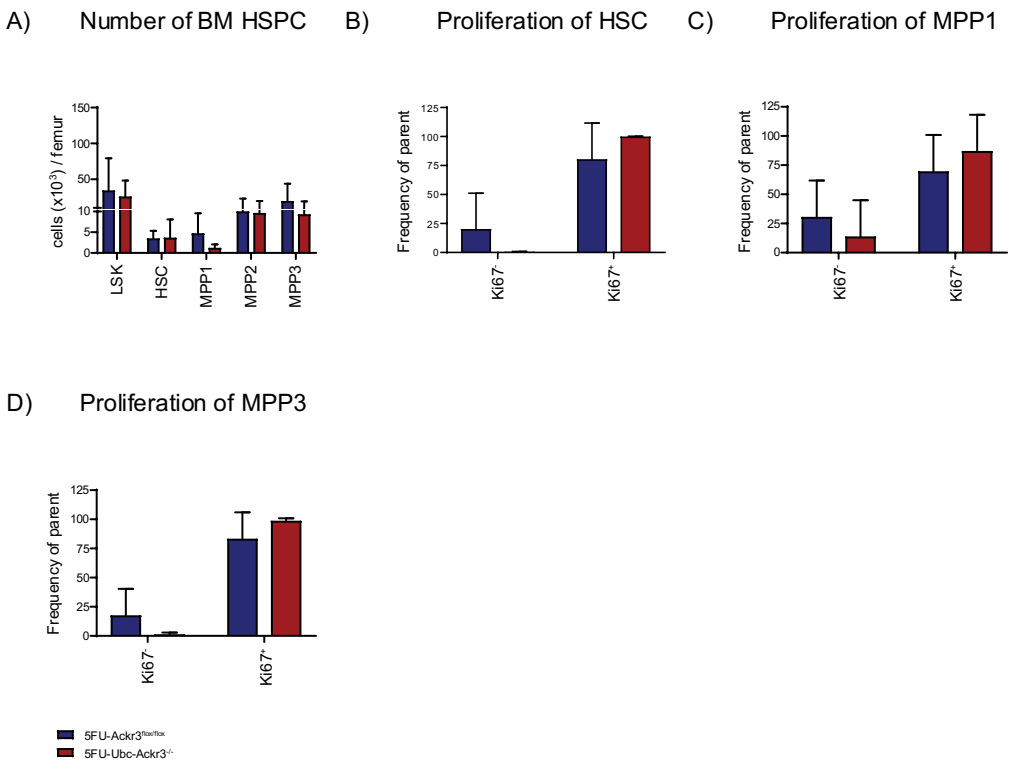

Figure 44 HSPC in *Ubc-Ackr3*$^{-/-}$ mice at day 10 after myeloablation.
A) Number of HSPC in the BM of 5FU- *Ackr3*$^{flox/flox}$ (blue) and 5FU-*Ubc-Ackr3*$^{-/-}$(red) mice (n=6-9, in 3 independent experiments), assessed by flow cytometry. B) Frequency of quiescent Ki67^{-} and proliferative Ki67^{+} cells in HSC, C) MPP1 and D) MPP3 cells (n=6-9, in 3 independent experiments). Data are shown as mean ± SEM. A) 2way ANOVA, with Šidák post hoc test. B-D) Multiple unpaired *t* test, with 5% FDR correction according to Benjamini, Hochberg step up approach.

The presence of HSCs in both 5FU-treated groups already at day 10 resulted, as expected, in fully reconstituted tissues at day 21. Mature leukocytes of all lineages were similarly present in the two groups in the secondary lymphoid organs, blood (Figure 45A) and spleen (Figure 45B), as well as in the BM (Figure 45C). The number of HSPC was identical in the two groups (Figure 46A). At day 21, HSPC proliferation was less prominent, as approximately 50% of HSCs had returned to quiescent in both groups (Figure 46B). A similar proliferation status was observed in the progenitor populations MPP1 and MPP3 (Figure 46C-D). Thus, it was concluded that although *Ubc-Ackr3*$^{-/-}$ mice exhibited high mortality and reduced number of B cells in secondary tissues early after the myeloablation, the reconstitution was successful in the mice that survived the turning point of day 10.

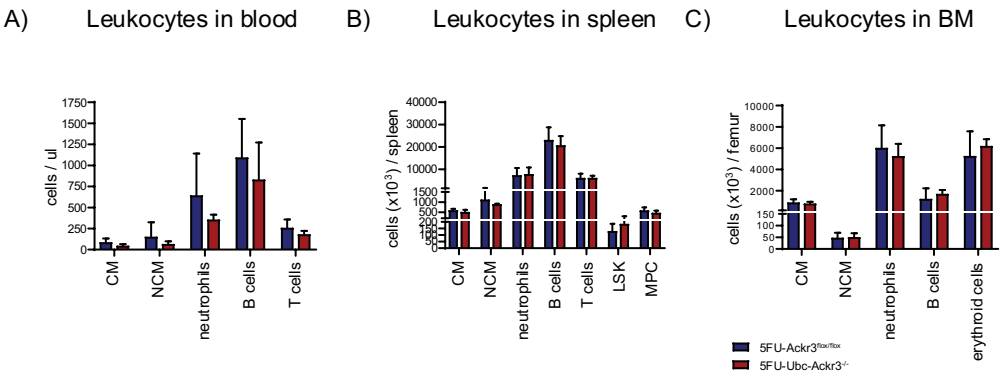

Figure 45 Reconstitution of mature leukocytes in *Ubc-Ackr3*$^{-/-}$ mice at day 21 after myeloablation.
A) Number of mature cells in the circulation of 5FU- *Ackr3*$^{flox/flox}$ (blue) and 5FU-*Ubc-Ackr3*$^{-/-}$(red) mice, assessed by flow cytometry. B) Number of splenic cells. C) Number of cells in BM. Data are shown as mean ± SEM. A-C) 2-way ANOVA, with Šidák *post hoc* test, (n=3-7, in 2 independent experiments).

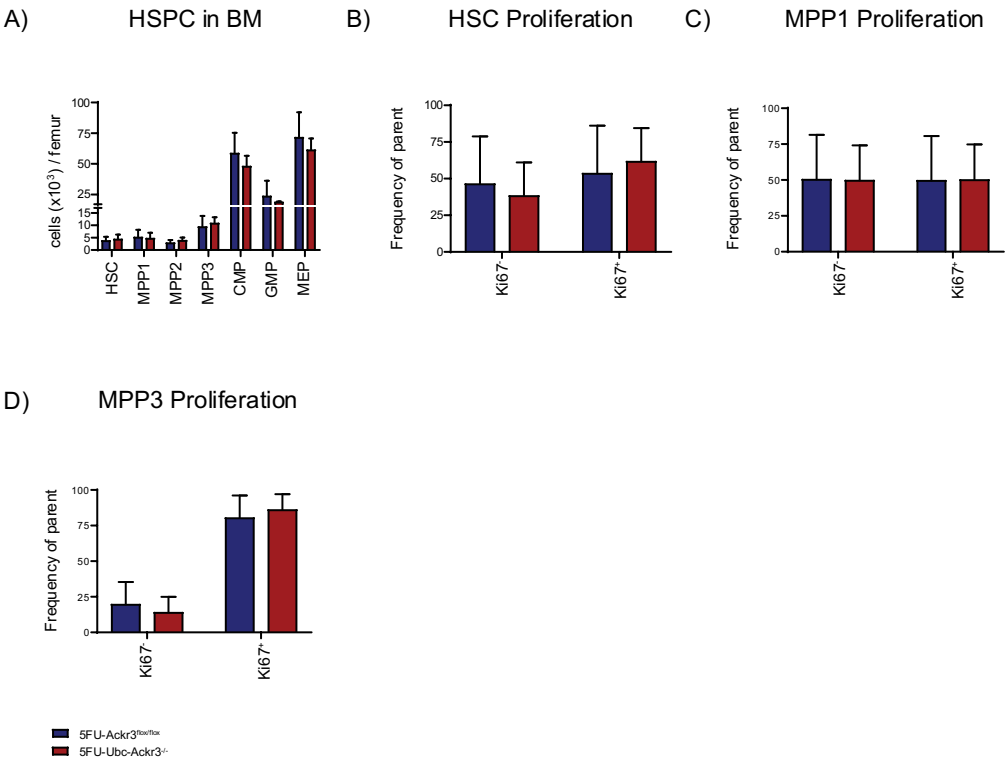

Figure 46 HSPC in *Ubc-Ackr3*$^{-/-}$ mice at day 21 after myeloablation.
A) Number of HSPC in the BM of 5FU-*Ackr3*$^{flox/flox}$ (blue) and 5FU-*Ubc-Ackr3*$^{-/-}$(red) mice (n=2-7, in 2 independent experiments), assessed by flow cytometry. B) Frequency of quiescent Ki67^{-} and proliferative Ki67^{+} cells in HSC, C) MPP1 and D) MPP3 cells (n=3-7, in 2 independent experiments). Data are shown as mean ± SEM. A) 2-way ANOVA, with Šidák *post hoc* test. B-D) Multiple unpaired *t* test, with 5% FDR correction according to Benjamini, Hochberg step up approach.

The high mortality and the delayed initiation of the BM reconstitution in *Ubc-Ackr3*$^{-/-}$ mice, as noted at day 10, prompted me to scrutinize the mechanism of the response. To this end, I screened the consistency of plasma and BM supernatant in 5FU treated *Ackr3*$^{flox/flox}$ mice and *Ubc-Ackr3*$^{-/-}$ mice. As shown in Figure 47A, the average values of TPO and IL-6 concentration were nearly 10-fold upregulated in the circulation of *Ubc-Ackr3*$^{-/-}$ mice compared to the *Ackr3*$^{flox/flox}$ mice (Figure 47A). Nevertheless, the most interesting finding was that, in contrast to steady state mice, the average concentration of circulating CXCL12 was 6 times increased in the *Ubc-Ackr3*$^{-/-}$ mice (Figure 47A). When analyzing the BM supernatant, no major differences were observed. However, there was a tendency for increased concentration of SCF in the *Ubc-Ackr3*$^{-/-}$ mice, compared to the *Ackr3*$^{flox/flox}$ mice and on the contrary, a 4-fold decrease in CXCL12 concentration (Figure 47B).

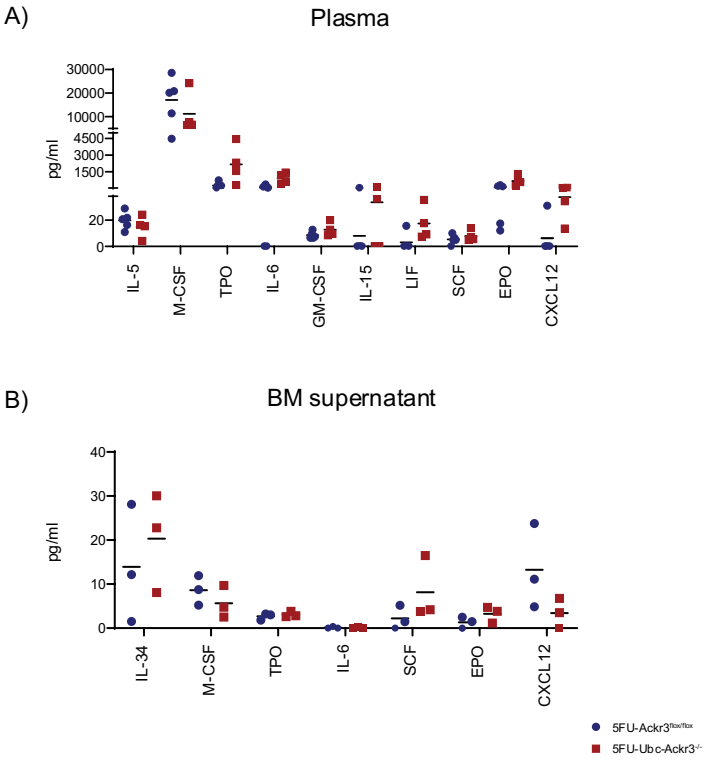

Figure 47 Protein analysis of blood and BM in *Ubc-Ackr3*$^{-/-}$ mice after myeloablation.
A) LEGENDplex assay for the quantification of cytokines in the plasma and B) the BM supernatant of 5FU-*Ackr3*$^{flox/flox}$ (blue) and 5FU-*Ubc-Ackr3*$^{-/-}$ (red) mice (n=3). Data are shown as individual values with mean. Multiple unpaired *t* test, with 5% FDR correction according to Benjamini, Hochberg step up approach.

TPO, via its receptor c-Mpl is detrimental for the megakaryocyte production (Geddis, 2010). Thus, I assessed the number of platelets in the blood of 5FU treated mice. As shown in Figure 48A, no significant difference was observed in the number of circulating platelets between the two groups. On the contrary, IL-6 has been correlated with anemia (Noguchi-Sasaki et al., 2016,

Yacoub et al., 2020). Thus, the hematological parameters of the 5FU treated mice were assessed. Although there was a tendency for decreased number of circulating red blood cells in the *Ubc-Ackr3*$^{-/-}$ mice compared to the 5FU-treated *Ackr3*$^{flox/flox}$ mice, the effect was not significant (Figure 49A). Nevertheless, the two main factors determining the oxygen concentration in the circulation were significantly affected. Hemoglobin (Hgb) and hematocrit (Hct) were significantly decreased by approximately 25% in mice lacking ACKR3 (Figure 49B-C). Of note, this was not accompanied by a reduction in the size of erythrocytes, as the Mean Corpuscular Volume (MCV) was comparable among the two groups (Figure 49D). Hence, it can be concluded that 5FU-treated *Ubc-Ackr3*$^{-/-}$ mice were anemic at the crucial day 10 after the myeloablation, which could be correlated with the increased mortality observed in the group.

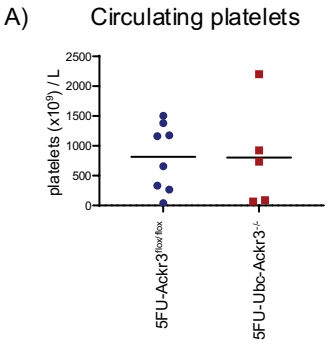

Figure 48 Platelet counts in 5FU-*Ubc-Ackr3*$^{-/-}$ mice.
A) Count of circulating platelets in 5FU-*Ackr3*$^{flox/flox}$ (blue) and 5FU-*Ubc-Ackr3*$^{-/-}$(red) mice (n=5-8, in 3 independent experiments). Data are shown as individual values with mean. Unpaired *t* test.

To verify the tendencies observed in the BM supernatant, I assessed by ELISA the concentration of the two HSC cytokines, the SCF and CXCL12. As shown in Figure 50A, in accordance with the data originating from the protein array, there was a slight increase in BM SCF levels, which, however, was not significant. On the contrary, at day 10, the protein levels of BM CXCL12 were decreased from 100 to approximately 37pg per femur, when assessed by ELISA (Figure 51A). At the same time, circulating CXCL12 was drastically elevated by approximately 3 times, reaching an average of 999 pg/ml in the 5FU-treated *Ubc-Ackr3*$^{-/-}$ mice (Figure 51B). The effect was rather transient, as the concentration of CXCL12 in both BM supernatant (Figure 51C) and plasma (Figure 51D) was equal to that of *Ackr3*$^{flox/flox}$ mice at day 21.

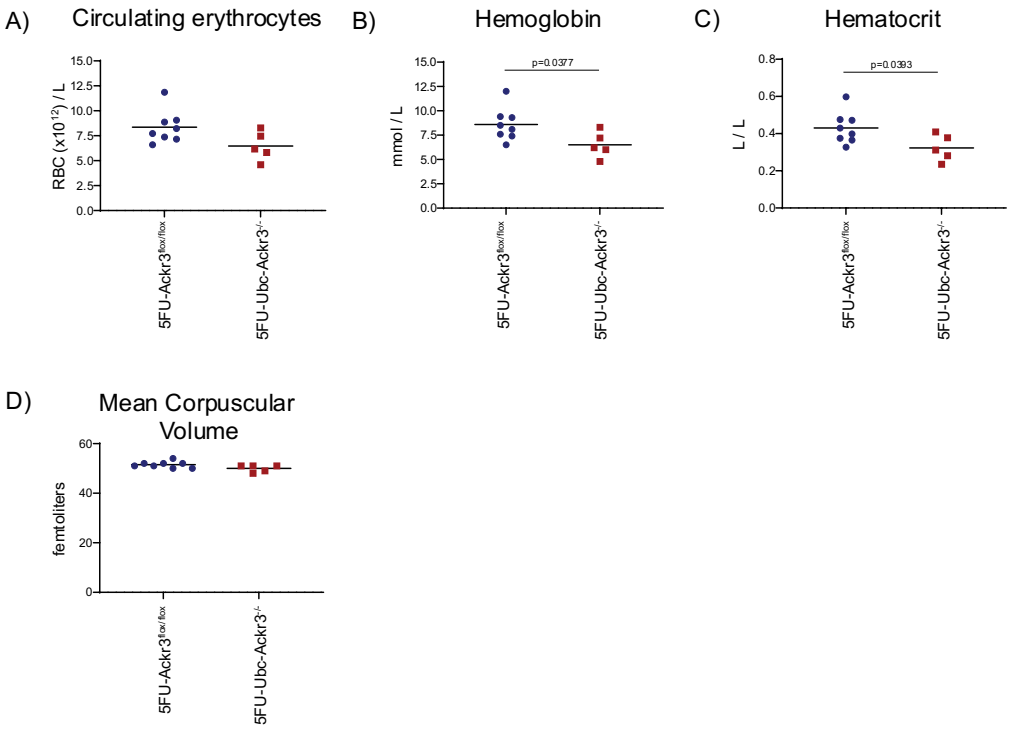

Figure 49 ACKR3 affects erythropoiesis after myeloablation.
A) Count of circulating erythrocytes in 5FU-*Ackr3*$^{flox/flox}$ (blue) and 5FU-*Ubc-Ackr3*$^{-/-}$(red) mice. B) Hgb and C) Hct in blood. D) MCV measurement of circulating erythrocytes (n=5-8, in 3 independent experiments). Data are shown as individual values with mean. A-D) Unpaired *t* test.

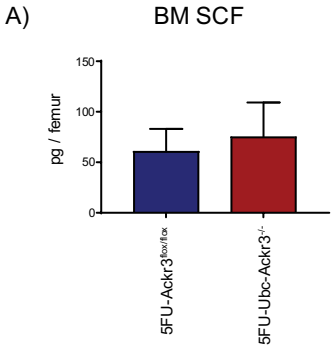

Figure 50 Concentration of SCF in BM supernatant of 5FU-*Ubc-Ackr3*$^{-/-}$ mice.
A) ELISA for SCF in the BM supernatant of 5FU- *Ackr3*$^{flox/flox}$ (blue) and 5FU-*Ubc-Ackr3*$^{-/-}$(red) mice (n=7-8, in 3 independent experiments). Data are shown as mean ± SEM. Unpaired *t* test.

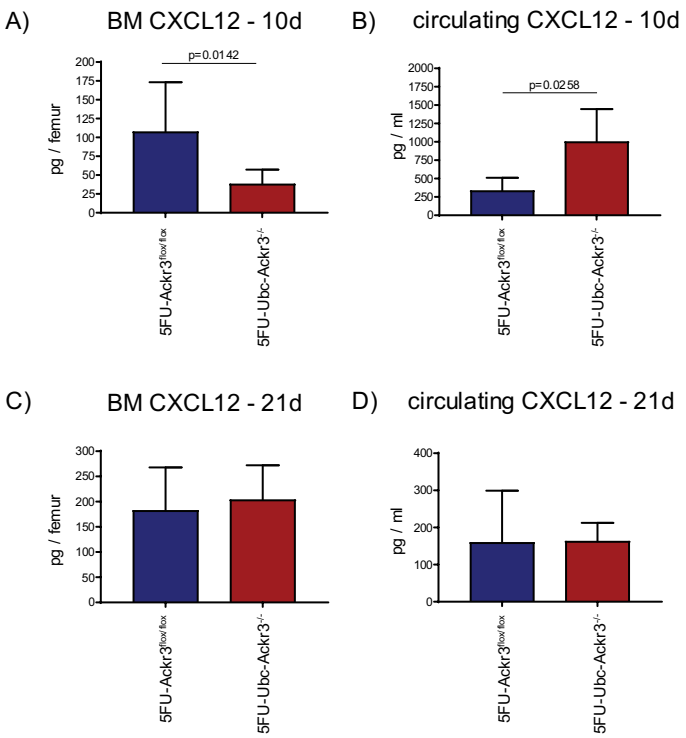

Figure 51 Concentration of CXCL12 in BM supernatant and plasma of 5FU-*Ubc-Ackr3*$^{-/-}$ mice.
A) ELISA for CXCL12a in the BM supernatant (n=6-9, in 3 independent experiments) and B) plasma at day 10 after 5FU administration in *Ackr3*$^{flox/flox}$ (blue) and *Ubc-Ackr3*$^{-/-}$(red) mice (n=5-9, in 3 independent experiments). C) Concentration of CXCL12a in the BM supernatant (n=3-7, in 2 independent experiments) and D) plasma at day 21 after myeloablation (n=3-6, in 2 independent experiments). Data are shown as mean ± SEM. A-B) Unpaired *t* test with Welch´s correction. C-D) Unpaired *t* test.

The simultaneous decrease of BM CXCL12 together with the increase in the plasma, lead to the hypothesis that ACKR3 could play a role in transferring CXCL12 from circulation to the BM. However, as discussed above, ACKR3 is not expressed by BM endothelial cells neither at steady state (Figure 21A), nor after myeloablation (Figures 35B, 38B, 41B). Thus, the two events were considered independent and an alternative source of circulating CXCL12 was investigated. To this end, the expression of ACKR3 in endothelial cells of peripheral tissues was assessed. As shown in Figure 52A, alveolar endothelial cells significantly expressed ACKR3 after the administration of 5FU. Similar observations were made for the aortic endothelial cells, as myeloablation enhanced ACKR3 expression (Figure 52B). In kidney, endothelial cells were significantly expressing ACKR3 also at steady state, whereas the expression did not significantly change after the 5FU treatment (Figure 52C). On the contrary, endothelial cells in liver were ACKR3^{-} at all conditions tested (Figure 52D). The sustained expression of ACKR3 on endothelial cells in different tissues before and after the myeloablation, made me hypothesize that endothelial ACKR3 is necessary for the regulation of CXCL12 concentration during myeloablation and when absent the concentration of CXCL12

increases. I tested whether endothelial ACKR3 regulates *Cxcl12* gene expression during myeloablation. To this end, the expression of *Cxcl12* was assessed in murine aorta, which was a tissue in which ACKR3 expression was enhanced after the myeloablation. Aorta was, thus, harvested and RNA was isolated from whole tissue. As shown in Figure 53A, in 5FU-treated *Ubc-Ackr3*$^{-/-}$ mice there was a significant increase in the expression of *Cxcl12* in aortic cells. Thus, the expression of ACKR3 on endothelial cells in periphery is essential for the regulation of CXCL12 at the gene and subsequently protein level during emergency hematopoiesis.

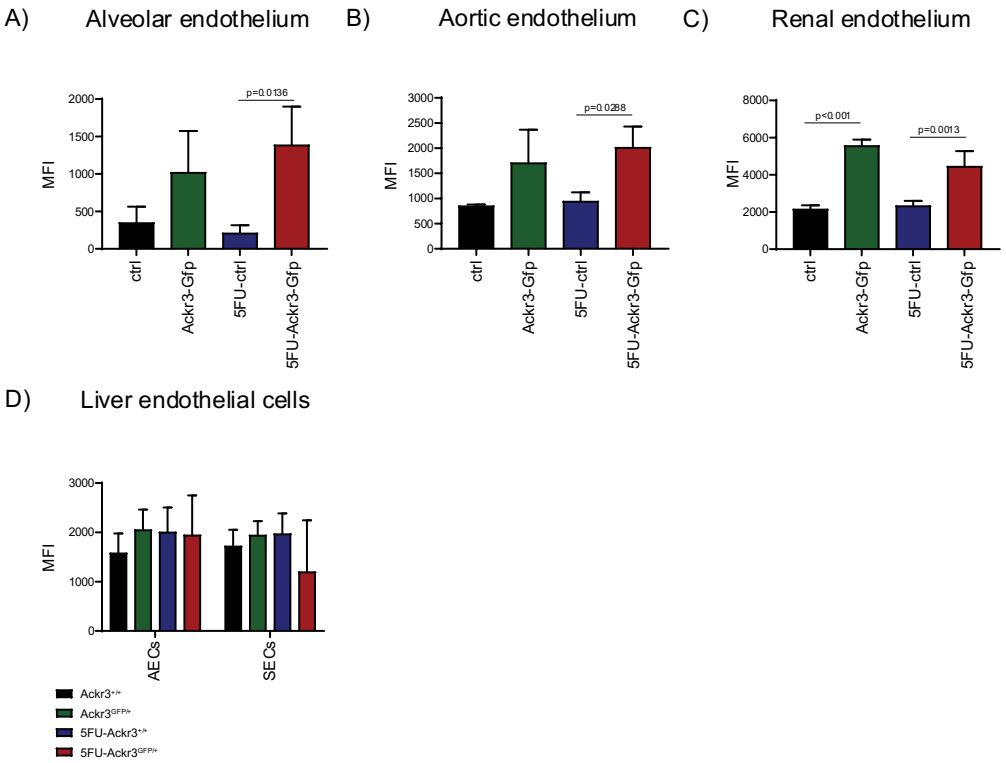

Figure 52 ACKR3 is expressed in the endothelial cells of multiple peripheral tissues after myeloablation. A) Expression of ACKR3 in alveolar endothelial cells B) aortic endothelial cells C) renal endothelial cells and D) endothelial cells in liver of *Ackr3*$^{+/+}$ (black), *Ackr3*$^{GFP/+}$ (green), 5FU- *Ackr3*$^{+/+}$ (blue) and 5FU-*Ackr3*$^{GFP/+}$ (red) mice, as assessed by flow cytometry. A-C) (n=3-4), D) (n=2-4). Data are shown as mean ± SEM. A) 2-way ANOVA, with Tukey *post hoc* test.

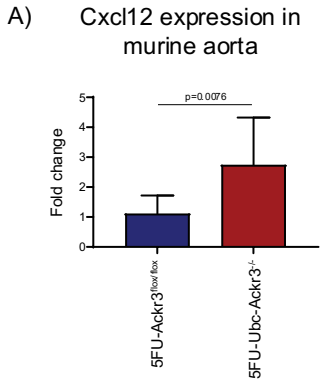

Figure 53 ACKR3 regulates *Cxcl12* expression *in vivo* after myeloablation.
A) PCR for the expression of *Cxcl12* in murine aorta in 5FU-*Ackr3*$^{flox/flox}$ (blue) and 5FU-Ubc-*Ackr3*$^{-/-}$ (red) mice (n=6-11, in 3 independent experiments). Data are shown as mean ± SEM. Unpaired *t* test.

In summary, ACKR3 is expressed in endosteal cells, but not in hematopoietic stem cells. Despite that, ACKR3 maintains HSC quiescent, by regulating the mitochondrial content and the ROS levels via the chemokine CXCL12. Hence, ACKR3 is essential for hematopoiesis, as ACKR3 ko mice exhibit decreased survival rates, and exacerbated anemia during emergency hematopoiesis. At these conditions, ACKR3 regulates *Cxcl12* expression in aortic endothelial cells and, thus, circulating CXCL12 concentration.

4.B Scrutinizing the mechanism of the HSPC retention

4.B.1 Investigation of the role of ACKR3 in BM HSPC retention

CXCL12 was shown to play an important role in BM HSPC retention (Nagasawa et al., 1996, Hopman and DiPersio, 2014, Day et al., 2015). Since I observed an increase of circulating CXCL12 in myeloablated *Ubc-Ackr3*$^{-/-}$ mice, I postulated that ACKR3 may act as a regulator of HSC retention. Thus, I hypothesized that inhibition of ACKR3 would lead to the formation of a CXCL12 gradient between BM and circulation that would eventually induce HSC mobilization to the circulation. To this end, the concentration of CXCL12 in plasma and BM supernatant, and the presence of HSC in the circulation were assessed in *Ubc-Ackr3*$^{-/-}$ mice, as well as in mice inhibited with the ACKR3 antagonist, compound X.

In contrast with the observations made with 5FU experiments, in steady state conditions depletion of ACKR3 did not alter CXCL12 concentration in BM (Figure 54A), nor in plasma (Figure 54B). Circulating CXCL12 was ranging from a mean of 546pg/ml in the *Ackr3*$^{flox/flox}$ mice to a mean of 605pg/ml in *Ubc-Ackr3*$^{-/-}$ mice (Figure 54A). Accordingly, the BM cellularity (Figure 55A), as well as the BM HSPC counts (Figure 55B) were identical between the two groups. To assess mobilization, the number of HSPC in spleen and blood were evaluated. Nevertheless, there was no increase in any HSPC population in the spleen (Figure 55C). In addition, the number of HSPC in blood remained low in both groups, as assessed by flow cytometry (Figure 55D). Finally, to exclude the possibility of mobilized HSPC cells that lack the typical stem cell markers for detection by flow cytometry, peripheral blood was plated in methylcellulose medium to assess the colony forming potency of the circulating cells and, hence, to identify the presence of progenitors in circulation. Nevertheless, the number of colonies formed from the *Ubc-Ackr3*$^{-/-}$ mice was very low and identical to those formed with the peripheral blood of *Ackr3*$^{flox/flox}$ mice. A representative picture of the colonies formed by the peripheral blood is shown in Figure 55E, whereas the quantification of the colonies formed is presented in Figure 55F.

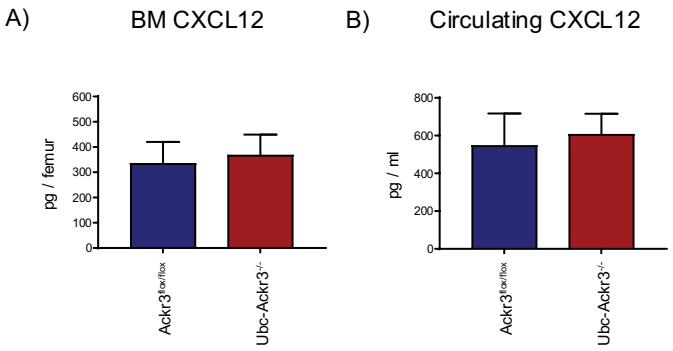

Figure 54 ACKR3 does not regulate the concentration of CXCL12 at steady state conditions.
A) ELISA for CXCL12a in the BM supernatant and B) plasma of *Ackr3*$^{flox/flox}$ (blue) and *Ubc-Ackr3*$^{-/-}$(red) mice. Data are shown as mean ± SEM. A-B) Unpaired *t* test (n=11, in 3 independent experiments).

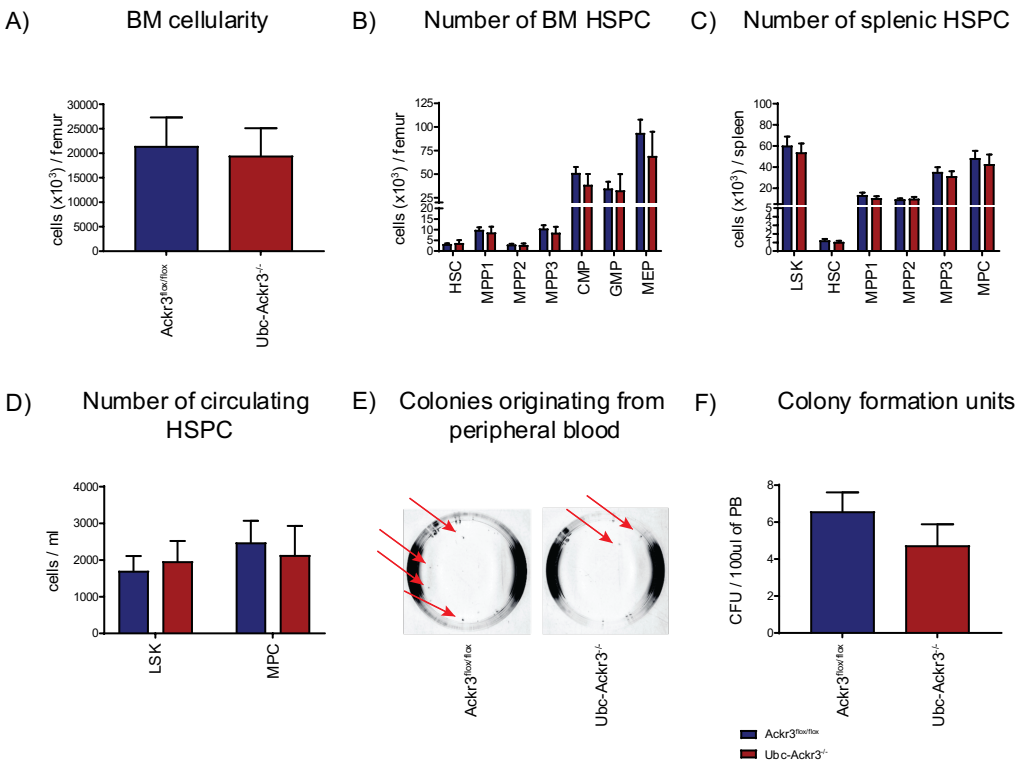

Figure 55 HSPC are not mobilized in *Ubc-Ackr3*$^{-/-}$ mice.
A) Total number of cells in the BM of *Ackr3*$^{flox/flox}$ (blue) and *Ubc-Ackr3*$^{-/-}$(red) mice, (n=8-11, in 2 independent experiments), assessed by flow cytometry. B-D) Numbers of HSPC (n=10-11, in 3 independent experiments) measured by flow cytometry in BM (B), spleen (n=9-12, in 3 independent experiments) (C), blood (D) (n=6-12, in 3 independent experiments). E) Representative picture of colonies formed by peripheral blood and F) quantification of the total colonies formed (n=7-9, in 3 independent experiments). Data are shown as mean ± SEM. A and F) Unpaired *t* test. B-D) 2-way ANOVA, with Šidák *post hoc* test.

The minor increase of circulating CXCL12 concentration in the *Ubc-Ackr3*$^{-/-}$ mice at steady state conditions, made me hypothesize that CXCL12 expression was compensated in the mouse model. Hence, ACKR3 was inhibited in C57Bl/6J mice using a new potent inhibitor X. The ACKR3 inhibitor was administered orally, and the concentration of circulating CXCL12 was assessed 1 hour, 6 hours and 3 days later. The short-term inhibition of ACKR3 was sufficient to increase the concentration of CXCL12. As shown in Figure 56, circulating CXCL12 increased 3 times at the 6-hour time point (Figure 56). Subsequently, the number of colonies formed from the peripheral blood of the ACKR3-inhibited mice was assessed. In addition, a group of animals was injected with the CXCR4 inhibitor, AMD3100, as a technical control for the colony formation assay. Nevertheless, as shown in Figure 57, no significant change in the colony formation potency of the peripheral blood was noted in the ACKR3-inhibited mice. On the contrary, the administration of AMD3100 resulted in an approximate 5-fold increase in the number of colonies formed (Figure 57). Thus, despite the

efficiency of this model in increasing the CXCL12 concentration in circulation, this increase was not sufficient to induce HSPC mobilization.

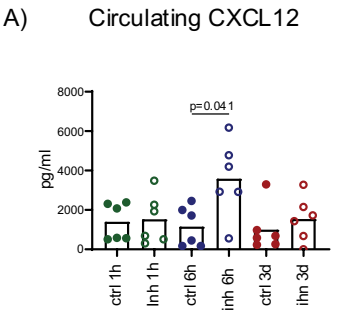

Figure 56 Pharmacological inhibition of ACKR3 increases circulating CXCL12 after 6h.
A) ELISA for circulating CXCL12a in control (solid points), and ACKR3 inhibited (open points) mice (n=6, in 2 independent experiments). Data are shown as individual points with mean. A) 1-way ANOVA, with Tukey *post hoc* test.

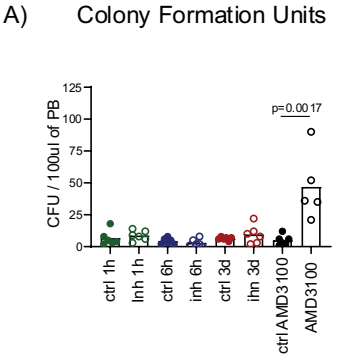

Figure 57 Pharmacological inhibition of ACKR3 does not mobilize HSPC.
A) Quantification of the total colonies formed from control (solid points), ACKR3 inhibited (open points) and CXCR4 inhibited (open black) mice (n=5-6, in 2 independent experiments). Data are shown as individual points with mean. A) 2-way ANOVA, with Šidák *post hoc* test. B) 1-way ANOVA, with Tukey post hoc test.

Finally, HSPC retention, was assessed in the myeloablated mice, in which the aberrant increase of CXCL12 was noted after the deletion of ACKR3 (Figure 51B). However, as shown in Figure 58A, the number of circulating HSPC remained low. Similarly, the colony production potency of the peripheral blood was comparable to that of the 5FU-*Ackr3*$^{flox/flox}$ mice (Figure 58B). Thus, our data in 3 different models of ACKR3 blockade suggest that the receptor regulates circulating CXCL12 concentration under specific conditions, but does not mediate the retention of HSPC in the BM.

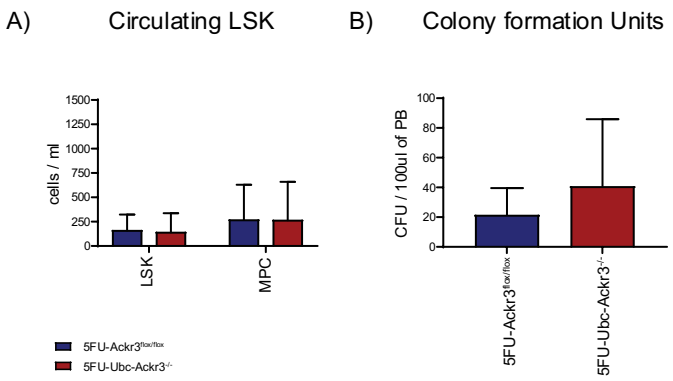

Figure 58 HSPC are not mobilized in 5FU-*Ubc-Ackr3*$^{-/-}$ mice.
A) Number of circulating LSK and MPC cells in 5FU- *Ackr3*$^{flox/flox}$ (blue) and 5FU-*Ubc-Ackr3*$^{-/-}$(red) mice (n=6-9, in 3 independent experiments) assessed by flow cytometry. B) Quantification of the total colonies formed by peripheral blood (n=6-11, in 3 independent experiments). Data are shown as individual points with mean. A) 2-way ANOVA, with Šidák *post hoc* test. B) Unpaired *t* test with Welch´s correction.

4.B.2 Evaluation of the "Gradient" hypothesis for HSPC retention

CXCL12 is considered a key element for the retention of HSPC (Tzeng et al., 2011, Dar et al 2011). Nevertheless, our findings contradict this notion, as changes in the concentration of CXCL12 in BM and blood did not affect HSPC BM retention. To determine whether CXCL12 is crucial for the retention of BM HSPC, we assessed the mobilization of HSPC in *Ubc-Cxcl12*$^{-/-}$ mouse model. Despite the great reduction of CXCL12 in both BM and circulation (Figure 29A-C), the total number of cells in the BM remained unaffected (Figure 59A). In addition, the number of BM HSPC did not change (Figure 59B), and there was no mobilization of HSPC to spleen (Figure 59C). The mobilization of progenitors in circulation was further excluded by assessing the number of circulating HSPC (Figure 59D), and the colony formation potency of peripheral blood. An average of 5 colonies were formed by plating 100ul of blood in both *Cxcl12*$^{flox/flox}$ and *Ubc-Cxcl12*$^{-/-}$ mice (Figure 59E), suggesting that the depletion of CXCL12 does not induce HSPC mobilization.

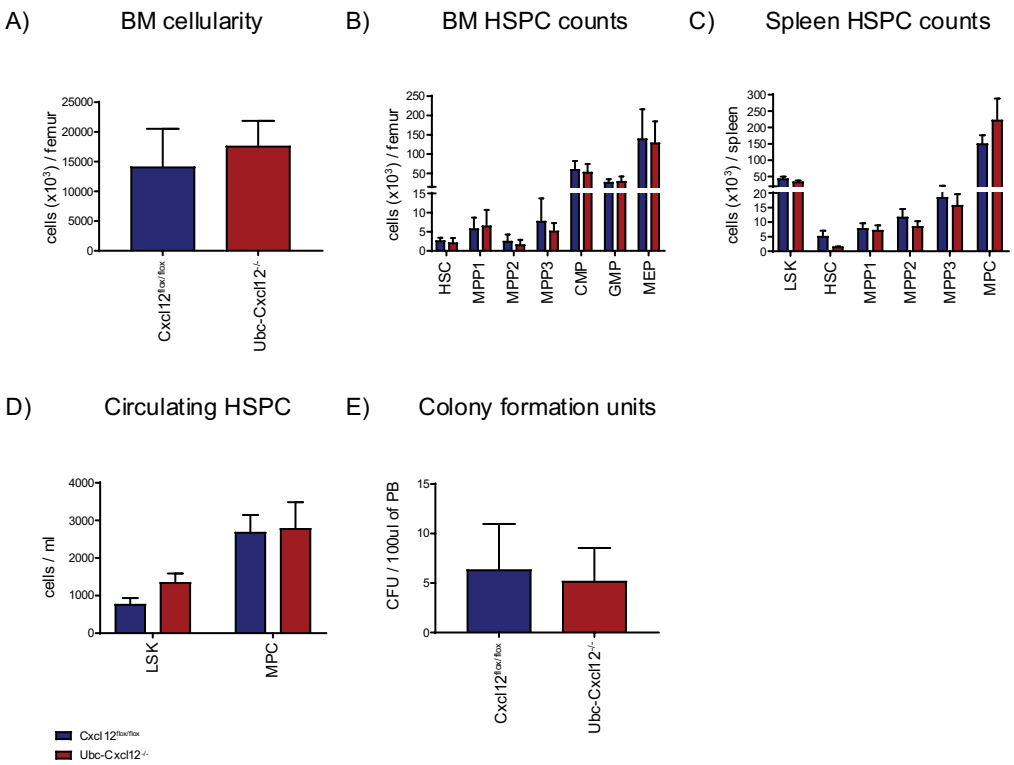

Figure 59 HSPC are not mobilized in *Ubc-Cxcl12*$^{-/-}$ mice.
A) BM cellularity in *Cxcl12*$^{flox/flox}$ (blue) and *Ubc-Cxcl12*$^{-/-}$(red) mice (n=6-8, in 3 independent experiments) assessed by flow cytometry. B) Number of HSPC in BM (n=6-8, in 3 independent experiments), C) spleen (n=6-8, in 3 independent experiments), D) blood (n=7-13, in 3 independent experiments). E) Quantification of the total colonies formed by peripheral blood (n=6, in 3 independent experiments). Data are shown as mean ± SEM. A and E) Unpaired *t* test. B-D) 2-way ANOVA, with Šidák *post hoc* test.

Of note, in *Ubc-Cxcl12*$^{-/-}$ mice CXCL12 protein levels are decreased in both BM and circulation (Figure 29A-C). Consequently, it could be argued that the model is inappropriate to investigate the role of the CXCL12 gradient between BM and circulation in HSPC mobilization, due to the complete absence of CXCL12 in both tissues. To this end, I developed two models in which, the concentration of circulating CXCL12 was artificially increased. It has been previously reported that AMD3100 increases the concentration of circulating CXCL12 (Jørgensen et al., 2021). In accordance with these data, the injection of AMD3100 in C57Bl/6J mice decreased by 40% the BM CXCL12 levels (Figure 60A), while increasing circulating CXCL12 concentration 9 times (Figure 60B). At the same time, the potency of the peripheral blood to form colonies increased 5 times (Figure 60C), supporting the role of the CXCL12 gradient in the regulation of BM HSPC retention and mobilization. Therefore, I injected AMD3100 in *Ubc-Cxcl12*$^{-/-}$ mice. Surprisingly the depletion of BM CXCL12 in *Ubc-Cxcl12*$^{-/-}$ mice was not efficient, as the concentration dropped by approximately 40% (Figure 61A). Nevertheless, the injection of AMD3100 significantly decreased

BM CXCL12 by 70% compared to the *Cxcl12*$^{flox/flox}$ mice (Figure 61A). Circulating CXCL12 was still efficiently depleted in *Ubc-Cxcl12*$^{-/-}$ mice (Figure 61B). Nevertheless, the effect was abrogated in the AMD3100-treated *Ubc-Cxcl12*$^{-/-}$ mice, as the concentration of CXCL12 reached an average of 197pg/ml (Figure 61B). Under these conditions, HSPC were mobilized. The number of LSK cells, as assessed by flow cytometry did not significantly differ (Figure 61C), but there was a 5-fold increase in the number of colonies formed by peripheral blood (Figure 61D). These data supported further the correlation between the relative difference in the CXCL12 concentration among tissues and cell mobilization.

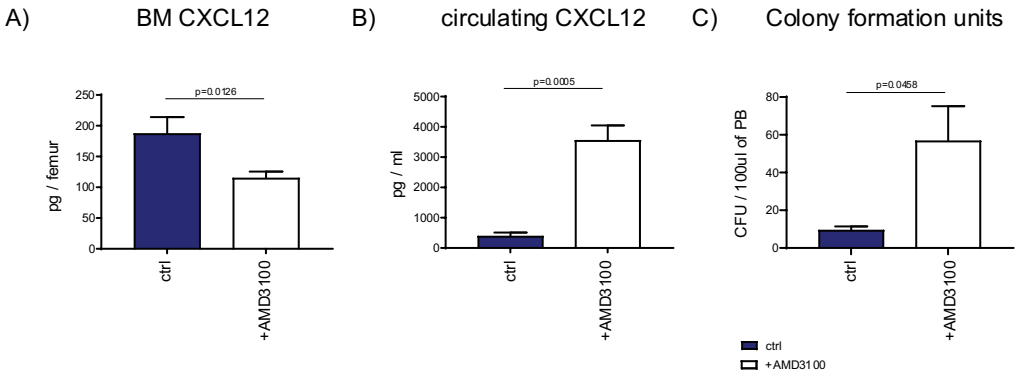

Figure 60 AMD3100-mediated HSPC mobilization affects CXCL12 concentration.
A) ELISA for CXCL12a in the BM and B) plasma of wild type (blue) and AMD3100-injected (white) mice. C) Quantification of the total colonies formed by peripheral blood. Data are shown as individual points with mean. A-B) Unpaired *t* test, (n=3). C) Unpaired *t* test with Welch´s correction (n=3).

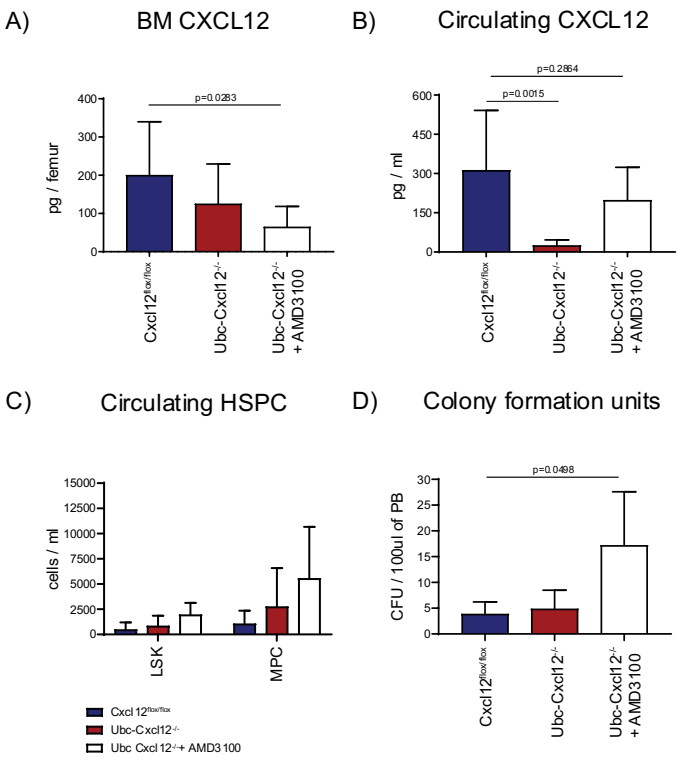

Figure 61 HSPC are mobilized in *Ubc-Cxcl12*$^{-/-}$ mice treated with AMD3100.
A) ELISA for CXCL12a in the BM and B) plasma of *Cxcl12*$^{flox/flox}$ (blue), *Ubc-Cxcl12*$^{-/-}$(red) and AMD3100-treated *Ubc-Cxcl12*$^{-/-}$ (white) mice (n=6-13, in 3 independent experiments). C) Number of circulating HSPC (n=3-4, in 2 independent experiments), assessed by flow cytometry. D) Quantification of the total colonies formed by peripheral blood (n=6-12, in 3 independent experiments). Data are shown as mean ± SEM. A) 1-way ANOVA, with Šidák *post hoc* test. B and D) Welch's ANOVA, with Dunnett's *post hoc* test. C) 2-way ANOVA, with Šidák *post hoc* test.

Because AMD3100 is a CXCR4-inhibitor, it is therefore difficult to determine if the mobilization of HSPC is due to its direct effect on CXCR4 expressed by HSPC and its alternative effect on CXCL12. I, thus, developed an alternative approach to answer this question. To this end, recombinant murine CXCL12 was injected i.v. in *Ubc-Cxcl12*$^{-/-}$ mice. Mice were sacrificed 30min later. Once again, although I observed a reduction of BM CLXCL12 in *Ubc-Cxcl12*$^{-/-}$ mice the depletion of the was not complete (Figure 62A). However, the injection of the recombinant protein did not affect the BM CXCL12 levels (Figure 62A). On the contrary, circulating CXCL12 was absent in *Ubc-Cxcl12*$^{-/-}$ mice (Figure 62B). The injection of the recombinant chemokine restored the circulating CXCL12 concentration (Figure 62B). However, there was no increase in the number of circulating HSPC, as assessed by both flow cytometry (Figure 62C) and the colony formation assay (Figure 62D). In summary, the absence of mobilization after the injection of the recombinant CXCL12 forced me to reject the theory about the existence of a CXCL12 gradient, as a mechanism for HSPC retention

and mobilization, and to hypothesize that the mobilization observed after the injection of AMD3100 is due to the blockade of the CXCR4-mediated signaling.

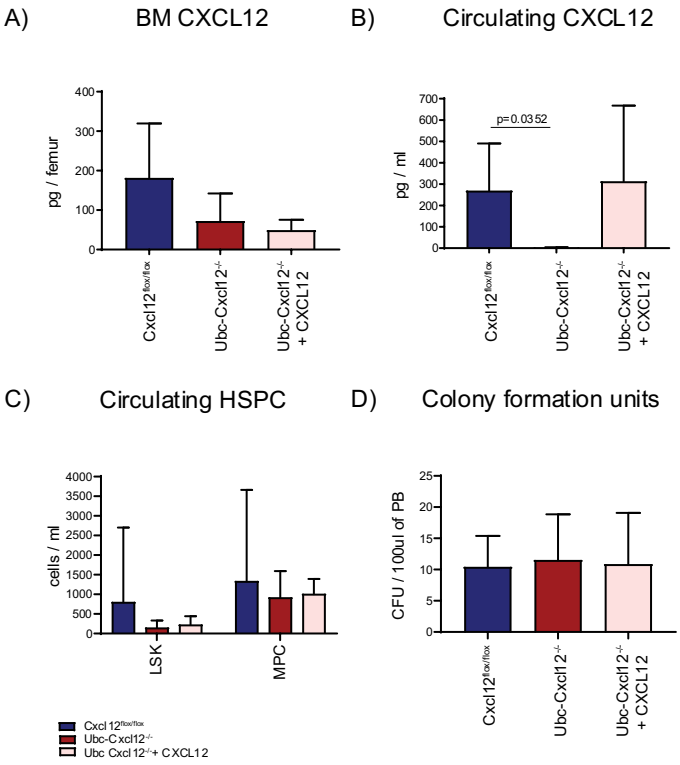

Figure 62 CXCL12 gradient is not sufficient for HSPC mobilization.
A) ELISA for CXCL12a in the BM and B) plasma of *Cxcl12*$^{flox/flox}$ (blue), *Ubc-Cxcl12*$^{-/-}$(red) and CXCL12-injected *Ubc-Cxcl12*$^{-/-}$ (pink) mice (n=6-7, in 2 independent experiments). C) Number of circulating HSPC (n=6-7, in 2 independent experiments), assessed by flow cytometry. D) Quantification of the total colonies formed by peripheral blood (n=6, in 2 independent experiments). Data are shown as mean ± SEM. A and B) Welch's ANOVA, with Dunnett's *post hoc* test. C) 2-way ANOVA, with Šidák *post hoc* test. D) 1-way ANOVA, with Šidák *post hoc* test.

4.B.3 Evaluation of the "constant CXCR4 activation" hypothesis for HSPC retention

For the assessment of the role of CXCR4 signaling on HSPC retention, I firstly evaluated HSPC mobilization in a conditional knockdown *Ubc-Cxcr4*$^{-/-}$ mouse model, by backcrossing the inducible *Ubc-Cre*^{ERT2} mice with a *Cxcr4*$^{flox/flox}$ line. In accordance with previous studies (Sugiyama et al., 2006), administration of tamoxifen and the subsequent global CXCR4 deletion led to HSPC mobilization. In *Ubc-Cxcr4*$^{-/-}$ mice, there was a robust increase in the number of circulating LSK cells and MPC cells four weeks after the initial tamoxifen injection, as shown in the representative Figure 63A. LSK cells in blood increased approximately 10 times, whereas the number of MPCs increased 5 times (Figure 63B). In addition, the number of colony-forming cells in the periphery elevated approximately 17 times after the deletion of CXCR4 (Figure 63C).

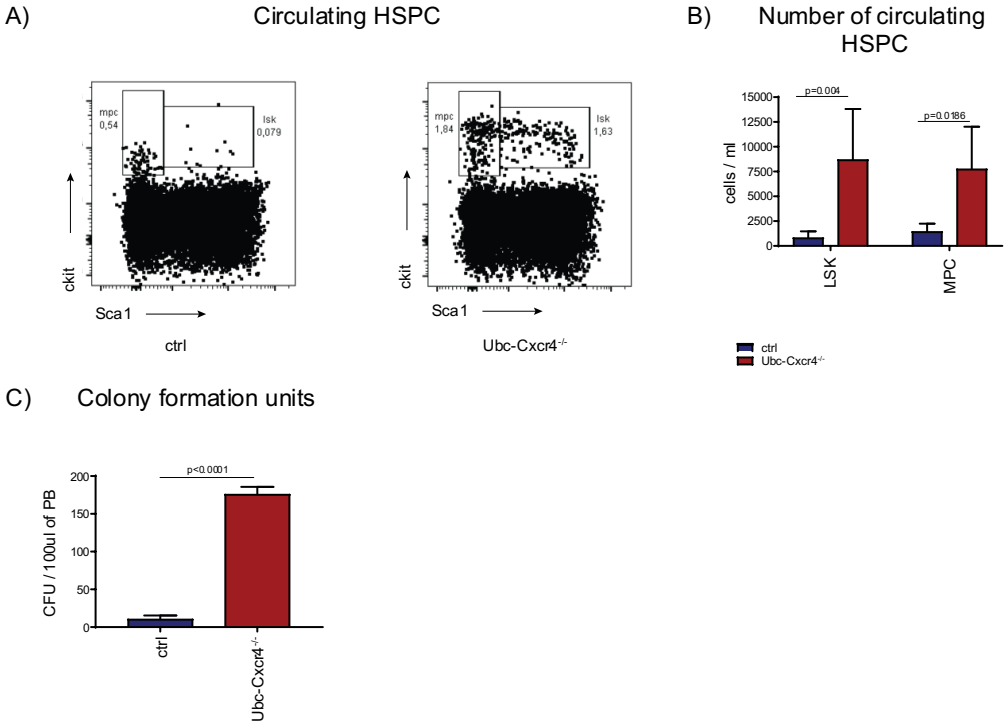

Figure 63 HSPC are mobilized in *Ubc-Cxcr4*$^{-/-}$ mice.

A) Representative figure of circulating LSK and MPC cells, gated as CD45^{+}Lin^{-} cells. B) Number of circulating HSPC in *Cxcr4*$^{flox/flox}$ (blue) and *Ubc-Cxcr4*$^{-/-}$ (red) mice (n=5, in 2 independent experiments), assessed by flow cytometry. D) Quantification of the total colonies formed by peripheral blood (n=3). Data are shown as mean ± SEM. B) 2-way ANOVA, with Šidák *post hoc* test. C) Unpaired *t* test.

These data supported the role of CXR4 on cell retention but did not prove that the effect is direct. To this end, it was necessary to, firstly, verify the expression of CXCR4 on HSC. To overcome the obstacle of the cell mobilization after CXCR4 deletion, I developed a flow cytometry-based binding assay to assess CXCR4 expression on HSPC in steady state mice. More specifically, I stained BM cells with fluorescently labeled CXCL12. The advantage of the binding assay, compared to the antibody staining was that the specificity of the assay was determined by blocking the ligand binding, adding the CXCR4 inhibitor, AMD3100. As shown in Figure 64, CXCL12 was bound to all BM leukocytes assessed. The highest MFI was observed in GMP and neutrophils, whereas the addition of the antagonist revealed a significant and specific CXCR4 expression in all cells, but MPP1 and erythroid cells. Binding of CXCL12 on HSCs was decreased by half after the addition of AMD3100 (Figure 64A) and, thus, it was concluded that HSCs do express CXCR4.

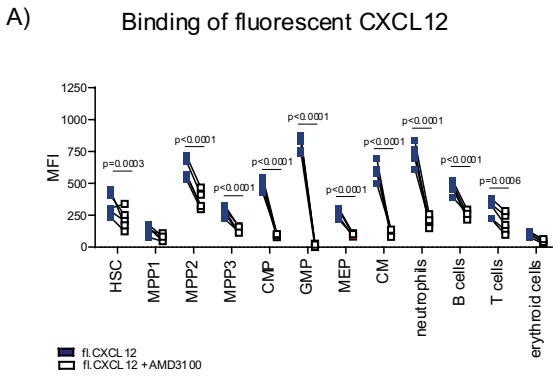

Figure 64 Expression of CXCR4 on BM leukocytes.
Binding of fluorescently labeled CXCL12 on PBS- (blue) and AMD3100-treated (white) BM cells (n=5). Data are shown as mean ± SEM. GLM ANOVA, with Šidák *post hoc* test.

After confirming the expression of the receptor on HSCs, an HSC-specific mouse model was employed to delete CXCR4 on HSCs and assess cell mobilization. The *Fgd5*$^{ZsGr.CreERT2}$ mice have been previously described to specifically target HSCs (Gazit et al., 2014). Due to the expression of the fluorescent molecule Zonathus Green (ZsGreen), the expression of *Fgd5* in BM cells was assessed by flow cytometry (Figure 65). As shown in Figure 65, *Fgd5* was highly expressed on HSCs and MPP1 cells whereas the expression decreased 3 times in the MPP2 and MPP3 subsets. In addition, BM mature cells were marked by the absence of the gene. Thus, the model was appropriate for the deletion of CXCR4 only on HSPC cells. Interestingly, *Fgd5* expression was also present in BM stromal cells and, more specifically, in the AECs (Figure 65).

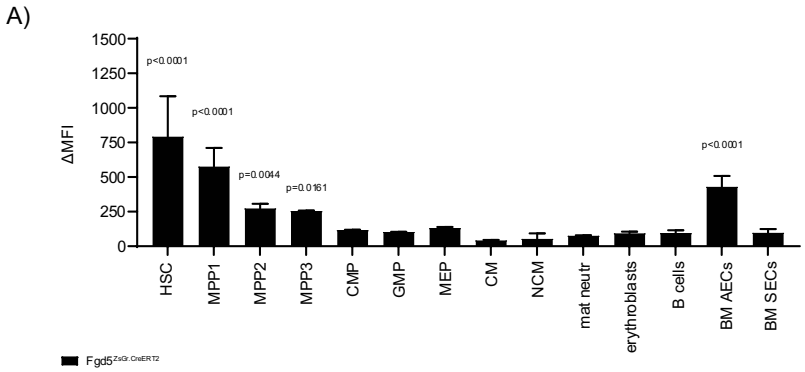

Figure 65 Expression of Fgd5 on BM leukocytes and stromal cells.
Expression of *Fgd5* in BM leukocytes and stromal cells in *Fgd5*$^{ZsGr.CreERT2}$ (black) mice normalized to the expression in *Cxcr4*$^{flox/flox}$ mice (n=2-4), as assessed by flow cytometry. Data are shown as mean ± SEM. Factorial ANOVA, with Šidák *post hoc* test.

Nevertheless, as shown in Figure 66, not all Fgd5^{+} HSCs were CXCR4^{+}, as assessed by flow cytometry using the anti-CXCR4 antibody 2B11. In fact, only the 13% of the total HSCs were Fgd5^{+}CXCR4^{+}. However, *Fgd5$^{ZsGr.CreERT2}$* mice were crossed with *Cxcr4$^{flox/flox}$* mice to generate *Fgd5-Cxcr4$^{-/-}$* mice. To induce the cell-specific deletion of CXCR4, tamoxifen was administered in *Fgd5-Cxcr4$^{-/-}$* mice and mice were sacrificed three weeks later. Nevertheless, I could not demonstrate the deletion of CXCR4 on the surface of the HSPC (Figure 67A). Cells were subsequently permeabilized and the presence of CXCR4 intracellularly was assessed. Although I observed a small reduction of intracellular CXCR4, the receptor was still present in the cells (Figure 67B). As a result, the number of circulating LSK and MPC cells was negligible (Figure 68A). Interestingly, the number of colonies generated from the peripheral blood of *Fgd5-Cxcr4$^{-/-}$* mice was nearly double compared to *Cxcr4$^{flox/flox}$* mice (Figure 68B), suggesting the mobilization of cells with clonogenic potency. On the contrary, the splenic LSK cells were not increased (Figure 68C). Thus, it was concluded that certain limitations arise in the usage of the *Fgd5$^{ZsGr.CreERT2}$* mice for the deletion of the CXCR4 receptor.

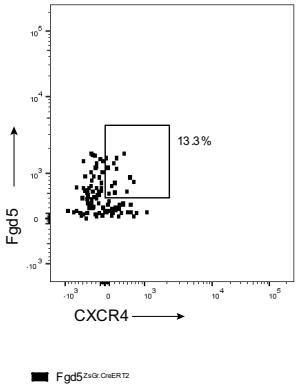

Figure 66 Representative figure of CXCR4 expression in Fgd5+ HSCs.
Representative figure showing the Fgd5^{+}CXCR4^{+} (gated) HSCs in *Fgd5$^{ZsGr.CreERT2}$* (black) mice.

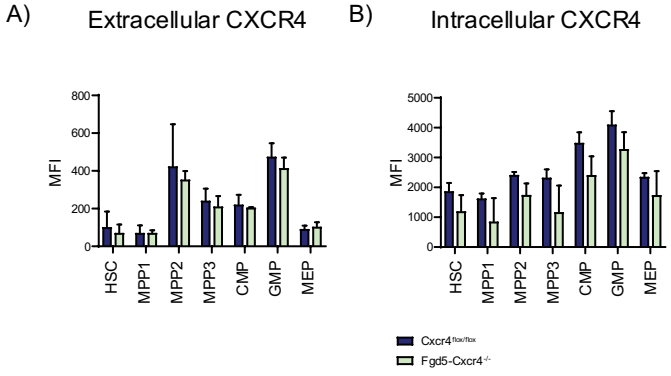

Figure 67 Inefficient suppression of CXCR4 expression in *Fgd5-Cxcr4$^{-/-}$* mice.

A) Expression of CXCR4 in the surface of BM HSPC in *Cxcr4*$^{flox/flox}$ (blue) and *Fgd5-Cxcr4*$^{-/-}$ (green) mice (n=2-5, in 2 independent experiments), assessed by flow cytometry. B) Intracellular staining for CXCR4 (n=2-4). Data are shown as mean ± SEM. A-B) 2-way ANOVA, with Šidák *post hoc* test.

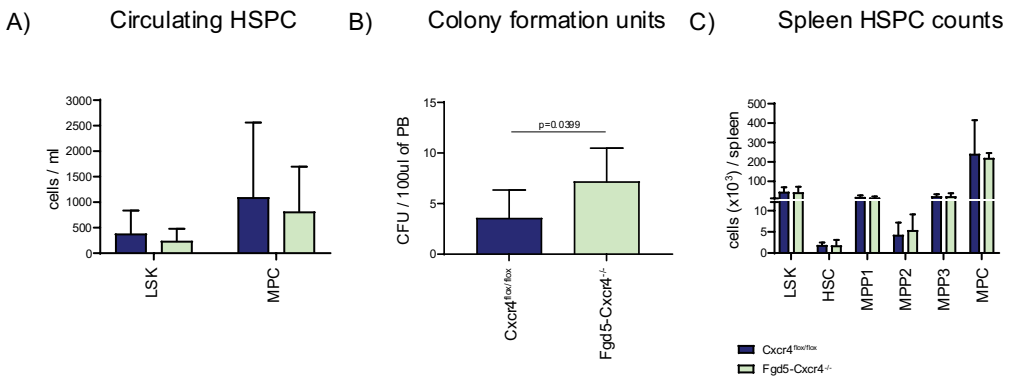

Figure 68 HSPC are not mobilized in *Fgd5-Cxcr4*$^{-/-}$ mice.
A) Number of circulating HSPC in *Cxcr4*$^{flox/flox}$ (blue) and *Fgd5-Cxcr4*$^{-/-}$ (green) mice (n=4-5, in 2 independent experiments) assessed by flow cytometry. B) Quantification of colonies formed by peripheral blood (n=4-5, in 2 independent experiments). C) Number of HSPC in spleen (n=3-5, in 2 independent experiments). Data are shown as mean ± SEM. A and C) 2-way ANOVA, with Šidák *post hoc* test. B) Unpaired *t* test.

The negligible deletion of CXCR4 with the HSC-specific mouse model, and the off-target expression of *Fgd5* in AECs prompted me to employ an alternative model. BM transplantation experiments were held to discriminate between the effect of the stromal cells and the hematopoietic cells in BM cell retention. To this end, BM cells from *Apoe*$^{-/-}$ *Cxcr4*$^{+/+}$ donors, were transplanted into *Cxcr4*$^{flox/flox}$ and *Ubc-Cxcr4*$^{-/-}$ recipient mice. After a short period of recovery, tamoxifen was administered and, thus, CXCR4 was deleted only on stromal cells in the *Ubc-Cxcr4*$^{-/-}$ recipient mice. Interestingly, despite a tendency for increased numbers of circulating HSPC, as assessed by flow cytometry (Figure 69A) and the colony-forming potency of the peripheral blood (Figure 69B), this effect was not significant. Accordingly, the number of splenic LSK cells was identical to that of the *Cxcr4*$^{flox/flox}$ recipients (Figure 69C), suggesting that CXCR4 on stromal cells does not mediate BM cell retention.

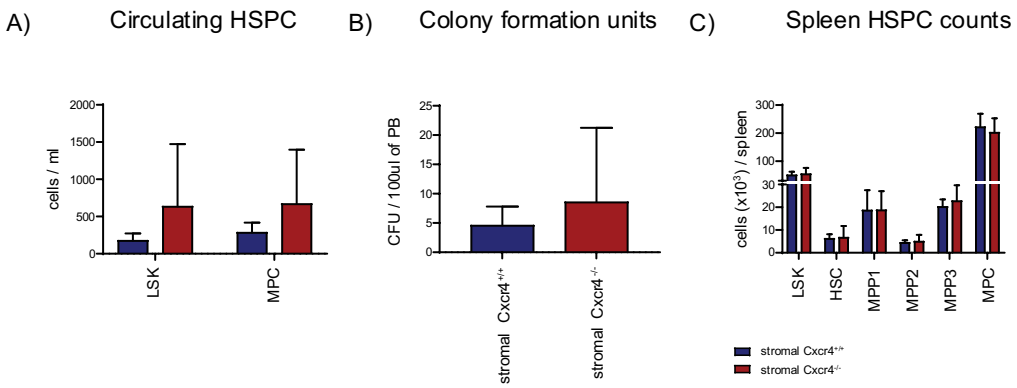

Figure 69 CXCR4 on stromal cells does not retain HSPC in the BM.
A) Number of circulating HSPC in *Cxcr4*$^{+/+}$ stromal cells (blue) and *Cxcr4*$^{-/-}$ stromal cells (red) mice, assessed by flow cytometry. B) Quantification of colonies formed by peripheral blood. C) Number of HSPC in spleen. Data are shown as mean ± SEM, (n=5-7). A and C) 2-way ANOVA, with Šidák *post hoc* test. B) Unpaired *t* test with Welch´s correction.

Thus, the inverse model was finally assessed. *Ubc-Cre*^{ERT} *Cxcr4*$^{flox/flox}$ and *Cxcr4*$^{flox/flox}$ BM cells were isolated and injected in irradiated *Apoe*$^{-/-}$ *Cxcr4*$^{+/+}$recipients. After recovery, CXCR4 was deleted in hematopoietic cells by tamoxifen injections. As a result, the number of MPC in blood elevated approximately 5 times (Figure 70A), whereas the colonies formed by 100µl of blood averaged to 35 in contrast to the 3 colonies per plate that were observed in the mice receiving BM leukocytes from *Cxcr4*$^{flox/flox}$ mice (Figure 70B). Nevertheless, no mobilization of HSPC was noted in spleen (Figure 70C).

Thus, our data contradict the role of CXCL12 in BM cell retention and rather support the direct role of CXCR4 on HSPC retention within the BM. Accordingly, blockade of CXCR4 or deletion of the gene results in cell mobilization to the circulation.

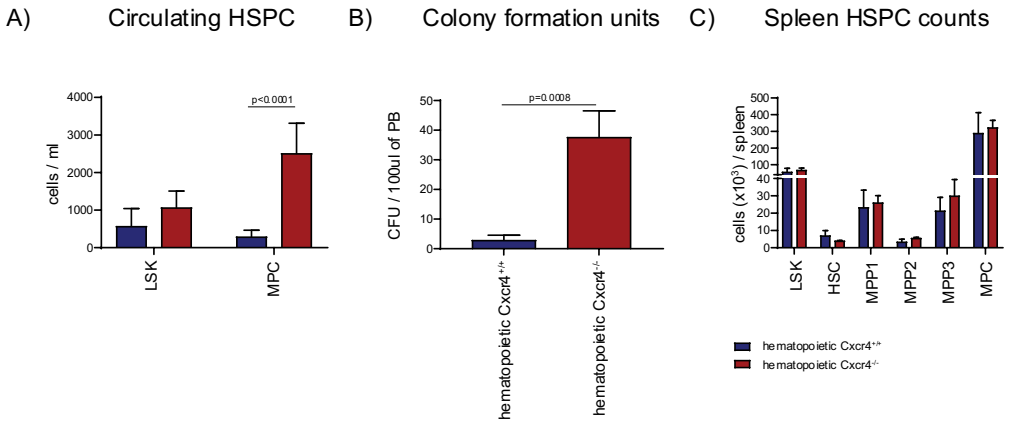

Figure 70 CXCR4 on HSPC retains cells in the BM.

A) Number of circulating HSPC in *Cxcr4*$^{+/+}$ hematopoietic cells (blue) and *Cxcr4*$^{-/-}$ hematopoietic cells (red) mice, (n=4-6), assessed by flow cytometry. B) Quantification of colonies formed by peripheral blood, (n=5-6). C) Number of HSPC in spleen, (n=5). Data are shown as mean ± SEM, (n=5-7). A and C) 2-way ANOVA, with Šidák *post hoc* test. B) Unpaired *t* test with Welch´s correction.

5. Discussion

HSCs are at the center of the immune system, as they produce all other hematopoietic cells at steady state and in case of emergency. A major regulator of HSCs is the chemokine CXCL12, which together with its receptor CXCR4, are considered to mediate cell retention in the BM (Zou et al., 1998, Ma et al., 1998, Nagasawa et al., 1996). The present study reveals for the first time a redundant role for ACKR3, the alternate CXCL12 receptor, in cell retention. More specifically, our data reveal a discrete expression pattern for ACKR3, compared to CXCR4, as it is not expressed in hematopoietic cells including HSCs. However, our data suggest that ACKR3 maintains HSC dormancy. As a result, although ACKR3 does not affect HSC differentiation at steady state definite murine hematopoiesis, the receptor is vital for the survival during emergency hematopoiesis. Under these conditions, ACKR3 regulates the transcription of the *Cxcl12* gene in the aorta, subsequently affecting the chemokine concentration in circulation. Finally, this study presents evidence that emphasize the role of the direct binding of CXCR4 to CXCL12 for cell retention in the BM, excluding alternate hypotheses on BM cell retention. Thus, our data reveal two discrete roles for the two chemokine receptors, with CXCR4 retaining HSCs in the BM and ACKR3 regulating cell biology, and under certain conditions the CXCL12 protein concentration.

5.1 ACKR3 is a tissue orchestrator

One major difference between the CXCR4 and ACKR3 is the cellular pattern of expression in the BM. The CXCL12 binding assay, that I developed in this study, unveiled the broad expression of CXCR4 is in both immature and mature hematopoietic cells. On the contrary, ACKR3 is not expressed on BM HSPC. In line with previous evidence (Gerrits et al., 2008), I detected a strong expression of GFP in the endosteum of the *Ackr3*^{GFP} mice, supporting the hypothesis that ACKR3 is expressed in cells of the endosteal lineage. In addition to the previously described expression of ACKR3 in the femoral endosteum (Gerrits et al., 2008), this study demonstrates ACKR3 expression in the endosteum of tibias and in the murine spine, suggesting that ACKR3 is a protein characterizing the endosteal cells. On the contrary, the expression of ACKR3 on vascular endothelial cells shows a complex mosaicism. I could not detect reliable GFP signal in endothelial cells in the BM, by both imaging and flow cytometry. However, the present study clearly demonstrates that ACKR3 is expressed in the endothelium of vessels in other tissues such as lung, kidney, and aorta. Of note, the proteomic profile of endothelial cells within a tissue exhibits great heterogeneity both in steady state (Marcu et al., 2018) and under immune responses (Gunawardana et al., 2021). Thus, ACKR3 expression in mice is not restricted to a single lineage, as it is present in both endothelial and endosteal cells, while a certain grade of discrepancy is observed among tissues. The expression on stromal cells suggests an indirect supportive role for ACKR3 in hematopoiesis.

In addition to the ACKR3 expression on stromal cells, we report here the expression of the receptor in murine BM plasma cells. In support of the present data, ACKR3 expression in human plasma cells and plasmablasts has been previously described (Humpert et al., 2012). The identification of an ACKR3^{+} B cell subtype in the murine spleen, which differentiate *in vitro* into plasma cells (Radice et al., 2020), make me hypothesize that this population differentiates and consequently migrates to the BM, while constantly expressing ACKR3. Nevertheless, the role of the receptor in the migration of these cell to the BM, and during immune responses remains elusive. Radice et al proposed that deletion of ACKR3 on CD19^{+} cells, affects the production of IgM during immune responses (Redice et al., 2020). Nevertheless, resting BM plasma cells do not express CD19 (Pracht et al., 2017, Brynjolfsson et al., 2018), and, hence, they were not targeted by this mouse model. In addition, plasma cells are characterized by the production of large amounts of IgG and IgA antibodies (Mei et al., 2009, Hallileyet al., 2015) for long periods after the B cell stimulation (Slifka et al., 1998). Thus, it would be interesting to assess the role of the ACKR3 receptor, both in the differentiation and the migration of the plasma cells, as well as its role in humoral immune responses.

In this regard, the present study suggests that ACKR3 does not affect HSC differentiation in steady state hematopoiesis. More specifically, the production of both myeloid and lymphoid cells remained unaltered after the deletion of ACKR3 in all tissues. It is important to note that all mice used in the present study were in *Apoe*$^{-/-}$ background. Hence, it is possible that changes on hematopoiesis and cell production were missed due to the low-grade inflammatory conditions induced by the absence of the gene (Zhang et al., 1992).

However, this study demonstrates for the first time a role for ACKR3 in the maintenance of the HSC dormancy in mice. The enhanced proliferation of the HSCs in the absence of the ACKR3, and the subsequent accumulation of intracellular ROS, demonstrates that ACKR3 is vital for the regulation of HSC metabolism. Nevertheless, the identification of the mechanism by which ACKR3 exerts its function has been proven to be a challenge. To this regard, the protein concentration of the ligand, CXCL12, remained unaltered in *Ubc-Ackr3*$^{-/-}$ mice. At the same time, no other cytokine was regulated, when I screened for 13 major cytokines involved in HSC biology. However, the deletion of CXCL12 in adult mice, phenocopied the accumulation of ROS in HSCs and the enhanced cell proliferation, observed in the *Ubc-Ackr3*$^{-/-}$ mice. Thus, it is possible that CXCL12 maintains HSC quiescence, preventing the accumulation of ROS in these cells. ACKR3 regulates CXCL12, promoting the hypoxic status in the cells, and consequently the absence of either the receptor or the chemokine induces the accumulation of ROS and promotes cells to exit dormancy. However, further experiments should be considered to fully elucidate the mechanism of the receptor in BM maintenance.

One hypothesis towards this aim, would be that ACKR3 deletion alters CXCL12 distribution locally, without affecting the total protein concentration. According to Kunz and Scroeder, who developed a system for CXCL12 protein detection, although CXCL12 does not form any gradient within the BM, there are some hotspots, where the chemokine accumulates, close to the endosteum (Kunz and Schroeder, 2019). Could the formation of these hotspots be due to the

proximal expression of ACKR3 in the endosteal cells? This assumption could be answered with the assessment of CXCL12 distribution in the BM in the *Ubc-Ackr3*$^{-/-}$ mice. An altered pattern of protein distribution in the BM could emphasize the role of ACKR3 in the distribution of the chemokine in the BM and the subsequent organization of the tissue.

It is detrimental to pinpoint the observation done by Radice et al that ACKR3 organizes spleen architecture, and in particular the development of the marginal zone, which is absent in ACKR3$^{-/-}$ mice (Radice et al., 2020). In this context, it is possible that ACKR3 also affects the localization of hematopoietic cells also in the BM. The assessment of HSC localization in *Ubc-Ackr3*$^{-/-}$ mice, could reveal whether the receptor regulates cell positioning within the BM environment, relatively to the endosteum, the sinusoids or the arterioles. Despite certain controversies (Acar et al., 2015, Nombela-Arrieta et al., 2013), HSC positioning in the BM has been correlated with the cell properties and the metabolic profile (Kunisaki et al 2013, Itkin et al., 2016). Thus, an altered HSC microenvironment could explain the altered metabolic phenotype of HSCs in the absence of ACKR3. A verification of this hypothesis would suggest that ACKR3, through the expression on stromal cells, is a major orchestrator of the HSC microenvironment, regulating the properties of the HSCs.

5.2 In the absence of ACKR3 mice are more susceptible to lethality after myeloablation

In addition to the role of ACKR3 in steady state hematopoiesis, the present study reveals for the first time that deletion of ACKR3 increases the susceptibility of the mouse model used after myeloablation with the chemotherapeutic agent 5FU. 5FU is a drug that interferes with RNA and DNA synthesis, evoking DNA repair mechanisms (Wyatt and Wilson, 2009), and is, thus, mainly affecting proliferating cells. Interestingly, the *Ubc-Ackr3*$^{-/-}$ mice that survived the turning point of day-10, fully reconstituted hematopoiesis. Thus, one hypothesis regarding the molecular mechanisms involved is that the aberrant proliferation of HSCs, in the absence of ACKR3, increase the vulnerability of these cells to 5FU, by inducing cell death. The HSCs that survive will, finally, reconstitute BM and restore hematopoiesis independently of ACKR3.

Another significant feature of the *Ubc-Ackr3*$^{-/-}$ mice, after the treatment with 5FU, which could also relate to the lethality, was the signs of anemia observed. This study reports a role for ACKR3 in red blood cell production, as the mice lacking ACKR3 exhibited reduced levels of hematocrit and hemoglobin after the 5FU treatment compared to the mice expressing ACKR3. To my knowledge this is the first time that the receptor is directly associated with these parameters. The only relevant data in literature demonstrate that infection with a Shiga toxin, which induces anemia *in vivo*, enhances ACKR3 expression in endothelial cells (Petruzziello-Pellegrini and Marsden, 2012). Interestingly, ACKR3 is not expressed on human erythroid cells (Berahovich et al., 2010), while our data further exclude the expression of the receptor on murine erythroid cells. Thus, it is hypothesized that ACKR3 regulates anemia indirectly via a distinct factor. In this regard,

IL-6, a cytokine that was significantly upregulated in the plasma of the 5FU-treated *Ubc-Ackr3*$^{-/-}$ mice, has been previously reported to exacerbate anemia (Yacoub et al., 2020). Thus, I propose the existence of an axis in which ACKR3 regulates the IL-6, affecting subsequently the production of red blood cells and their capacity to oxygenate tissues. In support of our hypothesis, overexpression of ACKR3 in cancer cells, induced the expression of IL-6 (Chen et al., 2016), whereas silencing of ACKR3 in an *in vitro* model of diabetes reduced the levels of the IL-6 protein (Yang et al., 2020). Thus, further experiments would help to identify the source of the circulating IL-6 and unveil the mechanism by which ACKR3 affects the erythrocytes. In addition, since the observations are based on a murine mouse model, the system should be translated to human biology at steady state, but also during emergency hematopoiesis induced by a cytotoxic drug, such as 5FU.

5.2 ACKR3 creates a regulatory loop for *Cxcl12* gene expression in murine aorta

In the present study, I inhibited ACKR3 in two independent models, using a transgenic mouse model in which ACKR3 was depleted in all cells after the treatment with tamoxifen, and a mouse model in which the receptor was inhibited via an antagonist. Nevertheless, there were no evidence of LSK mobilization in any of the models used, and thus, the present study provides for the first-time concrete evidence that ACKR3 is not involved in the retention of HSCs. As a result, it can be concluded that the role of ACKR3 in HSC maintenance is discrete from the role of CXCR4, which is involved in the retention of HSPC in the BM.

In addition, the present data reveal a role for ACKR3 in the regulation of CXCL12 concentration under specific conditions. More specifically, the conditional knock down of ACKR3 did not alter CXCL12 concentration in both plasma and BM at steady state mice. This result is contradicting to what previously observed in total ko mice, in which the concentration of circulating CXCL12 was significantly elevated (Berahovich et al., 2014). Of note, the total *Ackr3*$^{-/-}$ mice exhibit a survival rate of 30% (Gerrits et al., 2008), which stresses out concrete discrepancies with our model, in which the conditional deletion of the receptor was induced during definite hematopoiesis. Thus, our data are more reliable for the role of ACKR3 at steady state hematopoiesis and exclude the possibility of an artifact due to developmental malformations.

On the contrary, the administration of the ACKR3 pharmacological inhibitor resulted in a rapid increase of circulating CXCL12 6h after the administration. Intriguingly, this effect is observed in an even more pronounced way after the administration of the CXCR4 inhibitor, AMD3100, where circulating CXCL12 is increased within 1h. Due to the elapsed time to these responses, it can be assumed that the inhibitors regulate CXCL12 in the protein and not the gene level. The questions arising are whether these two inhibitors act via the same receptor, and which receptor that would be. In this regard, ACKR3 antagonist was reported not to interact with the CXCR4 (Richard-Bilstein et al., 2020). On the contrary, AMD3100 has been characterized as an agonist, but not an

antagonist, for ACKR3 (Kalatskaya et al., 2009). It could be hypothesized that the AMD3100-mediated elevation of the circulating CXCL12 concentration is due to an off-site effect to the receptor ACKR3. Dar et al supported that the altered concentration of CXCL12 in plasma and BM after AMD3100 is due to CXCL12 release from CXCR4+ BM stromal cells (Dar et al., 2011). Hence, it would be interesting to assess the AMD3100-dependent dysregulation of BM and circulating CXCL12 in ACKR3-/- mice. This model could answer the question on whether AMD3100 binding to ACKR3 affects CXCL12 concentration and give us new insights on the mechanism the routinely used drug, AMD3100, functions.

Atypical chemokine receptors act by scavenging, transferring, and presenting chemokines (Vacchini et al., 2016). The present data could, thus, elucidate the mechanism by which ACKR3 acts, regulating systemic CXCL12. To this end, it has been previously reported that ACKR3 degrades CXCL12 (Naumann et al., 2010). To verify or disprove this hypothesis, the BM CXCL12 concentration should be assessed in the mice treated with the AKCR3 antagonist at 6h, when the concentration of circulating CXCL12 reached a peak. If the BM CXCL12 levels remain unaltered after the treatment with the inhibitor, it could be considered that the elevation of the circulating CXCL12 concentration results from the blockade of the ACKR3-mediated CXCL12 scavenging.

On the contrary, a decrease in the BM CXCL12 after the administration of the ACKR3 inhibitor, would support the role of ACKR3 in regulating chemokine transferring among tissues. Nevertheless, in the present study the expression of ACKR3 on BM endothelial cells was extensively investigated, and disproved. Thus, it could be hypothesized that the role of ACKR3 on chemokine transferring is indirect, and an alternative hypothesis should be formed. One such hypothesis would be that the elevation of the systemic CXCL12 and the downregulation of CXCL12 in tissues is the result of vessel leakiness after the ACKR3 blockade. To this end, the assessment of endothelial cell integrity should be assessed with the injection of fluorescent dextran of different size. A confirmation of this theory would suggest that ACKR3 instead of a transferring receptor, is a protein maintaining vessel integrity.

Nevertheless, despite the exact mechanism by which ACKR3 pharmacological blockade results in the increase of circulating CXCL12, the fact that this effect is seen 6 hours after the inhibition, could explain the discrepancies with the inducible ko model, which was used in this study. It is possible that alternative mechanisms have been activated in our *in vivo* model to balance the dysregulation of the CXCL12 axis after the deletion of the ACKR3 receptor. In accordance with this hypothesis, the administration of ACKR3 antagonist in healthy volunteers results only in a transient increase of CXCL12 that peaks within the first 24h (Huynh et al., 2021). Hence, the elapsed time after the ACKR3 inhibition is important for the effect on CXCL12 concentration, as secondary mechanisms restore the concentration of CXCL12 in the plasma.

Changes in the experimental model with the administration of 5FU and the consequent myeloablation, altered the balance of the system, and resulted in a profound increase of circulating CXCL12, during the recovery phase. Although, a potent role of ACKR3 on vessel integrity, as analyzed above, would explain the changes observed in both circulation and BM after

the 5FU, the enhanced expression of ACKR3 on aortic cells after the myeloablation, prompted me to also investigate the expression of *Cxcl12* in these cells, relatively to ACKR3.

As shown by Döring et al, a major source of the circulating CXCL12 is BMX^{+} endothelial cells (Döring et al., 2019). Thus, I assessed the expression of CXCL12 in aortic cells isolated from the 5FU treated mice. Strikingly, aortic cells lacking ACKR3 exhibited significantly enhanced *Cxcl12* expression. Thus, it could be concluded that the binding of CXCL12 to ACKR3 activates an intracellular pathway that inhibits the gene transcription in these cells. The depletion of the receptor prevents the inhibition leading to aberrant gene expression and potentially the accumulation of circulating CXCL12. To our knowledge this is the first time that it is reported that ACKR3 regulates CXCL12 gene expression.

5.3 CXCL12/CXCR4 interaction retain hematopoietic cells in the BM

In addition to the role of ACKR3 in HSC maintenance and CXCL12 regulation, the mouse models developed for this study provided the tools to draw conclusions on the mechanisms retaining LSK cells in the BM. To this end, in contrast to the hypothesis correlating the elevation of the circulating CXCL12 concentration with the mobilization of LSK to the blood (Dar et al., 2011), our data do not support this hypothesis. Increase of the circulating CXCL12 was observed after the pharmacological inhibition of ACKR3 and during the myeloablation in *Ubc-Ackr3*$^{-/-}$ mice. However, no LSK cells were detected in the periphery. Similarly, the artificial increase of circulating CXCL12 by injection of the chemokine in mice depleted of CXCL12 did not affect the number of LSK cells in the BM nor the periphery. Hence, it is concluded, that the concentration of CXCL12 does not affect HSPC retention nor mobilization.

On the contrary, the present data strengthen the evidence regarding the direct role of CXCR4 for HSPC anchoring. To this end, unfortunately the *Fgd5-Cxcr4*$^{-/-}$ mice employed did not provide reliable data. Despite the mobilization of colony-forming cells in the circulation of *Fgd5-Cxcr4*$^{-/-}$ mice, the expression of CXCR4 in the surface and the cytoplasm of HSCs did not significantly change. The low percentage of cells expressing both Fgd5 and CXCR4 suggest that the *Fgd5*$^{ZsGr.CreERT2}$ model is not ideal for the assessment of the role of CXCR4. Thus, another HSC specific model should be employed to assess HSC mobilization after the deletion of CXCR4 in these cells. Nevertheless, the mobilization observed when knocking out CXCR4 in BM cells, but not in BM stromal cells, underlines that the direct activation of CXCR4 on hematopoietic cells mediates cell retention in the BM.

Whether this effect is only mediated by anchoring of CXCR4 on hematopoietic cells to the immobilized CXCL12 on BM stromal cells, or whether indirect anchoring molecules are involved has yet to be elucidated. The absence of mobilization in *Ubc-Cxcl12*$^{-/-}$ mice favors the hypothesis that additional extracellular molecules are involved in the CXCR4-dependent retention. Of note, a limitation of the model is that BM CXCL12 exhibited a 6-fold reduction, which suggests a significant depletion of the chemokine, but not a total deletion. It is proposed that the

administration of tamoxifen for a longer time period than the 2 months may assist the complete removal of the chemokine from the system. However, the absence of any reduction in the number of BM HSPC or in the number of circulating LSK, strengthens the hypothesis that additional molecules are involved in CXCR4-mediated cell retention.

To this end, *in vitro* system could be developed to study the binding of LSK cells to immobilized integrins in the presence and absence of the CXCR4/CXCL12. In this system, the screening of downstream kinase pathways, and the assessment of extracellular integrins on cell surface could reveal the molecular details of the mechanism. In this manner, the identification of novel and more efficient therapeutic targets for cell mobilization in clinic could be enabled. Moreover, G-CSF, a drug that has the disadvantage of the multiple dosing, could be replaced by other molecules, targeting the identified integrins, or the CXCR4/CXCL12 axis and thus eliminating the side effects of G-CSF injection (bone pain, redness, fever)

Finally, it is always possible that a novel undescribed ligand for CXCR4 mediates cell retention. In this regard, ubiquitin, the small protein involved in protein degradation, has been identified as a ligand for CXCR4 on myeloid cells. In addition, extracellular ubiquitin signals through CXCR4, inducing a Ca^{2+} mediated response (Saini et al., 2010). Other ligands that have been described for CXCR4 include the viral chemokine CCL2 and β-defensins (Adlere et al., 2019). Thus, it would be interesting to abrogate the binding of ubiquitin to CXCR4 *in vivo* and consequently to assess the role of the interaction in cell mobilization. Alternatively, an *in silico* High Throughput Screening should be employed to identify novel ligands for CXCR4.

5.4 Translational perspectives of the study

ACKR3 has been previously detected in human B cells (Humpert et al., 2012, Zabel et al., 2011, Sierro et al., 2007), but not in $CD34^+$ hematopoietic stem cells (Berahovich et al., 2010). Moreover, ACKR3 has been found to be expressed in human primary endothelial cells (Naumann et al., 2010). Our data on murine tissues reveal a similar expression profile of the receptor between the two species and, although further evaluation on the ACKR3 expressing cells within the human BM is needed, it is possible that ACKR3 exerts a comparable supportive role in human hematopoiesis, too. Lately, there has been a development of bone marrow organoids enabling the *ex vivo* mimicking of human hematopoiesis (Iordachescu et al., 2021, Giger et al., 2021). Thus, in order to elucidate the role of ACKR3 on human HSCs, the development of an organoid system is proposed, which would allow the *ex vivo* culture of HSCs in the presence of $ACKR3^+$ stromal cells. The data generated could reveal the role of ACKR3 in human hematopoiesis and enable us to evaluate the translation of our murine data.

HSC biology is detrimental during aging, malignancies and the development of cardiovascular diseases. Thus, unveiling the role of ACKR3 and targeting the receptor via small molecules would find multiple applications in clinic. During aging, HSCs exhibit an altered extracellular marker phenotype, skewed differentiation toward cells of the myeloid lineage, increased mobilization,

enhanced proliferative capacity and accumulation of DNA mutations (Geiger et al., 2013, de Haan and Lazare, 2018, Verovskaya et al., 2019). Thus, ACKR3 could transform into a key target to regulate HSC metabolism and functionality. In addition, certain changes occur in the environment of an aged BM. Osteoblast regeneration is downregulated, whereas the vessel network changes. Finally, aged BM is characterized by the enhanced deposition of fat cells (Verovskaya et al., 2019), a phenomenon that also affects the concentration of CXCL12, as the increased BM adiposity has been correlated with a reduction in circulating CXCL12 (Tuljapurkar et al., 2011). In summary, ACKR3 as a potent orchestrator of the BM microenvironment and a regulator of HSC biology, would be a novel target for the prevention of HSC aging.

In addition, both ACKR3 chemokine ligands, CXCL12 and CXCL11 have been correlated with CVD, whereas the role of ACKR3 remains elusive (Gencer et al., 2019). Nevertheless, it is important to note that during CVD, HSCs exhibit a senescent phenotype (Fabiola et al., 2013). More specifically, due to cellular proliferation, the telomeric DNA regions shorten. As a result, HSCs inherit mutations. The accumulation of mutations in HSCs due to proliferation and senescence results in the generation and prevail of certain HSC clones, a phenomenon termed as Clonal Hematopoiesis of Intermediate Potential (CHIP) (de Haan and Lazare, 2018, Evans et al., 2020, Jaiswal and Ebert, 2019). Individuals carrying mutated HSC clones were twice likely to exhibit a coronary heart disease, and increased risk for myocardial infraction (Jaiswal et al., 2017). Mechanistically, it has been presumed that the exacerbated atherosclerosis is due to the IL-1b production by the mutated clones. Additionally, IL-6 is considered to further induce CVD establishment (Lee et al., 2020, Jaiswal et al., 2017). Thus, an ACKR3-based therapeutic line could target HSC metabolism and consequently CHIP, as well as the production of inflammatory cytokines.

In hematopoietic malignancies, HSCs alter their oxidative profile. The pathway of oxidative phosphorylation is markedly used to produce energy, while the intracellular ROS levels remain low (Panuzzo et al., 2020). The regulated expression of transcription factors and antioxidant genes favor the maintenance of low ROS levels, which facilitates the maintenance of the HSCs and the establishment of the disease (Samimi et al., 2018). At the same time, the acquisition of favoring mutations, enhancing HSC survival and proliferation further predispose HSCs towards leukemia (Shlush et al., 2014). Moreover, CHIP is also a hallmark of hematopoietic malignancies, as mutations in specific genes induce the clonal expansion of HSCs (Genovese et al., 2014). Last but not least, 5FU is a frontline drug in the treatment of malignancies (Heidelberger et al., 1957, Casale and Crane, 2020). Thus, the interpretation of the present murine data on the role of ACKR3 in HSC susceptibility to 5FU to human biology would be of high value to ease chemotherapies' adverse effects.

Finally, Hematopoietic autologous and allogeneic stem cell transplantation (HSCT) is an established treatment for patients with hematopoietic malignancies (Dessie et al., 2020, Khaddour et al., 2021). Thus, our concrete data on the mechanism involved in CXCR4-dependent retention of HSCs could further facilitate the development of novel HSCT protocols for the remedy of hematopoietic diseases and beyond.

In summary, this study identifies the endosteal and endothelial cells as major ACKR3-expressing populations and reveals the role of the receptor in the regulation of HSC quiescence. In addition, the present data reveal that ACKR3 regulates CXCL12 concentration, and, consequently, short-term ACKR3 blockade triggers an increase of CXCL12 concentration in plasma. Nevertheless, CXCL12, and, thus, ACKR3 do not mediate HSC retention, for which CXCR4 is the key factor.

References

1. Abe, P., Mueller, W., Schütz, D., MacKay, F., Thelen, M., Zhang, P., & Stumm, R. (2014). CXCR7 prevents excessive CXCL12-mediated downregulation of CXCR4 in migrating cortical interneurons. *Development*, *141*(9), 1857–1863. https://doi.org/10.1242/dev.104224

2. Acar, M., Kocherlakota, K. S., Murphy, M. M., Peyer, J. G., Oguro, H., Inra, C. N., Jaiyeola, C., Zhao, Z., Luby-Phelps, K., & Morrison, S. J. (2015). Deep imaging of bone marrow shows non-dividing stem cells are mainly perisinusoidal. *Nature*, *526*(7571), 126–130. https://doi.org/10.1038/nature15250

3. Adapala, N. S., Root, S., Lorenzo, J., Aguila, H., & Sanjay, A. (2019). PI3K activation increases SDF-1 production and number of osteoclast precursors, and enhances SDF-1-mediated osteoclast precursor migration. *Bone Reports*, *10*, 100203. https://doi.org/10.1016/j.bonr.2019.100203

4. Adlere, I., Caspar, B., Arimont, M., Dekkers, S., Visser, K., Stuijt, J., Graaf, C. de, Stocks, M., Kellam, B., Briddon, S., Wijtmans, M., Esch, I. de, Hill, S., & Leurs, R. (2019). Modulators of CXCR4 and CXCR7/ACKR3 Function. *Molecular Pharmacology*, *96*(6), 737–752. https://doi.org/10.1124/mol.119.117663

5. Alampour-Rajabi, S., El Bounkari, O., Rot, A., Müller-Newen, G., Bachelerie, F., Gawaz, M., Weber, C., Schober, A., & Bernhagen, J. (2015). MIF interacts with CXCR7 to promote receptor internalization, ERK1/2 and ZAP-70 signaling, and lymphocyte chemotaxis. *The FASEB Journal*, *29*(11), 4497–4511. https://doi.org/10.1096/fj.15-273904

6. Almeida, M. J. de, Luchsinger, L. L., Corrigan, D. J., Williams, L. J., & Snoeck, H.-W. (2017). Dye-Independent Methods Reveal Elevated Mitochondrial Mass in Hematopoietic Stem Cells. *Cell Stem Cell*, *21*(6), 725-729.e4. https://doi.org/10.1016/j.stem.2017.11.002

7. Amjad, M. T., Chidharla, A., & Kasi, A. (2021). Cancer Chemotherapy. In *StatPearls*. StatPearls Publishing. http://www.ncbi.nlm.nih.gov/books/NBK564367/

8. Angelopoulou, M. K., Tsirkinidis, P., Boutsikas, G., Vassilakopoulos, T. P., & Tsirigotis, P. (2014). New Insights in the Mobilization of Hematopoietic Stem Cells in Lymphoma and Multiple Myeloma Patients. *BioMed Research International*, *2014*, 835138. https://doi.org/10.1155/2014/835138

9. Aoki, K., Kurashige, M., Ichii, M., Higaki, K., Sugiyama, T., Kaito, T., Ando, W., Sugano, N., Sakai, T., Shibayama, H., Takaori-Kondo, A., Morii, E., Kanakura, Y., & Nagasawa, T. (2021). Identification of CXCL12-abundant reticular cells in human adult bone marrow. *British Journal of Haematology*, *193*(3), 659–668. https://doi.org/10.1111/bjh.17396

10. Asada, N., Katayama, Y., Sato, M., Minagawa, K., Wakahashi, K., Kawano, H., Kawano, Y., Sada, A., Ikeda, K., Matsui, T., & Tanimoto, M. (2013). Matrix-Embedded Osteocytes Regulate Mobilization of Hematopoietic Stem/Progenitor Cells. *Cell Stem Cell*, *12*(6), 737–747. https://doi.org/10.1016/j.stem.2013.05.001

11. Asada, N., Takeishi, S., & Frenette, P. S. (2017). Complexity of bone marrow hematopoietic stem cell niche. *International Journal of Hematology*, *106*(1), 45–54. https://doi.org/10.1007/s12185-017-2262-9

12. Baba, M., Toyama, H., Sun, L., Takubo, K., Suh, H.-C., Hasumi, H., Nakamura-Ishizu, A., Hasumi, Y., Klarmann, K. D., Nakagata, N., Schmidt, L. S., Linehan, W. M., Suda, T., & Keller, J. R. (2016). Loss of Folliculin Disrupts Hematopoietic Stem Cell Quiescence and Homeostasis Resulting in Bone Marrow Failure. *STEM CELLS*, *34*(4), 1068–1082. https://doi.org/10.1002/stem.2293

13. Bachelerie, F., Ben-Baruch, A., Burkhardt, A. M., Combadiere, C., Farber, J. M., Graham, G. J., Horuk, R., Sparre-Ulrich, A. H., Locati, M., Luster, A. D., Mantovani, A., Matsushima, K., Murphy, P. M., Nibbs, R., Nomiyama, H., Power, C. A., Proudfoot, A. E. I., Rosenkilde, M. M., Rot, A., … Zlotnik, A. (2014). International Union of Basic and Clinical Pharmacology. LXXXIX. Update on the Extended Family of Chemokine Receptors and Introducing a New Nomenclature for Atypical Chemokine Receptors. *Pharmacological Reviews*, *66*(1), 1–79. https://doi.org/10.1124/pr.113.007724

14. Bai, L., Best, G., Xia, W., Peters, L., Wong, K., Ward, C., & Greenwood, M. (2018). Expression of Intracellular Reactive Oxygen Species in Hematopoietic Stem Cells Correlates with Time to Neutrophil and Platelet Engraftment in Patients Undergoing Autologous Bone Marrow Transplantation. *Biology of Blood and Marrow Transplantation*, *24*(10), 1997–2002. https://doi.org/10.1016/j.bbmt.2018.06.014

15. Balabanian, K., Brotin, E., Biajoux, V., Bouchet-Delbos, L., Lainey, E., Fenneteau, O., Bonnet, D., Fiette, L., Emilie, D., & Bachelerie, F. (2012). Proper desensitization of CXCR4 is required for lymphocyte development and peripheral compartmentalization in mice. *Blood*, *119*(24), 5722–5730. https://doi.org/10.1182/blood-2012-01-403378

16. Balabanian, K., Lagane, B., Infantino, S., Chow, K. Y. C., Harriague, J., Moepps, B., Arenzana-Seisdedos, F., Thelen, M., & Bachelerie, F. (2005). The Chemokine SDF-1/CXCL12 Binds to and Signals through the Orphan Receptor RDC1 in T Lymphocytes. *Journal of Biological Chemistry*, *280*(42), 35760–35766. https://doi.org/10.1074/jbc.M508234200

17. Banisadr, G., Podojil, J. R., Miller, S. D., & Miller, R. J. (2016). Pattern of CXCR7 Gene Expression in Mouse Brain Under Normal and Inflammatory Conditions. *Journal of Neuroimmune Pharmacology : The Official Journal of the Society on NeuroImmune Pharmacology*, *11*(1), 26–35. https://doi.org/10.1007/s11481-015-9616-y

18. Becker, N. B., Günther, M., Li, C., Jolly, A., & Höfer, T. (2019). Stem cell homeostasis by integral feedback through the niche. *Journal of Theoretical Biology*, *481*, 100–109. https://doi.org/10.1016/j.jtbi.2018.12.029

19. Berahovich, R. D., Zabel, B. A., Lewén, S., Walters, M. J., Ebsworth, K., Wang, Y., Jaen, J. C., & Schall, T. J. (2014). Endothelial expression of CXCR7 and the regulation of systemic CXCL12 levels. *Immunology*, *141*(1), 111–122. https://doi.org/10.1111/imm.12176

20. Berahovich, R. D., Zabel, B. A., Penfold, M. E. T., Lewén, S., Wang, Y., Miao, Z., Gan, L., Pereda, J., Dias, J., Slukvin, I. I., McGrath, K. E., Jaen, J. C., & Schall, T. J. (2010). CXCR7 Protein Is Not Expressed on Human or Mouse Leukocytes. *The Journal of Immunology*, *185*(9), 5130–5139. https://doi.org/10.4049/jimmunol.1001660

21. Bernitz, J. M., Kim, H.-S., MacArthur, B., Sieburg, H., & Moore, K. (2016). Hematopoietic Stem Cells Count and Remember Self-Renewal Divisions. *Cell*, *167*(5), 1296-1309.e10. https://doi.org/10.1016/j.cell.2016.10.022

22. Boldajipour, B., Mahabaleshwar, H., Kardash, E., Reichman-Fried, M., Blaser, H., Minina, S., Wilson, D., Xu, Q., & Raz, E. (2008). Control of Chemokine-Guided Cell Migration by Ligand Sequestration. *Cell*, *132*(3), 463–473. https://doi.org/10.1016/j.cell.2007.12.034

23. Bonecchi, R., Locati, M., Galliera, E., Vulcano, M., Sironi, M., Fra, A. M., Gobbi, M., Vecchi, A., Sozzani, S., Haribabu, B., Van Damme, J., & Mantovani, A. (2004). Differential recognition and scavenging of native and truncated macrophage-derived chemokine (macrophage-derived chemokine/CC chemokine ligand 22) by the D6 decoy receptor. *Journal of Immunology (Baltimore, Md.: 1950)*, *172*(8), 4972–4976.

24. Boneyard, L. F. (2011). The Amazing Osteocyte. *Journal of Bone and Mineral Research*, *26*(2), 229–238. https://doi.org/10.1002/jbmr.320

25. Bourke, V. A., Watchman, C. J., Reith, J. D., Jorgensen, M. L., Dieudonnè, A., & Bolch, W. E. (2009). Spatial gradients of blood vessels and hematopoietic stem and progenitor cells within the marrow cavities of the human skeleton. *Blood*, *114*(19), 4077–4080. https://doi.org/10.1182/blood-2008-12-192922

26. Breitbach, M., Kimura, K., Luis, T. C., Fuegemann, C. J., Woll, P. S., Hesse, M., Facchini, R., Rieck, S., Jobin, K., Reinhardt, J., Ohneda, O., Wenzel, D., Geisen, C., Kurts, C., Kastenmüller, W., Hölzel, M., Jacobsen, S. E. W., & Fleischmann, B. K. (2018). In Vivo Labeling by CD73 Marks Multipotent Stromal Cells and Highlights Endothelial Heterogeneity in the Bone Marrow Niche. *Cell Stem Cell*, *22*(2), 262-276.e7. https://doi.org/10.1016/j.stem.2018.01.008

27. Broxmeyer, H. E., Orschell, C. M., Clapp, D. W., Hangoc, G., Cooper, S., Plett, P. A., Liles, W. C., Li, X., Graham-Evans, B., Campbell, T. B., Calandra, G., Bridger, G., Dale, D. C., & Srour, E. F. (2005). Rapid mobilization of murine and human hematopoietic stem and progenitor cells with AMD3100, a CXCR4 antagonist. *Journal of Experimental Medicine*, *201*(8), 1307–1318. https://doi.org/10.1084/jem.20041385

28. Bruns, I., Lucas, D., Pinho, S., Ahmed, J., Lambert, M. P., Kunisaki, Y., Scheiermann, C., Schiff, L., Poncz, M., Bergman, A., & Frenette, P. S. (2014). Megakaryocytes regulate hematopoietic stem cell quiescence through CXCL4 secretion. *Nature Medicine*, *20*(11), 1315–1320. https://doi.org/10.1038/nm.3707

29. Brynjolfsson, S. F., Persson Berg, L., Olsen Ekerhult, T., Rimkute, I., Wick, M.-J., Mårtensson, I.-L., & Grimsholm, O. (2018). Long-Lived Plasma Cells in Mice and Men. *Frontiers in Immunology*, *9*, 2673. https://doi.org/10.3389/fimmu.2018.02673

30. Burns, J. M., Summers, B. C., Wang, Y., Melikian, A., Berahovich, R., Miao, Z., Penfold, M. E. T., Sunshine, M. J., Littman, D. R., Kuo, C. J., Wei, K., McMaster, B. E., Wright, K., Howard, M. C., & Schall, T. J. (2006). A novel chemokine receptor for SDF-1 and I-TAC involved in cell survival, cell adhesion, and tumor development. *Journal of Experimental Medicine*, *203*(9), 2201–2213. https://doi.org/10.1084/jem.20052144

31. Busch, K., Klapproth, K., Barile, M., Flossdorf, M., Holland-Letz, T., Schlenner, S. M., Reth, M., Höfer, T., & Rodewald, H.-R. (2015). Fundamental properties of unperturbed haematopoiesis from stem cells in vivo. *Nature*, *518*(7540), 542–546. https://doi.org/10.1038/nature14242

32. Canals, M., Scholten, D. J., Munnik, S. de, Han, M. K. L., Smit, M. J., & Leurs, R. (2012). Ubiquitination of CXCR7 Controls Receptor Trafficking. *PLOS ONE*, *7*(3), e34192. https://doi.org/10.1371/journal.pone.0034192

33. Carroll, D., & St. Clair, D. K. (2018). Hematopoietic Stem Cells: Normal Versus Malignant. *Antioxidants & Redox Signaling*, *29*(16), 1612–1632. https://doi.org/10.1089/ars.2017.7326

34. Cao, Y., Fang, Y., Cai, J., Li, X., Xu, F., Yuan, N., Zhang, S., & Wang, J. (2016). ROS functions as an upstream trigger for autophagy to drive hematopoietic stem cell differentiation. *Hematology*, *21*(10), 613–618. https://doi.org/10.1080/10245332.2016.1165446

35. Capitano, M. L., Hangoc, G., Cooper, S., & Broxmeyer, H. E. (2015). Mild Heat Treatment Primes Human CD34+ Cord Blood Cells for Migration Toward SDF-1α and Enhances Engraftment in an NSG Mouse Model. *STEM CELLS*, *33*(6), 1975–1984. https://doi.org/10.1002/stem.1988

36. Casale, J., & Crane, J. S. (2020). Fluorouracil. In *StatPearls*. StatPearls Publishing. http://www.ncbi.nlm.nih.gov/books/NBK549808/

37. Cascio, M. J., & DeLoughery, T. G. (2017). Anemia: Evaluation and Diagnostic Tests. *Medical Clinics of North America*, *101*(2), 263–284. https://doi.org/10.1016/j.mcna.2016.09.003

38. Chavakis, T., Mitroulis, I., & Hajishengallis, G. (2019). Hematopoietic progenitor cells as integrative hubs for adaptation to and fine-tuning of inflammation. *Nature Immunology*, *20*(7), 802–811. https://doi.org/10.1038/s41590-019-0402-5

39. Chen, K., Bao, Z., Tang, P., Gong, W., Yoshimura, T., & Wang, J. M. (2018). Chemokines in homeostasis and diseases. *Cellular and Molecular Immunology*, *15*(4), 324–334. https://doi.org/10.1038/cmi.2017.134

40. Chen, Q., Liu, Y., Jeong, H.-W., Stehling, M., Dinh, V. V., Zhou, B., & Adams, R. H. (2019). Apelin+ Endothelial Niche Cells Control Hematopoiesis and Mediate Vascular Regeneration after Myeloablative Injury. *Cell Stem Cell*, *25*(6), 768-783.e6. https://doi.org/10.1016/j.stem.2019.10.006

41. Chen, Y., Teng, F., Wang, G., & Nie, Z. (2016). Overexpression of CXCR7 induces angiogenic capacity of human hepatocellular carcinoma cells via the AKT signaling pathway. *Oncology Reports*, *36*(4), 2275–2281. https://doi.org/10.3892/or.2016.5045

42. Cheng, M., Zhou, J., Wu, M., Boriboun, C., Thorne, T., Liu, T., Xiang, Z., Zeng, Q., Tanaka, T., Tang, Y. L., Kishore, R., Tomasson, M. H., Miller, R. J., Losordo, D. W., & Qin, G. (2010). CXCR4-mediated bone marrow progenitor cell maintenance and mobilization are modulated by c-kit activity. *Circulation Research*, *107*(9), 1083–1093. https://doi.org/10.1161/CIRCRESAHA.110.220970

43. Chow, A., Lucas, D., Hidalgo, A., Méndez-Ferrer, S., Hashimoto, D., Scheiermann, C., Battista, M., Leboeuf, M., Prophete, C., van Rooijen, N., Tanaka, M., Merad, M., & Frenette, P. S. (2011). Bone marrow CD169+ macrophages promote the retention of hematopoietic stem and progenitor cells in the mesenchymal stem cell niche. *Journal of Experimental Medicine*, *208*(2), 261–271. https://doi.org/10.1084/jem.20101688

44. Christodoulou, C., Spencer, J. A., Yeh, S.-C. A., Turcotte, R., Kokkaliaris, K. D., Panero, R., Ramos, A., Guo, G., Seyedhassantehrani, N., Esipova, T. V., Vinogradov, S. A., Rudzinskas, S., Zhang, Y., Perkins, A. S., Orkin, S. H., Calogero, R. A., Schroeder, T., Lin, C. P., & Camargo, F. D. (2020). Live-animal imaging of native haematopoietic stem and progenitor cells. *Nature*, *578*(7794), 278–283. https://doi.org/10.1038/s41586-020-1971-z

45. Christopher, M. J., Liu, F., Hilton, M. J., Long, F., & Link, D. C. (2009). Suppression of CXCL12 production by bone marrow osteoblasts is a common and critical pathway for cytokine-induced mobilization. *Blood*, *114*(7), 1331–1339. https://doi.org/10.1182/blood-2008-10-184754

46. Christopher, M. J., Rao, M., Liu, F., Woloszynek, J. R., & Link, D. C. (2011). Expression of the G-CSF receptor in monocytic cells is sufficient to mediate hematopoietic progenitor mobilization by G-CSF in mice. *Journal of Experimental Medicine*, *208*(2), 251–260. https://doi.org/10.1084/jem.20101700

47. Comazzetto, S., Murphy, M. M., Berto, S., Jeffery, E., Zhao, Z., & Morrison, S. J. (2019). Restricted Hematopoietic Progenitors and Erythropoiesis Require SCF from Leptin Receptor+ Niche Cells in the Bone Marrow. *Cell Stem Cell*, *24*(3), 477-486.e6. https://doi.org/10.1016/j.stem.2018.11.022

48. Connell, B. J., Sadir, R., Baleux, F., Laguri, C., Kleman, J.-P., Luo, L., Arenzana-Seisdedos, F., & Lortat-Jacob, H. (2016). Heparan sulfate differentially controls CXCL12α- and CXCL12γ-mediated cell migration through differential presentation to their receptor CXCR4. *Science Signaling*, *9*(452), ra107. https://doi.org/10.1126/scisignal.aaf1839

49. Coutu, D. L., Kokkaliaris, K. D., Kunz, L., & Schroeder, T. (2017). Three-dimensional map of nonhematopoietic bone and bone-marrow cells and molecules. *Nature Biotechnology*, *35*(12), 1202–1210. https://doi.org/10.1038/nbt.4006

50. Crump, M. P., Gong, J.-H., Loetscher, P., Rajarathnam, K., Amara, A., Arenzana-Seisdedos, F., Virelizier, J.-L., Baggiolini, M., Sykes, B. D., & Clark-Lewis, I. (1997). Solution structure and basis for functional activity of stromal cell-derived factor-1; dissociation of CXCR4 activation from binding and inhibition of HIV-1. *The EMBO Journal*, *16*(23), 6996–7007. https://doi.org/10.1093/emboj/16.23.6996

51. Cruz-Orengo, L., Holman, D. W., Dorsey, D., Zhou, L., Zhang, P., Wright, M., McCandless, E. E., Patel, J. R., Luker, G. D., Littman, D. R., Russell, J. H., & Klein, R. S. (2011). CXCR7 influences leukocyte entry into the CNS parenchyma by controlling abluminal CXCL12 abundance during autoimmunity. *Journal of Experimental Medicine*, *208*(2), 327–339. https://doi.org/10.1084/jem.20102010

52. Dar, A., Goichberg, P., Shinder, V., Kalinkovich, A., Kollet, O., Netzer, N., Margalit, R., Zsak, M., Nagler, A., Hardan, I., Resnick, I., Rot, A., & Lapidot, T. (2005). Chemokine receptor CXCR4–dependent internalization and resecretion of functional chemokine SDF-1 by bone marrow endothelial and stromal cells. *Nature Immunology*, *6*(10), 1038–1046. https://doi.org/10.1038/ni1251

53. Dar, A., Schajnovitz, A., Lapid, K., Kalinkovich, A., Itkin, T., Ludin, A., Kao, W.-M., Battista, M., Tesio, M., Kollet, O., Cohen, N. N., Margalit, R., Buss, E. C., Baleux, F., Oishi, S., Fujii, N., Larochelle, A., Dunbar, C. E., Broxmeyer, H. E., … Lapidot, T. (2011). Rapid mobilization of hematopoietic progenitors by AMD3100 and catecholamines is mediated by CXCR4-dependent SDF-1 release from bone marrow stromal cells. *Leukemia*, *25*(8), 1286–1296. https://doi.org/10.1038/leu.2011.62

54. Day, R. B., Bhattacharya, D., Nagasawa, T., & Link, D. C. (2015). Granulocyte colony-stimulating factor reprograms bone marrow stromal cells to actively suppress B lymphopoiesis in mice. *Blood*, *125*(20), 3114–3117. https://doi.org/10.1182/blood-2015-02-629444

55. De Clercq, E. (2003). The bicyclam AMD3100 story. *Nature Reviews Drug Discovery*, *2*(7), 581–587. https://doi.org/10.1038/nrd1134

56. de Haan, G., & Lazare, S. S. (2018). Aging of hematopoietic stem cells. *Blood*, *131*(5), 479–487. https://doi.org/10.1182/blood-2017-06-746412

57. Décaillot, F. M., Kazmi, M. A., Lin, Y., Ray-Saha, S., Sakmar, T. P., & Sachdev, P. (2011). CXCR7/CXCR4 Heterodimer Constitutively Recruits β-Arrestin to Enhance Cell Migration. *Journal of Biological Chemistry*, *286*(37), 32188–32197. https://doi.org/10.1074/jbc.M111.277038

58. Deshpande, O. A., & Mohiuddin, S. S. (2021). Biochemistry, Oxidative Phosphorylation. In *StatPearls*. StatPearls Publishing. http://www.ncbi.nlm.nih.gov/books/NBK553192/

59. Dessie, G., Derbew Molla, M., Shibabaw, T., & Ayelign, B. (2020). Role of Stem-Cell Transplantation in Leukemia Treatment. *Stem Cells and Cloning : Advances and Applications*, *13*, 67–77. https://doi.org/10.2147/SCCAA.S262880

60. DeWire, S. M., Ahn, S., Lefkowitz, R. J., & Shenoy, S. K. (2007). β-Arrestins and Cell Signaling. *Annual Review of Physiology*, *69*(1), 483–510. https://doi.org/10.1146/annurev.physiol.69.022405.154749

61. Di Giandomenico, S., Kermani, P., Mollé, N., Yabut, M. M., Abu-Zeinah, G., Stephens, T., Messali, N., Schreiner, R., Brenet, F., Rafii, S., & Scandura, J. M. (2020). Megakaryocyte TGFβ1 partitions erythropoiesis into immature progenitor/stem cells and maturing precursors. *Blood*, *136*(9), 1044–1054. https://doi.org/10.1182/blood.2019003276

62. Ding, L., & Morrison, S. J. (2013). Haematopoietic stem cells and early lymphoid progenitors occupy distinct bone marrow niches. *Nature*, *495*(7440), 231–235. https://doi.org/10.1038/nature11885

63. Ding, L., Saunders, T. L., Enikolopov, G., & Morrison, S. J. (2012). Endothelial and perivascular cells maintain haematopoietic stem cells. *Nature*, *481*(7382), 457–462. https://doi.org/10.1038/nature10783

64. Domingues, M. J., Nilsson, S. K., & Cao, B. (2017). New agents in HSC mobilization. *International Journal of Hematology*, *105*(2), 141–152. https://doi.org/10.1007/s12185-016-2156-2

65. Donzella, G. A., Schols, D., Lin, S. W., Esté, J. A., Nagashima, K. A., Maddon, P. J., Allaway, G. P., Sakmar, T. P., Henson, G., DeClercq, E., & Moore, J. P. (1998). AMD3100, a small molecule inhibitor of HIV-1 entry via the CXCR4 co-receptor. *Nature Medicine*, *4*(1), 72–77. https://doi.org/10.1038/nm0198-072

66. Döring, Y., van der Vorst, E. P. C., Duchene, J., Jansen, Y., Gencer, S., Bidzhekov, K., Atzler, D., Santovito, D., Rader, D. J., Saleheen, D., & Weber, C. (2019). CXCL12 Derived From Endothelial Cells Promotes Atherosclerosis to Drive Coronary Artery Disease. *Circulation*, *139*(10), 1338–1340. https://doi.org/10.1161/CIRCULATIONAHA.118.037953

67. Driessen, R. L., Johnston, H. M., & Nilsson, S. K. (2003). Membrane-bound stem cell factor is a key regulator in the initial lodgment of stem cells within the endosteal marrow region. *Experimental Hematology*, *31*(12), 1284–1291. https://doi.org/10.1016/j.exphem.2003.08.015

68. Emmons, R., Niemiro, G. M., & De Lisio, M. (2017). Hematopoiesis with Obesity and Exercise: Role of the Bone Marrow Niche. *Exercise Immunology Review*, *23*, 82–95.

69. Esplin, B. L., Shimazu, T., Welner, R. S., Garrett, K. P., Nie, L., Zhang, Q., Humphrey, M. B., Yang, Q., Borghesi, L. A., & Kincade, P. W. (2011). Chronic Exposure to a TLR Ligand Injures Hematopoietic Stem Cells. *Journal of Immunology (Baltimore, Md. : 1950)*, *186*(9), 5367–5375. https://doi.org/10.4049/jimmunol.1003438

70. Evans, M. A., Sano, S., & Walsh, K. (2020). Cardiovascular Disease, Aging, and Clonal Hematopoiesis. *Annual Review of Pathology*, *15*, 419–438. https://doi.org/10.1146/annurev-pathmechdis-012419-032544

71. Fabiola, O., Rina, R., Fiorella, M., Angela, M. A., Gabriele, S., Giulia, B., Roberto, A., & Antonio, D. P. (2013). Cellular Senescence in Cardiovascular Diseases: Potential Age-Related Mechanisms and Implications for Treatment. *Current Pharmaceutical Design*, *19*(9), 1710–1719.

72. Feil, R., Wagner, J., Metzger, D., & Chambon, P. (1997). Regulation of Cre recombinase activity by mutated estrogen receptor ligand-binding domains. *Biochemical and Biophysical Research Communications*, *237*(3), 752–757. https://doi.org/10.1006/bbrc.1997.7124

73. Ferrucci, L., & Fabbri, E. (2018). Inflammageing: Chronic inflammation in ageing, cardiovascular disease, and frailty. *Nature Reviews Cardiology*, *15*(9), 505–522. https://doi.org/10.1038/s41569-018-0064-2

74. Fischer, A., Notarangelo, L. D., Neven, B., Cavazzana, M., & Puck, J. M. (2015). Severe combined immunodeficiencies and related disorders. *Nature Reviews Disease Primers*, *1*(1), 1–18. https://doi.org/10.1038/nrdp.2015.61

75. Freitas, C., Wittner, M., Nguyen, J., Rondeau, V., Biajoux, V., Aknin, M.-L., Gaudin, F., Beaussant-Cohen, S., Bertrand, Y., Bellanné-Chantelot, C., Donadieu, J., Bachelerie, F., Espéli, M., Dalloul, A., Louache, F., & Balabanian, K. (2017). Lymphoid differentiation of hematopoietic stem cells requires efficient Cxcr4 desensitization. *The Journal of Experimental Medicine*, *214*(7), 2023–2040. https://doi.org/10.1084/jem.20160806

76. Frost, H. M. (1969). Tetracycline-based histological analysis of bone remodeling. *Calcified Tissue Research*, *3*(3), 211–237. https://doi.org/10.1007/bf02058664

77. Fumagalli, A., Zarca, A., Neves, M., Caspar, B., Hill, S. J., Mayor, F., Smit, M. J., & Marin, P. (2019). CXCR4/ACKR3 phosphorylation and recruitment of interacting proteins: Key mechanisms regulating their functional status. *Molecular Pharmacology*. https://doi.org/10.1124/mol.118.115360

78. Fukuma, N., Akimitsu, N., Hamamoto, H., Kusuhara, H., Sugiyama, Y., & Sekimizu, K. (2003). A role of the Duffy antigen for the maintenance of plasma chemokine concentrations. *Biochemical and Biophysical Research Communications*, *303*(1), 137–139. https://doi.org/10.1016/S0006-291X(03)00293-6

79. Fukushima, T., Tanaka, Y., Hamey, F. K., Chang, C.-H., Oki, T., Asada, S., Hayashi, Y., Fujino, T., Yonezawa, T., Takeda, R., Kawabata, K. C., Fukuyama, T., Umemoto, T., Takubo, K., Takizawa, H., Goyama, S., Ishihama, Y., Honda, H., Göttgens, B., & Kitamura, T. (2019). Discrimination of Dormant and Active Hematopoietic Stem Cells by G0 Marker Reveals Dormancy Regulation by Cytoplasmic Calcium. *Cell Reports*, *29*(12), 4144-4158.e7. https://doi.org/10.1016/j.celrep.2019.11.061

80. Galliera, E., Jala, V. R., Trent, J. O., Bonecchi, R., Signorelli, P., Lefkowitz, R. J., Mantovani, A., Locati, M., & Haribabu, B. (2004). β-Arrestin-dependent Constitutive Internalization of the Human Chemokine Decoy Receptor D6 *. *Journal of Biological Chemistry*, *279*(24), 25590–25597. https://doi.org/10.1074/jbc.M400363200

81. Gao, X., Enten, G. A., DeSantis, A. J., Volkman, B. F., Gaponenko, V., & Majetschak, M. (2020). Characterization of heteromeric complexes between chemokine (C-X-C motif) receptor 4 and α1-adrenergic receptors utilizing intermolecular bioluminescence resonance energy transfer assays. *Biochemical and Biophysical Research Communications*. https://doi.org/10.1016/j.bbrc.2020.02.094

82. Gao, X., Zhang, D., Xu, C., Li, H., Caron, K. M., & Frenette, P. S. (2021). Nociceptive nerves regulate haematopoietic stem cell mobilization. *Nature*, *589*(7843), 591–596. https://doi.org/10.1038/s41586-020-03057-y

83. Gardner, L., Patterson, A. M., Ashton, B. A., Stone, M. A., & Middleton, J. (2004). The human Duffy antigen binds selected inflammatory but not homeostatic chemokines. *Biochemical and Biophysical Research Communications*, *321*(2), 306–312. https://doi.org/10.1016/j.bbrc.2004.06.146

84. Gazit, R., Mandal, P. K., Ebina, W., Ben-Zvi, A., Nombela-Arrieta, C., Silberstein, L. E., & Rossi, D. J. (2014). Fgd5 identifies hematopoietic stem cells in the murine bone marrow. *The Journal of Experimental Medicine*, *211*(7), 1315–1331. https://doi.org/10.1084/jem.20130428

85. Gębura, K., Butrym, A., Chaszczewska-Markowska, M., Wróbel, T., Kuliczkowski, K., & Bogunia-Kubik, K. (2019). G-CSF administration favours SDF-1 release and activation of neutrophils and monocytes in recipients of autologous peripheral blood progenitor cells. *Cytokine*, *116*, 38–47. https://doi.org/10.1016/j.cyto.2018.12.011

86. Geddis, A. E. (2010). Megakaryopoiesis. *Seminars in Hematology*, *47*(3), 212–219. https://doi.org/10.1053/j.seminhematol.2010.03.001

87. Geiger, H., de Haan, G., & Florian, M. C. (2013). The ageing haematopoietic stem cell compartment. *Nature Reviews Immunology*, *13*(5), 376–389. https://doi.org/10.1038/nri3433

88. Gencer, S., van der Vorst, E. P. C., Aslani, M., Weber, C., Döring, Y., & Duchene, J. (2019). Atypical Chemokine Receptors in Cardiovascular Disease. *Thrombosis and Haemostasis*, *119*(4), 534–541. https://doi.org/10.1055/s-0038-1676988

89. Genovese, G., Kähler, A. K., Handsaker, R. E., Lindberg, J., Rose, S. A., Bakhoum, S. F., Chambert, K., Mick, E., Neale, B. M., Fromer, M., Purcell, S. M., Svantesson, O., Landén, M., Höglund, M., Lehmann, S., Gabriel, S. B., Moran, J. L., Lander, E. S., Sullivan, P. F., … McCarroll, S. A. (2014). Clonal Hematopoiesis and Blood-Cancer Risk Inferred from Blood DNA Sequence. *The New England Journal of Medicine*, *371*(26), 2477–2487. https://doi.org/10.1056/NEJMoa1409405

90. Gerrits, H., Schenau, D. S. van I., Bakker, N. E. C., Disseldorp, A. J. M. van, Strik, A., Hermens, L. S., Koenen, T. B., Krajnc-Franken, M. A. M., & Gossen, J. A. (2008). Early postnatal lethality and cardiovascular defects in CXCR7-deficient mice. *Genesis*, *46*(5), 235–245. https://doi.org/10.1002/dvg.20387

91. Giger, S., Hofer, M., Miljkovic-Licina, M., Hoehnel, S., Brandenberg, N., Guiet, R., Ehrbar, M., Kleiner, E., Gegenschatz, K., Matthes, T., & Lutolf, M. P. (2021). *Microarrayed human bone marrow organoids for modeling blood stem cell dynamics* (p. 2021.05.26.445803). https://doi.org/10.1101/2021.05.26.445803

92. Gomariz, A., Helbling, P. M., Isringhausen, S., Suessbier, U., Becker, A., Boss, A., Nagasawa, T., Paul, G., Goksel, O., Székely, G., Stoma, S., Nørrelykke, S. F., Manz, M. G., & Nombela-Arrieta, C. (2018). Quantitative spatial analysis of haematopoiesis-regulating stromal cells in the bone marrow

microenvironment by 3D microscopy. *Nature Communications*, *9*. https://doi.org/10.1038/s41467-018-04770-z

93. Goodman, O. B., Krupnick, J. G., Santini, F., Gurevich, V. V., Penn, R. B., Gagnon, A. W., Keen, J. H., & Benovic, J. L. (1996). β-Arrestin acts as a clathrin adaptor in endocytosis of the β 2 -adrenergic receptor. *Nature*, *383*(6599), 447–450. https://doi.org/10.1038/383447a0

94. Gosling, J., Dairaghi, D. J., Wang, Y., Hanley, M., Talbot, D., Miao, Z., & Schall, T. J. (2000). Cutting Edge: Identification of a Novel Chemokine Receptor That Binds Dendritic Cell- and T Cell-Active Chemokines Including ELC, SLC, and TECK. *The Journal of Immunology*, *164*(6), 2851–2856. https://doi.org/10.4049/jimmunol.164.6.2851

95. Göttgens, B. (2015). Regulatory network control of blood stem cells. *Blood*, *125*(17), 2614–2620. https://doi.org/10.1182/blood-2014-08-570226

96. Graham, G. J., Handel, T. M., & Proudfoot, A. E. I. (2019). Leukocyte Adhesion: Reconceptualizing Chemokine Presentation by Glycosaminoglycans. *Trends in Immunology*, *40*(6), 472–481. https://doi.org/10.1016/j.it.2019.03.009

97. Graham, G. J., Locati, M., Mantovani, A., Rot, A., & Thelen, M. (2012). The biochemistry and biology of the atypical chemokine receptors. *Immunology Letters*, *145*(1), 30–38. https://doi.org/10.1016/j.imlet.2012.04.004

98. Greenbaum, A., Hsu, Y.-M. S., Day, R. B., Schuettpelz, L. G., Christopher, M. J., Borgerding, J. N., Nagasawa, T., & Link, D. C. (2013). CXCL12 in early mesenchymal progenitors is required for haematopoietic stem-cell maintenance. *Nature*, *495*(7440), 227–230. https://doi.org/10.1038/nature11926

99. Gunawardana, H., Romero, T., Yao, N., Heidt, S., Mulder, A., Elashoff, D. A., & Valenzuela, N. M. (2021). Tissue-specific endothelial cell heterogeneity contributes to unequal inflammatory responses. *Scientific Reports*, *11*(1), 1949. https://doi.org/10.1038/s41598-020-80102-w

100. Gustavsson, M., Dyer, D. P., Zhao, C., & Handel, T. M. (2019). Kinetics of CXCL12 binding to atypical chemokine receptor 3 reveal a role for the receptor N-terminus in chemokine binding. *Science Signaling*, *12*(598). https://doi.org/10.1126/scisignal.aaw3657

101. Haas, S., Trumpp, A., & Milsom, M. D. (2018). Causes and Consequences of Hematopoietic Stem Cell Heterogeneity. *Cell Stem Cell*, *22*(5), 627–638. https://doi.org/10.1016/j.stem.2018.04.003

102. Halliley, J. L., Tipton, C. M., Liesveld, J., Rosenberg, A. F., Darce, J., Gregoretti, I. V., Popova, L., Kaminiski, D., Fucile, C. F., Albizua, I., Kyu, S., Chiang, K.-Y., Bradley, K. T., Burack, R., Slifka, M., Hammarlund, E., Wu, H., Zhao, L., Walsh, E. E., … Lee, F. E.-H. (2015). Long-Lived Plasma Cells Are Contained within the CD19(-)CD38(hi)CD138(+) Subset in Human Bone Marrow. *Immunity*, *43*(1), 132–145. https://doi.org/10.1016/j.immuni.2015.06.016

103. Hansell, C. A. H., Hurson, C. E., & Nibbs, R. J. B. (2011). DARC and D6: Silent partners in chemokine regulation? *Immunology and Cell Biology*, *89*(2), 197–206. https://doi.org/10.1038/icb.2010.147

104. Harper, J. M., Wilkinson, J. E., & Miller, R. A. (2010). Macrophage migration inhibitory factor-knockout mice are long lived and respond to caloric restriction. *The FASEB Journal*, *24*(7), 2436–2442. https://doi.org/10.1096/fj.09-152223

105. Heesen, M., Berman, M. A., Charest, A., Housman, D., Gerard, C., & Dorf, M. E. (1998). Cloning and chromosomal mapping of an orphan chemokine receptor: Mouse RDC1. *Immunogenetics*, *47*(5), 364–370. https://doi.org/10.1007/s002510050371

106. Heidelberger, C., Chaudhuri, N. K., Danneberg, P., Mooren, D., Griesbach, L., Duschinsky, R., Schnitzer, R. J., Pleven, E., & Scheiner, J. (1957). Fluorinated Pyrimidines, A New Class of Tumour-Inhibitory Compounds. *Nature*, *179*(4561), 663–666. https://doi.org/10.1038/179663a0

107. Hendrix, C. W., Flexner, C., MacFarland, R. T., Giandomenico, C., Fuchs, E. J., Redpath, E., Bridger, G., & Henson, G. W. (2000). Pharmacokinetics and Safety of AMD-3100, a Novel Antagonist of the CXCR-4 Chemokine Receptor, in Human Volunteers. *Antimicrobial Agents and Chemotherapy*, *44*(6), 1667–1673. https://doi.org/10.1128/AAC.44.6.1667-1673.2000

108. Hermetet, F., Buffière, A., Aznague, A., Pais de Barros, J.-P., Bastie, J.-N., Delva, L., & Quéré, R. (2019). High-fat diet disturbs lipid raft/TGF-β signaling-mediated maintenance of hematopoietic stem cells in mouse bone marrow. *Nature Communications*, *10*(1), 1–11. https://doi.org/10.1038/s41467-018-08228-0

109. Hilger, D., Masureel, M., & Kobilka, B. K. (2018). Structure and dynamics of GPCR signaling complexes. *Nature Structural & Molecular Biology*, *25*(1), 4–12. https://doi.org/10.1038/s41594-017-0011-7

110. Hoggatt, J., Kfoury, Y., & Scadden, D. T. (2016). Hematopoietic Stem Cell Niche in Health and Disease. *Annual Review of Pathology: Mechanisms of Disease*, *11*(1), 555–581. https://doi.org/10.1146/annurev-pathol-012615-044414

111. Holmbeck, K., Bianco, P., Pidoux, I., Inoue, S., Billinghurst, R. C., Wu, W., Chrysovergis, K., Yamada, S., Birkedal-Hansen, H., & Poole, A. R. (2005). The metalloproteinase MT1-MMP is required for normal development and maintenance of osteocyte processes in bone. *Journal of Cell Science*, *118*(1), 147–156. https://doi.org/10.1242/jcs.01581

112. Hook, C., Yamaguchi, K., Scheid, P., & Piiper, J. (1988). Oxygen transfer of red blood cells: Experimental data and model analysis. *Respiration Physiology*, *72*(1), 65–82. https://doi.org/10.1016/0034-5687(88)90080-1

113. Hopman, R. K., & DiPersio, J. F. (2014). Advances in stem cell mobilization. *Blood Reviews*, *28*(1), 31–40. https://doi.org/10.1016/j.blre.2014.01.001

114. Hughes, C. E., & Nibbs, R. J. B. (2018). A guide to chemokines and their receptors. *The FEBS Journal*, *285*(16), 2944–2971. https://doi.org/10.1111/febs.14466

115. Humpert, M.-L., Pinto, D., Jarrossay, D., & Thelen, M. (2014). CXCR7 influences the migration of B cells during maturation. *European Journal of Immunology*, *44*(3), 694–705. https://doi.org/10.1002/eji.201343907

116. Humpert, M.-L., Tzouros, M., Thelen, S., Bignon, A., Levoye, A., Arenzana-Seisdedos, F., Balabanian, K., Bachelerie, F., Langen, H., & Thelen, M. (2012). Complementary methods provide evidence for the expression of CXCR7 on human B cells. *PROTEOMICS*, *12*(12), 1938–1948. https://doi.org/10.1002/pmic.201100581

117. Huynh, C., Henrich, A., Strasser, D. S., Boof, M.-L., Al-Ibrahim, M., Meyer Zu Schwabedissen, H. E., Dingemanse, J., & Ufer, M. (2021). A Multipurpose First-in-Human Study With the Novel CXCR7 Antagonist ACT-1004-1239 Using CXCL12 Plasma Concentrations as Target Engagement Biomarker. *Clinical Pharmacology & Therapeutics*, *109*(6), 1648–1659. https://doi.org/10.1002/cpt.2154

118. Ikuta, K., & Weissman, I. L. (1992). Evidence that hematopoietic stem cells express mouse c-kit but do not depend on steel factor for their generation. *Proceedings of the National Academy of Sciences of the United States of America*, *89*(4), 1502–1506.

119. Infantino, S., Moepps, B., & Thelen, M. (2006). Expression and Regulation of the Orphan Receptor RDC1 and Its Putative Ligand in Human Dendritic and B Cells. *The Journal of Immunology*, *176*(4), 2197–2207. https://doi.org/10.4049/jimmunol.176.4.2197

120. Iordachescu, A., Hughes, E. A. B., Joseph, S., Hill, E. J., Grover, L. M., & Metcalfe, A. D. (2021). Trabecular bone organoids: A micron-scale 'humanised' prototype designed to study the effects of microgravity and degeneration. *Npj Microgravity*, *7*(1), 1–21. https://doi.org/10.1038/s41526-021-00146-8

121. Israels, L. G. (1969). Chemotherapy of Hematological Malignancies. *Canadian Family Physician*, *15*(1), 36–39.

122. Itkin, T., Gur-Cohen, S., Spencer, J. A., Schajnovitz, A., Ramasamy, S. K., Kusumbe, A. P., Ledergor, G., Jung, Y., Milo, I., Poulos, M. G., Kalinkovich, A., Ludin, A., Kollet, O., Shakhar, G., Butler, J. M., Rafii, S., Adams, R. H., Scadden, D. T., Lin, C. P., & Lapidot, T. (2016). Distinct bone marrow blood vessels differentially regulate hematopoiesis. *Nature*, *532*(7599), 323–328. https://doi.org/10.1038/nature17624

123. Ito, K., Hirao, A., Arai, F., Takubo, K., Matsuoka, S., Miyamoto, K., Ohmura, M., Naka, K., Hosokawa, K., Ikeda, Y., & Suda, T. (2006). Reactive oxygen species act through p38 MAPK to limit the lifespan of hematopoietic stem cells. *Nature Medicine*, *12*(4), 446–451. https://doi.org/10.1038/nm1388

124. Ito, K., Turcotte, R., Cui, J., Zimmerman, S. E., Pinho, S., Mizoguchi, T., Arai, F., Runnels, J. M., Alt, C., Teruya-Feldstein, J., Mar, J. C., Singh, R., Suda, T., Lin, C. P., Frenette, P. S., & Ito, K. (2016). Self-renewal of a purified Tie2+ hematopoietic stem cell population relies on mitochondrial clearance. *Science*, *354*(6316), 1156–1160. https://doi.org/10.1126/science.aaf5530

125. Jaiswal, S., & Ebert, B. L. (2019). Clonal hematopoiesis in human aging and disease. *Science (New York, N.Y.)*, *366*(6465), eaan4673. https://doi.org/10.1126/science.aan4673

126. Jaiswal, S., Natarajan, P., Silver, A. J., Gibson, C. J., Bick, A. G., Shvartz, E., McConkey, M., Gupta, N., Gabriel, S., Ardissino, D., Baber, U., Mehran, R., Fuster, V., Danesh, J., Frossard, P., Saleheen, D., Melander, O., Sukhova, G. K., Neuberg, D., … Ebert, B. L. (2017). Clonal Hematopoiesis and Risk of Atherosclerotic Cardiovascular Disease. *The New England Journal of Medicine*, *377*(2), 111–121. https://doi.org/10.1056/NEJMoa1701719

127. Jamieson, T., Cook, D. N., Nibbs, R. J. B., Rot, A., Nixon, C., Mclean, P., Alcami, A., Lira, S. A., Wiekowski, M., & Graham, G. J. (2005). The chemokine receptor D6 limits the inflammatory response *in vivo*. *Nature Immunology*, *6*(4), 403–411. https://doi.org/10.1038/ni1182

128. Janssens, R., Struyf, S., & Proost, P. (2018). The unique structural and functional features of CXCL12. *Cellular & Molecular Immunology*, *15*(4), 299–311. https://doi.org/10.1038/cmi.2017.107

129. Jin, G., Xu, C., Zhang, X., Long, J., Rezaeian, A. H., Liu, C., Furth, M. E., Kridel, S., Pasche, B., Bian, X.-W., & Lin, H.-K. (2018). Atad3a suppresses Pink1-dependent mitophagy to maintain homeostasis of hematopoietic progenitor cells. *Nature Immunology*, *19*(1), 29–40. https://doi.org/10.1038/s41590-017-0002-1

130. Jørgensen, A. S., Daugvilaite, V., De Filippo, K., Berg, C., Mavri, M., Benned-Jensen, T., Juzenaite, G., Hjortø, G., Rankin, S., Våbenø, J., & Rosenkilde, M. M. (2021). Biased action of the CXCR4-targeting drug plerixafor is essential for its superior hematopoietic stem cell mobilization. *Communications Biology*, *4*(1), 1–12. https://doi.org/10.1038/s42003-021-02070-9

131. Kalatskaya, I., Berchiche, Y. A., Gravel, S., Limberg, B. J., Rosenbaum, J. S., & Heveker, N. (2009). AMD3100 Is a CXCR7 Ligand with Allosteric Agonist Properties. *Molecular Pharmacology*, *75*(5), 1240–1247. https://doi.org/10.1124/mol.108.053389

132. Kashiwazaki, M., Tanaka, T., Kanda, H., Ebisuno, Y., Izawa, D., Fukuma, N., Akimitsu, N., Sekimizu, K., Monden, M., & Miyasaka, M. (2003). A high endothelial venule-expressing promiscuous chemokine receptor DARC can bind inflammatory, but not lymphoid, chemokines and is dispensable for lymphocyte homing under physiological conditions. *International Immunology*, *15*(10), 1219–1227. https://doi.org/10.1093/intimm/dxg121

133. Katayama, Y., Battista, M., Kao, W.-M., Hidalgo, A., Peired, A. J., Thomas, S. A., & Frenette, P. S. (2006). Signals from the Sympathetic Nervous System Regulate Hematopoietic Stem Cell Egress from Bone Marrow. *Cell*, *124*(2), 407–421. https://doi.org/10.1016/j.cell.2005.10.041

134. Kato, G. J., Piel, F. B., Reid, C. D., Gaston, M. H., Ohene-Frempong, K., Krishnamurti, L., Smith, W. R., Panepinto, J. A., Weatherall, D. J., Costa, F. F., & Vichinsky, E. P. (2018). Sickle cell disease. *Nature Reviews Disease Primers*, *4*(1), 1–22. https://doi.org/10.1038/nrdp.2018.10

135. Kawaguchi, N., Zhang, T.-T., & Nakanishi, T. (2019). Involvement of CXCR4 in Normal and Abnormal Development. *Cells*, *8*(2). https://doi.org/10.3390/cells8020185

136. Khaddour, K., Hana, C. K., & Mewawalla, P. (2021). Hematopoietic Stem Cell Transplantation. In *StatPearls*. StatPearls Publishing. http://www.ncbi.nlm.nih.gov/books/NBK536951/

137. Kiel, M. J., He, S., Ashkenazi, R., Gentry, S. N., Teta, M., Kushner, J. A., Jackson, T. L., & Morrison, S. J. (2007). Haematopoietic stem cells do not asymmetrically segregate chromosomes or retain BrdU. *Nature*, *449*(7159), 238–242. https://doi.org/10.1038/nature06115

138. Klasen, C., Ohl, K., Sternkopf, M., Shachar, I., Schmitz, C., Heussen, N., Hobeika, E., Levit-Zerdoun, E., Tenbrock, K., Reth, M., Bernhagen, J., & Bounkari, O. E. (2014). MIF Promotes B Cell Chemotaxis through the Receptors CXCR4 and CD74 and ZAP-70 Signaling. *The Journal of Immunology*, *192*(11), 5273–5284. https://doi.org/10.4049/jimmunol.1302209

139. Klener, P., Etrych, T., & Klener, P. (2019). Biological Therapy of Hematologic Malignancies: Toward a Chemotherapy- free Era. *Current Medicinal Chemistry*, *26*(6), 1002–1018. https://doi.org/10.2174/0929867324666171006144725

140. Kondo, M., Wagers, A. J., Manz, M. G., Prohaska, S. S., Scherer, D. C., Beilhack, G. F., Shizuru, J. A., & Weissman, I. L. (2003). Biology of Hematopoietic Stem Cells and Progenitors: Implications for Clinical Application. *Annual Review of Immunology*, *21*(1), 759–806. https://doi.org/10.1146/annurev.immunol.21.120601.141007

141. Kufareva, I., Gustavsson, M., Zheng, Y., Stephens, B. S., & Handel, T. M. (2017). What Do Structures Tell Us About Chemokine Receptor Function and Antagonism? *Annual Review of Biophysics*, *46*, 175–198. https://doi.org/10.1146/annurev-biophys-051013-022942

142. Kufareva, I., Stephens, B. S., Holden, L. G., Qin, L., Zhao, C., Kawamura, T., Abagyan, R., & Handel, T. M. (2014). Stoichiometry and geometry of the CXC chemokine receptor 4 complex with CXC ligand 12: Molecular modeling and experimental validation. *Proceedings of the National Academy of Sciences*, *111*(50), E5363–E5372. https://doi.org/10.1073/pnas.1417037111

143. Kunisaki, Y., Bruns, I., Scheiermann, C., Ahmed, J., Pinho, S., Zhang, D., Mizoguchi, T., Wei, Q., Lucas, D., Ito, K., Mar, J. C., Bergman, A., & Frenette, P. S. (2013). Arteriolar niches maintain haematopoietic stem cell quiescence. *Nature*, *502*(7473), 637–643. https://doi.org/10.1038/nature12612

144. Kunz, L., & Schroeder, T. (2019). A 3D Tissue-wide Digital Imaging Pipeline for Quantitation of Secreted Molecules Shows Absence of CXCL12 Gradients in Bone Marrow. *Cell Stem Cell*, *25*(6), 846-854.e4. https://doi.org/10.1016/j.stem.2019.10.003

145. Kurosawa, S., & Iwama, A. (2020). Aging and leukemic evolution of hematopoietic stem cells under various stress conditions. *Inflammation and Regeneration*, *40*, 29. https://doi.org/10.1186/s41232-020-00138-3

146. Laporte, S. A., Miller, W. E., Kim, K.-M., & Caron, M. G. (2002). β-Arrestin/AP-2 Interaction in G Protein-coupled Receptor Internalization: IDENTIFICATION OF A β-ARRESTIN BINDING SITE IN β2-

ADAPTIN*. *Journal of Biological Chemistry*, *277*(11), 9247–9254. https://doi.org/10.1074/jbc.M108490200

147. Levoye, A., Balabanian, K., Baleux, F., Bachelerie, F., & Lagane, B. (2009). CXCR7 heterodimerizes with CXCR4 and regulates CXCL12-mediated G protein signaling. *Blood*, *113*(24), 6085–6093. https://doi.org/10.1182/blood-2008-12-196618

148. Lau, S., Feitzinger, A., Venkiteswaran, G., Wang, J., Lewellis, S. W., Koplinski, C. A., Peterson, F. C., Volkman, B. F., Meier-Schellersheim, M., & Knaut, H. (2020). A negative-feedback loop maintains optimal chemokine concentrations for directional cell migration. *Nature Cell Biology*, *22*(3), 266–273. https://doi.org/10.1038/s41556-020-0465-4

149. Laurenti, E., & Göttgens, B. (2018). From haematopoietic stem cells to complex differentiation landscapes. *Nature*, *553*(7689), 418–426. https://doi.org/10.1038/nature25022

150. Lee, M. K. S., Dragoljevic, D., Bertuzzo Veiga, C., Wang, N., Yvan-Charvet, L., & Murphy, A. J. (2020). Interplay between Clonal Hematopoiesis of Indeterminate Potential and Metabolism. *Trends in Endocrinology & Metabolism*, *31*(7), 525–535. https://doi.org/10.1016/j.tem.2020.02.005

151. Liang, R., Arif, T., Kalmykova, S., Kasianov, A., Lin, M., Menon, V., Qiu, J., Bernitz, J. M., Moore, K., Lin, F., Benson, D. L., Tzavaras, N., Mahajan, M., Papatsenko, D., & Ghaffari, S. (2020). Restraining Lysosomal Activity Preserves Hematopoietic Stem Cell Quiescence and Potency. *Cell Stem Cell*, *26*(3), 359-376.e7. https://doi.org/10.1016/j.stem.2020.01.013

152. Libert, F., Parmentier, M., Lefort, A., Dumont, J. E., & Vassart, G. (1990). Complete nucleotide sequence of a putative G protein coupled receptor: RDC1. *Nucleic Acids Research*, *18*(7), 1917.

153. Lipfert, J., Ödemis, V., Wagner, D.-C., Boltze, J., & Engele, J. (2013). CXCR4 and CXCR7 form a functional receptor unit for SDF-1/CXCL12 in primary rodent microglia. *Neuropathology and Applied Neurobiology*, *39*(6), 667–680. https://doi.org/10.1111/nan.12015

154. Liu, Q., Li, Z., Gao, J.-L., Wan, W., Ganesan, S., McDermott, D. H., & Murphy, P. M. (2015). The CXCR4 antagonist AMD3100 redistributes leukocytes from primary immune organs to secondary immune organs, lung and blood in mice. *European Journal of Immunology*, *45*(6), 1855–1867. https://doi.org/10.1002/eji.201445245

155. Ma, Q., Jones, D., Borghesani, P. R., Segal, R. A., Nagasawa, T., Kishimoto, T., Bronson, R. T., & Springer, T. A. (1998). Impaired B-lymphopoiesis, myelopoiesis, and derailed cerebellar neuron migration in CXCR4- and SDF-1-deficient mice. *Proceedings of the National Academy of Sciences*, *95*(16), 9448–9453. https://doi.org/10.1073/pnas.95.16.9448

156. Ma, Q., Jones, D., & Springer, T. A. (1999). The Chemokine Receptor CXCR4 Is Required for the Retention of B Lineage and Granulocytic Precursors within the Bone Marrow Microenvironment. *Immunity*, *10*(4), 463–471. https://doi.org/10.1016/S1074-7613(00)80046-1

157. Marcu, R., Choi, Y. J., Xue, J., Fortin, C. L., Wang, Y., Nagao, R. J., Xu, J., MacDonald, J. W., Bammler, T. K., Murry, C. E., Muczynski, K., Stevens, K. R., Himmelfarb, J., Schwartz, S. M., & Zheng, Y. (2018). Human Organ-Specific Endothelial Cell Heterogeneity. *IScience*, *4*, 20–35. https://doi.org/10.1016/j.isci.2018.05.003

158. Maryanovich, M., Zaltsman, Y., Ruggiero, A., Goldman, A., Shachnai, L., Zaidman, S. L., Porat, Z., Golan, K., Lapidot, T., & Gross, A. (2015). An MTCH2 pathway repressing mitochondria metabolism regulates haematopoietic stem cell fate. *Nature Communications*, *6*(1), 7901. https://doi.org/10.1038/ncomms8901

159. Matsuoka, Y., Nakatsuka, R., Sumide, K., Kawamura, H., Takahashi, M., Fujioka, T., Uemura, Y., Asano, H., Sasaki, Y., Inoue, M., Ogawa, H., Takahashi, T., Hino, M., & Sonoda, Y. (2015). Prospectively Isolated Human Bone Marrow Cell-Derived MSCs Support Primitive Human CD34-Negative Hematopoietic Stem Cells. *STEM CELLS*, *33*(5), 1554–1565. https://doi.org/10.1002/stem.1941

160. McDermott, D. H., Gao, J.-L., Liu, Q., Siwicki, M., Martens, C., Jacobs, P., Velez, D., Yim, E., Bryke, C. R., Hsu, N., Dai, Z., Marquesen, M. M., Stregevsky, E., Kwatemaa, N., Theobald, N., Priel, D. A. L., Pittaluga, S., Raffeld, M. A., Calvo, K. R., … Murphy, P. M. (2015). Chromothriptic Cure of WHIM Syndrome. *Cell*, *160*(4), 686–699. https://doi.org/10.1016/j.cell.2015.01.014

161. McDermott, D. H., Lopez, J., Deng, F., Liu, Q., Ojode, T., Chen, H., Ulrick, J., Kwatemaa, N., Kelly, C., Anaya-O'Brien, S., Garofalo, M., Marquesen, M., Hilligoss, D., DeCastro, R., Malech, H. L., & Murphy, P. M. (2011). AMD3100 is a potent antagonist at CXCR4R334X, a hyperfunctional mutant chemokine receptor and cause of WHIM syndrome. *Journal of Cellular and Molecular Medicine*, *15*(10), 2071–2081. https://doi.org/10.1111/j.1582-4934.2010.01210.x

162. Medzhitov, R. (2008). Origin and physiological roles of inflammation. *Nature*, *454*(7203), 428–435. https://doi.org/10.1038/nature07201

163. Mei, H. E., Yoshida, T., Sime, W., Hiepe, F., Thiele, K., Manz, R. A., Radbruch, A., & Dörner, T. (2009). Blood-borne human plasma cells in steady state are derived from mucosal immune responses. *Blood*, *113*(11), 2461–2469. https://doi.org/10.1182/blood-2008-04-153544

164. Méndez-Ferrer, S., Lucas, D., Battista, M., & Frenette, P. S. (2008). Haematopoietic stem cell release is regulated by circadian oscillations. *Nature*, *452*(7186), 442–447. https://doi.org/10.1038/nature06685

165. Méndez-Ferrer, S., Michurina, T. V., Ferraro, F., Mazloom, A. R., MacArthur, B. D., Lira, S. A., Scadden, D. T., Ma'ayan, A., Enikolopov, G. N., & Frenette, P. S. (2010). Mesenchymal and haematopoietic stem cells form a unique bone marrow niche. *Nature*, *466*(7308), 829–834. https://doi.org/10.1038/nature09262

166. Miao, M., Clercq, E. D., & Li, G. (2020). Clinical significance of chemokine receptor antagonists. *Expert Opinion on Drug Metabolism & Toxicology*, *16*(1), 11–30. https://doi.org/10.1080/17425255.2020.1711884

167. Miller, M. C., & Mayo, K. H. (2017). Chemokines from a Structural Perspective. *International Journal of Molecular Sciences*, *18*(10), 2088. https://doi.org/10.3390/ijms18102088

168. Min, K., Yoon, H.-J., Park, J. Y., Baidya, M., Dwivedi-Agnihotri, H., Maharana, J., Chaturvedi, M., Chung, K. Y., Shukla, A. K., & Lee, H. H. (2020). Crystal Structure of β-Arrestin 2 in Complex with CXCR7 Phosphopeptide. *Structure*. https://doi.org/10.1016/j.str.2020.06.002

169. Mitroulis, I., Chen, L.-S., Singh, R. P., Kourtzelis, I., Economopoulou, M., Kajikawa, T., Troullinaki, M., Ziogas, A., Ruppova, K., Hosur, K., Maekawa, T., Wang, B., Subramanian, P., Tonn, T., Verginis, P., Bonin, M. von, Wobus, M., Bornhäuser, M., Grinenko, T., … Chavakis, T. (2017). Secreted protein Del-1 regulates myelopoiesis in the hematopoietic stem cell niche. *The Journal of Clinical Investigation*, *127*(10), 3624–3639. https://doi.org/10.1172/JCI92571

170. Mitroulis, I., Ruppova, K., Wang, B., Chen, L.-S., Grzybek, M., Grinenko, T., Eugster, A., Troullinaki, M., Palladini, A., Kourtzelis, I., Chatzigeorgiou, A., Schlitzer, A., Beyer, M., Joosten, L. A. B., Isermann, B., Lesche, M., Petzold, A., Simons, K., Henry, I., … Chavakis, T. (2018). Modulation of Myelopoiesis Progenitors Is an Integral Component of Trained Immunity. *Cell*, *172*(1), 147-161.e12. https://doi.org/10.1016/j.cell.2017.11.034

171. Nagai, Y., Garrett, K. P., Ohta, S., Bahrun, U., Kouro, T., Akira, S., Takatsu, K., & Kincade, P. W. (2006). Toll-like Receptors on Hematopoietic Progenitor Cells Stimulate Innate Immune System Replenishment. *Immunity*, *24*(6), 801–812. https://doi.org/10.1016/j.immuni.2006.04.008

172. Nagasawa, T., Hirota, S., Tachibana, K., Takakura, N., Nishikawa, S., Kitamura, Y., Yoshida, N., Kikutani, H., & Kishimoto, T. (1996). Defects of B-cell lymphopoiesis and bone-marrow myelopoiesis in mice lacking the CXC chemokine PBSF/SDF-1. *Nature*, *382*(6592), 635–638. https://doi.org/10.1038/382635a0

173. Nagasawa, T., Nakajima, T., Tachibana, K., Iizasa, H., Bleul, C. C., Yoshie, O., Matsushima, K., Yoshida, N., Springer, T. A., & Kishimoto, T. (1996). Molecular cloning and characterization of a murine pre-B-cell growth-stimulating factor/stromal cell-derived factor 1 receptor, a murine homolog of the human immunodeficiency virus 1 entry coreceptor fusin. *Proceedings of the National Academy of Sciences*, *93*(25), 14726–14729. https://doi.org/10.1073/pnas.93.25.14726

174. Nakamura-Ishizu, A., Takizawa, H., & Suda, T. (2014). The analysis, roles and regulation of quiescence in hematopoietic stem cells. *Development*, *141*(24), 4656–4666. https://doi.org/10.1242/dev.106575

175. Naumann, U., Cameroni, E., Pruenster, M., Mahabaleshwar, H., Raz, E., Zerwes, H.-G., Rot, A., & Thelen, M. (2010). CXCR7 Functions as a Scavenger for CXCL12 and CXCL11. *PLOS ONE*, *5*(2), e9175. https://doi.org/10.1371/journal.pone.0009175

176. Nie, Y., Waite, J., Brewer, F., Sunshine, M.-J., Littman, D. R., & Zou, Y.-R. (2004). The role of CXCR4 in maintaining peripheral B cell compartments and humoral immunity. *The Journal of Experimental Medicine*, *200*(9), 1145–1156. https://doi.org/10.1084/jem.20041185

177. Nilsson, S. K., Johnston, H. M., Whitty, G. A., Williams, B., Webb, R. J., Denhardt, D. T., Bertoncello, I., Bendall, L. J., Simmons, P. J., & Haylock, D. N. (2005). Osteopontin, a key component of the hematopoietic stem cell niche and regulator of primitive hematopoietic progenitor cells. *Blood*, *106*(4), 1232–1239. https://doi.org/10.1182/blood-2004-11-4422

178. Noguchi-Sasaki, M., Sasaki, Y., Shimonaka, Y., Mori, K., & Fujimoto-Ouchi, K. (2016). Treatment with anti-IL-6 receptor antibody prevented increase in serum hepcidin levels and improved anemia in mice inoculated with IL-6–producing lung carcinoma cells. *BMC Cancer*, *16*, 270. https://doi.org/10.1186/s12885-016-2305-2

179. Nombela-Arrieta, C., & Manz, M. G. (2017). Quantification and three-dimensional microanatomical organization of the bone marrow. *Blood Advances*, *1*(6), 407–416. https://doi.org/10.1182/bloodadvances.2016003194

180. Nombela-Arrieta, C., Pivarnik, G., Winkel, B., Canty, K. J., Harley, B., Mahoney, J. E., Park, S.-Y., Lu, J., Protopopov, A., & Silberstein, L. E. (2013). Quantitative imaging of haematopoietic stem and progenitor cell localization and hypoxic status in the bone marrow microenvironment. *Nature Cell Biology*, *15*(5), 533–543. https://doi.org/10.1038/ncb2730

181. Notta, F., Zandi, S., Takayama, N., Dobson, S., Gan, O. I., Wilson, G., Kaufmann, K. B., McLeod, J., Laurenti, E., Dunant, C. F., McPherson, J. D., Stein, L. D., Dror, Y., & Dick, J. E. (2016). Distinct routes of lineage development reshape the human blood hierarchy across ontogeny. *Science (New York, N.Y.)*, *351*(6269), aab2116. https://doi.org/10.1126/science.aab2116

182. O'Boyle, G., Mellor, P., Kirby, J. A., & Ali, S. (2009). Anti-inflammatory therapy by intravenous delivery of non-heparan sulfate-binding CXCL12. *The FASEB Journal*, *23*(11), 3906–3916. https://doi.org/10.1096/fj.09-134643

183. Oberlin, E., Amara, A., Bachelerie, F., Bessia, C., Virelizier, J.-L., Arenzana-Seisdedos, F., Schwartz, O., Heard, J.-M., Clark-Lewis, I., Legler, D. F., Loetscher, M., Baggiolini, M., & Moser, B. (1996). The CXC chemokine SDF-1 is the ligand for LESTR/fusin and prevents infection by T-cell-line-adapted HIV-1. *Nature*, *382*(6594), 833–835. https://doi.org/10.1038/382833a0

184. Ogawa, M., Matsuzaki, Y., Nishikawa, S., Hayashi, S., Kunisada, T., Sudo, T., Kina, T., Nakauchi, H., & Nishikawa, S. (1991). Expression and function of c-kit in hemopoietic progenitor cells. *Journal of Experimental Medicine*, *174*(1), 63–71. https://doi.org/10.1084/jem.174.1.63

185. Orfao, A., Matarraz, S., Pérez-Andrés, M., Almeida, J., Teodosio, C., Berkowska, M. A., & van Dongen, J. J. M. (2019). Immunophenotypic dissection of normal hematopoiesis. *Journal of Immunological Methods*, *475*, 112684. https://doi.org/10.1016/j.jim.2019.112684

186. Panch, S. R., Szymanski, J., Savani, B. N., & Stroncek, D. F. (2017). Sources of Hematopoietic Stem and Progenitor Cells and Methods to Optimize Yields for Clinical Cell Therapy. *Biology of Blood and Marrow Transplantation*, *23*(8), 1241–1249. https://doi.org/10.1016/j.bbmt.2017.05.003

187. Panuzzo, C., Jovanovski, A., Pergolizzi, B., Pironi, L., Stanga, S., Fava, C., & Cilloni, D. (2020). Mitochondria: A Galaxy in the Hematopoietic and Leukemic Stem Cell Universe. *International Journal of Molecular Sciences*, *21*(11), 3928. https://doi.org/10.3390/ijms21113928

188. Passegué, E., Jamieson, C. H. M., Ailles, L. E., & Weissman, I. L. (2003). Normal and leukemic hematopoiesis: Are leukemias a stem cell disorder or a reacquisition of stem cell characteristics? *Proceedings of the National Academy of Sciences of the United States of America*, *100 Suppl 1*, 11842–11849. https://doi.org/10.1073/pnas.2034201100

189. Pelus, L. M., & Broxmeyer, H. E. (2018). Peripheral blood stem cell mobilization; a look ahead. *Current Stem Cell Reports*, *4*(4), 273–281. https://doi.org/10.1007/s40778-018-0141-9

190. Petruzziello-Pellegrini, T. N., & Marsden, P. A. (2012). Shiga toxin-associated hemolytic uremic syndrome: Advances in pathogenesis and therapeutics. *Current Opinion in Nephrology and Hypertension*, *21*(4), 433–440. https://doi.org/10.1097/MNH.0b013e328354a62e

191. Piedrahita, J. A., Zhang, S. H., Hagaman, J. R., Oliver, P. M., & Maeda, N. (1992). Generation of mice carrying a mutant apolipoprotein E gene inactivated by gene targeting in embryonic stem cells. *Proceedings of the National Academy of Sciences of the United States of America*, *89*(10), 4471–4475. https://doi.org/10.1073/pnas.89.10.4471

192. Pietras, E. M. (2017). Inflammation: A key regulator of hematopoietic stem cell fate in health and disease. *Blood*, *130*(15), 1693–1698. https://doi.org/10.1182/blood-2017-06-780882

193. Pilo, F., & Angelucci, E. (2018). A storm in the niche: Iron, oxidative stress and haemopoiesis. *Blood Reviews*, *32*(1), 29–35. https://doi.org/10.1016/j.blre.2017.08.005

194. Ponomaryov, T., Peled, A., Petit, I., Taichman, R. S., Habler, L., Sandbank, J., Arenzana-Seisdedos, F., Magerus, A., Caruz, A., Fujii, N., Nagler, A., Lahav, M., Szyper-Kravitz, M., Zipori, D., & Lapidot, T. (2000). Induction of the chemokine stromal-derived factor-1 following DNA damage improves human stem cell function. *The Journal of Clinical Investigation*, *106*(11), 1331–1339. https://doi.org/10.1172/JCI10329

195. Poulos, M. G., Guo, P., Kofler, N. M., Pinho, S., Gutkin, M. C., Tikhonova, A., Aifantis, I., Frenette, P. S., Kitajewski, J., Rafii, S., & Butler, J. M. (2013). Endothelial Jagged-1 Is Necessary for Homeostatic and Regenerative Hematopoiesis. *Cell Reports*, *4*(5), 1022–1034. https://doi.org/10.1016/j.celrep.2013.07.048

196. Pracht, K., Meinzinger, J., Daum, P., Schulz, S. R., Reimer, D., Hauke, M., Roth, E., Mielenz, D., Berek, C., Côrte-Real, J., Jäck, H.-M., & Schuh, W. (2017). A new staining protocol for detection of murine antibody-secreting plasma cell subsets by flow cytometry. *European Journal of Immunology*, *47*(8), 1389–1392. https://doi.org/10.1002/eji.201747019

197. Radice, E., Ameti, R., Melgrati, S., Foglierini, M., Antonello, P., Stahl, R. A. K., Thelen, S., Jarrossay, D., & Thelen, M. (2020). Marginal Zone Formation Requires ACKR3 Expression on B Cells. *Cell Reports*, *32*(5), 107951. https://doi.org/10.1016/j.celrep.2020.107951

198. Rajagopal, S., Kim, J., Ahn, S., Craig, S., Lam, C. M., Gerard, N. P., Gerard, C., & Lefkowitz, R. J. (2010). β-arrestin- but not G protein-mediated signaling by the "decoy" receptor CXCR7. *Proceedings of the National Academy of Sciences*, *107*(2), 628–632. https://doi.org/10.1073/pnas.0912852107

199. Ramalingam, P., Poulos, M. G., & Butler, J. M. (2017). Regulation of the Hematopoietic Stem Cell Lifecycle by the Endothelial Niche. *Current Opinion in Hematology*, *24*(4), 289–299. https://doi.org/10.1097/MOH.0000000000000350

200. Ramirez, P., Rettig, M. P., Uy, G. L., Deych, E., Holt, M. S., Ritchey, J. K., & DiPersio, J. F. (2009). BIO5192, a small molecule inhibitor of VLA-4, mobilizes hematopoietic stem and progenitor cells. *Blood*, *114*(7), 1340–1343. https://doi.org/10.1182/blood-2008-10-184721

201. Ratajczak, M. Z., & Adamiak, M. (2015). Membrane lipid rafts, master regulators of hematopoietic stem cell retention in bone marrow and their trafficking. *Leukemia*, *29*(7), 1452–1457. https://doi.org/10.1038/leu.2015.66

202. Ray, P. D., Huang, B.-W., & Tsuji, Y. (2012). Reactive oxygen species (ROS) homeostasis and redox regulation in cellular signaling. *Cellular Signalling*, *24*(5), 981–990. https://doi.org/10.1016/j.cellsig.2012.01.008

203. Redpath, A. N., François, M., Wong, S.-P., Bonnet, D., & Rankin, S. M. (2017). Two distinct CXCR4 antagonists mobilize progenitor cells in mice by different mechanisms. *Blood Advances*, *1*(22), 1934–1943. https://doi.org/10.1182/bloodadvances.2017006064

204. Regan-Komito, D., Swann, J. W., Demetriou, P., Cohen, E. S., Horwood, N. J., Sansom, S. N., & Griseri, T. (2020). GM-CSF drives dysregulated hematopoietic stem cell activity and pathogenic extramedullary myelopoiesis in experimental spondyloarthritis. *Nature Communications*, *11*(1), 155. https://doi.org/10.1038/s41467-019-13853-4

205. Richard-Bildstein, S., Aissaoui, H., Pothier, J., Schäfer, G., Gnerre, C., Lindenberg, E., Lehembre, F., Pouzol, L., & Guerry, P. (2020). Discovery of the Potent, Selective, Orally Available CXCR7 Antagonist ACT-1004-1239. *Journal of Medicinal Chemistry*, *63*(24), 15864–15882. https://doi.org/10.1021/acs.jmedchem.0c01588

206. Rodrigues, C. P., Shvedunova, M., & Akhtar, A. (2021). Epigenetic Regulators as the Gatekeepers of Hematopoiesis. *Trends in Genetics*, *37*(2), 125–142. https://doi.org/10.1016/j.tig.2020.09.015

207. Rodriguez, S., Chora, A., Goumnerov, B., Mumaw, C., Goebel, W. S., Fernandez, L., Baydoun, H., HogenEsch, H., Dombkowski, D. M., Karlewicz, C. A., Rice, S., Rahme, L. G., & Carlesso, N. (2009). Dysfunctional expansion of hematopoietic stem cells and block of myeloid differentiation in lethal sepsis. *Blood*, *114*(19), 4064–4076. https://doi.org/10.1182/blood-2009-04-214916

208. Rodrigues-Moreira, S., Moreno, S. G., Ghinatti, G., Lewandowski, D., Hoffschir, F., Ferri, F., Gallouet, A.-S., Gay, D., Motohashi, H., Yamamoto, M., Joiner, M. C., Gault, N., & Romeo, P.-H. (2017). Low-Dose Irradiation Promotes Persistent Oxidative Stress and Decreases Self-Renewal in Hematopoietic Stem Cells. *Cell Reports*, *20*(13), 3199–3211. https://doi.org/10.1016/j.celrep.2017.09.013

209. Rönn, R. E., Guibentif, C., Saxena, S., & Woods, N.-B. (2017). Reactive Oxygen Species Impair the Function of CD90+ Hematopoietic Progenitors Generated from Human Pluripotent Stem Cells. *STEM CELLS*, *35*(1), 197–206. https://doi.org/10.1002/stem.2503

210. Rot, A. (2010). Chemokine patterning by glycosaminoglycans and interceptors. *Frontiers in Bioscience*, *15*(1), 645. https://doi.org/10.2741/3638

211. Rucci, N. (2008). Molecular biology of bone remodelling. *Clinical Cases in Mineral and Bone Metabolism*, *5*(1), 49–56.

212. Ruzankina, Y., Pinzon-Guzman, C., Asare, A., Ong, T., Pontano, L., Cotsarelis, G., Zediak, V. P., Velez, M., Bhandoola, A., & Brown, E. J. (2007). Deletion of the developmentally essential gene ATR in adult mice leads to age-related phenotypes and stem cell loss. *Cell Stem Cell*, *1*(1), 113–126. https://doi.org/10.1016/j.stem.2007.03.002

213. Saini, V., Marchese, A., & Majetschak, M. (2010). CXC Chemokine Receptor 4 Is a Cell Surface Receptor for Extracellular Ubiquitin*. *Journal of Biological Chemistry*, *285*(20), 15566–15576. https://doi.org/10.1074/jbc.M110.103408

214. Samimi, A., Kalantari, H., Lorestani, M. Z., Shirzad, R., & Saki, N. (2018). Oxidative stress in normal hematopoietic stem cells and leukemia. *APMIS*, *126*(4), 284–294. https://doi.org/10.1111/apm.12822

215. Säwen, P., Eldeeb, M., Erlandsson, E., Kristiansen, T. A., Laterza, C., Kokaia, Z., Karlsson, G., Yuan, J., Soneji, S., Mandal, P. K., Rossi, D. J., & Bryder, D. (n.d.). Murine HSCs contribute actively to native hematopoiesis but with reduced differentiation capacity upon aging. *ELife*, *7*. https://doi.org/10.7554/eLife.41258

216. Scadden, D. T. (2006). The stem-cell niche as an entity of action. *Nature*, *441*(7097), 1075–1079. https://doi.org/10.1038/nature04957

217. Scadden, D. T. (2012). Rethinking Stroma: Lessons from the Blood. *Cell Stem Cell*, *10*(6), 648–649. https://doi.org/10.1016/j.stem.2012.05.011

218. Schönemeier, B., Kolodziej, A., Schulz, S., Jacobs, S., Hoellt, V., & Stumm, R. (2008). Regional and cellular localization of the CXCl12/SDF-1 chemokine receptor CXCR7 in the developing and adult rat brain. *Journal of Comparative Neurology*, *510*(2), 207–220. https://doi.org/10.1002/cne.21780

219. Schofield, R. (1978). The relationship between the spleen colony-forming cell and the haemopoietic stem cell. *Blood Cells*, *4*(1–2), 7–25.

220. Schwartz, V., Lue, H., Kraemer, S., Korbiel, J., Krohn, R., Ohl, K., Bucala, R., Weber, C., & Bernhagen, J. (2009). A functional heteromeric MIF receptor formed by CD74 and CXCR4. *FEBS Letters*, *583*(17), 2749–2757. https://doi.org/10.1016/j.febslet.2009.07.058

221. Seita, J., & Weissman, I. L. (2010). Hematopoietic Stem Cell: Self-renewal versus Differentiation. *Wiley Interdisciplinary Reviews. Systems Biology and Medicine*, *2*(6), 640–653. https://doi.org/10.1002/wsbm.86

222. Semenza, G. L. (2007). Life with Oxygen. *Science*, *318*(5847), 62–64. https://doi.org/10.1126/science.1147949

223. Shaikh, A. C., & Sadowski, P. D. (1997). The Cre Recombinase Cleaves the lox Site in trans *. *Journal of Biological Chemistry*, *272*(9), 5695–5702. https://doi.org/10.1074/jbc.272.9.5695

224. Shlush, L. I., Zandi, S., Mitchell, A., Chen, W. C., Brandwein, J. M., Gupta, V., Kennedy, J. A., Schimmer, A. D., Schuh, A. C., Yee, K. W., McLeod, J. L., Doedens, M., Medeiros, J. J. F., Marke, R., Kim, H. J., Lee, K., McPherson, J. D., Hudson, T. J., Brown, A. M. K., … Dick, J. E. (2014). Identification of pre-leukemic hematopoietic stem cells in acute leukemia. *Nature*, *506*(7488), 328–333. https://doi.org/10.1038/nature13038

225. Sierro, F., Biben, C., Martínez-Muñoz, L., Mellado, M., Ransohoff, R. M., Li, M., Woehl, B., Leung, H., Groom, J., Batten, M., Harvey, R. P., Martínez-A, C., Mackay, C. R., & Mackay, F. (2007). Disrupted cardiac development but normal hematopoiesis in mice deficient in the second CXCL12/SDF-1 receptor, CXCR7. *Proceedings of the National Academy of Sciences*, *104*(37), 14759–14764. https://doi.org/10.1073/pnas.0702229104

226. Simpson, E., & Dazzi, F. (2019). Bone Marrow Transplantation 1957-2019. *Frontiers in Immunology*, *10*, 1246. https://doi.org/10.3389/fimmu.2019.01246

227. Simsek, T., Kocabas, F., Zheng, J., DeBerardinis, R. J., Mahmoud, A. I., Olson, E. N., Schneider, J. W., Zhang, C. C., & Sadek, H. A. (2010). The Distinct Metabolic Profile of Hematopoietic Stem Cells Reflects Their Location in a Hypoxic Niche. *Cell Stem Cell*, *7*(3), 380–390. https://doi.org/10.1016/j.stem.2010.07.011

228. Slifka, M. K., Antia, R., Whitmire, J. K., & Ahmed, R. (1998). Humoral immunity due to long-lived plasma cells. *Immunity*, *8*(3), 363–372. https://doi.org/10.1016/s1074-7613(00)80541-5

229. Sreedharan, S. P., Patel, D. R., Huang, J. X., & Goetzl, E. J. (1993). Cloning and Functional Expression of a Human Neuroendocrine Vasoactive Intestinal Peptide Receptor. *Biochemical and Biophysical Research Communications*, *193*(2), 546–553. https://doi.org/10.1006/bbrc.1993.1658

230. Sreedharan, S. P., Robichon, A., Peterson, K. E., & Goetzl, E. J. (1991). Cloning and expression of the human vasoactive intestinal peptide receptor. *Proceedings of the National Academy of Sciences of the United States of America*, *88*(11), 4986–4990.

231. Steen, A., Larsen, O., Thiele, S., & Rosenkilde, M. M. (2014). Biased and G Protein-Independent Signaling of Chemokine Receptors. *Frontiers in Immunology*, *5*. https://doi.org/10.3389/fimmu.2014.00277

232. Stone, M. J., Hayward, J. A., Huang, C., E. Huma, Z., & Sanchez, J. (2017). Mechanisms of Regulation of the Chemokine-Receptor Network. *International Journal of Molecular Sciences*, *18*(2), 342. https://doi.org/10.3390/ijms18020342

233. Sugiyama, T., Kohara, H., Noda, M., & Nagasawa, T. (2006). Maintenance of the Hematopoietic Stem Cell Pool by CXCL12-CXCR4 Chemokine Signaling in Bone Marrow Stromal Cell Niches. *Immunity*, *25*(6), 977–988. https://doi.org/10.1016/j.immuni.2006.10.016

234. Szabo, M. C., Soo, K. S., Zlotnik, A., & Schall, T. J. (1995). Chemokine class differences in binding to the Duffy antigen-erythrocyte chemokine receptor. *The Journal of Biological Chemistry*, *270*(43), 25348–25351. https://doi.org/10.1074/jbc.270.43.25348

235. Szade, K., Gulati, G. S., Chan, C. K. F., Kao, K. S., Miyanishi, M., Marjon, K. D., Sinha, R., George, B. M., Chen, J. Y., & Weissman, I. L. (2017). Where Hematopoietic Stem Cells Live: The Bone Marrow Niche. *Antioxidants & Redox Signaling*, *29*(2), 191–204. https://doi.org/10.1089/ars.2017.7419

236. Tachibana, K., Hirota, S., Iizasa, H., Yoshida, H., Kawabata, K., Kataoka, Y., Kitamura, Y., Matsushima, K., Yoshida, N., Nishikawa, S., Kishimoto, T., & Nagasawa, T. (1998). The chemokine receptor CXCR4 is essential for vascularization of the gastrointestinal tract. *Nature*, *393*(6685), 591–594. https://doi.org/10.1038/31261

237. Takubo, K., Goda, N., Yamada, W., Iriuchishima, H., Ikeda, E., Kubota, Y., Shima, H., Johnson, R. S., Hirao, A., Suematsu, M., & Suda, T. (2010). Regulation of the HIF-1α Level Is Essential for Hematopoietic Stem Cells. *Cell Stem Cell*, *7*(3), 391–402. https://doi.org/10.1016/j.stem.2010.06.020

238. Tarnowski, M., Liu, R., Wysoczynski, M., Ratajczak, J., Kucia, M., & Ratajczak, M. Z. (2010). CXCR7: A new SDF-1-binding receptor in contrast to normal CD34+ progenitors is functional and is expressed at higher level in human malignant hematopoietic cells. *European Journal of Haematology*, *85*(6), 472–483. https://doi.org/10.1111/j.1600-0609.2010.01531.x

239. Tassone, L., Notarangelo, L. D., Bonomi, V., Savoldi, G., Sensi, A., Soresina, A., Smith, C. I. E., Porta, F., Plebani, A., Notarangelo, L. D., & Badolato, R. (2009). Clinical and genetic diagnosis of warts, hypogammaglobulinemia, infections, and myelokathexis syndrome in 10 patients. *Journal of Allergy and Clinical Immunology*, *123*(5), 1170-1173.e3. https://doi.org/10.1016/j.jaci.2008.12.1133

240. Thelen, M. (2001). Dancing to the tune of chemokines. *Nature Immunology*, *2*(2), 129–134. https://doi.org/10.1038/84224

241. Thomas, E. D., Lochte, H. L. J., Lu, W. C., & Ferrebee, J. W. (2010, January 12). *Intravenous Infusion of Bone Marrow in Patients Receiving Radiation and Chemotherapy* (world) [Research-article]. Http://Dx.Doi.Org/10.1056/NEJM195709122571102; Massachusetts Medical Society. https://doi.org/10.1056/NEJM195709122571102

242. Torisawa, Y., Mosadegh, B., Bersano-Begey, T., Steele, J. M., Luker, K. E., Luker, G. D., & Takayama, S. (2010). Microfluidic platform for chemotaxis in gradients formed by CXCL12 source-sink cells. *Integrative Biology*, *2*(11–12), 680–686. https://doi.org/10.1039/c0ib00041h

243. Torossian, F., Anginot, A., Chabanon, A., Clay, D., Guerton, B., Desterke, C., Boutin, L., Marullo, S., Scott, M. G. H., Lataillade, J.-J., & Le Bousse-Kerdilès, M.-C. (2014). CXCR7 participates in CXCL12-induced CD34+ cell cycling through β-arrestin–dependent Akt activation. *Blood*, *123*(2), 191–202. https://doi.org/10.1182/blood-2013-05-500496

244. Torres, R., & Ramirez, J. C. (2009). A Chemokine Targets the Nucleus: Cxcl12-Gamma Isoform Localizes to the Nucleolus in Adult Mouse Heart. *PLoS ONE*, *4*(10), e7570. https://doi.org/10.1371/journal.pone.0007570

245. Tuljapurkar, S. R., McGuire, T. R., Brusnahan, S. K., Jackson, J. D., Garvin, K. L., Kessinger, M. A., Lane, J. T., Kane, B. J. O., & Sharp, J. G. (2011). Changes in human bone marrow fat content associated with changes in hematopoietic stem cell numbers and cytokine levels with aging. *Journal of Anatomy*, *219*(5), 574–581. https://doi.org/10.1111/j.1469-7580.2011.01423.x

246. Tzeng, Y.-S., Li, H., Kang, Y.-L., Chen, W.-C., Cheng, W.-C., & Lai, D.-M. (2011). Loss of Cxcl12/Sdf-1 in adult mice decreases the quiescent state of hematopoietic stem/progenitor cells and alters the pattern of hematopoietic regeneration after myelosuppression. *Blood*, *117*(2), 429–439. https://doi.org/10.1182/blood-2010-01-266833

247. Uckelmann, H., Blaszkiewicz, S., Nicolae, C., Haas, S., Schnell, A., Wurzer, S., Wagener, R., Aszodi, A., & Essers, M. A. G. (2016). Extracellular matrix protein Matrilin-4 regulates stress-induced HSC proliferation via CXCR4. *The Journal of Experimental Medicine*, *213*(10), 1961–1971. https://doi.org/10.1084/jem.20151713

248. Vacchini, A., Locati, M., & Borroni, E. M. (2016). Overview and potential unifying themes of the atypical chemokine receptor family. *Journal of Leukocyte Biology*, *99*(6), 883–892. https://doi.org/10.1189/jlb.2MR1015-477R

249. Valent, P., Kern, W., Hoermann, G., Milosevic Feenstra, J. D., Sotlar, K., Pfeilstöcker, M., Germing, U., Sperr, W. R., Reiter, A., Wolf, D., Arock, M., Haferlach, T., & Horny, H.-P. (2019). Clonal Hematopoiesis with Oncogenic Potential (CHOP): Separation from CHIP and Roads to AML. *International Journal of Molecular Sciences*, *20*(3), 789. https://doi.org/10.3390/ijms20030789

250. Veldkamp, C. T., Ziarek, J. J., Su, J., Basnet, H., Lennertz, R., Weiner, J. J., Peterson, F. C., Baker, J. E., & Volkman, B. F. (2009). Monomeric structure of the cardioprotective chemokine SDF-1/CXCL12. *Protein Science*, *18*(7), 1359–1369. https://doi.org/10.1002/pro.167

251. Velten, L., Haas, S. F., Raffel, S., Blaszkiewicz, S., Islam, S., Hennig, B. P., Hirche, C., Lutz, C., Buss, E. C., Nowak, D., Boch, T., Hofmann, W.-K., Ho, A. D., Huber, W., Trumpp, A., Essers, M. A. G., & Steinmetz, L. M. (2017). Human haematopoietic stem cell lineage commitment is a continuous process. *Nature Cell Biology*, *19*(4), 271–281. https://doi.org/10.1038/ncb3493

252. Verovskaya, E. V., Dellorusso, P. V., & Passegué, E. (2019). Losing Sense of Self and Surroundings: Hematopoietic Stem Cell Aging and Leukemic Transformation. *Trends in Molecular Medicine*, *25*(6), 494–515. https://doi.org/10.1016/j.molmed.2019.04.006

253. Wescott, M. P., Kufareva, I., Paes, C., Goodman, J. R., Thaker, Y., Puffer, B. A., Berdougo, E., Rucker, J. B., Handel, T. M., & Doranz, B. J. (2016). Signal transmission through the CXC chemokine receptor 4 (CXCR4) transmembrane helices. *Proceedings of the National Academy of Sciences*, *113*(35), 9928–9933. https://doi.org/10.1073/pnas.1601278113

254. Wilson, A., Fu, H., Schiffrin, M., Winkler, C., Koufany, M., Jouzeau, J.-Y., Bonnet, N., Gilardi, F., Renevey, F., Luther, S. A., Moulin, D., & Desvergne, B. (2018). Lack of Adipocytes Alters Hematopoiesis in Lipodystrophic Mice. *Frontiers in Immunology*, *9*. https://doi.org/10.3389/fimmu.2018.02573

255. Wilson, A., Laurenti, E., Oser, G., van der Wath, R. C., Blanco-Bose, W., Jaworski, M., Offner, S., Dunant, C. F., Eshkind, L., Bockamp, E., Lió, P., MacDonald, H. R., & Trumpp, A. (2008). Hematopoietic Stem Cells Reversibly Switch from Dormancy to Self-Renewal during Homeostasis and Repair. *Cell*, *135*(6), 1118–1129. https://doi.org/10.1016/j.cell.2008.10.048

256. Winkler, I. G., Pettit, A. R., Raggatt, L. J., Jacobsen, R. N., Forristal, C. E., Barbier, V., Nowlan, B., Cisterne, A., Bendall, L. J., Sims, N. A., & Lévesque, J.-P. (2012). Hematopoietic stem cell mobilizing agents G-CSF, cyclophosphamide or AMD3100 have distinct mechanisms of action on bone marrow HSC niches and bone formation. *Leukemia*, *26*(7), 1594–1601. https://doi.org/10.1038/leu.2012.17

257. Winkler, I. G., Sims, N. A., Pettit, A. R., Barbier, V., Nowlan, B., Helwani, F., Poulton, I. J., van Rooijen, N., Alexander, K. A., Raggatt, L. J., & Lévesque, J.-P. (2010). Bone marrow macrophages maintain hematopoietic stem cell (HSC) niches and their depletion mobilizes HSCs. *Blood*, *116*(23), 4815–4828. https://doi.org/10.1182/blood-2009-11-253534

258. Wyatt, M. D., & Wilson, D. M. (2009). Participation of DNA repair in the response to 5-fluorouracil. *Cellular and Molecular Life Sciences : CMLS*, *66*(5), 788–799. https://doi.org/10.1007/s00018-008-8557-5

259. Yacoub, M. F., Ferwiz, H. F., & Said, F. (2020). Effect of Interleukin and Hepcidin in Anemia of Chronic Diseases. *Anemia*, *2020*, 3041738. https://doi.org/10.1155/2020/3041738

260. Yahata, T., Takanashi, T., Muguruma, Y., Ibrahim, A. A., Matsuzawa, H., Uno, T., Sheng, Y., Onizuka, M., Ito, M., Kato, S., & Ando, K. (2011). Accumulation of oxidative DNA damage restricts the self-renewal capacity of human hematopoietic stem cells. *Blood*, *118*(11), 2941–2950. https://doi.org/10.1182/blood-2011-01-330050

261. Yamazaki, S., Ema, H., Karlsson, G., Yamaguchi, T., Miyoshi, H., Shioda, S., Taketo, M. M., Karlsson, S., Iwama, A., & Nakauchi, H. (2011). Nonmyelinating Schwann Cells Maintain Hematopoietic Stem Cell Hibernation in the Bone Marrow Niche. *Cell*, *147*(5), 1146–1158. https://doi.org/10.1016/j.cell.2011.09.053

262. Yang, Y., Zhou, Y., Wang, Y., Wei, X., Wu, L., Wang, T., & Ma, A. (2020). Exendin-4 reverses high glucose-induced endothelial progenitor cell dysfunction via SDF-1β/CXCR7–AMPK/p38-MAPK/IL-6 axis. *Acta Diabetologica*, *57*(11), 1315–1326. https://doi.org/10.1007/s00592-020-01551-3

263. Yu, S., Crawford, D., Tsuchihashi, T., Behrens, T. W., & Srivastava, D. (2011). The chemokine receptor CXCR7 functions to regulate cardiac valve remodeling. *Developmental Dynamics*, *240*(2), 384–393. https://doi.org/10.1002/dvdy.22549

264. Yung, Y., Lee, E., Chu, H.-T., Yip, P.-K., & Gill, H. (2021). Targeting Abnormal Hematopoietic Stem Cells in Chronic Myeloid Leukemia and Philadelphia Chromosome-Negative Classical Myeloproliferative Neoplasms. *International Journal of Molecular Sciences*, *22*(2), 659. https://doi.org/10.3390/ijms22020659

265. Zabel, B. A., Lewén, S., Berahovich, R. D., Jaén, J. C., & Schall, T. J. (2011). The novel chemokine receptor CXCR7 regulates trans-endothelial migration of cancer cells. *Molecular Cancer*, *10*(1), 73. https://doi.org/10.1186/1476-4598-10-73

266. Zabel, B. A., Wang, Y., Lewén, S., Berahovich, R. D., Penfold, M. E. T., Zhang, P., Powers, J., Summers, B. C., Miao, Z., Zhao, B., Jalili, A., Janowska-Wieczorek, A., Jaen, J. C., & Schall, T. J. (2009). Elucidation of CXCR7-Mediated Signaling Events and Inhibition of CXCR4-Mediated Tumor Cell Transendothelial Migration by CXCR7 Ligands. *The Journal of Immunology*, *183*(5), 3204–3211. https://doi.org/10.4049/jimmunol.0900269

267. Zarbock, A., Schmolke, M., Bockhorn, S. G., Scharte, M., Buschmann, K., Ley, K., & Singbartl, K. (2007). The Duffy antigen receptor for chemokines in acute renal failure: A facilitator of renal chemokine presentation. *Critical Care Medicine*, *35*(9), 2156. https://doi.org/10.1097/01.CCM.0000280570.82885.32

268. Zhang, S. H., Reddick, R. L., Piedrahita, J. A., & Maeda, N. (1992). Spontaneous hypercholesterolemia and arterial lesions in mice lacking apolipoprotein E. *Science (New York, N.Y.)*, *258*(5081), 468–471. https://doi.org/10.1126/science.1411543

269. Zhang, D.-E., Zhang, P., Wang, N., Hetherington, C. J., Darlington, G. J., & Tenen, D. G. (1997). Absence of granulocyte colony-stimulating factor signaling and neutrophil development in CCAAT enhancer binding protein α-deficient mice. *Proceedings of the National Academy of Sciences*, *94*(2), 569–574. https://doi.org/10.1073/pnas.94.2.569

270. Zhao, M., Perry, J. M., Marshall, H., Venkatraman, A., Qian, P., He, X. C., Ahamed, J., & Li, L. (2014). Megakaryocytes maintain homeostatic quiescence and promote post-injury regeneration of hematopoietic stem cells. *Nature Medicine*, *20*(11), 1321–1326. https://doi.org/10.1038/nm.3706

271. Zhou, B. O., Yue, R., Murphy, M. M., Peyer, J. G., & Morrison, S. J. (2014). Leptin-Receptor-Expressing Mesenchymal Stromal Cells Represent the Main Source of Bone Formed by Adult Bone Marrow. *Cell Stem Cell*, *15*(2), 154–168. https://doi.org/10.1016/j.stem.2014.06.008

272. Zlotnik, A., & Yoshie, O. (2012). The Chemokine Superfamily Revisited. *Immunity*, *36*(5), 705–716. https://doi.org/10.1016/j.immuni.2012.05.008

273. Zlotnik, A., Yoshie, O., & Nomiyama, H. (2006). The chemokine and chemokine receptor superfamilies and their molecular evolution. *Genome Biology*, *7*(12), 243. https://doi.org/10.1186/gb-2006-7-12-243

274. Zou, Y. R., Kottmann, A. H., Kuroda, M., Taniuchi, I., & Littman, D. R. (1998). Function of the chemokine receptor CXCR4 in haematopoiesis and in cerebellar development. *Nature*, *393*(6685), 595–599. https://doi.org/10.1038/31269

Appendix A:

Primer Sequence for end point PCR

Gene		*Sequence (5´> 3´)*	*Expected size (in base pair)*
Apoe$^{-/-}$	Forward (common)	GCC TAG CCG AGG GAG AGC CG	
	Reverse (1)	TGT GAC TTG GGA GCT CTG CAG C	wildtype: 150bp
	Reverse (2)	GCC GCC CCG ACT GCA TCT	transgenic: 245bp
Ubc^{CreERT2}	Forward	CAT GTC TTT AAT CTA CCT CGA TGG	
	Reverse	CTC TTC CCT CGT GAT CTG CAA CTC C	wildtype: 299bp
	Forward	CAG CAT GAA GTG CAA GAA CG	
	Reverse	CAC CAG GTT AGC CTT TAA GCC	transgenic: 500bp
Cxcr4$^{flox/flox}$	Forward (common)	CAC TAC GCA TGA CTC GAA ATG	
	Reverse (1)	GTG TGC GGT GGT ATC CAG C	wildtype: 330bp
	Reverse (2)	GTG CTC CTC GGA ATG AAG AG	transgenic: 430bp
Ackr3$^{flox/flox}$	Forward	GGA ACC CAG GCG AAG TCT GAG	wildtype: 362bp
	Reverse	CCT GTA CTT CAG TAG GAG TCC AC	transgenic: 396bp
Fgd5^{CreERT2}	Forward (common)	GGA AGC TCC AGA TGA AGA GG	
	Reverse (1)	ATG ACC TCA TTG GGG AAG G	wildtype: 302bp
	Reverse (2)	GCG GTT GCC GTA CAT GAA G	transgenic: 265bp
Cxcl12$^{flox/flox}$	Forward	GGACACCAGAACCTTGAAAC	wildtype: 280bp
	Reverse	AGCCTCGGACTTGGCATAAC	transgenic: 320bp
Ackr3^{Gfp}	Forward (common)	GTC ACT TGG TCG CTC TCC TC	
	Reverse (1)	GAT GTA GCA GTG CGT GTC GT	wildtype: 280bp
	Reverse (2)	GAA CTT CAG GGT CAG CTT GC	transgenic: 150bp
Ackr3$^{-/-}$ *(after tamoxifen)*	Forward	GAG TCA ATT GAG TGG GCA AGG	wildtype: 1900bp
	Reverse	GCT ACA TTG CTT TCT TGA AGA AAC C	transgenic: 2300bp ko: 300bp

Appendix B:

List of antibodies used for flow cytometry

Target name	*Fluorescent molecule*	*Clone*	*Provider*	*Catalogue Number*	*Concentration used*
CD3	Pacific Blue	17A2	Biolegend	100214	1/200
CD3	Biotin	17A2	Biolegend	100244	1/500
CD3	BUV737	17A2	BD Biosciences	564380	1/200
CD11b	Pacific Blue	M1/70	Biolegend	101224	1/1000
CD11b	APC	M1/70	Biolegend	101211	1/500
CD11b	FITC	M170	Biolegend	101206	1/500
CD11b	Biotin	M1/70	Biolegend	101204	1/500
CD11b	PE Dazzle 594	M1/70	Biolegend	101256	1/1000
CD16/32	APC/Cy7	93	Biolegend	101328	1/500
Cd16/32	PE	93	Biolegend	101307	1/500
CD16/32	-	93	Biolegend	101302	1/500
CD16/32	Alexa Fluor 700	93	eBioscience	56-0161-80	1/500
CD19	PE/Cy7	6D5	Biolegend	115519	1/1000
CD19	BUV737	1D3	BD Biosciences	612782	1/500
CD21	APC	7E9	Biolegend	123412	1/1000
CD23	BV421	B3B4	Biolegend	101621	1/1000
CD31	PerCP-Cy5.5	390	Biolegend	102419	1/500
CD31	FITC	MEC 13.3	BD biosciences	553372	1/500
CD31	Alexa Fluor 594	MEC13.3	Biolegend	102520	1/500
CD34	FITC	RAM34	BD Biosciences	560238	1/500
CD34	Alexa Fluor 647	RAM34	BD biosciences	560233	1/500
CD34	BV421	RAM34	BD Biosciences	562608	1/500
CD44	BV510	IM7	Biolegend	103044	1/500
CD45	APC e-fluor 780	30-F11	eBioscience	47-0451-82	1/500
CD45	BV711	30F-11	Biolegend	103147	1/500
CD45	FITC	30-F11	Biolegend	103108	1/500

CD45	PercP-Cy5.5.5	30-F11	Biolegend	103131	1/500
CD48	BV510	HM48-1	Biolegend	103443	1/500
CD48	APCCy7	HM48-1	Biolegend	103431	1/500
CD48	PE Dazzle 594	HM48-1	Biolegend	103437	1/500
CD51	PE	RMV-7	Biolegend	104105	1/500
CD106 (VCAM)	PerCP-Cy5.5	429	Biolegend	105715	1/500
CD106	PE	429	Biolegend	105713	1/500
CD115	APC	Alexa Fluor S98	Biolegend	135510	1/500
CD115	PE	Alexa Fluor S98	Biolegend	135506	1/500
CD115	BUV395	T38-320	BD Biosciences	743642	1/200
CD140a (PDGFRa)	PE	APA5	Invitrogen	12-1401-81	1/100
CD150	PerCP-Cy5.5	TC15-12F12.2	Biolegend	115922	1/500
CD150	APC	TC15-12F12.2	Biolegend	115910	1/500
CXCR4	PE	2B11	ThermoFisher	12-9991-82	1/200
CXCR4	BV421	2B11	BD biosciences	562738	1/200
CXCR4	Alexa Fluor 488	2B11	ThermoFisher	53-9991-80	1/300
CXCR7	Alexa Fluor 594	11G8	R&D Systems	FAB42273T	1/100
B220	Pacific Blue	RA3-6B2	Biolegend	103227	1/1000
B220	BV510	RA3-6B2	Biolegend	103247	1/500
B220	Biotin	RA3-6B2	Biolegend	103204	1/500
c-kit	PE/Cy7	2B8	Biolegend	105814	1/1000
c-kit	BV785	ACK2	Biolegend	135138	1/500
c-kit	Alexa Fluor 594	2B8	Biolegend	105831	1/500
Gr1	Pacific Blue	RB6-8C5	Biolegend	108430	1/1000
Gr1	Biotin	RB6-8C5	Biolegend	108403	1/500
F4/80	BV510	BM8	Biolegend	123135	1/500
F4/80	FITC	BM8	Biolegend	123107	1/500

F4/80	PerCP-Cy5.5	BM8	Biolegend	123127	1/500
F4/80	APC	BM8	Biolegend	123115	1/500
Ki67	FITC	16A8	Biolegend	652410	1/300
Ki67	PE/Cy7	16A8	Biolegend	652425	1/400
Ly6C	BV421	HK1.4	Biolegend	128032	1/1000
Ly6C	PE/Cy7	HK1.4	Biolegend	128018	1/2000
Ly6C	BV510	HK1.4	Biolegend	128033	1/500
Ly6C	Alexa Fluor 700	HK1.4	Biolegend	128023	1/500
Ly6G	APC/Cy7	1A8	Biolegend	127624	1/500
Ly6G	FITC	1A8	Biolegend	127606	1/500
Ly6G	BV510	1A8	Biolegend	127633	1/500
Ly6G	BV605	1A8	Biolegend	127639	1/500
Sca1	APC/Cy7	D7	Biolegend	582906	1/500
Sca1	BV605	D7	Biolegend	108134	1/500
Sca1	APC	D7	Biolegend	108111	1/500
Sca1	PerCP-Cy5.5	D7	Biolegend	108121	1/500
Ter119	Pacific Blue	TER-119	Biolegend	116232	1/200
Ter119	PE	TER-119	Biolegend	116208	1/500
Ter119	Alexa Fluor 647	Ter-119	Biolegend	116218	1/500
Ter119	Biotin	Ter-119	Biolegend	116204	1/200
Streptavidin	Alexa Fluor 594		Biolegend	405240	1/500
Streptavidin	Alexa Fluor 647		Biolegend	405237	1/500

Acknowledgements

I thank Prof. Weber and Dr. Johan Duchêne for their supervision and offering the possibility to complete my PhD thesis in IPEK. Ms. Iliriana Vatovci, Mr. Emanuel Putz, Ms. Brigitte Stöger and especially Ms. Catherine Gunczi for the assistance, whenever it was requested.
I thank my parents for their support in all stages of my studies and their financial support, especially during the first difficult months of my PhD. I thank Dr. Emiel van der Vorst and Prof. Yvonne Döring, for believing in me and their technical support. I, finally, thank Dr. Raquel Guillamat Prats and Dr. Donato Santovito for their technical and personal support and Yvonne Jansen for the technical assistance, whenever it was requested.

List of Publications

1. Bianchini, M., Duchêne, J., Santovito, D., Schloss, M. J., Evrard, M., Winkels, H., **Aslani, M.**, Mohanta, S. K., Horckmans, M., Blanchet, X., Lacy, M., von Hundelshausen, P., Atzler, D., Habenicht, A., Gerdes, N., Pelisek, J., Ng, L. G., Steffens, S., Weber, C., & Megens, R. T. A. (2019). PD-L1 expression on nonclassical monocytes reveals their origin and immunoregulatory function. *Science Immunology*, *4*(36), eaar3054. https://doi.org/10.1126/sciimmunol.aar3054

2. Bongiovanni, D., Santamaria, G., Klug, M., Santovito, D., Felicetta, A., Hristov, M., von Scheidt, M., **Aslani, M.**, Cibella, J., Weber, C., Moretti, A., Laugwitz, K.-L., Peano, C., & Bernlochner, I. (2019). Transcriptome Analysis of Reticulated Platelets Reveals a Prothrombotic Profile. *Thrombosis and Haemostasis*, *119*(11), 1795–1806. https://doi.org/10.1055/s-0039-1695009

3. Döring, Y., Jansen, Y., Cimen, I., **Aslani, M.**, Gencer, S., Peters, L. J. F., Duchene, J., Weber, C., & van der Vorst, E. P. C. (2020). B-Cell-Specific CXCR4 Protects Against Atherosclerosis Development and Increases Plasma IgM Levels. *Circulation Research*, *126*(6), 787–788. https://doi.org/10.1161/CIRCRESAHA.119.316142

4. Gencer, S., van der Vorst, E. P. C., **Aslani, M.**, Weber, C., Döring, Y., & Duchene, J. (2019). Atypical Chemokine Receptors in Cardiovascular Disease. *Thrombosis and Haemostasis*, *119*(4), 534–541. https://doi.org/10.1055/s-0038-1676988

5. Santovito, D., Egea, V., Bidzhekov, K., Natarelli, L., Mourão, A., Blanchet, X., Wichapong, K., **Aslani, M.**, Brunßen, C., Horckmans, M., Hristov, M., Geerlof, A., Lutgens, E., Daemen, M. J. A. P., Hackeng, T., Ries, C., Chavakis, T., Morawietz, H., Naumann, R., … Weber, C. (2020). Noncanonical inhibition of caspase-3 by a nuclear microRNA confers endothelial protection by autophagy in atherosclerosis. *Science Translational Medicine*, *12*(546), eaaz2294. https://doi.org/10.1126/scitranslmed.aaz2294

6. Santovito, D., Egea, V., Bidzhekov, K., Natarelli, L., Mourão, A., Blanchet, X., Wichapong, K., **Aslani, M.**, Brunßen, C., Horckmans, M., Hristov, M., Geerlof, A., Lutgens, E., Daemen, M. J. A. P., Hackeng, T., Ries, C., Chavakis, T., Morawietz, H., Naumann, R., … Weber, C. (2020). Autophagy unleashes noncanonical microRNA functions. *Autophagy*, *16*(12), 2294–2296. https://doi.org/10.1080/15548627.2020.1830523

7. Seijkens, T. T. P., van Tiel, C. M., Kusters, P. J. H., Atzler, D., Soehnlein, O., Zarzycka, B., Aarts, S. A. B. M., Lameijer, M., Gijbels, M. J., Beckers, L., den Toom, M., Slütter, B., Kuiper, J., Duchene, J., **Aslani, M.**, Megens, R. T. A., van 't Veer, C., Kooij, G., Schrijver, R., … Lutgens, E. (2018). Targeting CD40-Induced TRAF6 Signaling in Macrophages Reduces Atherosclerosis. *Journal of the American College of Cardiology*, *71*(5), 527–542. https://doi.org/10.1016/j.jacc.2017.11.055

8. van der Vorst, E. P. C., Daissormont, I., **Aslani, M.**, Seijkens, T., Wijnands, E., Lutgens, E., Duchene, J., Santovito, D., Döring, Y., Halvorsen, B., Aukrust, P., Weber, C., Höpken, U. E., & Biessen, E. A. L. (2020). Interruption of the CXCL13/CXCR5 Chemokine Axis Enhances Plasma IgM Levels and Attenuates Atherosclerosis Development. *Thrombosis and Haemostasis*, *120*(2), 344–347. https://doi.org/10.1055/s-0039-3400746

LMU LUDWIG-MAXIMILIANS-UNIVERSITÄT MÜNCHEN

Dekanat Medizinische Fakultät
Promotionsbüro

Affidavit

Aslani, Maria

Surname, first name

Pettenkoferstr. 9a, 80336 Munich

Address

I hereby declare, that the submitted thesis entitled

The role of the atypical chemokine receptor ACKR3 in Bone Marrow homeostasis

is my own work. I have only used the sources indicated and have not made unauthorised use of services of a third party. Where the work of others has been quoted or reproduced, the source is always given.

I further declare that the submitted thesis or parts thereof have not been presented as part of an examination degree to any other university.

Munich, 18/11/2021

Place, Date

Maria Aslani

Signature doctoral candidate

LMU LUDWIG-MAXIMILIANS-UNIVERSITÄT MÜNCHEN

Dekanat Medizinische Fakultät
Promotionsbüro

Confimation of congruency between printed and electronic version of the doctoral thesis

Doctoral Candidate: Maria Aslani

Address: Pettenkoferstr. 9a, 80336 Munich

I hereby declare that the electronic version of the submitted thesis, entitled

The role of the atypical chemokine receptor ACKR3 in Bone Marrow homeostasis

is congruent with the printed version both in content and format.

Munich, 18/11/2021

Place, Date

Maria Aslani

Signature doctoral candidate

Supervisor Declaration for Admission to the Oral Defense

I hereby confirm that the candidate:

Aslani	Maria
Name	First name(s) *please underline name used*

fullfilled all necessary requirements to be admitted to the doctoral examination.

Prof. Dr.	Christian	Weber
Title	First name	Name

Munich, 18.11.21

Place, Date

Signature supervisor

LMU LUDWIG-MAXIMILIANS-UNIVERSITÄT MÜNCHEN

Promotionsbüro
Medizinische Fakultät

MMRS

Stellungnahme für die Überprüfung von Textübereinstimmungen mit iThenticate

Sehr geehrte Betreuerin,
sehr geehrter Betreuer,

Bitte machen Sie vollständige Angaben. Die Stellungnahme muss bei Einreichen der Dissertation miteingereicht werden.

Als Betreuerin bzw. Betreuer dürfen Sie eine Dissertation maximal zweimal von iThenticate überprüfen lassen. Nach der ersten Überprüfung hat die Doktorandin bzw. der Doktorand einmal die Gelegenheit die Dissertation bei Bedarf zu überarbeiten.

Name Betreuer(in): Prof. Dr. Christian Weber

Name Accountinhaber
(falls abweichend von Betreuer)

Klinik oder Institut: Institut für Prophylaxe & Epidemiologie der Kreislaufkrankheiten (IPEK)

Name Doktorand(in): Maria Aslani

Titel der Dissertation:

☒ 1. Prüfbericht angefertigt am 25.10.2021 Prozentangabe: 11 %

☒ 2. Prüfbericht angefertigt am 17.11.2021 Prozentangabe: 11 %

Auf Basis des Prüfberichts liegt ein Plagiatsverdacht

☒ nicht vor. ☐ vor.

Bitte tragen Sie hier zusätzliche Kommentare ein. Sollten Sie mehr Platz benötigen, so verwenden Sie bitte ein neues Blatt.

Hiermit versichere ich, dass ich den Prüfbericht nach bestem Wissen und Gewissen bewertet habe und dass meine Angaben zum Vorliegen bzw. nicht Vorliegen eines Plagiatsverdachts korrekt sind.

17.11.21, München

Datum und Ort

Unterschrift Betreuer(in)

Form for the ”Münchner Universitätsgesellschaft”

Dear Sir / Madam,

The Münchener Universitätsgesellschaft e.V. would like to win further friends and sponsors for the Ludwig-Maximilians-Universität München. In order to support this, the Doctoral Committee plans to forward your address to the Münchener Universitätsgesellschaft upon successful completion of your doctoral degree.

Sincerely,

Doctoral Committee

Declaration

I agree to have my address forwarded to the Münchener Universitätsgesellschaft:

☒ yes ☐ no

Name, first name:	Aslani, Maria
Address:	Pettenkoferstr. 9a 80336 Munich
E-Mail Address:	Maria.Aslani@med.uni-muenchen.de

Munich, 18/11/2021

Place, Date

Signature

LMU LUDWIG-MAXIMILIANS-UNIVERSITÄT MÜNCHEN

Dekanat Medizinische Fakultät
Promotionsbüro

Dekanat Medizinische Fakultät LMU München
Bavariaring 19, 80336 München

Dr. Antje Hentrich
Leiterin der Munich
Medical Research School
Telefon: 089/4400-58935
Telefax: 089/4400-58902

mmrs@med.uni-muenchen.de
www.med.uni-muenchen.de

Postanschrift:
MMRS
Dekanat Medizinische Fakultät
Bavariaring 19
80336 München

Ihr Zeichen, Ihre Nachricht vom

Unser Zeichen

18. November 2021

Ph.D. Medical Research
Transcript of Records

Name: Maria Aslani Date of birth: 06.07.1993

Institute or Clinic: Klinische Einrichtungen des KUMs, Klinische Einrichtungen, Institut für Prophylaxe und Epidemiologie der Kreislaufkrankheiten (IPEK) - Großhadern

Methods

Title	Date	ECTS
External lab visit	06.11.2017 - 11.11.2017	2.0
Qualifikation nach TierSchVersV	27.11.2016 - 27.01.2017	3.0
Confocal Training	15.01.2020 - 16.01.2020	0.5
External lab visit	15.11.2019 - 15.11.2019	0.5
Development of assay - NE	01.01.2020 - 01.01.2020	0.5
Development of assay - Methylcellulose	01.03.2020 - 01.03.2020	1.0
Development of assay - LSK culturing	06.01.2020 - 06.08.2020	2.0
Webinars summer semester	01.04.2020 - 01.08.2020	0.5
Good Scientific Practice	01.10.2020 - 22.11.2020	0.5
Visual Communication of Science	23.11.2020 - 24.11.2020	1.0
Webinars WS	01.10.2020 - 01.02.2021	1.0
Weekly Lab Meetings WSe20/21	01.10.2020 - 01.02.2021	0.5
Introduction to R course	28.01.2021 - 29.01.2021	1.0
Editing, Processing and Analysis of Scientific Images	25.01.2021 - 27.01.2021	1.5
Ädvanced statistical methods course”	08.04.2021 - 09.04.2021	1.0
”BioImaging Day 2021	11.05.2021 - 11.05.2021	0.5
		17.0/17.0

Conferences

Title	Date	ECTS
Chemotactic Cytokines (GRS) - Gordon Research Seminar	02.06.2018 - 03.06.2018	1.5

Chemotactic Chemokines - Gordon Research Conference - The Chemokine System at the Crossroads of Physiology and Disease	03.06.2018 - 08.06.2018	3.0
IRTG1123 kicoff event- Projects presentation	28.11.2018 - 28.11.2018	0.5
Annual Retreat IRTG1123 and CRC1123	08.10.2019 - 11.10.2019	3.0
IRTG1123 Lecture Series WSe18-19	01.10.2018 - 31.03.2019	0.5
SFB1123 Lecture Series 19	01.01.2019 - 31.12.2019	0.5
		9.0/8.0

Skills

Title	Date	ECTS
Paper writing	01.11.2018 - 01.04.2019	1.0
Paper review Computational Biology and Chemistry	26.01.2019 - 13.02.2019	1.0
Conference Abstracts and Posters	12.11.2018 - 13.11.2018	1.0
Networking for Junior Scientists	16.11.2018 - 16.11.2018	0.5
Course vhb Scientific Writing SS 2020	25.04.2020 - 10.05.2020	0.5
Fundamentals of Project Management	01.06.2020 - 01.08.2020	3.0
		7.0/5.0

LMU LUDWIG-MAXIMILIANS-UNIVERSITÄT MÜNCHEN

Dean's Office
Medical Faculty

MMRS MUNICH MEDICAL RESEARCH SCHOOL

Application for Admission to the Ph.D. Examination

1. I hereby apply for admission to the final examination for the Ph.D. "Medical Research"

Aslani		Maria
Name	Maiden name	First name(s) *please underline name used*
Panorama-Thessaloniki	06-07-1993	Hellenic
Place of birth	Date of birth	Nationality

Pettenkoferstr. 9a
Address

+491631305341	Maria.Aslani@med.uni-muenchen.de
Telephone number	Email address
12006119	Medical Research
Matriculation number	Specialisation (i.e. "International Health" or "Oral Sciences", etc.)

2. The title of my dissertation is:

The role of the atypical chemokine receptor ACKR3 in Bone Marrow homeostasis

Institute for Cardiovascular Prevention (IPEK)
Institute(s) where dissertation was carried out

3. Dissertation

☒ The submitted dissertation has not been published to date

☐ The submitted dissertation or parts thereof have been published in:

Journal title(s)

Journal title(s)

4. The following documents are attached to this application:

- ☒ Dissertation (2x) printed and bound
- ☒ Dissertation (1x) in PDF-format
- ☒ Curriculum vitae *(must be included in bound version of dissertation)*
- ☒ Affidavit *(must be included in bound version of dissertation)*
- ☒ Declaration that bound and electronic versions of the dissertation are in accordance with one another *(must be included in bound version of dissertation*
- ☒ List of all scientific publications to date *(must be included in bound version of dissertation)*
- ☐ Declaration of all authors in case of cumulative dissertation
- ☒ Current proof of enrolment
- ☐ Doctoral supervision agreement(s) and target agreement
- ☒ Supervisor declaration for admission to oral defence
- ☒ iThenticate report
- ☒ Confirmation that all required ECTS have been achieved (transcript of records from your campus portal account)

I am aware that I will be denied admittance to the PhD examination if the documents are incomplete or I have given incorrect particulars. I have been informed that I will only be entitled to bear the title "Ph.D." once I have received my Doctor's Certificate.

Munich, 18/11/2021

Place, Date

Signature doctoral candidate